HAL
open science

Structural arquitecture, sedimentary balance and hydrocarbon potential of a "wedgetop-foredeep" transition zone of retro-foreland basin : example of the Marañon and Huallaga basins of northern Peru

Ysabel Calderón

To cite this version:

Ysabel Calderón. Structural arquitecture, sedimentary balance and hydrocarbon potential of a "wedgetop-foredeep" transition zone of retro-foreland basin : example of the Marañon and Huallaga basins of northern Peru. Tectonics. Université Paul Sabatier - Toulouse III, 2018. English. NNT : 2018TOU30038 . tel-02078737

HAL Id: tel-02078737

https://theses.hal.science/tel-02078737

Submitted on 25 Mar 2019

HAL is a multi-disciplinary open access archive for the deposit and dissemination of scientific research documents, whether they are published or not. The documents may come from teaching and research institutions in France or abroad, or from public or private research centers.

L'archive ouverte pluridisciplinaire **HAL**, est destinée au dépôt et à la diffusion de documents scientifiques de niveau recherche, publiés ou non, émanant des établissements d'enseignement et de recherche français ou étrangers, des laboratoires publics ou privés.

Université Fédérale
Toulouse Midi-Pyrénées

THÈSE

En vue de l'obtention du

DOCTORAT DE L'UNIVERSITÉ DE TOULOUSE

Délivré par :

Université Toulouse 3 Paul Sabatier (UT3 Paul Sabatier)

Présentée et soutenue par :
Ysabel Calderón
le mardi 20 mars 2018

Titre :

Architecture structurale, bilans sédimentaires et potentiel hydrocarburifère d'une zone de transition "wedgetop-foredeep" de rétro-bassin d'avant-pays: exemple des bassins Marañón et Huallaga du Nord-Pérou

---

École doctorale et discipline ou spécialité :
ED SDU2E : Sciences de la Terre et des Planètes Solides

Unité de recherche :
Géosciences Environnement Toulouse, UPS/CNRS UMR 5563/ IRD UR 234/ CNES

Directeur/trice(s) de Thèse :

Patrice BABY; Gérôme CALVES

Jury :

Isabelle MORETTI (Rapporteure)
Jaume VERGES (Rapporteur)
Jean-Paul CALLOT (Examinateur)
Didier BEZIAT (Examinateur)
Jean-François BALLARD (Examinateur)
Stéphane BRUSSET (Invité)

Résumé

Cette thèse, par son approche multidisciplinaire et l'interprétation d'une quantité importante de données industrielles, apporte de nouveaux éléments dans la compréhension des systèmes de bassin d'avant-pays, en particulier dans le domaine andino-amazonien du nord-Pérou. Elle propose un nouveau modèle stratigraphique et structural de cette région, et reconstitue l'histoire de la déformation et de la sédimentation tout en les quantifiant, données indispensables pour modéliser les systèmes pétroliers et réduire les risques en exploration. Les résultats montrent que l'architecture structurale du bassin d'avant-pays de MarañónMarañón, le plus grand des Andes centrales, évolue latéralement d'une zone de wedgetop au SE à une zone de foredeep au NW. Au SE, il forme un prisme de chevauchements en partie érodé, connecté aux bassins wedgetop de Huallaga et Moyabamba. Cet ensemble constitue un seul système de bassin d'avant-pays, déformé par l'interférence d'une tectonique de couverture à vergence Est et d'une tectonique de socle en grande partie à vergence Ouest. Le raccourcissement horizontal total varie entre 70 et 76 km. La vergence Ouest de cette tectonique de socle est contrôlée par l'héritage de l'orogénèse Gondwanide (Permien moyen). Nous montrons qu'elle est à l'origine des importants séismes crustaux et destructeurs dans le bassin de Moyabamba. La tectonique de couverture, à vergence Est, présente un fort raccourcissement et est limitée aux bassins wedgetop de Huallaga et Moyabamba, où elle est contrôlée par la distribution géographique d'un important niveau d'évaporites d'âge permien terminal scellant les structures de l'orogénèse Gondwanide. Vers le NW, la déformation du bassin Marañón s'amortit progressivement, ce qui se manifeste par la transition vers une zone de dépôt de type « foredeep ». La déformation, bien que peu importante, y est toujours active et responsable de séismes de faible profondeur. D'un point de vue sédimentaire, cette thèse a permis de différencier quatre mégaséquences d'avant-pays dans le bassin de MarañónMarañón, définies à partir de corrélations stratigraphiques de puits et des discontinuités régionales identifiées en sismique. Une coupe structurale traversant le système MarañónMarañón-Huallaga a été restaurée en trois étapes depuis l'Eocène moyen pour reconstituer et quantifier la propagation du système de bassin d'avant-pays. Les quatre mégaséquences d'avant-pays et la restauration séquentielle montrent que le système MarañónMarañón-Huallaga s'est développé depuis l'Albien en deux étapes séparées par une importante période d'érosion durant l'Eocène moyen. Elles ont enregistrées successivement les soulèvements des cordillères occidentale et orientale des Andes du nord-Pérou, et celui de l'Arche de Fitzcarrald. D'un point de vue quantitatif, les taux de sédimentation calculés montrent une augmentation progressive depuis l'Albien, interrompue par l'érosion de l'Eocène moyen. Les modélisations pétrolières 2D, réalisées à partir d'une révision des systèmes pétroliers et de la restauration séquentielle du système Huallaga-MarañónMarañón, valorisent une grande partie des résultats obtenus dans cette thèse en simulant l'expulsion des hydrocarbures aux différentes étapes de la déformation du système Huallaga-MarañónMarañón et en montrant ses zones de piégeage potentielles.

Abstract

This thesis, through its multidisciplinary approach and the interpretation of a large amount of industrial data, brings new elements in the understanding of foreland basin systems, especially in the Andino-Amazonian field of northern Peru. It proposes a new stratigraphic and structural model of this region, reconstructs and quantifies the history of the deformation and sedimentation that constitutes the key data to model the petroleum systems and to reduce the risks in exploration. The results show that the structural architecture of the MarañónMarañón Foreland Basin, the largest of the central Andes, evolves laterally from a wedgetop zone in the SE to a foredeep zone in the NW. In the SE, it forms a thrust wedge partly eroded, connected to the wedgetop basins of Huallaga and Moyabamba. This set constitutes a single foreland basin system, deformed by the interference of an east-verging thin-skinned tectonics and largely west-verging tectonics. The total horizontal shortening varies between 70 and 76 km. The western vergence of these thick-skinned tectonics is controlled by the inheritance of the Gondwanide orogeny (Middle Permian). We show that it is at the origin of the important crustal and destructive earthquakes in the Moyabamba basin. The east-verging thin-skinned tectonics shows a strong shortening and is confined to the wedgetop basins of Huallaga and Moyabamba, where it is controlled by the geographical distribution of a large level of Late Permian evaporites sealing the structures of the Gondwanide orogenesis. Towards the NW, the deformation of the Marañón basin is progressively amortized, which is reflected in the transition to a foredeep type deposition zone. The deformation, although not very important, is still active and responsible for shallow earthquakes. From a sedimentary point of view, this thesis has made it possible to differentiate four foreland mega-sequences in the Marañón basin, defined from well stratigraphic correlations and regional discontinuities identified in seismic. A structural section through the Marañón-Huallaga system has been restored in three stages since the Middle Eocene to reconstruct and quantify the propagation of the foreland basin system. The four foreland mega-sequences and the sequential restoration show that the Marañón-Huallaga system developed since the Albian during two stages separated by an important period of erosion during the Middle Eocene. They recorded successively the uplifts of the western and eastern Cordilleras of the Andes of northern Peru, and that of the Arch of Fitzcarrald. From a quantitative point of view, the calculated sedimentation rates show a gradual increase since the Albian, interrupted by the erosion of the Middle Eocene. The 2D petroleum modeling, carried out from a revision of the petroleum systems and the sequential restoration of the Huallaga-Marañón system, valorizes a large part of the results obtained in this thesis by simulating the expulsion of the hydrocarbons at the different stages of the deformation of the Huallaga-Marañón system, and showing its potential trapping areas.

Resumen

Esta tesis por su alcance multidisciplinario y la interpretación de una cantidad importante de información de la industria del petróleo aporta nuevos elementos en la comprensión del sistema de cuenca de ante-país, en particular en el dominio andino amazónico del norte de Perú. Este trabajo propone un nuevo modelo estratigráfico y estructural de esta región, reconstruye y cuantifica la historia de la deformación y de la sedimentación, información indispensable para modelizar los sistemas petroleros y reducir los riesgos de exploración. Los resultados muestran que la arquitectura estructural de la cuenca de ante-país de Marañón, la cuenca más grande de los Andes centrales, evoluciona lateralmente de una zona de wedgetop al sureste a una zona de foredeep al noroeste. Al suroeste, forma un prisma de cabalgamientos en parte erosionado, conectado a las cuencas wedgetop de Huallaga y Moyobamba. Este ensamble constituye un solo sistema de cuenca de ante-país, deformado por la interferencia de una tectónica de cobertura con vergencia Este y de una tectónica de basamento en gran parte con vergencia Oeste. El acortamiento horizontal total varía entre 70 y 76 km. La vergencia Oeste de esta tectónica de basamento está controlada por la herencia de la orogenia Gondwanide (Pérmico Medio). Nosotros mostramos que esta es el origen de importantes sismos crustales y destructores en la cuenca Moyobamba. La tectónica de cobertura, con vergencia Este, presenta un fuerte acortamiento y está limitada a las cuencas wedgetop de Huallaga y Moyobamba, donde está controlada por la distribución geográfica de un importante nivel de evaporitas de edad pérmico terminal sellando las estructuras de la orogenia Gondwaniana. Hacia el Noroeste, la deformación de la cuenca Marañón se amortiza progresivamente, la cual se manifiesta por la transición hacia una zona de depositación de tipo foredeep. La deformación, aunque poco importante, ha sido siempre activa y responsable de los sismos de baja profundidad. Desde un punto de vista sedimentario, esta tesis ha permitido diferenciar cuatro megasecuencias de ante-país en la cuenca Marañón, definidas a partir de la correlación estratigráfica de pozos y de discontinuidades regionales identificadas en la sísmica. Un corte estructural atravesando el sistema Marañón – Huallaga ha sido restaurado en tres etapas desde el Eoceno medio para reconstituir y cuantificar la propagación del sistema de cuenca ante-país. Las cuatro megasecuencas de ante-país y la restauración secuencial muestran que el sistema Marañón-Huallaga se ha desarrollado desde el Albiano en dos etapas separadas por un importante periodo de erosión durante el Eoceno medio. Estos han registrado sucesivamente los levantamientos de la cordillera occidental y oriental de los Andes del norte de Perú, y el del Arco de Fitzcarrald. Desde un punto de vista cuantitativo, las tasas de sedimentación calculadas muestran un aumento progresivo desde el Albiano, interrumpido por la erosión del Eoceno medio. Las modelizaciones petroleras 2D, realizadas a partir de una revisión de los sistemas petroleros y de la restauración secuencia del sistema Huallaga-Marañón, valorizan una gran parte de los resultados obtenidos en esta tesis simulando la expulsión de los hidrocarburos a diferentes etapas de la deformación del sistema Huallaga-Marañón y mostrando las zonas de potenciales entrampamiento.

Remerciements

Esta tesis se ha realizado dentro del Convenio de Cooperación entre el Institut de Recherche pour le Développement (IRD) y PERUPETRO, el cual tiene inicio desde el 2003 con el objetivo de realizar estudios en conjunto sobre los fenómenos geológicos y su implicancia en el desarrollo de las cuencas hidrocarburíferas a ambos lados de la cadena andina. Asimismo, ha brindado a lo largo de su trayectoria el soporte científico a diversos estudiantes peruanos y franceses para desarrollar trabajos de investigación y así obtener los grados académicos correspondientes. Es en este ámbito que agradezco enormemente las facilidades brindadas a ambas entidades a través de las gestiones realizadas por las personas que lo conforman.

Finalmente, después de varios años de tesis, mejor no nombrar, puedo expresar mi más sincero agradecimiento a las personas que me han permitido realizar este trabajo. Debo agradecer de manera especial y sincera a mis directores de tesis: Patrice Baby, por alentarme en realizar esta tesis doctoral bajo su dirección, apoyo, confianza y amistad en este extenso periodo, el cual me ha permitido incursionar en el mundo de la investigación. A Gérôme Calves, por sus recomendaciones en el trabajo y comprensión por el tiempo que tome en realizar el trabajo.

Quisiera agradecer en PERUPETRO a muchos colegas y amigos, algunos ellos no presentes en la empresa pero que me alentaron a seguir. Asimismo en especial a la Gerencia de Exploración liderado por Asaid Bandach.

También agradezco a las personas que me brindaron su apoyo durante mis estadías en el Laboratorio GET de Toulouse, Martin Roddaz, Stephane Brusset, Stephanie Brichau, Pierre Olivier así como los amigos que me brindaron alguna ayuda en estos largos años.

Agradezco por el tiempo brindado a los miembros del jurado y examinadores, Isabelle Moretti, Jaume Verges, Jean-Paul Callot, Didier Beziat, Jean-Francois Ballard y Stephane Brusset que aceptaron revisar y corregir el trabajo.

Un especial agradecimiento a mi familia y sobre todo a mis hijos Miguel y Luis Anibal por acompañarme en este proyecto que empezó también con la llegada de ellos.

Table of contents

Table of contents 1

List of figures 4

List of tables 10

Chapter 1: Introduction en Français 11

Chapter 1: Introduction 17

1.1. Topic and objectives 17

1.2. The subandean basins of northern Peru: generalities 19

1.3. Methodology 23

1.3.1. Structural Analysis 23

1.3.2. Lithostratigraphic analysis and sedimentation rates 25

1.3.3. Sequential Restoration 25

1.3.4. Petroleum System Modeling 25

1.4. Structure of the thesis 26

Chapter 2: Structural architecture of the retro-foreland basin system of northern Peru 29

2.1. Introduction 29

2.2. Thrust tectonics in the Andean retro-foreland basin of northern Peru: Permian inheritances and petroleum implications 31

Résumé en français 31

Abstract 32

2.2.1. Introduction 33

2.2.2. Geologic background 35

2.2.3. Stratigraphy 38

2.2.4. Structural analysis and balanced cross-sections 42

2.2.5. Discussion 55

2.2.6. Conclusions 57

2.3. The northern Marañón foreland basin system structure 58

2.3.1. Geologic framework, stratigraphy and method 58
2.3.2. The hinge zone: regional structural cross-section R3 61
2.3.3. The Santiago-Marañón foreland basin system: regional structural cross-section R4 63
2.3.4. The northern Situche deformation: regional structural cross-section R5 68
2.3.5. Summary and conclusion 70
Chapter 3: Marañón foreland basin system – the stratigraphic record 73
3.1. Introduction 73
3.2. Sequential restauration of the southern Marañón foreland basin system 75
3.3. Stratigraphic architecture 78
3.3.1. Previous studies and definition of long term foreland basin sequences 78
3.3.2 Wells stratigraphic correlations 80
3.3.3 Seismic and porosity logs calibration 87
3.4. Quantification of sedimentation rates in the foreland basin system 91
3.4.1. Long term foreland basin sequences in structural cross-sections 91
3.4.2. Wedge-top eroded thicknesses 95
3.4.3. Sedimentation rates 100
3.5. Summary and conclusions 105
Chapter 4: Petroleum systems restoration of the Huallaga-Marañón Andean retro-foreland basin, Peru 107
Introduction au chapitre 107
Résumé en français 108
Abstract 109
4.1. Introduction 110
4.2. Tectonic background 110
4.3. Stratigraphy 114
4.4. Balanced cross-section, deformation timing and sequential restoration 117
4.5. Sources rocks 127
4.5.1. Late Cretaceous 127
4.5.2. Late Triassic/Lower Jurassic (Pucara) 131

4.5.3. Late Permian (Shinai) 131
4.5.4. Devonian Carboniferous (Cabanillas) 132
4.5.5. Oil affinity background 132
4.6. Petroleum systems modeling 134
4.6.1. Method and data gathering 134
4.6.2. 1D modeling results 135
4.6.3. 2D modeling results 138
4.7. Discussion and conclusion 139
Chapter 5: Conclusions 145
5.1. Structural Architecture 145
5.2. Stratigraphic Architecture and Evolution of the Foreland Basin System 146
5.3. Petroleum systems of the Huallaga-Marañón foreland basin 147
5.4. The Huallaga-Marañón Foreland Basin System in the Subandean Basins of Peru 148
Chapter 5: Conclusions en Français 149
References cited 153
Annex 1: Biostratigraphy 163
Annex 2: Methods of time-depth conversion, porosity calculation, compaction correction and volume and rate estimation 165
Annex 3: Vitrine Reflectance values used in the Basin Modeling 171
Annex 4: Structural maps in depth 177
Annex 5: THE PERUVIAN SUBANDEAN FORELAND BASIN SYSTEM: STRUCTURAL OVERVIEW, GEOCHRONOLOGIC CONSTRAINTS, AND UNEXPLORED PLAYS *in Petroleum Basins and Hydrocarbon Potential of the Andes of Peru and Bolivia. AAPG Memoir 117* 179

List of figures

Figure 1.1. Central Andes, with location of the subandean basins and the structural section of Figure 1.2 (EC: Eastern Cordillera, WC: Western Cordillera). 18

Figure 1.2. Structural cross-section through the central Andes, with location of the Huallaga-Marañón Andean - Amazonian foreland basin system (modified from Prudhomme et al., 2016; location of the section in Figure 1.1).....19

Figure 1.3. Lithostratigraphic diagram representing from west to east the different sedimentary units of the Andean-Amazonian foreland basin system of Northern Peru. The Cretaceous to Neogene foreland sequences overlie unconformably on Mesozoic and Paleozoic pre-Andean series. 21

Figure 1.4. Gravimetric map (3D inversion) (after Graterol, 2011) showing the structural partitioning of the subandean basins of northern Peru, the depozones of the Marañón basin and the Iquitos Arch (forebulge). 22

Figure 1.5. Schematic cross-section illustrating the Foreland Basin System concept *sensu* DeCelles & Giles (1996) applied to subandean basins (from Roddaz et al., 2010). 23

Figure 1.6. Structural map of the Base Cretaceous (TWT-Two Way Time) of the Marañón foreland basin with location of the regional structural cross-sections. Crustal earthquakes recorded in this region have been used to constrain the structural geometry of some thrusts. 24

Figure 2.1. Geological map of the Marañón foreland basin system with location of the regional cross-sections presented in this chapter (R1 to R6), wells and seismic sections used for their construction. 30

Figure 2.2.1. Tectonic map of the Subandean basins of northern and central Peru, showing the study area and the different morpho-tectonic units. The Huallaga-Marañón and Moyabamba-Marañón structural cross-sections are located. 34

Figure 2.2.2. Geological map of the Huallaga-Moyabamba-Marañón FBS with location of seismic sections, wells, balanced cross-sections, and mean earthquakes (Mw>5) relocated by Delvin et al. (2012). The geology map is adapted from INGEMMET 1:1’000,000 map and field observations. 36

Figure 2.2.3. TWT Base Cretaceous structural map of the Marañón foreland basin with location of the eastern border of the pre-Cretaceous long-term sequences and Middle Permian thrust faults. The TWT map is superimposed on the geologic contours of the Andean relieves. Seismic project used for the map construction is located. 37

Figure 2.2.4. Stratigraphic diagram and petroleum systems along the Huallaga-Moyabamba-Marañón FBS. The orogenic cycles names are those that are more commonly used in the Andes (see Ramos, 1988; Caputo, 2014; Chew et al., 2016). 39

Figure 2.2.5. Regional wells stratigraphic correlations in the southern Marañón basin (Shanusi 1X, Loreto 1X and Santa Lucia 2X, location in Fig. 2.2.2) showing the first order pre-Cretaceous sequences. The Late Cretaceous basal foreland unconformity (Cushabatay Fm.) is flattened and correlations have been made between long term pre-Cretaceous sequences. 40

Figure 2.2.6. Interpreted seismic sections 91MPH-23 and DX-23 (location in Fig. 2.2.2 and 2.2.3) 44

Figure 2.2.7. Interpreted seismic sections AH-3 and DX-51 (location in Fig. 2.2.2 and 2.2.3) 46

Figure 2.2.8. Interpreted seismic section AH-13 (location in Fig. 2.2.2 and 2.2.3) 48

Figure 2.2.9. Interpreted seismic section PSEP-135-2013-01 (location in Fig. 2.2.2 and 2.2.3) 49

Figure 2.2.10. Huallaga-Marañón and Moyabamba-Marañón balanced cross-sections (location in Figures 2.2.1 and 2.2.2). Initial sections were obtained by flattening the base of the Pozo Formation (± 45Ma). Mean regional earthquakes (Mw>5) relocated by Delvin et al. (2012) have been projected on the section. 52

Figure 2.2.11. Zoom of the structural balanced cross-sections in the Huallaga-Marañón and Moyabamba-Marañón wedge-top basins (location in Figs 2.2.1 and 2.2.2). Mean regional earthquakes (Mw>5) relocated by Delvin et al. (2012) have been projected on the section. 54

Figure 2.3.1. TWT Base Cretaceous structural map of the Marañón foreland basin with location of the eastern border of the pre-Cretaceous long term sequences. The TWT map is superimposed on the geologic contours of the Andean relieves. Regional cross-sections, wells and 3D seismic of Situche area are located. Two depocenters appear in the Marañón foredeep. 59

Figure 2.3.2. Stratigraphic diagram and petroleum systems along the Santiago-Marañón FBS. The orogenic cycles names are those that are more commonly used in the Andes (see Ramos, 1988; Caputo, 2014; Chew et al., 2016). 60

Figure 2.3.3. Structural regional cross-section R3 through the deepest part of the Marañón foredeep (location on Figures 2.1 and 2.3.1). 62

Figure 2.3.4. Structural regional cross-section R4 through the Santiago-Marañón foreland basin system (location on Figures 2.1 and 2.3.1).....64

Figure 2.3.5. Stratigraphic log of the Putuime X1 well used for the interpretation of the Santiago basin seismic section (Figure 2.3.4.).....66

Figure 2.3.6. Regional gravimetric map showing basement configuration (modified from Navarro et al., 2005; gravity acquisition and processing from EDCON Worldwide, 1997). It shows the foredeep geometry of the Marañón basin west of the Iquitos forebulge, and the importance of the sedimentary cover thickness and the presence of basement highs in the Santiago basin.....67

Figure 2.3.7. Structural regional cross-section R5 through the northern Marañón foreland basin system and the Situche oil field (location on Figures 2.1 and 2.3.1). 69

Figure 2.3.8. Amplitude map from the Campanian Vivian reflector (modified from Talisman's report, 2012) showing WNW-ESE faults oblique to the classic N-S Andean structures. The amplitude anomaly also reflects no deposition of Vivian sandstones in the northern block (north of the listric faults system), where was drilled Situche Norte 4X. 70

Figure 2.3.9. Latitudinal structural regional cross-section R6 through the Marañón foreland (location on Figures 2.1 and 2.3.1). Vertical scale is exaggerated.....72

Figure 3.1. Digital Elevation Map (DEM) map with stratigraphic and structural cross sections constructed for this study. Dotted lines represent the outline of the sedimentary basins: Marañón, Santiago, Huallaga and Bagua. Biostratigraphic studies from previous reports are showed in red dots (Talisman, 2011, Conoco, 2008). 74

Figure 3.2. Huallaga-Marañón balanced cross-section (R1) and sequential restoration. Initial section (Middle Eocene) was obtained by flattening the base of the Pozo Formation (± 45Ma), which sealed previous deformation and configuration of the FBS. Intermediary stage corresponds to the Late Early Miocene stage and is calibrated by AFT dating in the Chazuta Thrust and Biabo Anticline. AFT samples are projected on present-day cross-section (see location on the map of Figures 3.1 and 2.2.2). AFT samples and analyses are described in the Chapter 4. CTFW: Chazuta Thrust Foot-Wall. 77

Figure 3.3. Late Cretaceous and Cenozoic sequences on the Andean Basal Foreland Unconformity (modified from Figure 1.3.). F1 to F4 appoint long term foreland basin sequences defined in this study (see below).....78

Figure 3.4. Stratigraphic overview (Wheeler diagram) of the Paleogene-Neogene northern Peruvian foreland basin (from Roddaz et al., 2010). Fm: formation; Mb: member; SAZ: sub-Andean zone. 79

Figure 3.5. SW- NE wells stratigraphic correlation S1 (location on Fig. 3.1) crossing the southern Marañón basin, and flattened at the regional Basal Pozo erosional unconformity. BFU: Basal Foreland Unconformity. Depth is in meters. 83

Figure 3.6. SW- NE wells stratigraphic correlation S2 (location on Fig. 3.1) crossing the Marañón basin, and flattened at the regional Basal Pozo erosional unconformity. BFU: Basal Foreland Unconformity. Depth is in meters. 84

Figure 3.7. SW- NE wells stratigraphic correlation S3 (location on Fig. 3.1) in the Santiago and northern Marañón basin, and flattened at the regional Basal Pozo erosional unconformity. BFU: Basal Foreland Unconformity. Depth is in meters. 85

Figure 3.8. NW- SE wells stratigraphic correlation (S4, location on Fig. 3.1) crossing the Marañón basin, and flattened at the regional Basal Pozo erosional unconformity. BFU: Basal Foreland Unconformity. MFBS: Marañón Foreland Basin System. Depth is in meters.....86

Figure 3.9. Seismic section DX-31 in the Loreto antiform (see Fig. 3.1 for location) and its correlation with well log and porosity chart showing mean unconformities and long-term foreland basin sequences (see Figure 3.3). BFU: Basal Foreland Unconformity. 88

Figure 3.10. Seismic section Sun 16 in the Mahuaca area (see Fig. 3.1 for location) and its correlation with the well log and porosity chart showing mean unconformities and long term foreland basin sequences (see Figure 3.3). BFU: Basal Foreland Unconformity. 89

Figure 3.11. Inline 194 section from the 3D seismic cube of the Tucunare area (see Fig. 3.1 for location) and its correlation with well log and porosity chart showing mean unconformities and long term foreland basin sequences (see Figure 3.3). BFU: Basal Foreland Unconformity. 90

Figure 3.12. Inline 173 from the 3D seismic cube of the Situche area (see Fig. 3.1 for location) and its correlation with well log and porosity chart showing mean unconformities and long term foreland basin sequences (see Figure 3.3). BFU: Basal Foreland Unconformity. 91

Figure 3.13. Regional structural cross sections R1 (location in Fig. 3.1) showing long term foreland basin sequences (F1, F2, F3 and F4). Vertical scale exaggeration 93

Figure 3.14. Regional structural cross sections R1 (location in Fig. 3.1) showing long term foreland basin sequences (F1, F2, F3 and F4). Vertical scale exaggeration. 94

Figure 3.15. Regional structural cross sections R1 (location in Fig. 3.1) showing long term foreland basin sequences (F1, F2, F3 and F4) and the top Neogene paleosurface profile computed from 1D PetroMod modeling (see text). Vertical scale exaggeration. 97

Figure 3.16. Regional structural cross sections R3 (location in Fig. 3.1) showing long term foreland basin sequences (F1, F2, F3 and F4) and the top Neogene surface profile computed from 1D PetroMod modeling (see text). Vertical scale exaggeration. 98

Figure 3.17. Regional structural cross sections R5 (location in Fig. 3.1) showing long term foreland basin sequences (F1, F2, F3 and F4) and the top Neogene surface profile computed from 1D PetroMod modeling (see text). Vertical scale exaggeration. 99

Figure 3.18. Computed sedimentation rates along regional cross sections R1, R3 and R5. MFBS: Marañón Foreland Basin System. 102

Figure 3.19. (A) Sediment supply and flux computed for the Marañón Basin over the last 110 Ma. (B) Modern sediment supply corresponds to the flux measured at Obidos (Filizola

and Guyot 2014). In the Ucayali Basin, the modern sedimentation rates represent 220 Mt/y (Santini et al., 2014). Note the logarithmic scale to allow ‘comparison’ of the modern (high) and geological (low) rates. 104

Figure 4.1. Tectonic map of the Subandean basins of northern and central Peru, showing the study area and the different morpho-tectonic units. The Huallaga-Marañón structural cross-section is located. 111

Figure 4.2. Geological map of the study area, with location of the Huallaga-Marañón balanced cross-section, subsurface data, AFT datings and Ro analyses. 113

Figure 4.3. Stratigraphic diagram and petroleum systems along the Huallaga-Marañón cross-section. 116

Figure 4.4. Interpreted seismic sections crossing the Huallaga and Marañón wedge-top basins and used for the balanced cross-section construction. 119

Figure 4.5. Huallaga-Marañón balanced cross-section and sequential restoration. Initial section was obtained by flattening the base of the Pozo Formation (± 45Ma). Intermediary stage corresponds to the Late Early Miocene stage and is calibrated by AFT dating in the Chazuta Thrust and Biabo Anticline. AFT samples are projected on the cross-section (see location on the map of Figure 4.2). TG30, HUA338 and HUA330 have been analyzed for this study (see Table 4.1); ages correspond to youngest cooling events. TRU70 has been published by Eude et al. (2015); the AFT age corresponds to the Central Age. CTFW: Chazuta Thrust Foot-Wall. 120

Figure 4.6. Geographic distribution and TOC of the four studied source rocks in the Peruvian Subandean basins. (A) Late Cretaceous (Chonta), (B) Late Cretaceous (Raya), (C) Triassic (Pucara), (D) Late Permian (Shinai). 128

Figure 4.7. Geographic distribution and maturity of the four studied source rocks in the Peruvian Subandean basins. (A) Late Cretaceous (Chonta), (B) Late Cretaceous (Raya Fm.), (C) Triassic (Pucara), (D) Late Permian (Shinai). 129

Figure 4.8. Van Krevelen plots of the pyrolysis results from the studied sources rocks (Chonta, Raya, Pucara, Shinai) in the Huallaga-Marañón foreland basin system. 130

Figure 4.9. Oil to sources correlations in the Marañón basin from C28 / C29 Sterane Ratio versus C29 / C30 Hopane Ratio (modified from Idemitsu Oil & Gas Company Ltd., 2000). 133

Figure 4.10. Maturity state on the present structural cross-section using 1D modeling and Ro calibration of Tamanco 1X, La Frontera 1X, Santa Lucia 1X, Loreto 1X, Ponasillo 1X and Biabo fictive well. Three outcrop analyses (TG32, TRU70 and HUA332) have been used too. Wells and outcrops are located on the map of Figure 4.2. TG32 and TRU70 are projected. 136

Figure 4.11. 1D burial and maturity modeling along the structural cross-section. 137

Figure 4.12. Evolution of the maturity windows (Ro) through times for the four potential sources rocks and in the three stages of the sequential restoration of the regional cross-section. 140

Figure 4.13. Evolution of the maturity (TR) through times for the four potential sources rocks and in the three stages of the sequential restoration of the regional cross-section. Hydrocarbon accumulations computed by Petromod are represented. Source rock (SR) and reservoir are indicated for each numbered accumulation. 141

Figure 4.14. Hydrocarbon saturation and oil and gas migration vectors through time in the three stages of the sequential restoration of the regional cross section. Hydrocarbon accumulations computed by PetroMod ® are represented. Source rock (SR) and reservoir are indicated for each numbered accumulation 142

List of tables

Table 3.1. Marañón Basin volumetric, physical properties of sediments and sedimentation rates computed from regional cross sections R1, R3 and R5 and isopach map.....101

Table 4.1. New apatite fission-tracks (AFT) data. Analyses were done at *Geotrack International Pty Ltd* in 2014.....122

Table 4.2. Geochemical analyses of the PERUPETRO data bank (Petroleum System International, 2011; SPT Simon Petroleum, 1993) and new geochemical analyses done by Geo Lab Sur and Geotrack in new outcrop samples collected close to the regional cross-section. 123

Chapter 1: Introduction en Français

1.1. Problématique et objectifs

Les bassins subandins du Nord-Pérou (Marañón, Huallaga, Moyabamba, et Santiago; cf. Figures 1.1 et 1.2) se situent dans la zone de transition Andes-Amazonie et font partie du retro-bassin d'avant-pays nord amazonien (Espurt et al., 2007, 2011; Roddaz et al., 2010). Ils constituent des bassins pétroliers à potentiel reconnu et en cours d'exploration (Mathalone and Motaya, 1995; McGroder et al., 2014). La présence d'abondantes données de sous-sol permet d'y réaliser une analyse rigoureuse de l'architecture structurale et stratigraphique.

Les bassins Marañón et Huallaga (Figure 1.2) sont les plus importants de ces bassins et ne peuvent être dissociés pour comprendre la structure et l'évolution du système wedgetop-foredeep du retro-bassin d'avant-pays nord amazonien.

Ces bassins, déformés par des systèmes de plis et chevauchements, présentent un partitionnement structural complexe contrôlé par un héritage mésozoïque et/ou paléozoïque. La question du contrôle de la déformation subandine par des paléostructures telles que le rift triasique (Rosas et al., 2007; McGroder et al., 2014) et/ou les orogénèses paléozoïques (Laubacher et al., 1985; Dalmayrac et al., 1988; Bump et al., 2008; Espurt et al., 2008) reste d'actualité. Les synthèses proposées jusqu'à maintenant sont incomplètes et ne répondent pas de manière satisfaisante à cette question. Dans cette thèse, le premier objectif est donc de profiter de l'accès à la base de données de sub-surface et de surface de PERUPETRO (Agence nationale des hydrocarbures du Pérou) pour réviser l'architecture structurale des bassins Marañón et Huallaga, afin d'en proposer une nouvelle analyse géométrique et cinématique. Les bassins subandins moins importants comme Moyabamba et Santiago seront également considérés pour comprendre l'ensemble du système. Ce premier objectif permettra aussi de mieux cerner les risques structuraux qui freinent actuellement l'exploration pétrolière dans les bassins subandins du Nord-Pérou.

Dans un système de bassin d'avant-pays, le « timing » de la propagation des chevauchements peut être déchiffré à partir d'âges thermochronologiques et de l'enregistrement stratigraphique des dépôts syn-orogéniques. Dans les bassins Huallaga et

Marañón, la définition de ce calendrier permet de mieux comprendre la propagation du front orogénique d'arrière-arc des Andes centrales et le développement du bassin d'avant-pays andino-amazonien associé. Ce calendrier permet aussi de définir les moments critiques des systèmes pétroliers (Magoon and Dow, 1994). Le deuxième objectif est donc d'intégrer de nouvelles données thermochronologiques et une analyse des enregistrements sédimentaires dans nos modèles structuraux, en proposant quand cela est possible une restauration séquentielle de la déformation.

Les bilans sédimentaires dans la propagation des systèmes de bassin d'avant-pays sont des résultats relativement rares à l'échelle géologique. Ils ne peuvent être obtenus qu'à partir de données de sous-sol renseignant les épaisseurs sédimentaires et d'une stratigraphie relativement bien contrainte. Le troisième objectif de cette thèse est d'essayer de quantifier les taux de sédimentation et leur évolution tout au cours de l'histoire des bassins d'avant-pays Huallaga et Marañón. Les calculs ont été faits après révision de la stratigraphie et de l'architecture des remplissages sédimentaires syn-orogéniques reportée sur les nouvelles coupes structurales régionales construites dans le cadre de la thèse.

Enfin le dernier objectif consiste à exploiter les résultats obtenus dans une modélisation pétrolière 2D de la partie la plus complexe et la plus attractive du système de bassin d'avant-pays andino-amazonien du nord-Pérou : le système Huallaga-Marañón. Cette modélisation intègre la révision et définition de nouveaux systèmes pétroliers, et utilise les restaurations séquentielles de la déformation obtenues précédemment.

1.2. Les bassins subandins du nord-Pérou : généralités

Les bassins subandins du Nord-Pérou (Marañón, Huallaga, Moyabamba, et Santiago; cf. Figures 1.1 et 1.2) appartiennent à ce que nous appellerons le système de bassin d'avant-pays (FBS : Foreland Basin System) andino-amazonien, qui occupe une part relativement importante dans le dispositif structural de la chaîne andine comme le montre la coupe de la Figure 1.2. La déformation de ces bassins, pouvant présenter de forts taux de raccourcissement (Hermoza et al., 2005), est associée à la propagation du front orogénique d'arrière-arc et au soulèvement de la Cordillère Orientale qui a commencé entre 30 et 24 Ma (Eude et al., 2015). Au cours du Crétacé supérieur et du Paléogène, les bassins subandins se trouvaient en position beaucoup plus distale dans le système de bassin d'avant-pays et étaient beaucoup moins déformés. L'initiation de ce système de bassin d'avant-pays est marquée par une BFU (Basal Foreland Unconformity) qui se situe à la base de la première séquence transgressive du Crétacé supérieur et repose sur des séries mésozoïques,

paléozoïques ou précambriennes déformées et érodées reflétant une histoire pré-andine complexe. L'ensemble de ces séries sédimentaires et métamorphiques est représenté dans la Figure 1.3.

Le système de bassin d'avant-pays subandin du Nord-Pérou est compartimenté en sous bassins qui sont représentés sur les Figures 1.1 et 1.4. La paléogéographie des bassins pré-crétacés a joué un rôle important dans ce partitionnement structural. Les paléostructures les plus influentes correspondent au rift triasique (Rosas et al., 2007; McGroder et al., 2014) et à l'héritage des orogénèses de la fin du Jurassique et du Paléozoique (Laubacher et al., 1985; Dalmayrac et al., 1988; Ramos, 1988; Bump et al., 2008; Espurt et al., 2008; Caputo, 2014). Elles seront décrites et discutées dans le Chapitre II.

1.3. Méthodologie

Une approche pluridisciplinaire a été nécessaire pour intégrer et interpréter l'ensemble des données. Les études structurales, l'analyse des données thermochronologiques et des remplissages sédimentaires ont été menées de front, afin de proposer un modèle de propagation du système de chevauchements et des zones de dépôts associées. Nous avons pour cela utilisé le concept de système de bassin d'avant-pays de DeCelles & Gilles (1996).

1.3.1. Analyse structurale

L'analyse structurale a été réalisée à partir d'interprétation sismique 2D, calibrée à partir des puits d'exploration les plus profonds, de données de terrain et d'une révision stratigraphique (Figures 1.3 et 1.6). Les sections sismiques et les données de puits ont été fournies par PERUPETRO SA. Les sections sismiques ont été chargées et interprétées dans WinPICS (Divestco software) et MOVE (Midland Valley software). Les données de surface ont été obtenues à partir de nos campagnes de terrain et des cartes géologiques 1 : 100 000 d'INGEMMET (Institut National Géologique, Minier et Métallurgique du Pérou).

Des coupes structurales – pour la plupart équilibrées - ont été ensuite construites à l'échelle régionale à travers l'ensemble des bassins Marañón et Huallaga et des bassins frontaliers Moyabamba et Santiago (Figure 1.6), à l'aide du logiciel MOVE (Middland Valley).

1.3.2. Analyses lithostratigraphiques et taux de sédimentation

Afin d'étudier les remplissages sédimentaires des bassins Huallaga et Marañón en termes de propagation de zones de dépôt d'avant-pays (voir Figure 1.5), les séquences sédimentaires régionales (long terme) ont été définies et caractérisées à partir de corrélations lithostratigraphiques de puits et de la caractérisation des discontinuités majeures reconnues en sismique 2D et dans les logs de porosité. Les données de puits et la sismique ont été fournies par PERUPETRO SA. Les datations proviennent de publications académiques et de rapports industriels disponibles dans la base de données de PERUPETRO SA.

Les séquences sédimentaires de bassin d'avant-pays ainsi définies ont été ensuite cartées sur les coupes structurales régionales, avant d'être utilisées pour calculer des taux de sédimentation pour chaque coupe.

Enfin, des flux sédimentaires ont été calculés en volume pour l'ensemble du bassin Marañón à partir de cartes isopaques construites grâce à l'information sismique, qui ont été ensuite transformées en profondeur.

1.3.3. Restauration séquentielle

La coupe structurale régionale R1 (voir Figure 1.6) englobant le système Huallaga-Marañón a été équilibrée et restaurée en plusieurs étapes, avec le logiciel MOVE de Middland Valley, pour mieux comprendre la propagation des systèmes de chevauchements et des zones de dépôt d'avant-pays. Ces différentes étapes ont été reconstituées à partir 1) de données thermochronologiques nouvelles et antérieures, 2) de la surface d'érosion de l'Eocène moyen connue régionalement (Christophoul et al., 2002), qui a servi de niveau repère et qu'il a été possible d'identifier en sismique et sur le terrain, et 3) de l'analyse de strates de croissance apparaissant en sismique. Au total, trois étapes de déformation ont pu être reconstituées.

L'ensemble des données utilisées sont décrites en détails dans les chapitres 3 et 4.

1.3.4. Modélisation pétrolière

La restauration séquentielle obtenue pour la coupe régionale Huallaga-Marañón (R1) a été utilisée afin de réaliser pour la première fois une modélisation 2D des systèmes pétroliers de cette région. Ces systèmes pétroliers ont été préalablement révisés et partiellement redéfinis à partir de nouvelles analyses de roches mères et des données déjà existantes chez PERUPETRO SA.

La modélisation a été réalisée avec le logiciel Petromod de Schlumberger. Les données utilisées concernant roches mères, réservoirs, charges et géohistoire sont décrites en détails dans le Chapitre 4.

1.4. Structure de la thèse

Après une introduction générale (Chapitre 1) résumant objectifs et méthodologie, la thèse comprend trois chapitres.

Le Chapitre 2 présente une analyse structurale synthétique des bassins Huallaga et Marañón, et bassins frontaliers (Moyabamba et Santiago), à partir des données de sous-sol fournies par PERUPETRO SA et d'observations de terrain. Des coupes structurales régionales ont été construites à partir d'interprétations sismiques calibrées par des données de forage et de surface. Ces coupes structurales réparties sur l'ensemble de la région étudiée permettent de proposer une architecture structurale complexe, héritée de paléostructures paléozoïques et mésozoiques. Cette étude structurale a fait l'objet d'un article publié à *Marine and Petroleum Geology* en 2017, où est analysée aussi l'activité sismique de certains chevauchements mis en évidence dans ce travail.

Le Chapitre 3 s'intéresse aux dépôts des bassins d'avant-pays Huallaga et Marañón, et en définit les principales séquences sédimentaires à partir de corrélations stratigraphiques régionales de puits, et de l'interprétation de sismique 2D et de logs de porosité. Une restauration séquentielle de la propagation des chevauchements et des différentes zones de dépôts, contrainte par des données thermochronologiques et l'analyse de strates de croissance, est proposée. Finalement, des taux de sédimentation sont calculés pour chaque séquence sédimentaire majeure et discutés sur 3 coupes structurales régionales, puis à l'échelle de l'ensemble du bassin Marañón.

Le Chapitre 4 présente une modélisation pétrolière 2D réalisée à partir de la restauration du système d'avant-pays Huallaga-Marañón, après révision des systèmes pétroliers de la région, et intégration de nouvelles données. Ce type de modélisation 2D rare dans les systèmes de bassin d'avant-pays apporte indéniablement une plus-value pour l'exploration pétrolière de la région. Elle a fait l'objet d'une publication (2017) dans *l'AAPG Memoir 114 (Petroleum Systems Analysis – Case studies).*

La thèse comprend aussi 5 annexes: la première concerne les données biostratigraphiques utilisées dans le chapitre 3; la deuxième les méthodologies utilisées pour les calculs de porosité, transformation temps-profondeur des sections sismiques et correction de compaction; la troisième présente des données de réflectance de vitrinite de roches mères utilisées pour des modélisations PETROMOD 1D permettant d'évaluer des épaisseurs de sédiments érodés ; la quatrième présente les cartes isopaques du bassin Marañón construites à partir de données sismiques pour calculer les volumes de sédiments déposés dans le système d'avant-pays; la cinquième est un article sous presse présentant une synthèse sur les bassins péruviens.

Chapter 1: Introduction

1.1. Topic and objectives

The subandean basins of Northern Peru (Marañón, Huallaga, Moyabamba, and Santiago, see Figures 1.1 and 1.2) are located in the Andes-Amazon transition zone and are part of the Northern Amazonian retroforeland basin (Espurt et al., 2007, 2011; Roddaz et al., 2010). They constitute petroleum basins with proven potential and still under exploration (Mathalone and Motaya, 1995; McGroder et al., 2014). The presence of abundant sub-surface data allows for a rigorous analysis of the structural and stratigraphic architecture.

The Marañón and Huallaga basins (Figure 1.2) are the most important of these basins and cannot be dissociated to understand the structure and evolution of the wedgetop-foredeep system of the Northern Amazon retroforeland basin.

These basins, deformed by fold and thrust systems, exhibit complex structural partitioning controlled by a Mesozoic and/or Paleozoic inheritance. The question of the control of subandean deformation by paleostructures such as the Triassic rift (Rosas et al., 2007, McGroder et al., 2014) and/or Paleozoic orogenies (Laubacher et al., 1985; Dalmayrac et al. 1988; Bump et al., 2008; Espurt et al., 2008) remains relevant. The syntheses proposed so far are incomplete and do not respond satisfactorily to this question. In this thesis, the first objective is to take advantage of the access to the sub-surface and surface database of PERUPETRO (National Hydrocarbons Agency of Peru) to revise the structural architecture of the Marañón and Huallaga basins, in order to propose a new geometric and kinematic analysis. Less important subandean basins as Moyabamba and Santiago will also be considered to understand the whole system. This first objective will also permit to better identify the structural risks that currently hinder the petroleum exploration in the subandean basins of northern Peru.

In a foreland basin system, the timing of the thrust propagation can be deciphered from thermochronological ages and stratigraphic records of syn-orogenic deposits. In the Huallaga and Marañón basins, the definition of this timing allows to better understand the propagation of the orogenic front of the central Andes and the development of the associated Andean-Amazonian foreland basin. This calendar also helps to define critical moments in oil systems

(Magoon and Dow, 1994). The second objective is therefore to integrate new thermochronological data and a sedimentary record analysis in our structural models, proposing when possible a sequential restoration of the deformation.

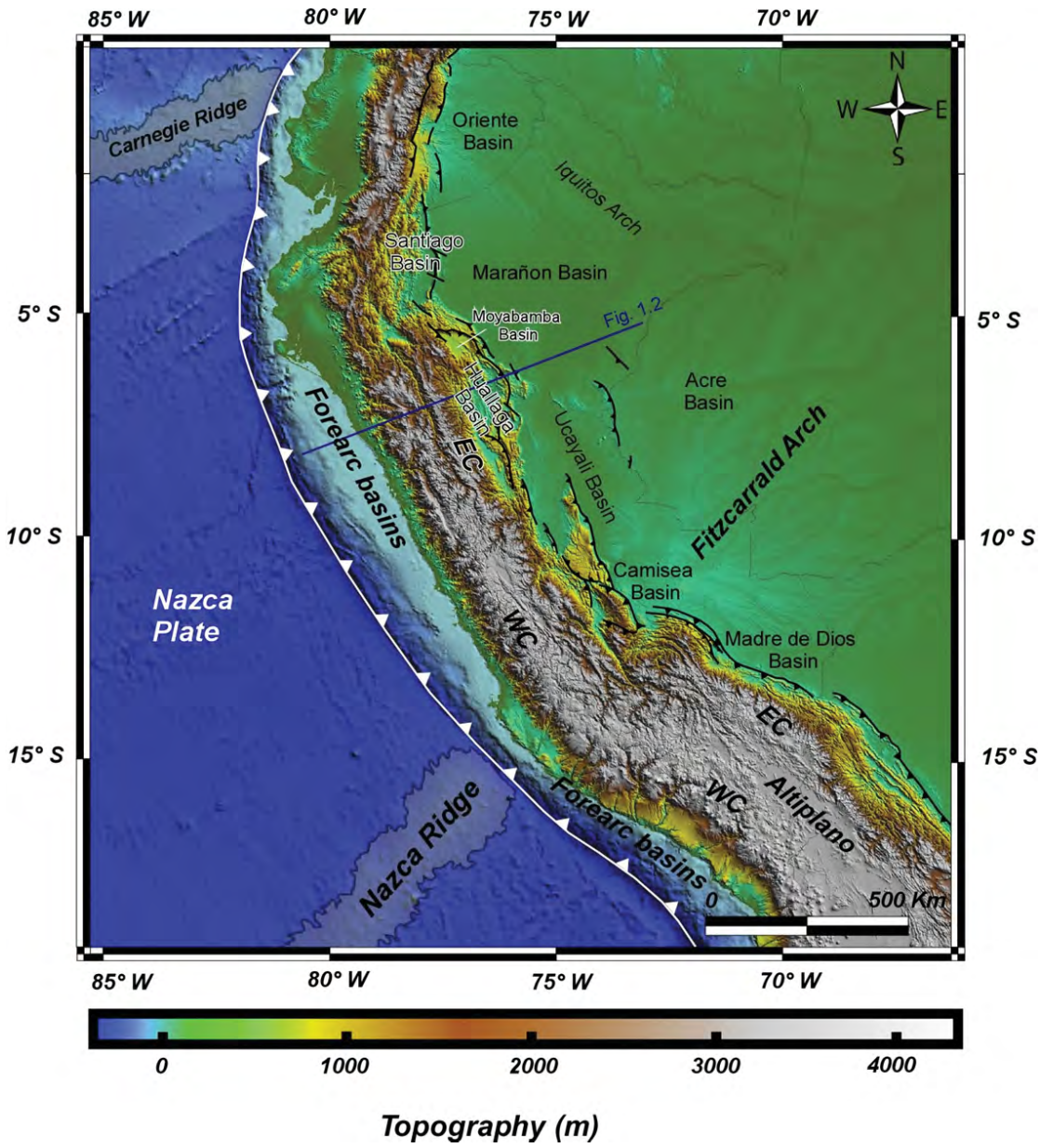

Figure 1.1. Central Andes, with location of the subandean basins and the structural section of Figure 1.2 (EC: Eastern Cordillera, WC: Western Cordillera).

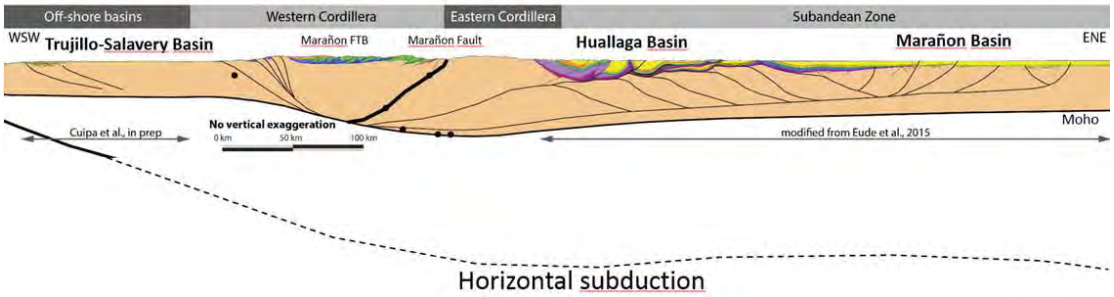

Figure 1.2. Structural cross-section through the central Andes, with location of the Huallaga-Marañón Andean - Amazonian foreland basin system (modified from Prudhomme et al., 2016; location of the section in Figure 1.1).

Sedimentary budgets associated to the propagation of foreland basin systems are relatively rare at the geological scale. They can only be obtained from subsurface data giving the sedimentary thicknesses and a relatively well constrained stratigraphy. The third objective of this thesis is to quantify the sedimentation rates and their evolution throughout the history of the Huallaga and Marañón foreland basins. The calculations were made after a revision of the stratigraphy and the architecture of the syn-orogenic sedimentary infills reported on the new regional structural cross-sections constructed for this thesis.

Finally, the last objective is to exploit the achieved results in a 2D petroleum modeling of the most complex and attractive part of the Andean-Amazonian foreland basin system of northern Peru: the Huallaga-Marañón system. This modeling integrates the revision and definition of new petroleum systems and uses the sequential restorations of the deformation obtained previously.

1.2. The subandean basins of northern Peru: generalities

The subandean basins of Northern Peru (Marañón, Huallaga, Moyabamba, and Santiago; see Figures 1.1 and 1.2) belong to what we will call the Andean-Amazonian Foreland Basin System (FBS), which represents an important part in the structure of the Andean mountain chain as shown in the cross-section of Figure 1.2. The deformation of these basins, which may present high rates of shortening (Hermoza et al., 2005), is associated to the propagation of the orogenic front and the uplift of the Eastern Cordillera that began between 30 and 24 Ma (Eude et al., 2015). During the upper Cretaceous and Paleogene, subandean basins were much more distal in the foreland basin system and much less deformed. The initiation of this foreland basin system is marked by a BFU (Basal Foreland Unconformity), located at the base of the late Cretaceous transgressive sequence, and overlaying deformed and

eroded Mesozoic, Paleozoic or Precambrian series that reflect a complex pre-Andean history. All of these sedimentary and metamorphic series are shown in Figure 1.3.

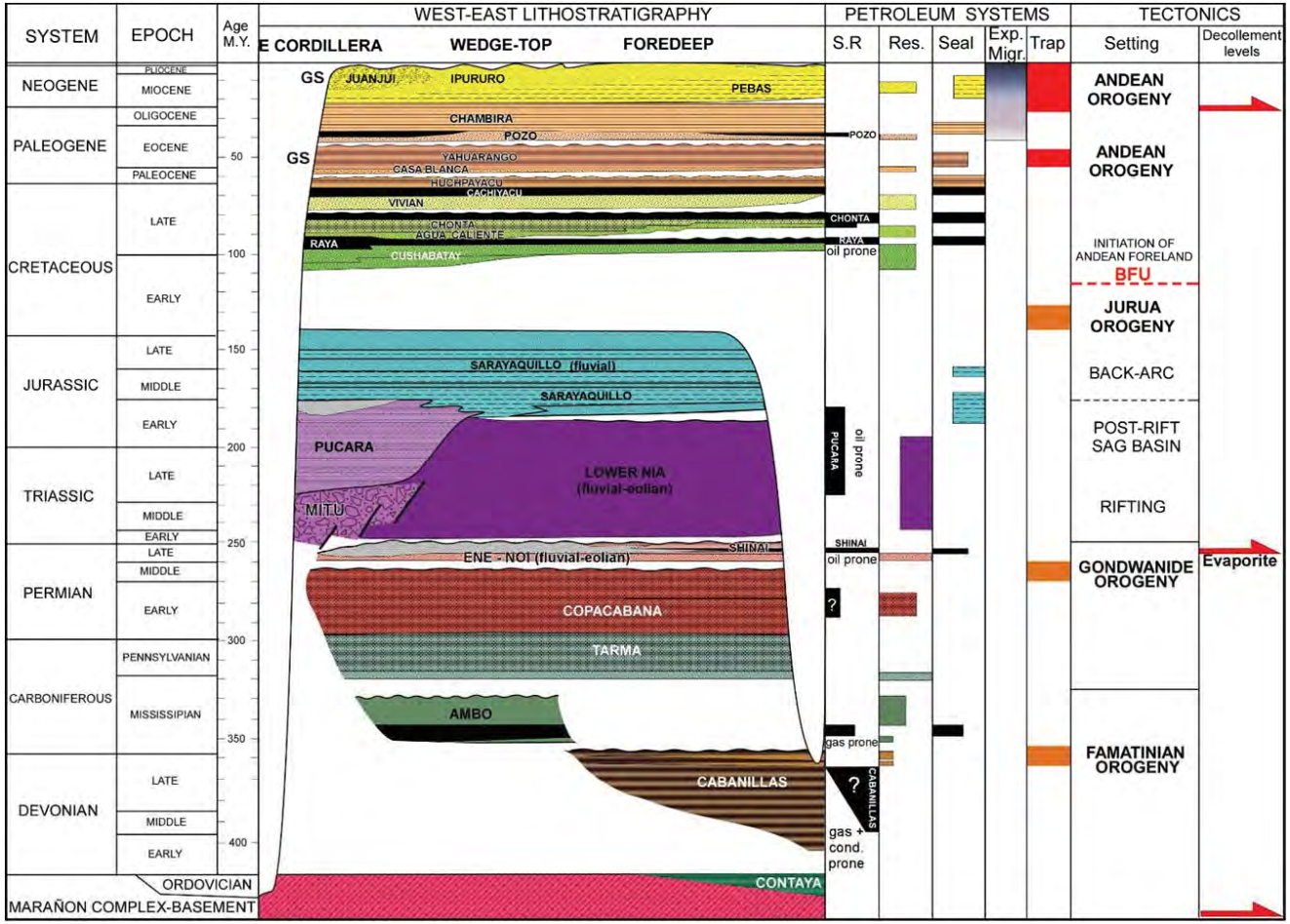

Figure 1.3. Lithostratigraphic diagram representing from west to east the different sedimentary units of the Andean-Amazonian foreland basin system of Northern Peru. The Cretaceous to Neogene foreland sequences overlie unconformably on Mesozoic and Paleozoic pre-Andean series.

.

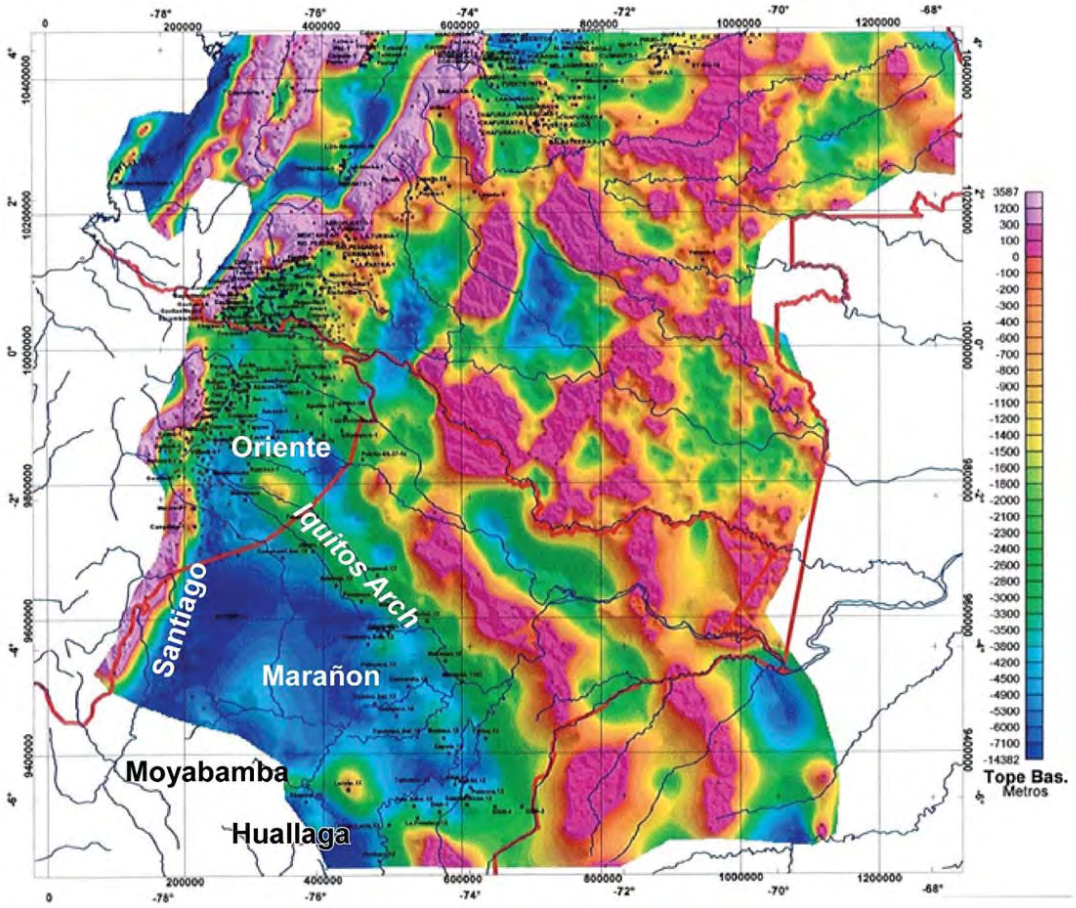

Figure 1.4. Gravimetric map (3D inversion) (after Graterol, 2011) showing the structural partitioning of the subandean basins of northern Peru, the depozones of the Marañón basin and the Iquitos Arch (forebulge).

The subandean foreland basin system in northern Peru is partitioned into sub-basins, which are shown in Figures 1.1 and 1.4. The paleogeography of pre-Cretaceous basins played an important role in this structural partitioning. The most influential paleostructures correspond to the Triassic rift (Rosas et al., 2007; McGroder et al., 2014) and to the inheritance of late Jurassic and Paleozoic orogenies (Laubacher et al., 1985; Dalmayrac et al. 1988; Ramos, 1988; Bump et al., 2008; Espurt et al., 2008; Caputo 2014). They will be described and discussed in Chapter II

1.3. Methodology

A multidisciplinary approach was needed to integrate and interpret the dataset. Structural studies, analysis of thermochronological data and sediment infills were conducted simultaneously in the study in order to propose a propagation model of the thrust system and associated depozones. For this study, we used the concept of foreland basin system by DeCelles & Gilles (1996).

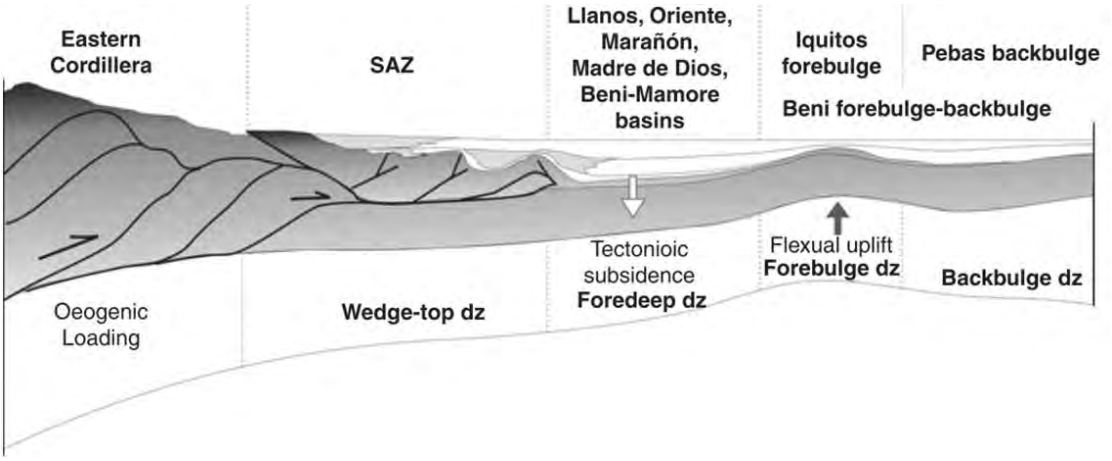

Figure 1.5. Schematic cross-section illustrating the Foreland Basin System concept *sensu* DeCelles & Giles (1996) applied to subandean basins (from Roddaz et al., 2010).

1.3.1. Structural Analysis

The structural analysis was based on 2D seismic interpretation, calibrated from the deepest exploration wells, field data and stratigraphic revision (Figures 1.3 and 1.6). Seismic sections and well data were provided by PERUPETRO S.A. The seismic sections have been loaded and interpreted in WinPICS (Divestco software) and MOVE (Midland Valley software). Surface data were obtained from our field surveys and 1: 100,000 geological maps of INGEMMET (Instituto Geológico Minero Metalurgico del Peru).

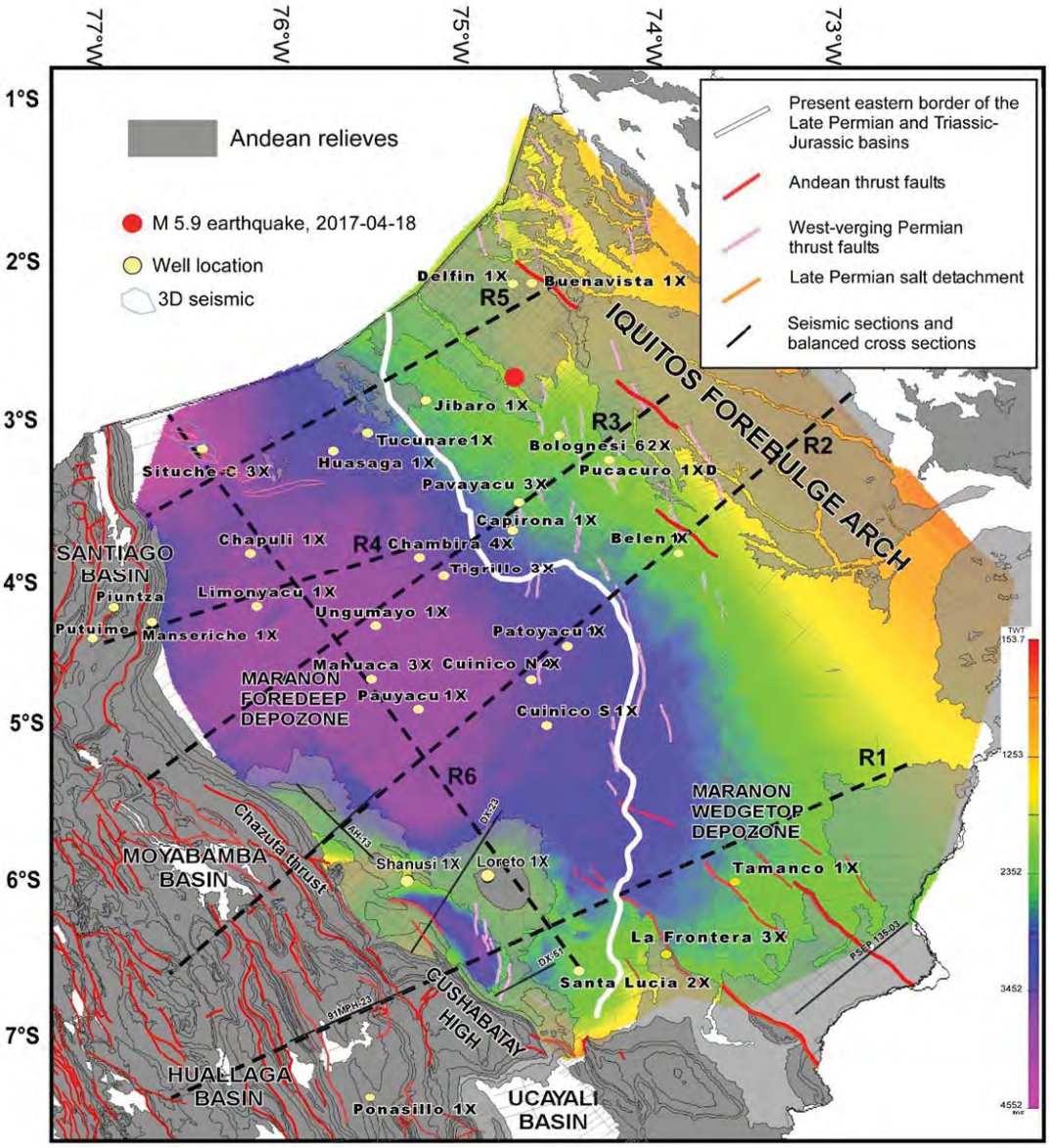

Figure 1.6. Structural map of the Base Cretaceous (TWT-Two Way Time) of the Marañón foreland basin with location of the regional structural cross-sections. Crustal earthquakes recorded in this region have been used to constrain the structural geometry of some thrusts.

Structural sections - mostly balanced - were then constructed regionally across the Marañón and Huallaga basins system and the Moyabamba and Santiago bordering basins (Figure 1.6), using the MOVE software (Middland Valley).

1.3.2. Lithostratigraphic analysis and sedimentation rates

In order to study the sedimentary infills of the Huallaga and Marañón basins in terms of propagation of foreland depozones (see Figure 1.5), (long-term) regional sedimentary sequences have been defined and characterized from wells lithostratigraphic correlations and the characterization of major discontinuities recognized in 2D seismic and in the porosity logs. Wells and seismic data were provided by PERUPETRO S.A. Stratigraphic datings come from academic publications and industrial reports available in the PERUPETRO S.A. database.

The foreland basin sedimentary sequences thus identified were then mapped in the regional structural cross-sections, before being used to calculate sedimentation rates for each cross-section.

Finally, sedimentary flows were calculated in volume for the entire Marañón basin from isopach maps constructed using seismic information, which were then transformed in depth.

1.3.3. Sequential Restoration

The regional structural section R1 (see Figure 1.6) encompassing the Huallaga-Marañón system has been balanced and restored in several stages, with the MOVE software from Middland Valley, to better understand the propagation of the thrust systems and the foreland basin depozones. These different stages were reconstructed from 1) new and previous thermochronological data, 2) the middle Eocene erosion surface known regionally (Christophoul et al., 2002), which served as key horizon in the initial stage, and that it was possible to identify in seismic and in the field, and 3) the analysis of growth strata that appears in seismic. In total, three deformation stages could be reconstructed.

All the data used are described in detail in Chapters 3 and 4.

1.3.4. Petroleum System Modeling

The sequential restoration obtained for the Huallaga-Marañón regional cross-section (R1) was used to carry out for the first time a 2D petroleum system modeling of this region. These

petroleum systems have been previously revised and partially redefined based on new source rock analyzes and existing data from PERUPETRO S.A.

The modeling was done with the Schlumberger's Petromod software. The data used for source rocks, reservoirs, charge and geohistory are described in detail in Chapter 4.

1.4. Structure of the thesis

After a general introduction (Chapter 1) summarizing objectives and methodology, the thesis comprises three chapters.

Chapter 2 presents a synthetic structural analysis of the Huallaga and Marañón basins, and the bordering basins (Moyabamba and Santiago), based on subsurface data provided by PERUPETRO S.A. and field observations. Regional structural cross-sections were constructed from seismic interpretations calibrated by drilling and surface data. These structural cross-sections distributed over the whole of the studied region allow to illustrate a complex structural architecture inherited from Paleozoic and Mesozoic paleostructures. This structural study was the subject of an article published in Marine and Petroleum Geology in 2017, which also analyzes the seismic activity of some thrusts faults highlighted in this work.

Chapter 3 looks at the deposits of the Huallaga and Marañón foreland basins, and defines the main sedimentary sequences from regional stratigraphic well correlations, and interpretation of 2D seismic and porosity logs. A sequential restoration of the thrust system propagation and associated depozones, constrained by thermochronological data and the analysis of growth strata, is proposed. Finally, sedimentation rates are calculated for each major sedimentary sequence and discussed on 3 regional structural cross-sections, and then on the scale of the whole Marañón basin.

Chapter 4 presents 2D petroleum system modeling based on the restoration of the Huallaga-Marañón foreland basin system, after reviewing the regional petroleum systems, and integrating new data. This type of 2D modeling, rare in foreland basin systems, brings added value to the hydrocarbon exploration in the region. It has been published (2017) in *AAPG Memoir 114 (Petroleum Systems Analysis – Case studies)*.

The thesis also includes 5 annexes: the first concerns the biostratigraphic data used in Chapter 3; the second presents the methodologies used for porosity calculations, time-depth transformation of seismic sections and compaction correction; the third presents source rock vitrinite reflectance data used for PETROMOD 1D modeling to evaluate eroded sediment

thicknesses; the fourth presents isopach maps of the Marañón basin constructed from seismic data to calculate the sediment volumes deposited in the foreland basin system; the fifth is an article in press presenting a synthesis on the Peruvian basins.

Chapter 2: Structural architecture of the retro-foreland basin system of northern Peru

2.1. Introduction

In this chapter, the structural architecture of the retro-foreland basin system of northern Peru is presented from south to north in two distinct parts.

The southern part corresponds to the Huallaga-Marañón and Moyabamba-Marañón foreland basin systems that are described in an article published in *Marine and Petroleum Geology* (2017). It is illustrated by two regional balanced cross-sections (R1 and R2 in Figure 2.1) and presents a new stratigraphic diagram of the region based on new regional correlations from surface and sub-surface data. It highlights a Paleozoic fold and thrust belt reactivated during Andean deformation and still active.

The northern part changes in orientation and style of deformation. It is illustrated by 3 regional cross-sections (R3, R4 and R5 in Figure 2.1), which permit to have an overview of this part of the Marañón foreland basin system. It comprises the complex Santiago N-S elongated wedge-top Subandean basin, where a new structural interpretation is presented and discussed.

A NNW-SSE regional cross-section (R6 in Figure 2.1) has been also constructed to illustrate the lateral geometric and stratigraphic evolution of the Marañón Basin.

Some regional cross-sections presented in this chapter will be used in the Chapter 3 to describe the Cenozoic stratigraphic architecture of the Marañón foreland basin system and calculate foreland sedimentation rates associated to Andean orogeny.

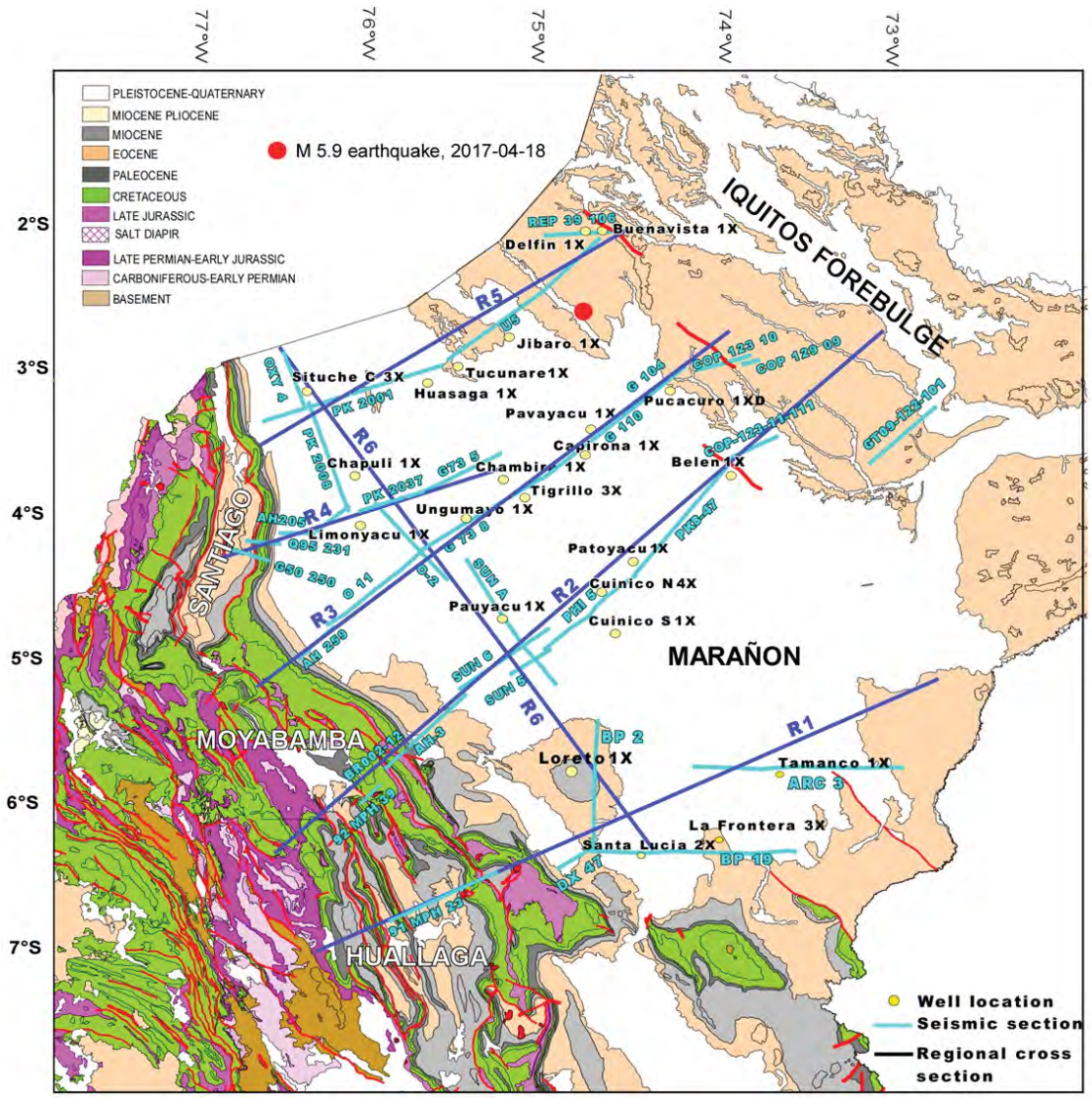

Figure 2.1. Geological map of the Marañón foreland basin system with location of the regional cross-sections presented in this chapter (R1 to R6), wells and seismic sections used for their construction.

2.2. Thrust tectonics in the Andean retro-foreland basin of northern Peru: Permian inheritances and petroleum implications

(Published in Marine and Petroleum Geology 82 (2017), 238-250)

Ysabel Calderon [a], Patrice Baby [b], Christian Hurtado [c], Stéphane Brusset [b]

[a] PERUPETRO S.A., Av. Luis Aldana 380, San Borja, Lima, Peru

[b] GET-UMR CNRS/IRD/Université Paul Sabatier, 13545, 14 Avenue Edouard Belin, 31400 Toulouse, France

[c] Instituto de Geociencias, Universidade de Brasília, Campus Universitario Darcy Ribeiro ICC - Ala Central, CEP 70.910-900 Brasília, DF, Brazil

Résumé en français

Dans le nord du Pérou, le système de bassin d'avant-pays Huallaga-Moyabamba-Marañón résulte de l'interaction entre tectonique de couverture et tectonique de socle. Des données de géophysique et la construction de coupes équilibrées montrent que cette configuration structurale a été contrôlée par l'héritage permien. Une chaine plissée fossilisée du Permien moyen, qui s'est développée durant l'orogénèse Gondwanide, a été partiellement réactivée pendant la compression andine et a contrôlé la propagation de la tectonique de socle. Ce système de chevauchements à vergence ouest est toujours actif et est à l'origine d'une sismicité crustale et destructrice dans la région de Moyabamba. Des évaporites du Permien terminal, qui ont scellé la chaine plissée d'âge permien moyen, ont contrôlé la propagation d'une tectonique de couverture et de développement du chevauchement le plus grand de la zone subandine péruvienne. La chaine plissée fossilisée et en partie réactivée du Permien moyen constitue un nouveau « play » pétrolier pour l'exploration des bassins subandins du nord Pérou. Les pièges structuraux de sous-chevauchements des bassins « wedge-top » de Moyabamba et Huallaga sont particulièrement attractifs, mais restent inexplorés.

Abstract

In northern Peru, the Huallaga-Moyabamba-Marañón Subandean foreland basin system results from the interaction between thin and thick-skinned tectonics. Geophysical data and the construction of two balanced cross-sections show that this structural configuration has been controlled by Permian inheritances. A fossilized west-verging Middle Permian fold and thrust belt, which developed during the Gondwanide orogeny, has been partly reactivated by the Andean compression and controlled thick skinned tectonics propagation. This west-verging thrust system is still active and causes the crustal and damaging seismicity of the Moyabamba region. Late Permian salt, which has sealed the Middle Permian fold and thrust belt, controlled thin-skinned tectonics propagation and the development of the must large overthrust of the Peruvian Subandean zone. The fossilized and partly reactivated Middle Permian fold and thrust belt constitutes a new petroleum play for the exploration in the northern Peruvian Subandean basins. Sub-thrust traps of the Moyabamba and Huallaga wedge-top basins are particularly attractive but stay unexplored.

Keywords: Thin and thick-skinned tectonics, Sub-Andes, Paleozoic petroleum system, Peru, Gondwanide orogeny, salt, Permian, crustal seismicity

2.2.1. Introduction

Importance of thin-skinned tectonics vs thick-skinned tectonics in fold and thrust belts has been largely debated (Coward, 1983; Tozer et al., 2002; Calabro et al., 2003). Thrusts propagation is controlled by parameters as structural inheritance, lithostratigraphy and erosion and/or sedimentation rates, which determine the style of deformation (Buchanan & McClay, 1991; Sassi et al., 1993; Mugnier et al., 1997; Leturmy et al., 2000; Teixell and Koyi, 2003; Poblet & Lisle, 2011). Thin-skinned tectonics requires the presence of regional detachment as shales or evaporites expanded in the sedimentary cover (Davis & Engelder, 1985; Costa & Vendeville, 2002) while thick-skinned tectonics is generally attributed to tectonic inversion (McClay, 1989; Buchanan & McClay, 1991; Colletta et al., 1996; Kley et al., 1999; Baby et al., 2013). In some cases, thick-skinned deformation can also be related to the reactivation of old fossilized fold and thrust belts (Giambiagi et al., 2014). In Central Andes, the eastern fold and thrust belt, commonly known as Subandean zone, presents a latitudinal structural variation ranging from pure thin-skinned tectonics in the south to complex interference of both thick and thin-skinned tectonics in the north (Kley et al., 1999; Gil et al., 2001; McGroder et al., 2014). Our aim is to discriminate these two styles of thrust deformation in the northern Central Andes of Peru, and identify their structural inheritance.

The study area corresponds to the Huallaga, Moyabamba and southern Marañón subandean foreland basin system (Figure 2.2.1), named in this paper Huallaga-Moyabamba-Marañón FBS. The eastward thrusts propagation of this FBS is controlled by thinned and thick-skinned tectonics (Eude et al., 2015; Calderon et al., 2017). The Moyabamba zone is characterized by crustal earthquakes constrained to shallow depths and related to reverse basement faults with westward vergence (Delvin et al., 2012). The geometry and origin of these faults have been poor investigated.

The purpose of this paper is a revision of the present day structural architecture of the Huallaga-Moyabamba-Marañón FBS and its relationship with pre-Cretaceous structures. Although our structural revision is based on the interpretation of an exhaustive compilation of seismic data, here just a few examples of seismic cross-sections are presented. They clearly show the main tectonic Andean and pre-Andean features of the study area. Two regional balanced cross-sections have been constructed to investigate the relationships between thick and thin-skinned tectonics, and to better understand the petroleum potential of the region. We show how seismic interpretation and stratigraphic revision from wells and field information allowed us to evidence the roles of a Permian fold and thrust belt sealed by a

regional salt level in the deformation of the Huallaga-Moyabamba-Marañón FBS. The extension, significance and petroleum implications of these Permian features are discussed.

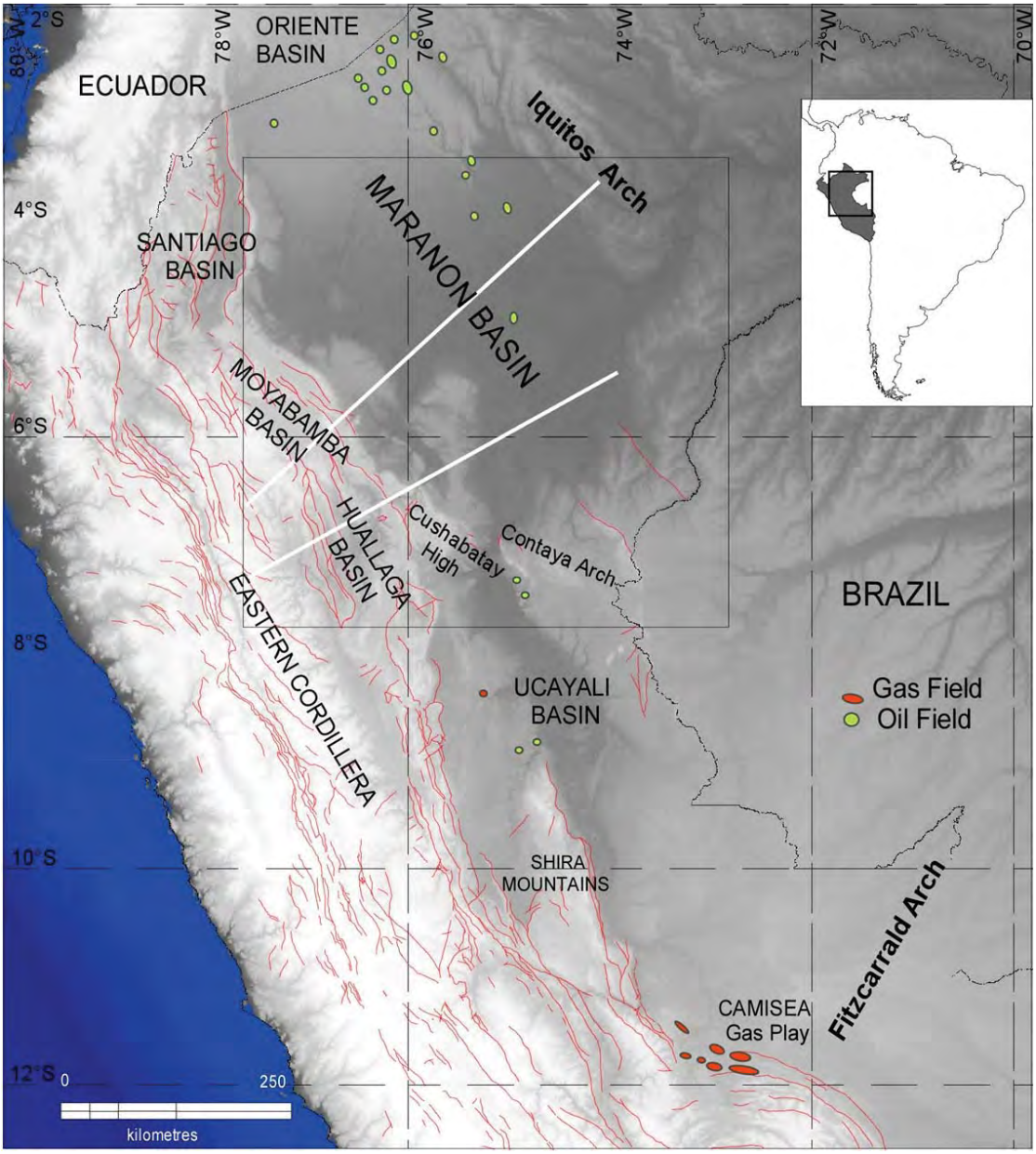

Figure 2.2.1. Tectonic map of the Subandean basins of northern and central Peru, showing the study area and the different morpho-tectonic units. The Huallaga-Marañón and Moyabamba-Marañón structural cross-sections are located.

2.2.2. Geologic background

The northern Central Andes of Peru are characterized by the absence of Altiplano, the flat slab subduction of the Nazca oceanic plate (Gutcher et al., 2000; Espurt et al., 2007) and an extensive deformation of the eastern Andean orogenic wedge with an amount of shortening greater than 140 km (Eude et al., 2015). As a result, this region shows the easternmost propagation of the Subandean orogenic front (Figure 2.2.1).

The Marañón, Huallaga and Moyabamba Subandean sub-basins are located in the Andean-Amazonian transitional area (Figures 2.2.1 and 2.2.2), the so-called Northern Amazonian Foreland Basin (Espurt et al., 2007, 2011). They are classically interpreted as the components of a wide retro-foreland basin system, where the Huallaga and Moyabamba Subandean areas are conventionally correlated to the wedge-top depozone and the Marañón area to the foredeep depozone (Hermoza et al., 2005; Roddaz et al., 2005; Calderon et al., 2017). Thermochronological dating shows that the North Amazonian Foreland Basin started to acquire its modern configuration between 30 and 24 Ma (Eude et al., 2015) with the development of the Huallaga syn-orogenic wedge-top basin (Hermoza et al., 2005). The Huallaga thrusts system is characterized by a strong horizontal shortening. To the west, the Andean Eastern Cordillera, which acted as the deformable backstop, corresponds to the tectonic inversion of the pre-Andean Triassic rift (Rosas et al., 2007; Eude et al., 2015; Calderon et al., 2017). The Moyabamba thrusts system is much more unknown and is analysed in this paper. Several versions of balanced cross-section have already been constructed in the Huallaga-Marañón foreland basin system (Gil, 2001; Hermoza et al., 2005; Eude et al., 2015; Calderon et al., 2017). They show the importance of thin-skinned tectonics controlled by a regional evaporitic layer whose age is discussed below. A total horizontal shortening around 70-90 km has been calculated by these authors. To the east of the Huallaga thrust front, the southern Marañón basin is deformed by a modern and still active thick-skinned tectonics, and should therefore be seen as the contemporaneous wedge-top rather than the foredeep of the foreland basin system. Seismic sections show east and west-verging basement thrusts, which branch on a deep detachment (Eude et al., 2015). This basement thrusts system plunges to the west below the Huallaga and Moyabamba piggyback basins and interferes with thin-skinned deformation of the sedimentary cover. The Cushabatay High, in the Huallaga-Marañón transition zone, is the geomorphologic expression of such structures. The Moyabamba basin structural geometry is much less known and is described for the first time in this paper. It is characterized by crustal shallow depths earthquakes (Tavera et al., 2001; Delvin et al., 2012), used in this work to constrain the thrusts geometry.

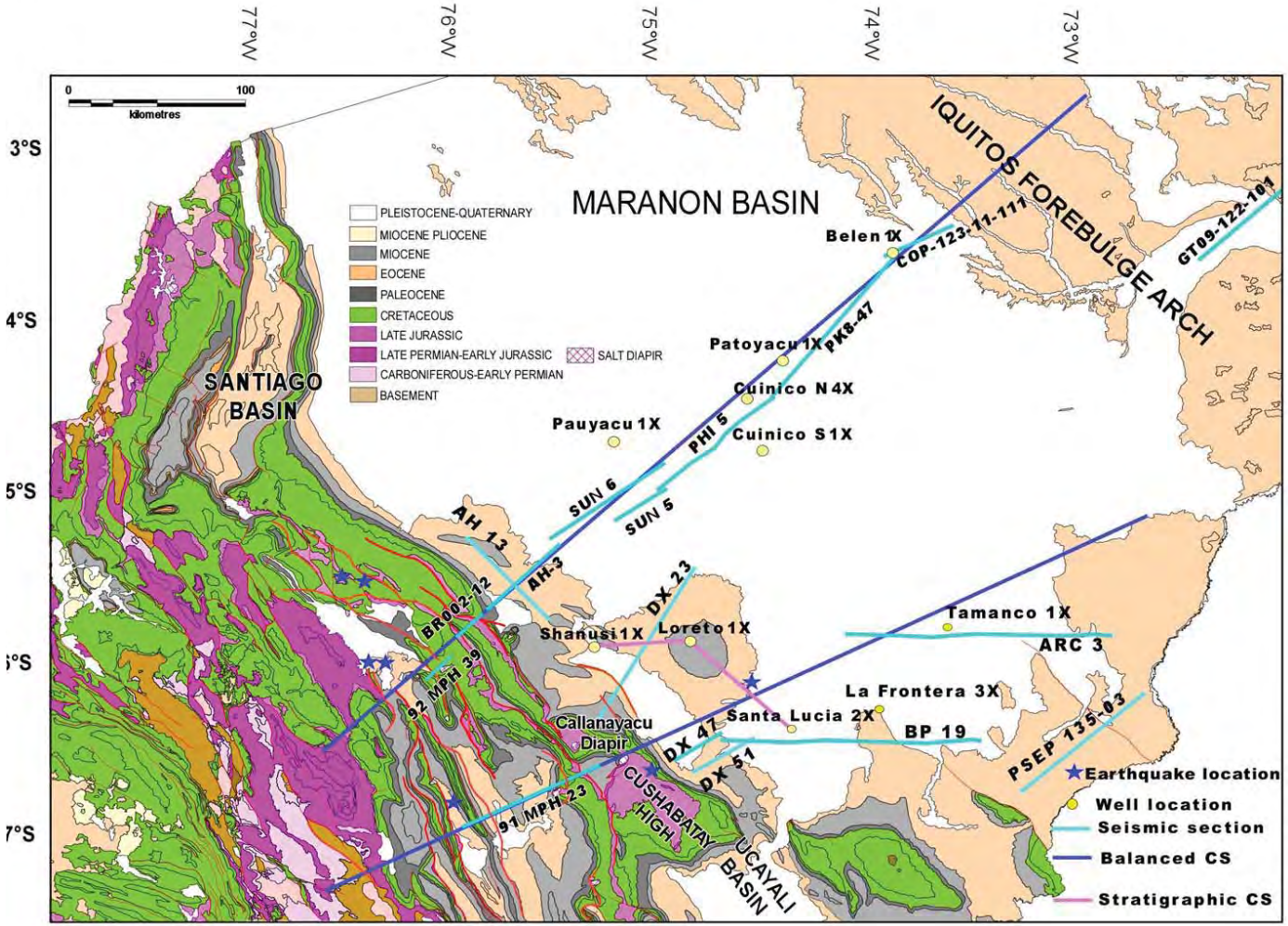

Figure 2.2.2. Geological map of the Huallaga-Moyabamba-Marañón FBS with location of seismic sections, wells, balanced cross-sections, and mean earthquakes (Mw>5) relocated by Delvin et al. (2012). The geology map is adapted from INGEMMET 1:1'000,000 map and field observations.

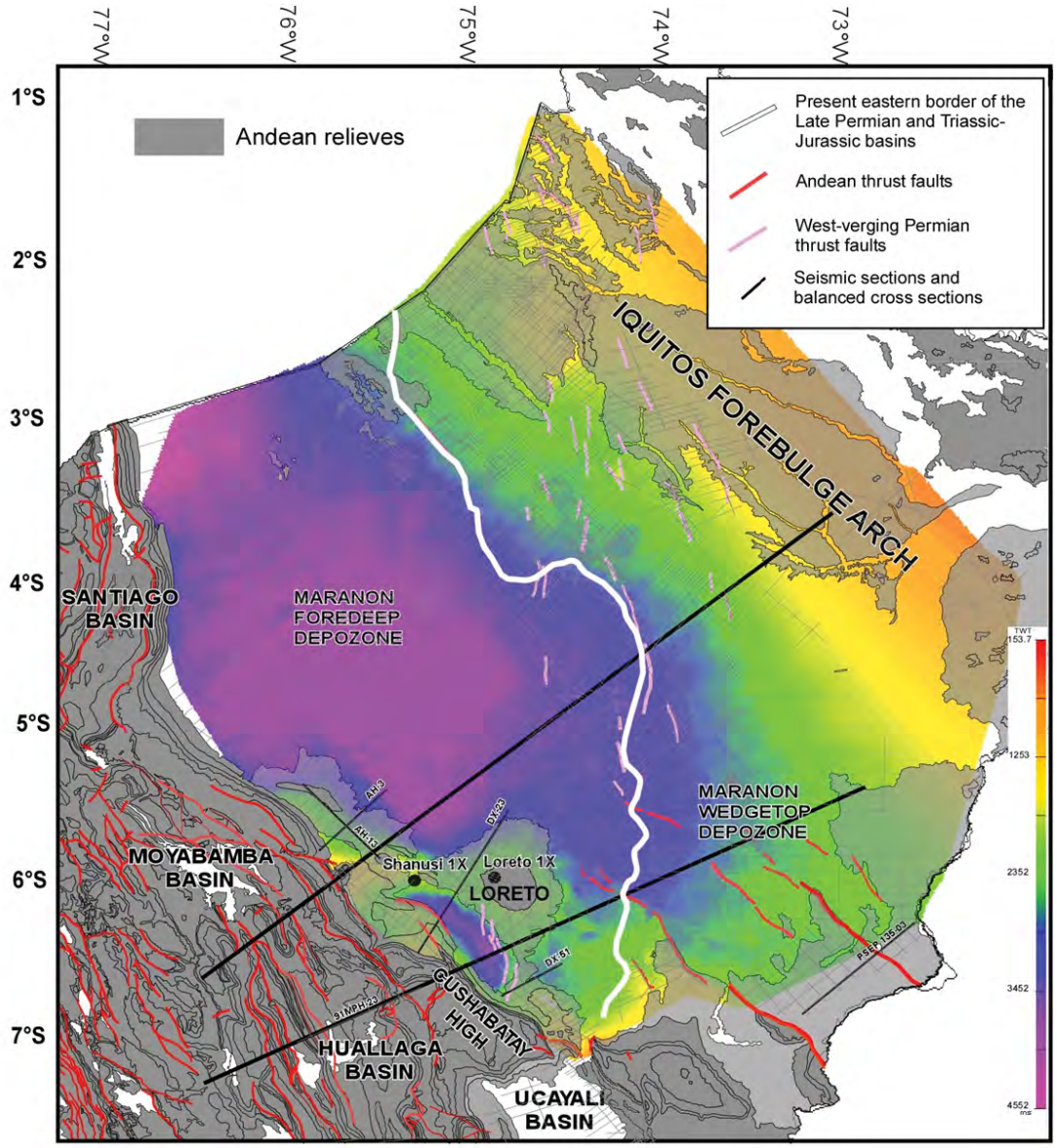

Figure 2.2.3. TWT Base Cretaceous structural map of the Marañón foreland basin with location of the eastern border of the pre-Cretaceous long-term sequences and Middle Permian thrust faults. The TWT map is superimposed on the geologic contours of the Andean relieves. Seismic project used for the map construction is located.

North of the studied area, the Marañón basin is progressively deepening and deformation is weaker (Figure 2.2.3). It constitutes a foredeep depozone limited in the west by the Santiago Subandean fold and thrust belt (PARSEP, 2001), and in the east by the Iquitos forebulge (Roddaz et al., 2005). To the north, it extends with the Oriente basin of Ecuador (Balkwill et al., 1995; Baby et al., 2013).

2.2.3. Stratigraphy

The sedimentary cover involved in the deformation of the Huallaga-Moyabamba-Marañón FBS consists of a pre-Andean series, unconformably overlain by a marine to continental late Cretaceous sedimentary wedge thinning to the NE, and by a Cenozoic foreland continental and shallow marine infill. It is illustrated by the stratigraphic diagram of the Figure 2.2.4.

The pre-Andean series comprises remnants of Ordovician, Devonian, Carboniferous and Permian clastic and carbonated marine deposits, overlain in the Subandean zone by a regional layer of evaporite, long regarded as Jurassic in age despite the absence of real dating (PARSEP, 2001; Moretti et al., 2013). Recent revisions of regional stratigraphy based on subsurface correlations, thanks to new seismic information (Perupetro S.A. database) and new field observations, allowed us to reconsider the stratigraphic position of this important regional layer of salt, which acted as the mean detachment of the Huallaga and Moyabamba thrusts system (Hurtado et al., 2014; Baby et al., 2014, Calderon et al., 2017). It outcrops on the Callanayacu Diapir, east of the Chazuta thrust (Huallaga thrust front; see Figure 2.2.2) along the Huallaga river, where evaporites are covered by marine black shales, limestones and dolomites. These marine deposits could never be dated. However, north-south seismic correlations from the South Marañón basin to the Ucayali basin show that they correspond to the Shinai Formation (Hurtado et al., 2014; Baby et al., 2014) defined and dated from the Late Permian in the Camisea area (Seminario et al., 2005 and reference therein). Therefore, we consider the regional salt layer as Late Permian. This salt age has previously been proposed in the Huallaga basin by Rodriguez and Chalco (1975). The regional salt layer extends to the north in the Santiago basin where Aleman & Marksteiner (1993) also mentioned the possibility of a Late Permian age. Along the Huallaga River, the Shinai Formation is overlain by approximately 2000 meters of aeolian and fluvial sandstones and silts, which can be correlated with the Lower Nia reservoir of the Camisea area (Seminario et al., 2005) and the overlaying Sarayaquillo Formation. These continental series are considered as Triassic and Jurassic in age (PARSEP, 2001; Seminario et al., 2005). They overlay a weak unconformity identified in the Marañón basin by seismic and wells (Figure 2.2.5) that marked the onset of a long period of rifting and post-rift regional sag (Rosas et al., 2007). To the west, the aeolian sandstones laterally pass to the continental Mitu rift and marine Pucara post-rift deposits outcropping in the Eastern Cordillera, where they overlay directly the basement known as Marañón Complex (Wilson, 1985).

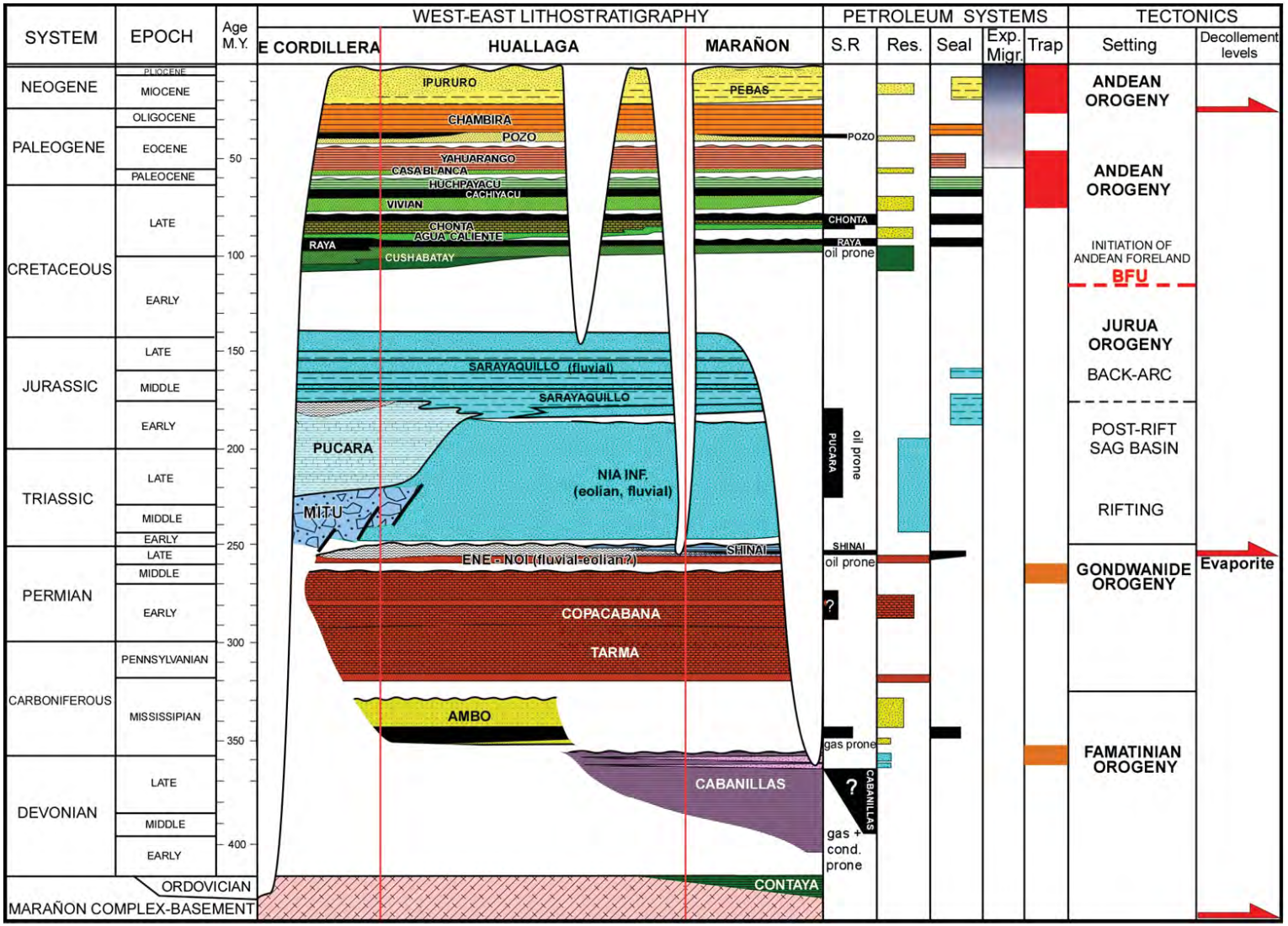

Figure 2.2.4. Stratigraphic diagram and petroleum systems along the Huallaga-Moyabamba-Marañón FBS. The orogenic cycles names are those that are more commonly used in the Andes (see Ramos, 1988; Caputo, 2014; Chew et al., 2016).

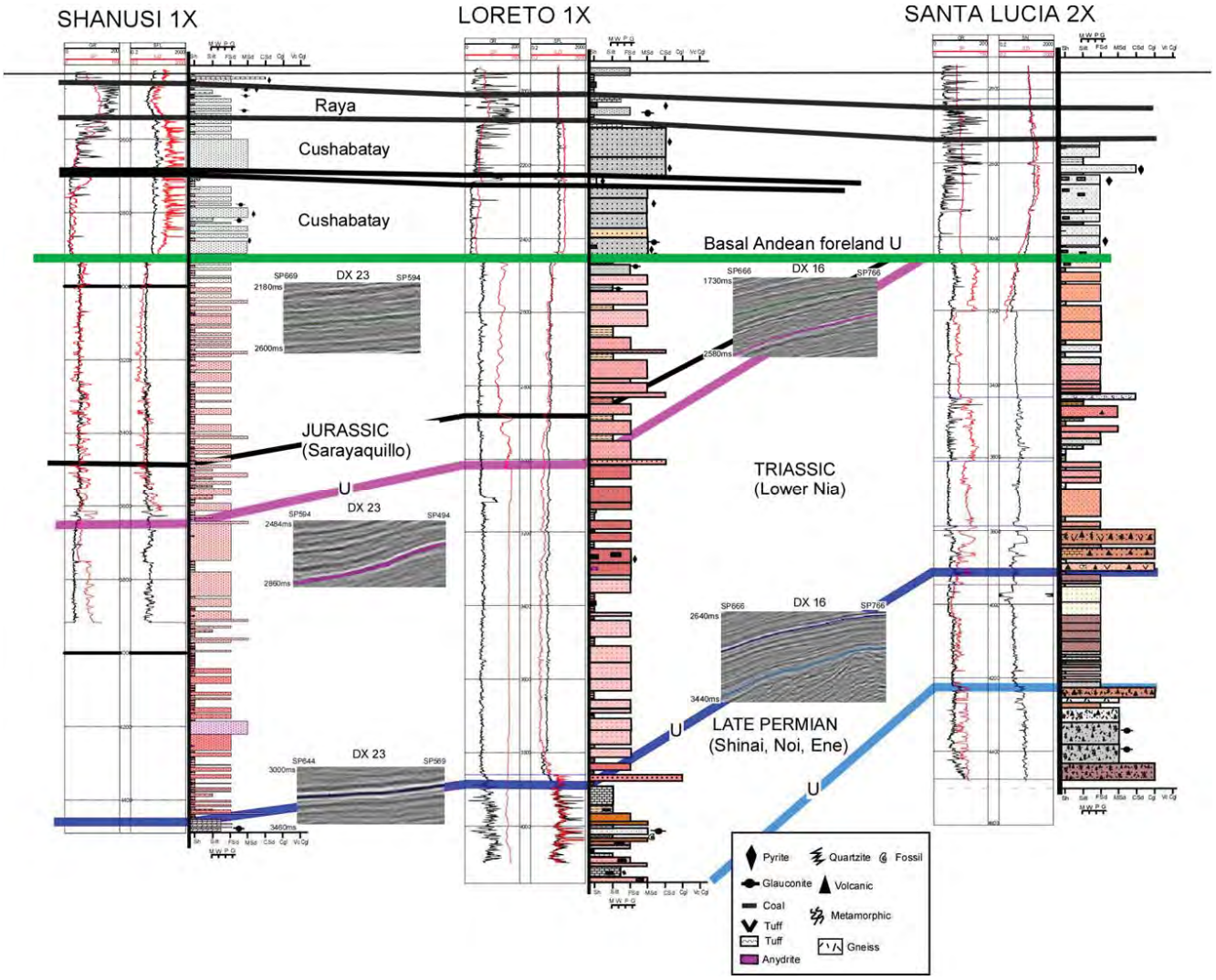

Figure 2.2.5. Regional wells stratigraphic correlations in the southern Marañón basin (Shanusi 1X, Loreto 1X and Santa Lucia 2X, location in Fig. 2.2.2) showing the first order pre-Cretaceous sequences. The Late Cretaceous basal foreland unconformity (Cushabatay Fm.) is flattened and correlations have been made between long term pre-Cretaceous sequences.

This lateral change occurs apparently in the Subandean-Eastern Cordillera transition zone and corresponds to the eastern Mitu rift border. The tectonic inversion of the Mitu rift has controlled the deformation and propagation of the Eastern Cordillera deformable backstop of the Subandean fold and thrust belt.

After a major sedimentary hiatus (110-120 Ma), corresponding probably to the Andean basal foreland unconformity, late Cretaceous sequences were deposited. They comprise Albian to Maastrichtian fluvial to shallow marine cyclic sequences of sandstones, shales and limestones (Cushabatay-Raya; Agua Caliente-Chonta; Vivian-Cachiyacu-Huchpayacu; see Figure 2.2.4). These eastward-thinning sequences were deposited in the Andean-proto-Amazonian retro-foreland basin controlled by the tectonic loading of the incipient Andean orogenic wedge. They constitute today the main petroleum systems of the Oriente-Marañón prolific oil province (Marksteiner & Aleman, 1997; Barragan et al., 2008). Reservoirs corresponds to fluvio-deltaic and tide-dominated estuarine deposits of the Cushabatay, Agua Caliente and Vivian formations, and source rocks are constituted by shales and limestones of the Raya and Chonta formations (Mathalone & Montoya, 1995; PARSEP, 2001).

The Cenozoic foreland infill presents important lateral variations from the Huallaga-Moyabamba hinterland to the Marañón foreland. It has been well described in terms of foreland system depositional environments controlled by thrusts propagation by Hermoza et al. (2005) and Roddaz et al. (2010). The Paleocene-Early Eocene sequence starts with the fluvial and tidal sandstones of the Casa Blanca Formation (Gil, 2001 and references therein), comparable to the Vivian reservoir. It passes gradually to red siltstones and mudstones forming distal fluvial deposits (Yahuarango Fm.). The Middle Eocene-Oligocene sequence overlies a regional erosional unconformity, which extends to the north in Ecuador and Colombia. This erosion has been interpreted as an unloading orogenic period (Christophoul et al., 2002; Roddaz et al., 2010). The Middle-Upper Pozo Formation developed in shallow marine environment and recorded a new orogenic loading period. It is overlaid by the Oligocene silts and sandstones of the Chambira Formation. The Neogene sequence recorded the development of the modern Huallaga-Moyabamba wedge-top depozone and a strong subsidence in a deltaic environment evolving progressively to an alluvial system (Hermoza et al., 2005). This thick Neogene sequence corresponds to the main charge of the petroleum systems.

In the southern Marañón basin, thicknesses and stratigraphy of pre-Cretaceous series are primarily constrained by the Shanusi 2X, Loreto 1X, and Santa Lucia 2X wells (location in Figure 2.2.2). Correlations between these wells (Figure 2.2.5) show Paleozoic, Triassic and Jurassic long term sequences separated by regional erosional unconformities. These

regional discontinuities can be clearly identified on the seismic (Figures 2.2.6 to 2.2.9) and have been represented in our structural cross-sections (Figure 2.2.10). They correspond to: 1) the base of the Late Permian Ene-Noi-Shinai sequence only reached in the Santa Lucia 2X well; 2) the base of the Triassic-Lower Jurassic Lower Nia eolian and fluvial sequence; 3) the base of the Upper Jurassic Sarayaquillo fluvial sequence; 4) the base of the Late Cretaceous fluvial and shallow marine Cushabatay sequence, which forms the basal Andean foreland unconformity.

2.2.4. Structural analysis and balanced cross-sections

2.2.4.1. Method

The structural analysis is based on 2D seismic interpretation, calibrated from the deepest wells of the region (Shanusi 1X, Loreto 1X, Santa Lucia 2X, La Frontera 3X, Tamanco 1X,, Pauyacu 1X, Cuinico Sur 1X, Cuinico Norte 4X, Patoyacu 1X, Belen 1X), field data and the stratigraphic revision presented above (Figures 2.2.4 and 2.2.5). Wells information includes composite log and lithological data, and check shots were acquired for the most representative wells.

Seismic sections and wells data (see Figure 2.2.2 for location) were provided by PERUPETRO S.A. The seismic sections have been loaded and interpreted in WinPICS (Divestco software) and the Midland Valley Move 2015 software. Surface data were obtained from our field surveys and 1:100,000 INGEMMET (Instituto Nacional Geológico, Minero y Metalúrgico del Perú) geologic maps.

The two balanced regional cross-sections have been constructed using the Midland Valley Move 2015 software on the basis of the flexural-slip algorithm, assuming constant bed length and thickness and constant area for salt units and Neogene infill. Their orientation is orthogonal to the arcuate shape of the Subandean thrust front (Figure 2.2.2) and is consistent with the thrust movement direction (bow-and-arrow rule). The cross-sections were restored at the base of the Pozo Formation, which sealed a regional erosive planar unconformity (Christophoul et al., 2002).

2.2.4.2. Geophysical data and interpretation

2.2.4.2.1. Seismic reflection

For this study, we have incorporated seismic sections from campaigns of Amerada, Deminex, British Petroleum, Arco, Mobil, Burlington, Sun, Phillips, Prakla, Conoco Phillips and Gran Tierra. They are unevenly distributed in the Marañón Basin, with section spacing between 5 and 10 km and in some cases up to 30 km. The dominant frequency of the 2D seismic data is approximately 20Hz, resulting in a vertical resolution of approximately 40 m. This seismic information, combined with wells data, allowed us to construct a two-way time (TWT) map of the Cretaceous base for the entire Marañón basin (Figure 2.2.3). This map illustrates the present-day Marañón basin structural architecture with their regional faults. It shows the eastward propagation of the Subandean frontal thrusts system in the southern wedge-top depozone and how it dies progressively to the north in the foredeep depozone. The eastern part of the Triassic and Jurassic basins has been eroded and sealed by the Late Early Cretaceous Andean basal foreland unconformity. The present border of these basins (see Figure 2.2.3) does not seem to have any control in the Subandean deformation.

Although our structural revision is based on the interpretation of an exhaustive compilation of seismic data, only the most representative examples of seismic cross-sections have been chosen to show the main tectonic Andean and pre-Andean features.

91MPH-23 seismic section (Figure 2.2.6A): this section is a good illustration of the interference between thick and thin-skinned tectonics in the Huallaga basin. It clearly shows the large overthrusting of the Chazuta thrust sheet that developed on the extensive and thick level of Late Permian evaporate, outcropping in various places of the Huallaga basin (Figure 2.2.2) and pinched out to the east. More to the west, the Biabo anticline is a major fault propagation fold that propagated in the thick almost continuous Neogene infill (Miocene and Pliocene). The Chazuta thrust sheet hanging-wall shows the autochthonous Cretaceous and Lower Cenozoic sedimentary series and two salt pillows. They are deformed by important west-verging basement thrusts whose origin will be discussed later. The easternmost west-verging basement structure is partly sealed by Late Cretaceous and Lower Cenozoic growth strata. This section was used in the Huallaga-Marañón balanced cross-section construction (Fig. 2.2.10).

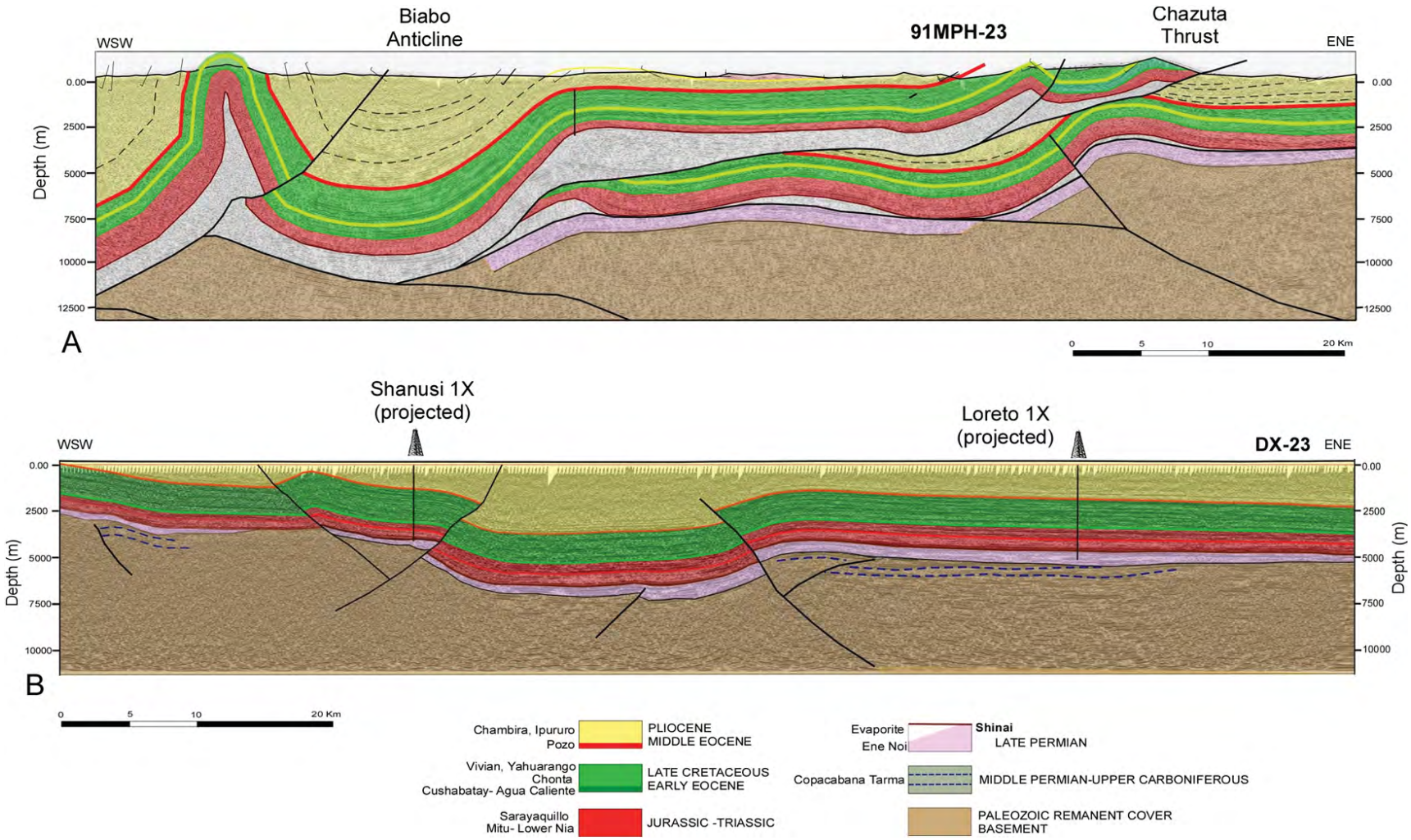

Figure 2.2.6. Interpreted seismic sections 91MPH-23 and DX-23 (location in Fig. 2.2.2 and 2.2.3)

DX-23 seismic section (Figure 2.2.6B): east of the Chazuta thrust, important thick-skinned Andean deformation is observed in the DX-23 seismic section where two exploratory wells could be projected (Loreto 1X and Shanusi 2X). The Late Permian evaporate level is not present in this part of the basin. This section shows that the wide and domed Loreto structure, well expressed in the structural map of the Figure 2.2.3, is a west verging structure with a recent consequent uplift. The seismic also shows an old contractional deformation preserved below the basal erosional unconformity of the Late Permian series and affecting the Permian and Carboniferous Copacabana-Tarma formations. To the west, the Shanusi pop-up structure is another important recent thick-skinned structure with a major east-verging basement thrust on the eastern limb of the Cushabatay High (see Figures 2.2.2 and 2.2.3). The western border of the seismic section shows a small west-verging structure sealed by the basal unconformity of the Late Permian series.

AH-3 seismic section (Figure 2.2.7A): this section was used for the construction of the Moyabamba-Marañón balanced cross-section (Fig. 2.2.10). It shows the northern continuity of the Loreto basement structure in the Chazuta thrust hanging-wall. Pre-Andean folds associated to west-verging thrust are sealed by the basal erosional unconformity of the Late Permian. They deformed the Permian and Upper Carboniferous Tarma and Copacabana formations imaged by characteristic strong reflectors well calibrated by deep wells in other parts of the Peruvian Subandean basins (PARSEP, 2001; Hurtado et al., 2014). Therefore, this compressive deformation can be considered as Permian in age.

DX-51 seismic section (Figure 2.2.7B): this section, located south to Loreto, is probably one of the most representative seismic sections of the Permian compressive deformation. As in the AH-3 seismic section, west-verging thrust folds are sealed by the basal Late Permian unconformity and deformed the Copacabana and Tarma formations. The westernmost fault-propagation-fold presents growth strata in the upper part of the Copacabana Formation. These Permian thrusts have been reactivated during the recent Andean deformation, and are apparently responsible of the large and smooth anticlines emerging in the Marañón basin. In the Loreto structure, west-verging Permian thrusts have been mapped (see Fig. 3) and present N-S orientation.

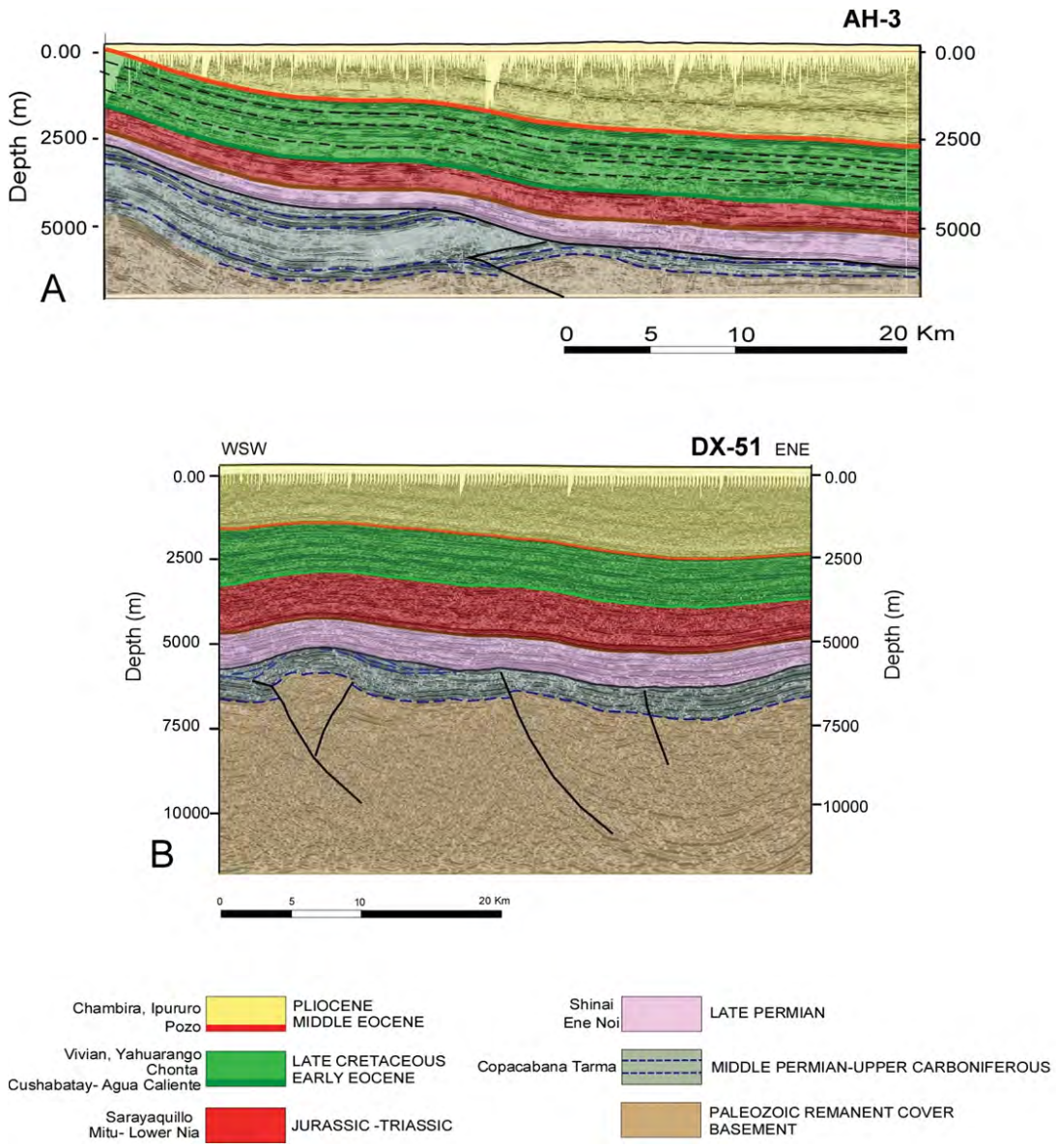

Figure 2.2.7. Interpreted seismic sections AH-3 and DX-51 (location in Fig. 2.2.2 and 2.2.3)

AH-13 seismic section (Figure 2.2.8): this section is parallel to the Andean structures and crosses the AH-3 section in the north of the study area. It confirms the presence of a Permian fold and thrusts belt below the Marañón foreland basin system. This fold and thrust belt is obviously sealed by the Late Permian series, and partly reactivated during the recent Andean compression.

PSEP-135-2013-01 seismic section (Figure 2.2.9): this section clearly shows a pre-Andean west-verging fold and thrust belt, eroded and sealed by the Cushabatay basal unconformity (Late Early Cretaceous) and cut by a recent major east-verging Andean thrust. In this part of the Marañón basin, deep wells as Tamanco X1 show that the Cretaceous Cushabatay Formation unconformably overlies the Permian Copacabana Formation. Therefore, this east-verging fold and thrust belt can be easily correlated with the Permian fold and thrust belt observed on the AH-3, DX-21 and AH-13 seismic sections.

2.2.4.2.2. Regional seismicity

The Moyabamba and Huallaga basins are located on the most seismically active segment of the Peruvian Subandean zone (Tavera et al., 2001; Delvin et al., 2012). According to these authors, Subandean crustal earthquakes occur from the surface to near the Moho depth and are associated to basement thrusts. In our balanced cross-sections construction, we have used the corrected depth locations and focal mechanisms of crustal earthquakes of the Central Andes published by Delvin et al. (2012) to define the geometry of the most western Subandean thrusts. In the study area, Delvin et al. (2012) have relocated 9 earthquakes between magnitude 5.2 and 6.6 that occurred between 1968 and 1999. They showed that focal mechanisms are consistent with horizontal shortening.

Three of these earthquakes have been projected along the Huallaga-Marañón cross-section between 33 and 24 km of depth (Figure 2.2.10). They have permitted to better constrain the lower crust detachment level depth of the basement thrusts system imaged by seismic reflection profiles (Figures 2.2.6 to 2.2.9).

In the Moyabamba-Marañón structural cross-section, four earthquakes between 24 and 14 km depth have been projected. They are consistent with the west-verging basement thrusts geometries imaged in the seismic sections of Figures 2.2.6 and 2.2.7. The 1990-91 damaging earthquakes of Moyabamba (Tavera et al., 2001) were probably associated to one of this important west-verging basement thrusts. Such reverse faults have been also recognized more to the south by Delvin et al. (2012) in the Ucayali basin.

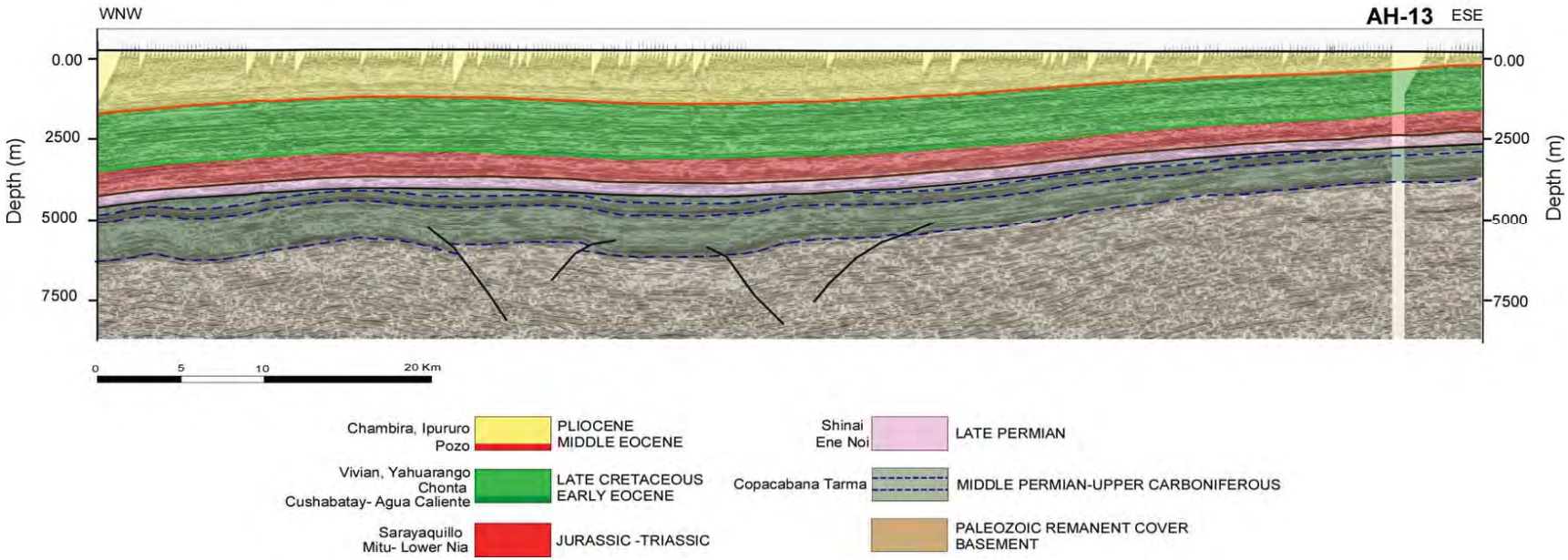

Figure 2.2.8. Interpreted seismic section AH-13 (location in Fig. 2.2.2 and 2.2.3)

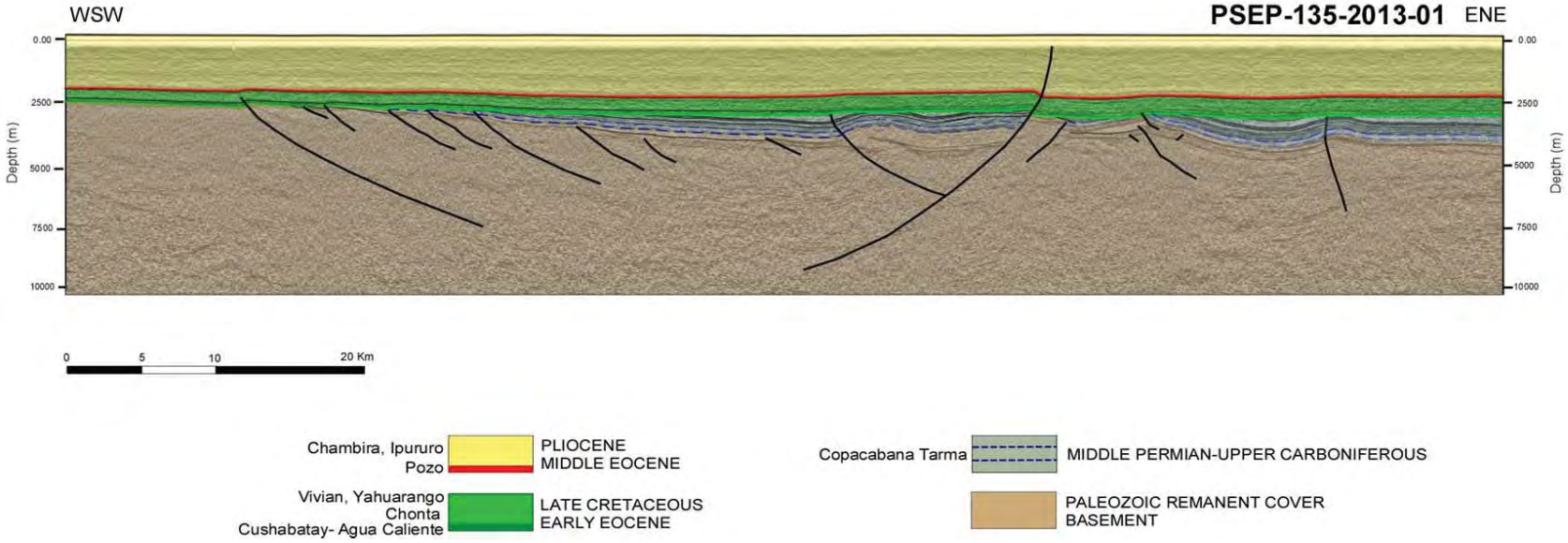

Figure 2.2.9. Interpreted seismic section PSEP-135-2013-01 (location in Fig. 2.2.2 and 2.2.3)

2.2.4.2.3. Thrusts regional distribution and shortening

The Huallaga balanced cross-section (Figure 2.2.10) has been updated from previous versions (Gil, 2001; Hermoza et al., 2005; Eude et al., 2015; Calderon et al., 2017), while the Moyabamba cross-section has been exclusively constructed for this study and is published for the first time. They are ~ 420 km and ~ 572 km long from the Eastern Cordillera to the Marañón foreland. To the west, the tectonic inversion of the Triassic Mitu rift has controlled the deformation and propagation of the Eastern Cordillera deformable backstop of the Huallaga and Moyabamba wedge-top basins. Both wedge-top basins are deformed by east verging thin-skinned large emerging thrusts and west verging thick-skinned deep blind thrusts. Thin-skinned thrusts have propagated on the thick and continuous Late Permian evaporate layer that expended above pre-Andean structures. To the east, the Marañón basin is characterized by east-verging basement thrusts branched on an intra-basement detachment, which deform the entire Neogene series. The Moyabamba cross-section reached the Iquitos Andean forebulge (Roddaz et al., 2005). Total horizontal shortenings are 70 km in the Huallaga cross-section and 76 km in the Moyabamba cross-section.

2.2.4.2.4. Basement deformation

Both balanced cross-sections show two types of basement deformation. The deformation is active as shown by the present crustal seismicity of the region (Tavera, 2011).

To the east, in the Marañón foreland, the orogenic deformation propagated normally towards the east with relatively deep thrust faults branched on an intra-basement detachment. The depth of this detachment (Figure 2.2.10) is constrained by the location of crustal earthquakes (Delvin et al., 2012; see above). East-verging basement thrusts have an Andean fabric with a typical NW-SE orientation perpendicular to the South American and Nazca plates convergence (Nocquet et al., 2014).

To the west, beneath the Huallaga and Moyabamba wedge-top basins, active west-verging thrusts are evidenced both by seismic reflexion data (Figures 2.2.6, 2.2.7, 2.2.8 and 2.2.9) and crustal earthquakes (Figures 2.2.10 and 2.2.11). The best topographic expression of this deep deformation coincides with the Cushabatay High, east of the Huallaga thrust front (Chazuta thrust), where merges the Callanayacu diapir (Figures 2.2.2 and 2.2.11). The Callanayacu structure is a diapir of Late Permian evaporite deformed at the top of the

Cushabatay High mega-duplex, which developed between the intra-basement detachment and the salt detachment (Figure 2.2.11). Such duplexes developed also under the Huallaga and Moyabamba salt detachment. Below the Moyabamba basin, one of these crustal west-verging thrusts is particularly active and responsible of the 1990-91 damaging earthquakes of Moyabamba (Tavera et al., 2001). At the limit between the Moyabamba basin and the Eastern Cordillera, the west-verging fault-propagation-fold of Cerro Blanco is the topographic expression of this fault propagation (Figure 2.2.11). East of the Chazuta thrust, seismic sections (Figures 2.2.6 to 2.2.9) show that the west-verging thrusts correspond to the reactivation of Middle Permian thrusts that deform the Copacabana Formation and are sealed by the Late Permian erosional basal unconformity. In the Loreto structure, seismic mapping of this Permian thrusts shows they are N-S oriented (see structural map of Figure 2.2.3). The seismic sections of Figures 2.2.7B, 2.2.8 and 2.2.9 show that they belong to a significant fold and thrust belt fossilized and partly reactivated under the Andean Marañón foreland basin. North of the Loreto structure, north-south faults have been mapped (Figure 2.2.3) and could correspond to the northern prolongation of the inherited Permian fold and thrust belt, although Permian strata are not preserved in this part of the Marañón basin to confirm the initial age of the faults. The geodynamic setting of the Permian fold and thrust belt will be discussed later.

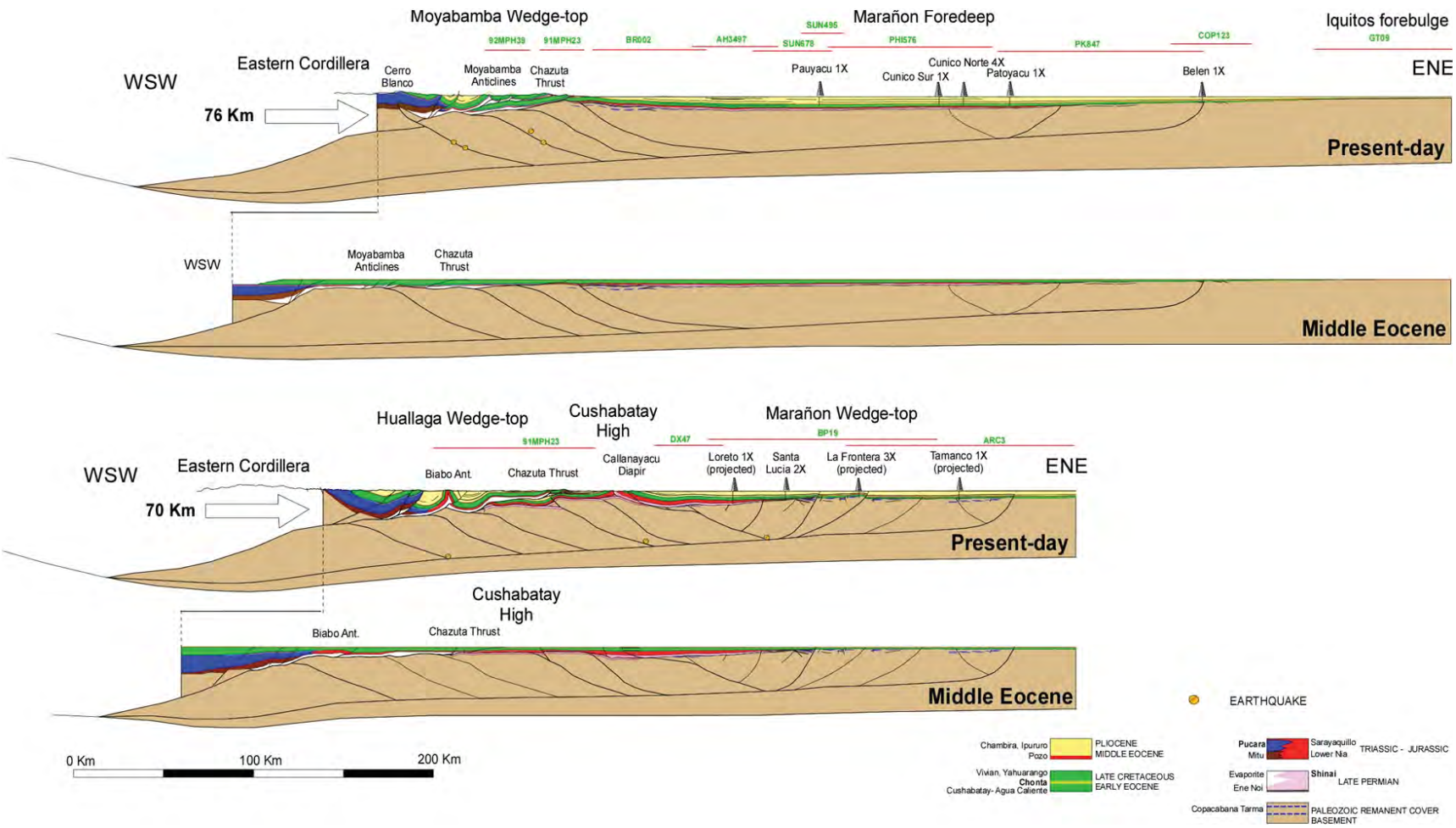

Figure 2.2.10. Huallaga-Marañón and Moyabamba-Marañón balanced cross-sections (location in Figures 2.2.1 and 2.2.2). Initial sections were obtained by flattening the base of the Pozo Formation (± 45Ma). Mean regional earthquakes (Mw>5) relocated by Delvin et al. (2012) have been projected on the section.

2.2.4.2.5. Salt tectonics distribution

Above the west-verging basement thrusts system, important salt thicknesses have been identified in both Huallaga and Moyabamba wedge-top basins thanks to seismic information (see Figure 2.2.6A for example). This salt is outcropping in some diapirs and emerging sole thrusts (Figures 2.2.2 and 2.2.10), where it is mainly composed of light gray halite, gypsum, and some levels of marl and mudstone. It strongly controlled the style of deformation and the development of extensive tectonic nappe as the Chazuta thrust and detachment folding illustrated by the Biabo and Moyabamba mega-folds (Figures 2.2.2 and 2.2.11). Its thickness decreases rapidly to the south in the Ucayali basin, where it is clearly identified and described thanks to the Camisea wells (Seminario et al., 2005), and increases to the north, in the Santiago basin, where a complex salt tectonics has been described (Aleman & Marksteiner, 1993; Mathalone & Montaya, 1995; Gil et al., 2001). The salt level disappears abruptly to the east in the Marañón basin, which explains the absence of thin-skinned tectonics in this part of the foreland basin system. Our stratigraphic revision proposed in the section 3 suggests a Late Permian age of this salt. It overlay the erosional unconformity that sealed the Permian west-verging fold and thrust belt described above. The salt deposits extension over the pre-Late Permian thrust system is well illustrated in the palinspastic restorations of the two balanced cross-sections (Figure 2.2.10). The eastern and western disappearance of the salt and the increase of its thickness to the north imply a marine transgression entering from the north, which agrees with published Permian paleogeographic maps (Williams, 1995; McGroder et al., 2014).

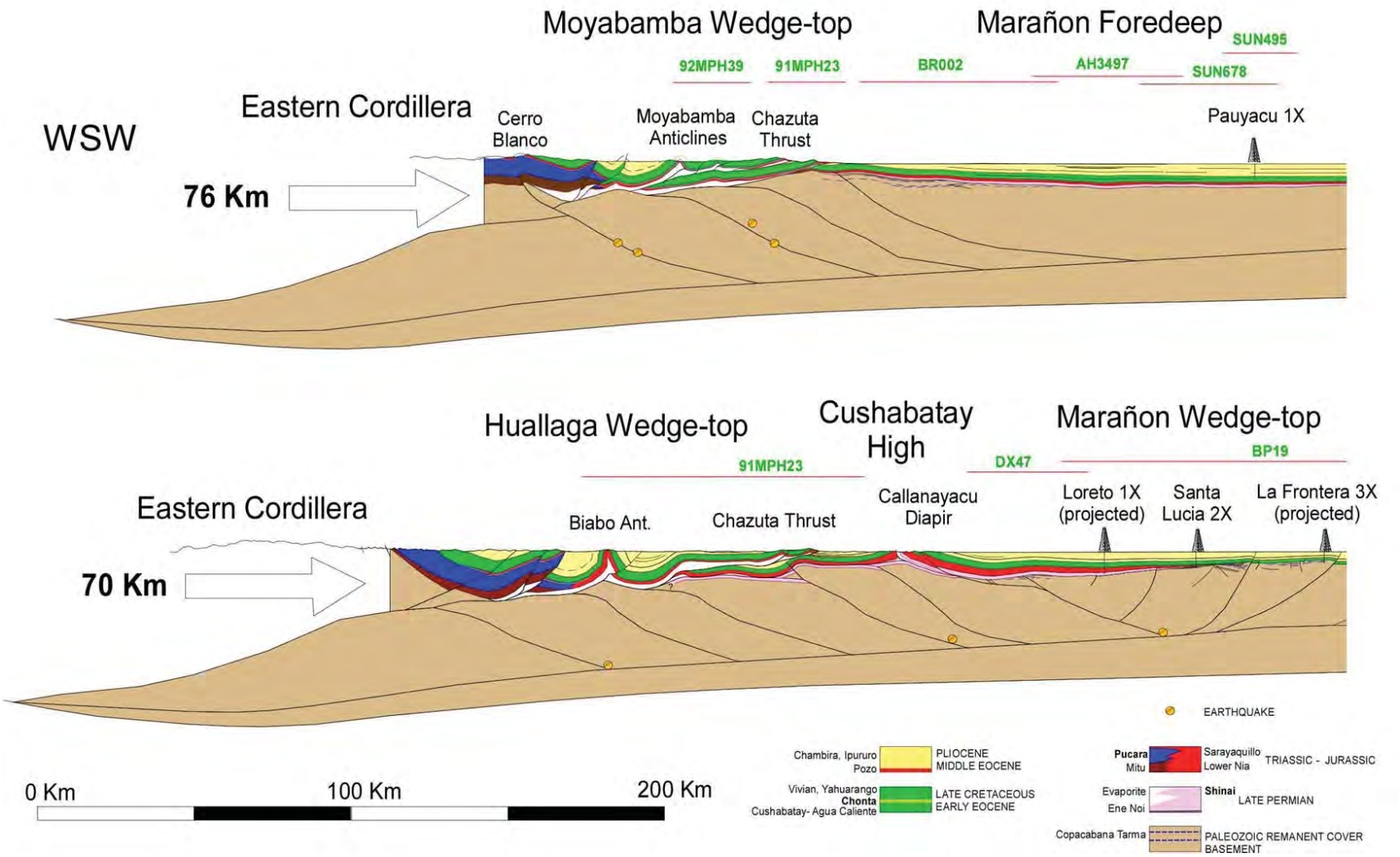

Figure 2.2.11. Zoom of the structural balanced cross-sections in the Huallaga-Marañón and Moyabamba-Marañón wedge-top basins (location in Figs 2.2.1 and 2.2.2). Mean regional earthquakes (Mw>5) relocated by Delvin et al. (2012) have been projected on the section.

2.2.5. Discussion

2.2.5.1. Permian orogeny

The seismic sections and balanced cross-sections presented in this study show that the Huallaga-Moyabamba-Marañón foreland thrusts system forms actually a complex wedge-top depozone characterized by active west-verging basement thrusts. Some seismic sections (Figures 2.2.6B, 2.2.7, 2.2.8 and 2.2.9) image a Permian inheritance of this thrusts system. It forms a Middle Permian fold and thrust belt, sealed by a Late Permian unconformity, and reactivated during the Andean orogeny. When seismic mapping is possible, it shows a N-S orientation of these fold and trust belt (Figure 2.2.3). This Paleozoic deformation has been yet suggested in the Huallaga basin by Rodriguez and Chalco (1975). These authors have proposed a tectonic uplift at the end of the Middle Permian in the eastern part of the Huallaga basin to explain the lack and probable erosion of the Copacabana Formation. They considered this tectonic uplift as the result of the Hercynian orogeny. In Southern Peru, Laubacher and Mégard (1985) showed an “early Hercynian belt partially reactivated by the late Hercynian pulse of deformation”. They identified in the Eastern Cordillera and the Altiplano a late Hercynian folding in the Carboniferous and early Permian strata, subsequently eroded and unconformably overlain by late Permian sedimentary series. As in the Huallaga-Moyabamba-Marañón thrust system, these Permian structures are west-verging and N-S oriented. They have been also suggested in northwestern Peru by Dalmayrac et al. (1988) and evidenced by subsurface data in the offshore forearc basins of northern Peru (Timoteo et al., 2012) at the same latitude as our balanced cross-sections. Apparently, the structural mapping published by these authors shows the same N-S trend orientation. Recently, Chew et al. (2016) have demonstrated that the Eastern Cordillera of Peru has experienced a high-grade orogenic event in the latest Middle Permian.

Andean reactivation of late Carboniferous to Middle Permian west-verging thrusts have been also described in the Southern Central Andes (Giambiagi et al., 2014). Therefore, it appears that the Middle Permian orogen fabric – known as Late Hercynian orogen in Peru (Laubacher and Mégard, 1985) o San Rafael orogen in Argentina (Ramos, 1988) – has a strong influence on the propagation of the Andean deformation. It was part of a long fold and thrust belt developed along the southern margin of Gondwana, and now preserved in South America, South Africa, Antartica and Australia (Catuneanu, 2004). For this raison, we prefer to use “Gondwanide orogeny” to describe this deformation (see Figure 2.2.4). This name is more commonly used in the Andes (Ramos, 1988; Chew et al., 2016). In the Huallaga-

Moyabamba-Marañón thrusts system, the middle Permian west-verging thrusts are nowadays reactivated and constitute origin structures for the earthquakes. In our balanced cross-sections, the abnormal deep detachment of the lower crust constructed in base of the regional seismicity results probably from the Middle Permian orogen inheritance.

2.2.5.2. Implications for petroleum exploration

Paleozoic petroleum systems of the Huallaga-Marañón foreland basin have been recently revaluated and described by Calderon et al. (2017). They are represented in the stratigraphic diagram of the Figure 2.2.4 and can be extrapolated to the poor known Moyabamba basin. Late Cretaceous classic source rocks are present in all the foreland basins and the Late Triassic-Early Jurassic Pucara source rock is confined to the Eastern Cordillera-Huallaga-Moyabamba transition zone above the inverted Triassic rift. Recently, a new Late Permian source rock (Shinai) has been suggested along a large proportion of the foreland basin system (Calderon et al., 2017).

Our study highlights a new petroleum play in the Huallaga, Moyabamba and southern Marañón basins. This new play corresponds to the reactivated, but preserved, Middle Permian fold and thrust evidenced in our structural analysis. It shows thrust related anticlines (see Figures 2.2.7B, 2.2.8 and 2.2.9 for example) that could be alimented by remnants of the classic Subandean Devonian Cabanillas source rock (Mathalone and Montaya, 1995; Jacques, 2004) and/or the Late Permian source rock recently evidenced in the study area (see Figure 2.2.3). As in the Camisea basin (Seminario et al., 2005), fluvial and aeolian sandstones of the Ene and Lower Nia formations can constitute good reservoirs for these structural traps. Most of these potential hydrocarbon structures are preserved in the unexplored Chazuta thrust foot-wall, making the Huallaga-Moyabamba-Marañón foreland system as one of the most sub-trap attractiveness of Peru.

Oil and gas discoveries have been made in the last decade in Paleozoic fractured reservoirs of offshore structures in the “Sechure Bahia” in the other side of the Andes at the same latitude as the Moyabamba basin (Alarcon and Borda, 2011). This petroleum play corresponds to reactivated Late Paleozoic compressive structures and is comparable to that we suggest in the Huallaga-Moyabamba-Marañon FBS. This augurs good prospects for future explorations.

2.2.6. Conclusions

Geophysical data and balanced cross-sections show that the Huallaga-Moyabamba-Marañón FBS is deformed by the interference of east-verging thin-skinned tectonics and west-verging thick-skinned tectonics. Total horizontal shortening varies between 70 and 76 km. Thick-skinned tectonics is still active and is propagating to the east in the Marañón sub-basin that corresponds to a wedge-top depozone at the latitude of the Huallaga and Moyabamba basins. More to the north, the Subandean thrust front propagation retreats to the hinterland and the Marañón basin evolves gradually to a foredeep depozone.

West-verging thick-skinned tectonics is controlled by the inheritance of the Middle Permian orogeny known as the Gondwanide orogeny, which is clearly identified for the first time in the Subandean basins of Peru. Such reactivated west-verging thrusts form high structures relieves as the Loreto and Cushabatay antiforms.

Thin-skinned tectonics propagation is controlled by the post-orogenic Late Permian salt distribution that results in the development of a regional décollement and the must large overthrust (+- 40 km of horizontal shortening) of the Peruvian Subandean zone. This implies an attractive sub-thrust play for the petroleum exploration that stays unexplored.

Crustal and damaging seismic activity in the Moyabamba basin is due to the reactivation of the west-verging Middle Permian thrusts. Our structural analysis shows that this lower crust seismic activity can be associated to two major west-verging reverse faults.

The fossilized and partly reactivated Middle Permian fold and thrust belt, now well-defined on seismic sections, constitutes a new petroleum play for the exploration in the Huallaga-Moyabamba-Marañón FBS. Thrust related anticlines are potential structural traps alimented by Paleozoic source rocks. As in the Camisea basin, Permian and/or Triassic fluvial and aeolian sandstones represent potential reservoirs. The Late Permian salt cover forms an excellent seal in the Huallaga and Moyabamba basins. This augurs good prospects for future explorations.

Acknowledgements: This research project was conducted thanks to the IRD-PERUPETRO S.A. research agreement and the Institut Carnot ISIFoR. It received financial support from TOTAL for field surveys and laboratory analysis. We thank Rolando Bolaños and Asaid Bandach for their support and participation throughout the long-term IRD-PERUPETRO S.A. research activities.

2.3. The northern Marañón foreland basin system structure

2.3.1. Geologic framework, stratigraphy and method

In the previous section 2.2., it has been shown that the southern part of the Marañón is currently deformed by the Subandean thrust system propagation and corresponds to the contemporaneous wedge-top depozone of the northern retro-foreland basin system. Towards the north, the Marañón basin is progressively deepening and deformation is weaker; it can be considered as a foredeep depozone limited in the west by the Santiago Subandean fold and thrust belt, and in the east by the Iquitos forebulge (Figure 2.3.1). It constitutes also the deepest depozone of the Marañón-Oriente-Putumayo foreland basin (Marksteiner and Aleman, 1997), and played an important role in the Cretaceous oil generation (Barragan et al., 2008). Thrust faults orientation changes from NNE-SSW to N-S, and extends in Ecuador to the Northern Andes domain.

The E-W stratigraphic diagram of Figure 2.3.2 shows some differences with the southern part. There is no evidence of the Triassic Mitu-Pucara rift system in the Subandean zone. However, the late Permian salt regional level is still present and well developed in the Santiago Basin and in the western part of the Marañón Basin (Aleman and Marksteiner, 1993; Mathalone and Montoya, 1995; Gil et al., 2001; Witte et al., 2011).

The method of interpretation and construction is the same that we used in the section 2.2.; it is described in the paper published in *Marine and Petroleum Geology*. Seismic sections and wells data were also provided by PERUPETRO S.A., and surface data were obtained from 1:100,000 INGEMMET (Instituto Nacional Geologico, Minero y Metalúrgico del Perú) geologic maps and PERUPETRO data base. Seismic sections and wells used for the cross-sections construction are located in Figure 2.1. Detailed lithostratigraphic logs of the wells are presented in the Chapter 3. The regional cross-sections are not balanced as in the southern part because horizontal shortening is negligible except for the R4 that comprises the Santiago wedgetop basin. Unfortunately, the cross-section R4 is oblique to the structures and does not allow to construct a rigorous balanced cross-section.

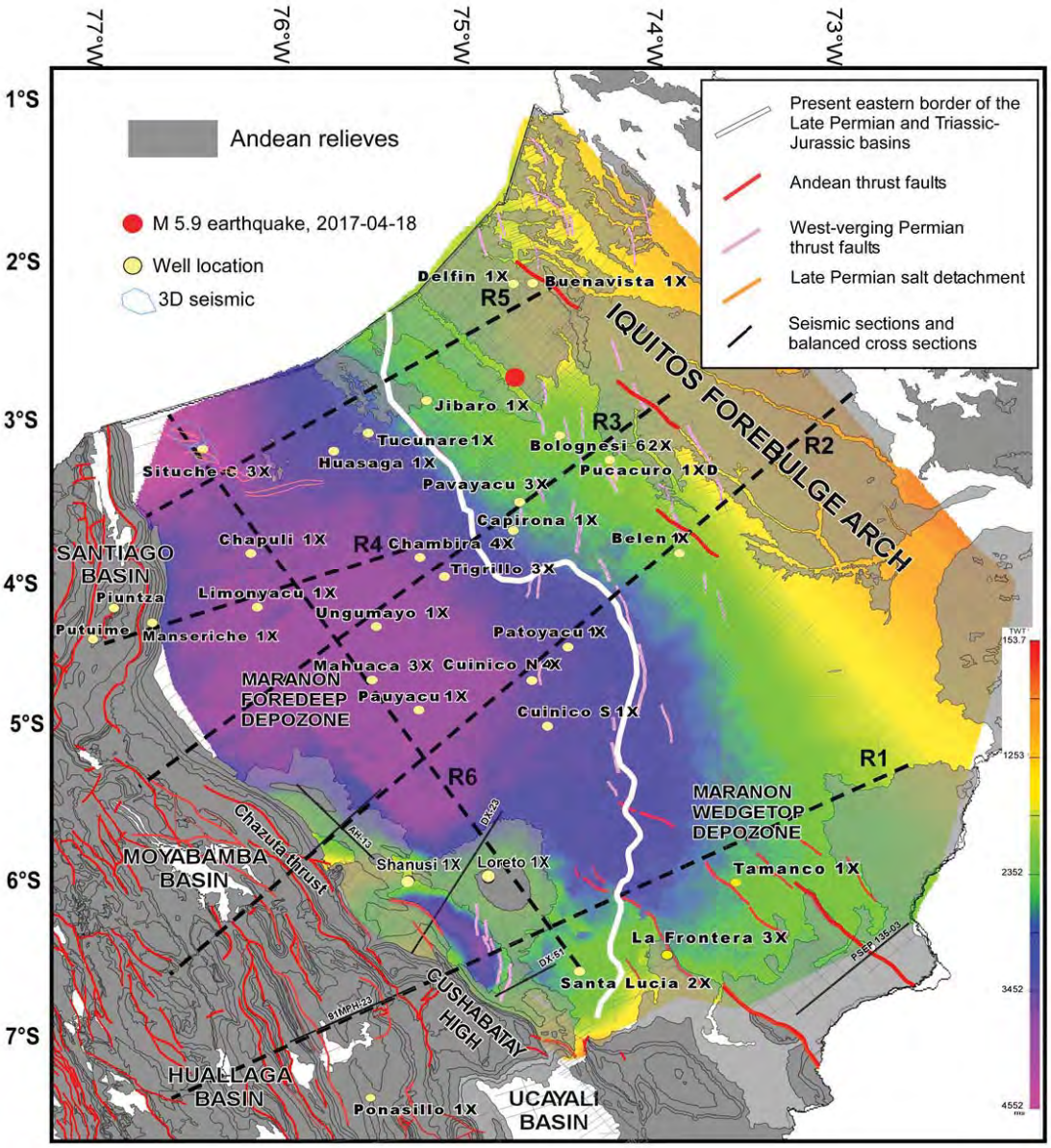

Figure 2.3.1. TWT Base Cretaceous structural map of the Marañón foreland basin with location of the eastern border of the pre-Cretaceous long term sequences. The TWT map is superimposed on the geologic contours of the Andean relieves. Regional cross-sections, wells and 3D seismic of Situche area are located. Two depocenters appear in the Marañón foredeep.

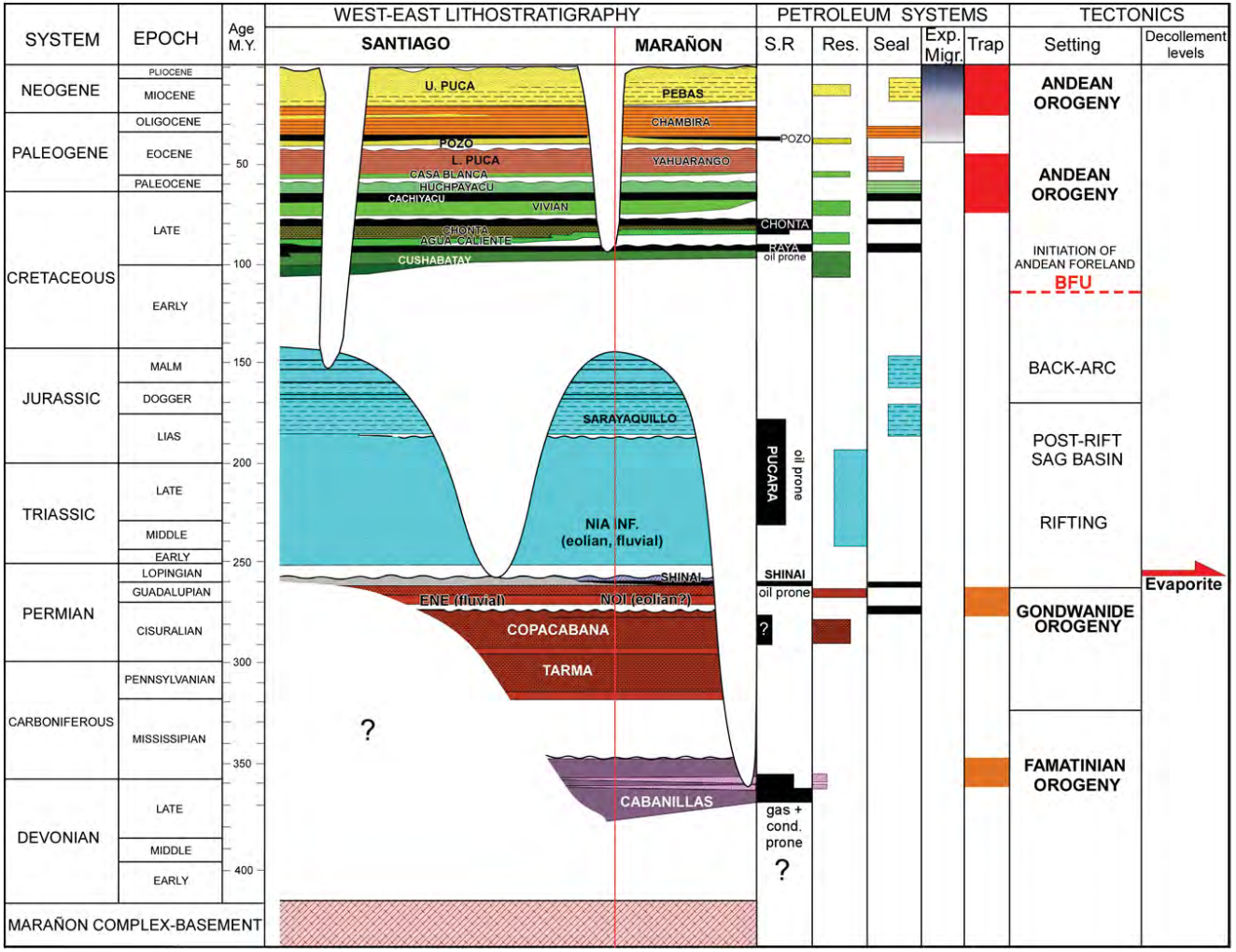

Figure 2.3.2. Stratigraphic diagram and petroleum systems along the Santiago-Marañón FBS. The orogenic cycles names are those that are more commonly used in the Andes (see Ramos, 1988; Caputo, 2014; Chew et al., 2016).

2.3.2. The hinge zone: regional structural cross-section R3

This part of the Marañón Basin is located in the hinge zone between the Central and Northern Andes, traditionally known as Huancabamba deflection (Mitouard et al., 1990), where Andean structures orientation changes from NNE-SSW in the south to N-S in the north. The TWT Base Cretaceous structural map of Figure 2.3.1 shows that this zone corresponds to one the two current depocenters of the Marañón foredeep (see structural map of Figure 2.3.1.), where the Cenozoic sediments can reach more than 4000 m of thickness.

The regional cross-section R3 (Figure 2.3.3) is 457 km long from the eastern flank of the Subandean zone to the western flank of the Iquitos Arch (forebulge). It has been constructed from 6 seismic sections and 5 wells (see also map of Figure 2.1). It shows as in the south (see section 2.2.) thick-skinned deformation, but a relative simple structural geometry without thin-skinned deformation probably due to the absence of the Late Permian evaporitic layer. The Chazuta thin-skinned thrust system no longer exists; it dies out between cross-sections R2 and R3 (Figure 2.3.1) with the disappearance of the salt layer, whose eastern border is probably located more in the hinterland. The eastern flank of the Subandean zone is just uplifted by a west-verging basement thrust, which belongs to the northern prolongation of Huallaga-Moyabamba west-verging basement thrust system interpreted as the reactivation of Gondwanian compressive structures (middle Permian, see 2.2. section). This fault is branched on the intra-basement detachment constrained by the location of crustal earthquakes and previously described in the southern Marañón Basin (see Figure 2.2.11). The seismic section AH 259 of Figure 2.3.3 shows a fossilized west-verging middle Permian thrust sealed by the Late Permian deposits.

To the east, the orogenic deformation propagated in sequence towards the east, and merges currently east of the Pucaruro well on the western flank of the Iquitos forebulge (Roddaz et al., 2005). This part of the Marañón Basin is poor deformed. It presents some weak structures as the Capirona-Pavayacu pop-up, but active deformation is proved by intra-basement seismicity as the recent M 5.9 earthquake (2017-04-18) at 14+-1.7 km depth (https://earthquake.usgs.gov/earthquakes/eventpage/us10008iq5#executive) (see Figure 2.3.1). This earthquake is located in the cross-section R3 (Figure 2.3.3) and appears to confirm the depth proposed for the intra-basement detachment.

Timing of deformation is poor constrained along the cross-section R3. No growth strata are visible on the seismic sections and no thermochronologic data exist.

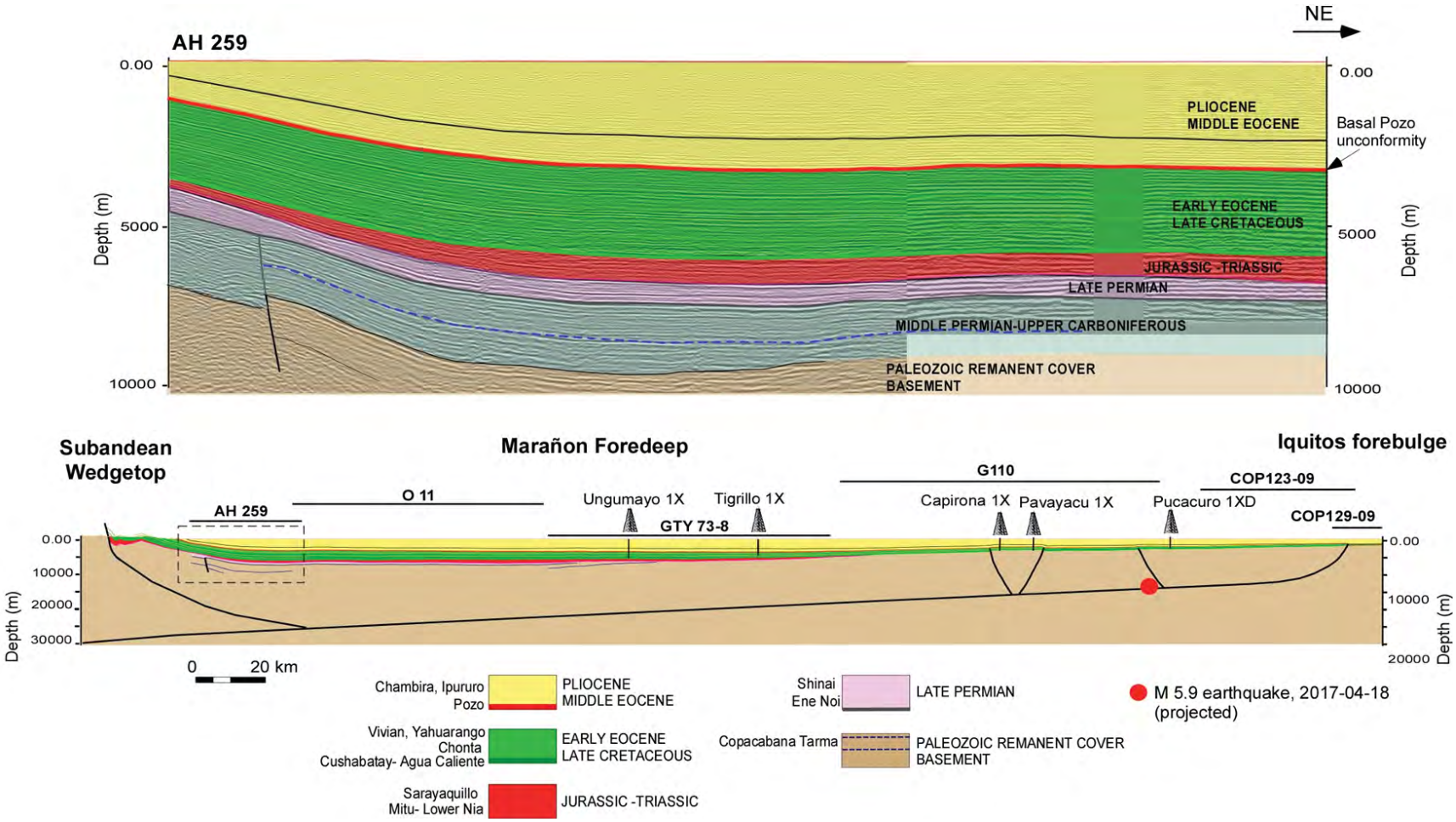

Figure 2.3.3. Structural regional cross-section R3 through the deepest part of the Marañón foredeep (location on Figures 2.1 and 2.3.1).

2.3.3. The Santiago-Marañón foreland basin system: regional structural cross-section R4

The regional cross-section R4 (Figure 2.3.4) shows the relationships between the Santiago wedge-top and the Marañón foredeep. It is 214 km long and extends from the middle part of the Santiago Basin to the depocenter of the northern Marañón foredeep. It has been constructed from 6 seismic sections (location in Figure 2.1.) and three wells. Seismic reflectors of the Santiago section have been calibrated from surface data (INGEMMET 1:100 000 Geological map) and from the Putuime X1 well (Figure 2.3.5), and then corroborated to the reflectors of the Marañón seismic sections.

The Santiago wedge-top Basin is well known for its salt tectonics, which is attested by diapiric structures and salt pillows evidenced in seismic (Aleman and Marksteiner, 1993; Mathalone and Montoya, 1995; Gil et al., 2001; Witte et al., 2011). The evaporites layer has been reached by the Putuime well (Figure 2.3.5), where it is directly overlaid by the Cushabatay late Cretaceous sandstones. As in the Huallaga Basin (see section 2.2.), seismic data (Figure 2.3.4) show that the evaporites thickness is important and can reach several thousands of meters. The age the evaporites are considerate as Late Permian as suggested by our stratigraphic revision of section 2.2.3. (See also stratigraphic diagram of Figure 2.3.2.).

As shown by the cross-section R4 (Figure 2.3.4), the Santiago wedge-top basin is also deformed by interference of thin and thick-skinned tectonics. To the east, beneath the salt-core anticline of the Campanquiz Cordillera, a west-verging basement thrust is evidenced by the seismic. It is probably due, as in the Huallaga basin, to the reactivation of a Late Permian thrust. To the west, the Putuime structure is interpreted as an east-verging basement structure. Shortening of this basement thrusts system is accommodated by thin-skinned and salt tectonics in the Late Permian evaporites layer and its Mesozoic and Cenozoic cover. The best expression of this deformation is the box-fold anticline of the Campanquiz Cordillera. Basement thrusts are branched on the intra-basement detachment already evidenced in the southern regional cross-sections (R., R2, R3 and R4).

The gravity map of Figure 2.3.6 shows the foredeep geometry of the Marañón basin west of the Iquitos forebulge, and the importance of the sedimentary cover thickness and the presence of basement highs in the Santiago basin, as proposed in the cross-section R4.

The Marañón foredeep of the cross-section R4 is weakly deformed and does not present major structures.

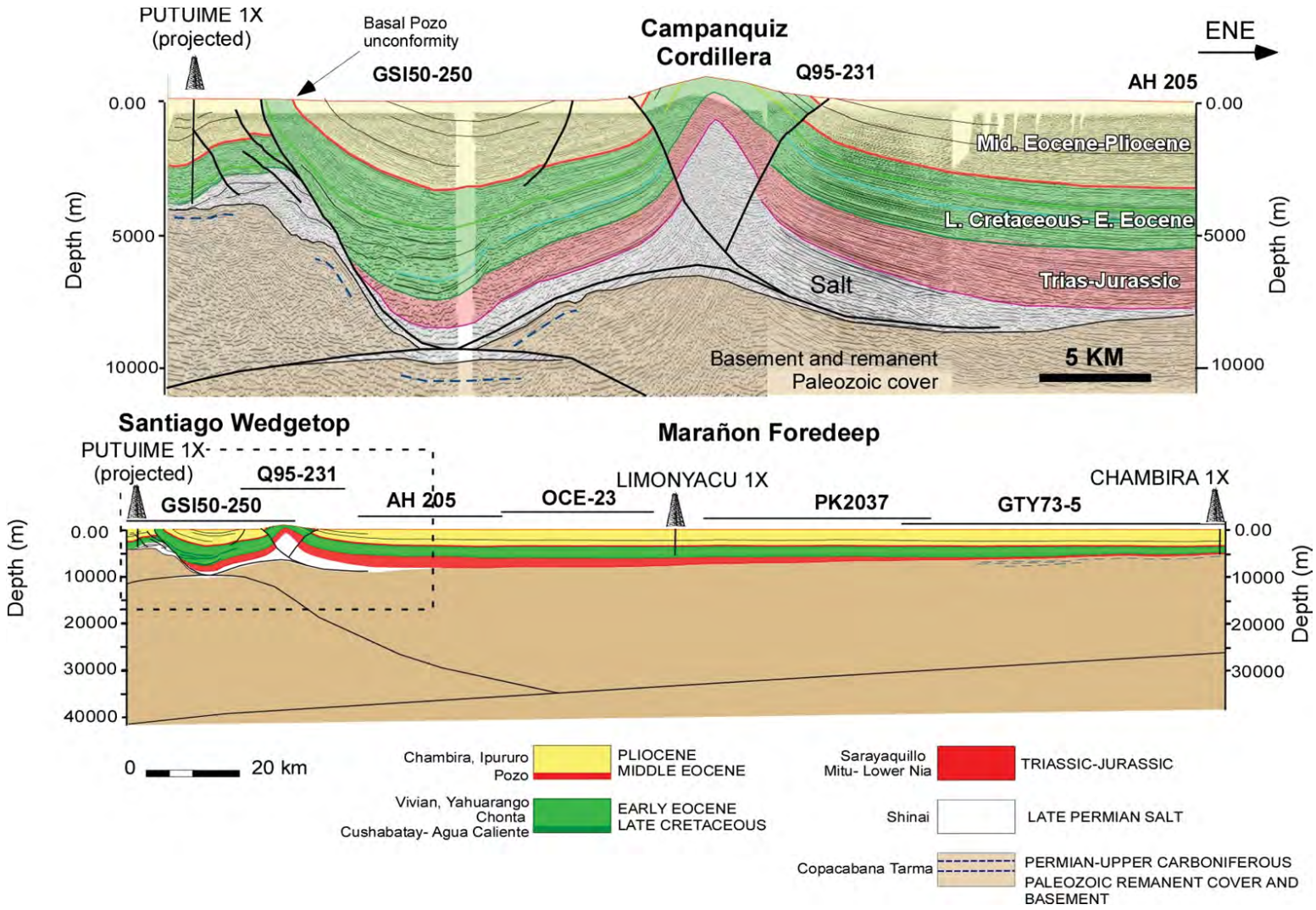

Figure 2.3.4. Structural regional cross-section R4 through the Santiago-Marañón foreland basin system (location on Figures 2.1 and 2.3.1).

Thermochronologic studies show that the Campanquiz anticline uplift separating the Santiago wedge-top from the Marañón foredeep is Late Miocene in age (Aleman and Marksteiner, 1993; Kennan, 2008). However, growth strata in the late Cretaceous infill (see seismic section of R4; Figure 2.3.4.) recorded a first stage of salt and basement tectonics. The seismic section shows that the Putuime basement thrust uplift started at the beginning of the late Cretaceous sedimentation (Cushabatay Fm.) and was progressively sealed by the late Cretaceous to early Eocene deposits. The Basal Pozo erosion marks the end of this first stage of Andean deformation and the beginning of a relative tectonic quiescence (Christophoul et al., 2002) before the late Miocene deformation, which will be discussed in the next chapters.

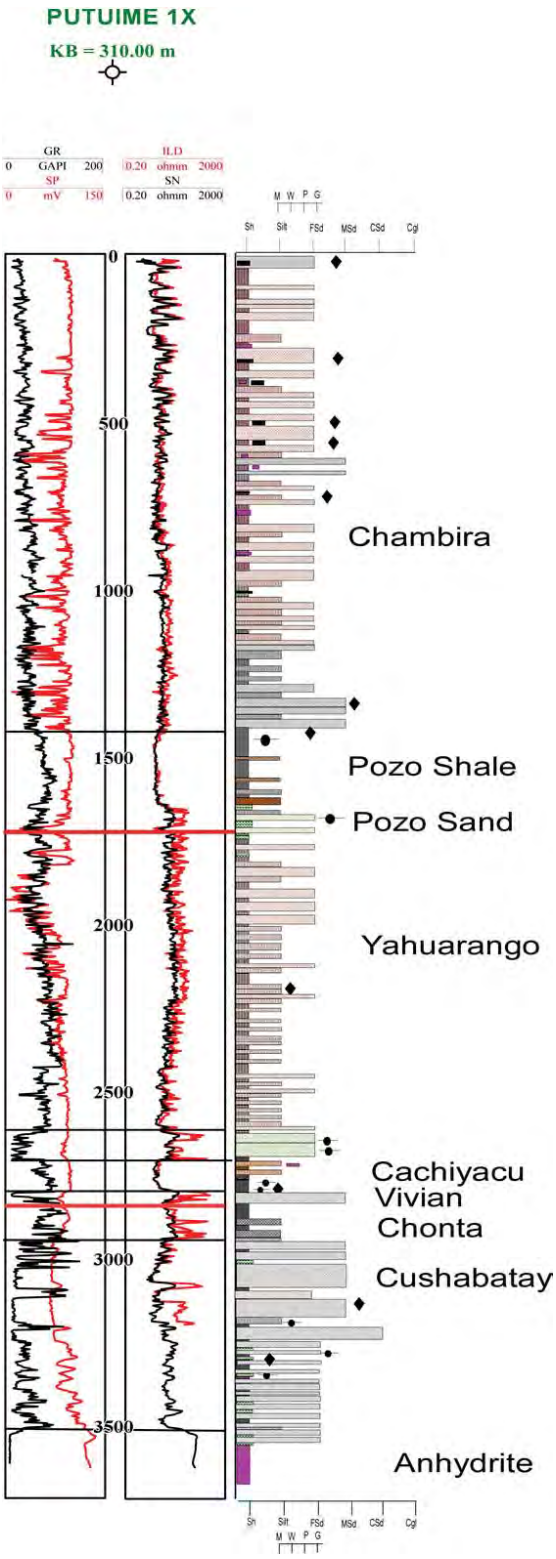

Figure 2.3.5. Stratigraphic log of the Putuime X1 well used for the interpretation of the Santiago basin seismic section (Figure 2.3.4.).

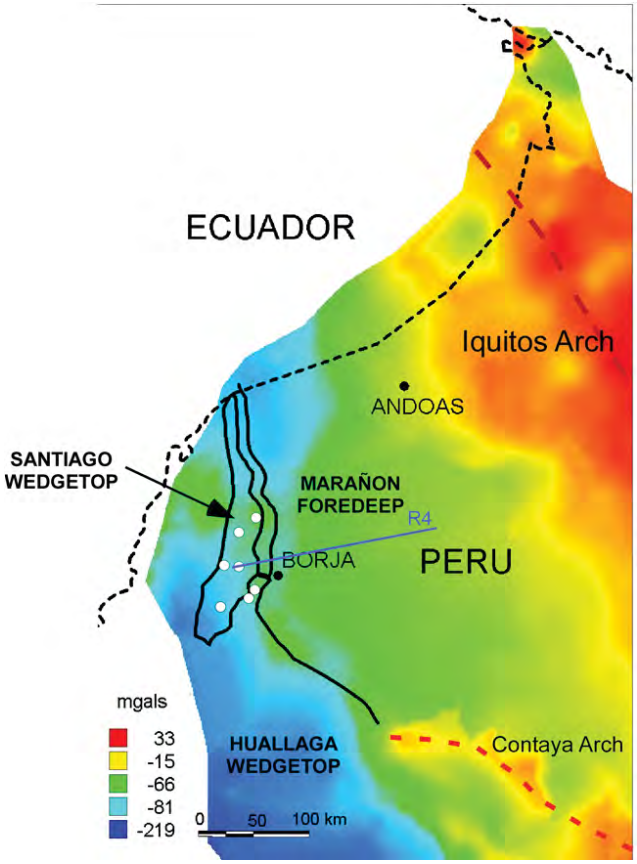

Figure 2.3.6. Regional gravimetric map showing basement configuration (modified from Navarro et al., 2005; gravity acquisition and processing from EDCON Worldwide, 1997). It shows the foredeep geometry of the Marañón basin west of the Iquitos forebulge, and the importance of the sedimentary cover thickness and the presence of basement highs in the Santiago basin.

2.3.4. The northern Situche deformation: regional structural cross-section R5

The regional cross-section R5 is constructed through the deepest part of the Marañón foredeep depozone (northern depocenter; see structural map of Figure 2.3.1.), where the Situche wells have passed 4500 m of Cenozoic sediments.

The cross-section R5 (Figure 2.3.7) is 309 km long from the western limit of the Marañón foredeep to the western flank of the Iquitos Arch (forebulge). It has been constructed from 5 seismic sections and 4 wells (see also map of Figure 2.1).

To the east, the Marañón foredeep is weakly deformed by the Tucunare, Delfin and Buena Vista east-verging basement thrust structures. As in the cross-section R3, the recent M 5.9 earthquake (2017-04-18) at 14+-1.7km depth (https://earthquake.usgs.gov/earthquakes/eventpage/us10008iq5#executive) has been projected to highlight the depth of the active intra-basement detachment.

This part of the Marañón foredeep basin is characterized by the peculiar deformation of the Situche structure (see section seismic of Figure 2.3.7 and structural map of Figure 2.3.8). The Situche oil field has been discovered by Occidental Petrolera del Peru in 2006. The reservoir that was tested corresponds to the Late Cretaceous Vivian sandstones (see Figure 2.2.4). The proven reserves for Situche are 25,752 MSTB (Libro de Reservas, 2016). The north and central 3D's merge data set was performed in 2011. The Situche Central 3D is a 199.2 sq km seismic survey that was acquired in 2007 and Situche Norte 3D is a 265.2 sq km seismic survey acquired in 2010, both being in the North Marañón Basin. The combined merged area of the two surveys is 449.34 sq km. The structural map from bloc 3D (Figure 2.3.8) shows that it is associated to WNW-ESE faults oblique to the classic N-S Andean structures. In the cross-section R5, the Situche anticline developed on an inverted normal listric fault that branches apparently on the Late Permian salt detachment. This normal fault controlled the sedimentation of the Campanian Vivian sandstones, which constitute the main reservoir, only present west of the fault as shown by exploratory wells and amplitude map of Figure 2.3.8. The inversion of the normal listric fault deformed al the Cenozoic cover and occurred undoubtedly in the late Neogene during the last Andean compressive period. The origin of this normal fault during the Campanian, curiously synchronous with the first Andean orogenic period, can only be explained by a gravitational salt deformation. It developed on the western flank of a structural high that could be Paleozoic in age and comparable to the middle Permian thick-skinned structures observed below the Huallaga and Moyabamba basins (Figure 2.2.11).

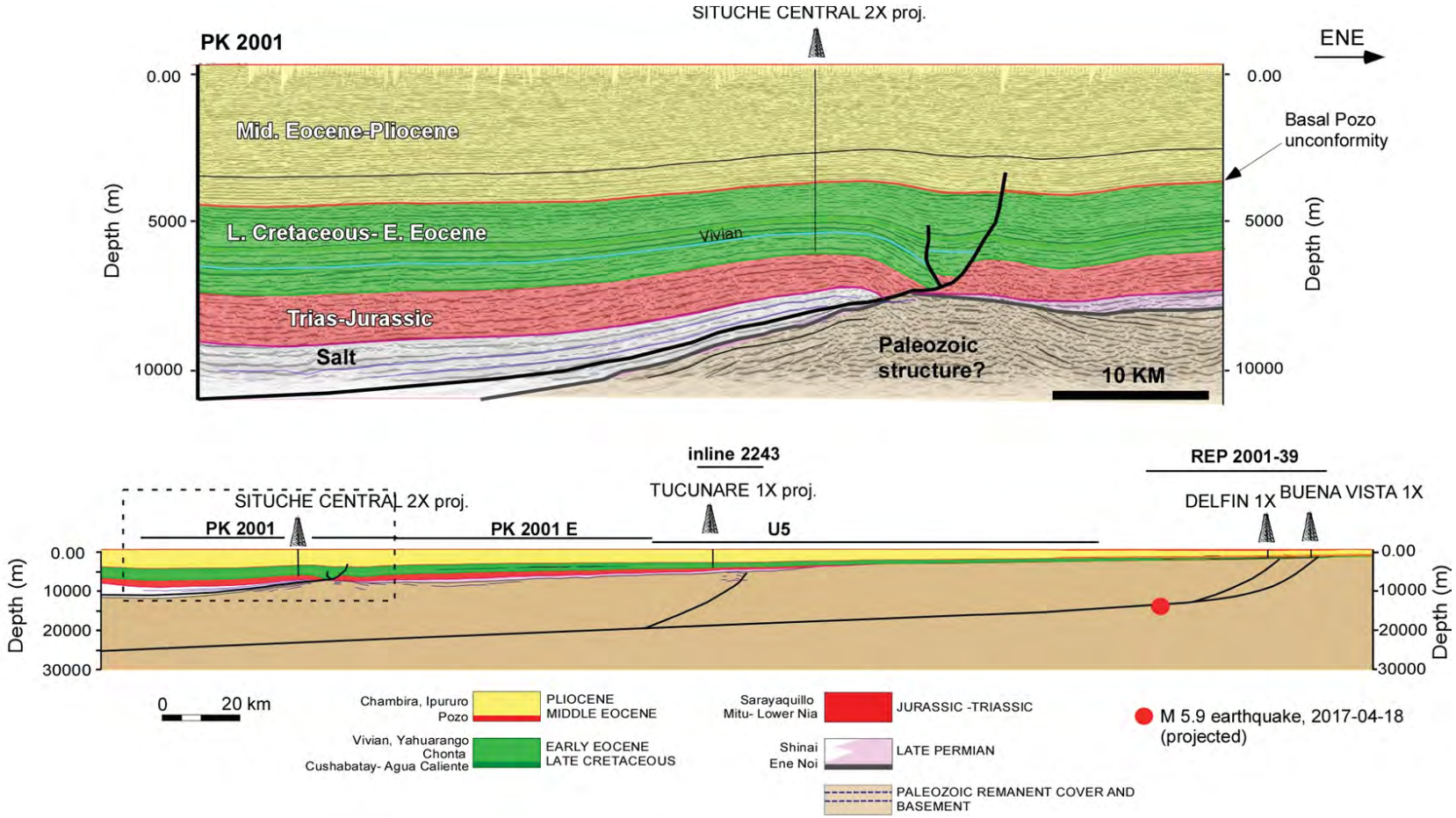

Figure 2.3.7. Structural regional cross-section R5 through the northern Marañón foreland basin system and the Situche oil field (location on Figures 2.1 and 2.3.1).

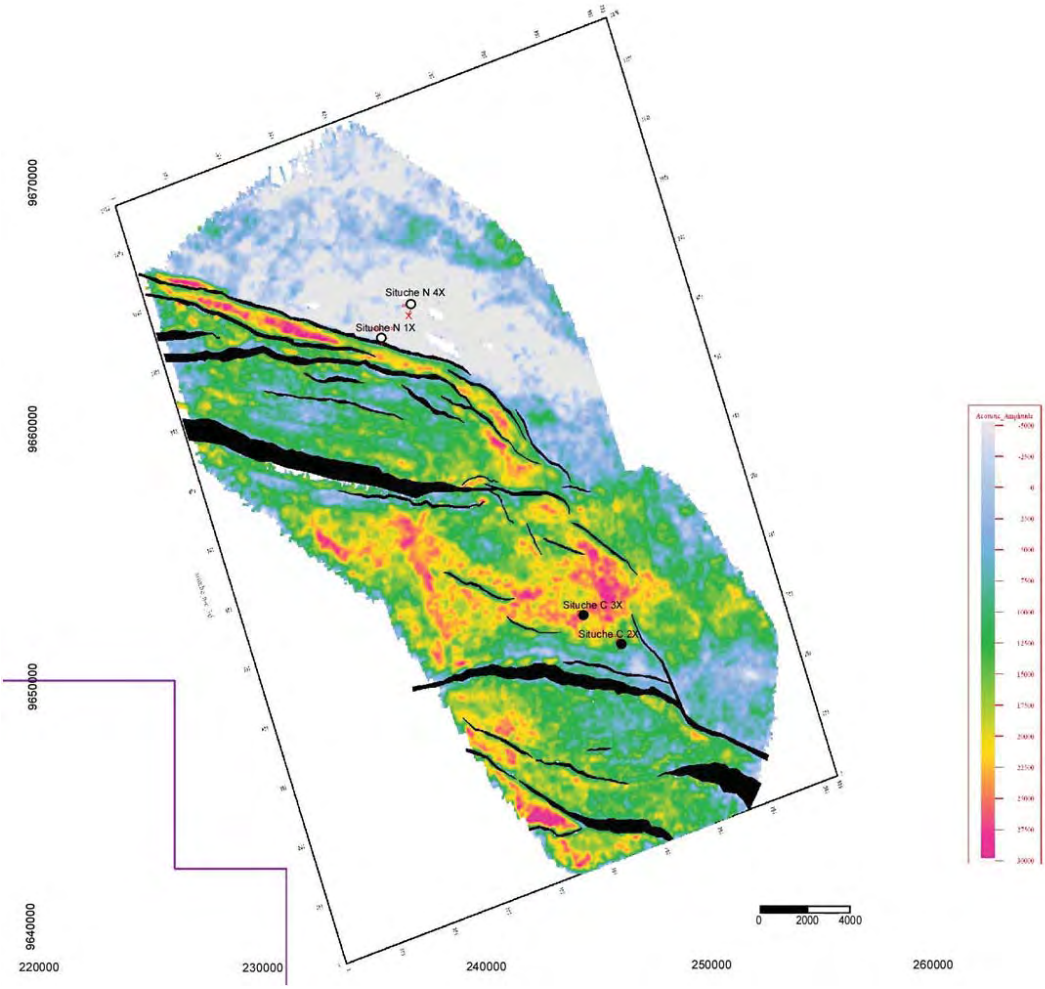

Figure 2.3.8. Amplitude map from the Campanian Vivian reflector (modified from Talisman's report, 2012) showing WNW-ESE faults oblique to the classic N-S Andean structures. The amplitude anomaly also reflects no deposition of Vivian sandstones in the northern block (north of the listric faults system), where was drilled Situche Norte 4X.

2.3.5. Summary and conclusion

The structural map (Figure 2.3.1) and the N-S cross-section R6 (Figure 2.3.9) illustrate the south-north "wedgetop-foredeep" transition of the Marañón foreland basin. In the south, the Marañón basin is still deformed and uplifted by the Subandean thick-skinned tectonics. To the north, this deformation progressively dies and the Marañón basin converts into foredeep depozone with two depocenters, where more than 4000 m of Cenozoic sediments have been passed by exploratory wells (4500 m in Situche wells). This deep part of the Marañón Basin

corresponds to the zone of maximal hydrocarbon generation (see “Situche kitchen” of Barragan et al., 2008).

As in the southern Huallaga and Moyabamba basins, deformation is linked to an intra-basement detachment with active deformation, probably also inherited from the middle Permian west-verging Gondwanide orogeny. Giant southern structure as the Loreto Hight (see R6; Figure 2.3.9) results from this west-verging basement thrust tectonics.

The Santiago structural architecture results as in the south (Huallaga and Moyabamba basins) from the interference of thick and thin-skinned salt tectonics. Salt detachment corresponds to the Late Permian regional evaporites layer that reach some thousand meters of thickness. Growth strata in the late Cretaceous infill of the Santiago Basin recorded a first stage of salt and basement tectonics. Basement thrusts uplift started at the beginning of the Cretaceous sedimentation (Cushabatay Fm.) and was progressively sealed by the late Cretaceous to early Eocene deposits.

In the north of the Marañón foredeep, the Situche structure, one of the most important oil field, is characterized by an atypical deformation. It corresponds to the late Neogene inversion of a Campanian listric normal fault branched on the late Permian salt detachment, which controlled the sedimentation of the Campanian Vivian sandstones (reservoir).

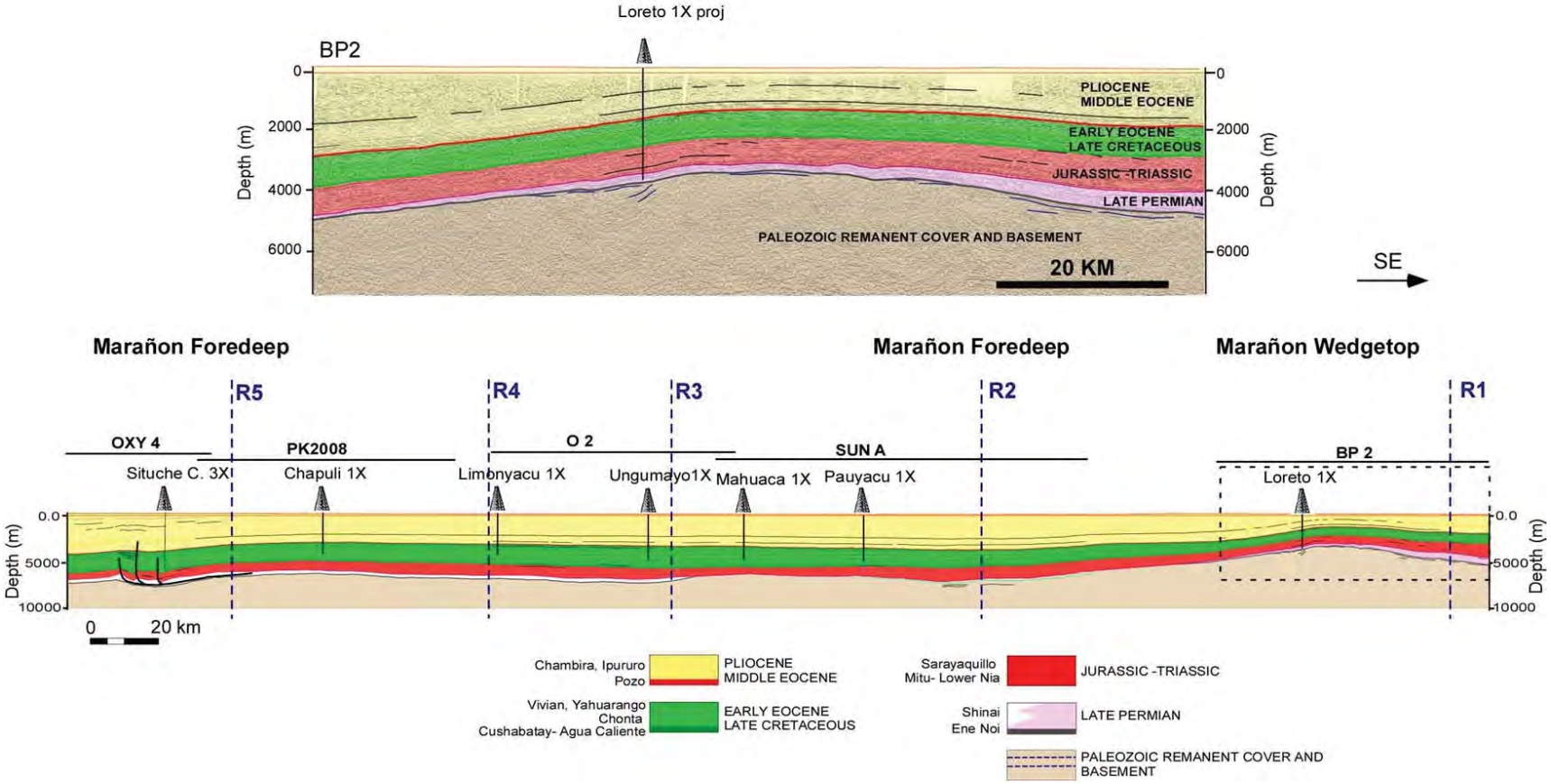

Figure 2.3.9. Latitudinal structural regional cross-section R6 through the Marañón foreland (location on Figures 2.1 and 2.3.1). Vertical scale is exaggerated.

Chapter 3: Marañón foreland basin system – the stratigraphic record

3.1. Introduction

Quantification of sedimentary basin is one of the numerous steps to understand the interaction and resulting product of the solid earth with the external envelopes of the Earth (Sediment Routing Systems; e.g. Allen, 2017). Foreland basins represent one of the repositories of the mountain building history and its evolution (Pelletier, 2007). Vertical movements and horizontal shortening of the sedimentary wedge (Vergès et al., 1998) is the main topics of interest of foreland basin studies whereas the movements of mass and flux associated to sedimentary signal represent of least studied aspect of these geological structures (Allen et al., 2013). Due to the focus of interest on the uplifted structures at the transition between the main relief and sedimentary basin, efforts have been made towards the qualification and quantification of erosion in the hinterland (e.g. Pelletier, 2007; Bayona et al., 2008).

The aim of this study is (1) to obtain a regional knowledge of the Marañón Basin sedimentary infill in terms of foreland basin evolution, (2) constrain the chronostratigraphic framework to establish this evolution, (3) estimate the sedimentary rates for each long-term sequence in the foreland basin system.

Major long-term sequences are defined from wells stratigraphic correlations and reported in three of the six regional structural cross-sections (see Figure 3.1.1. for location). Wedge-top eroded thicknesses are estimated from seismic reflection and vitrinite reflectance data. Sedimentation rates are calculated for each structural cross-section and each long-term sequence, and then in 3D at the scale of the Marañón Basin.

The geologic framework of the Marañón foreland basin system has already been detailed in the Chapter 2.

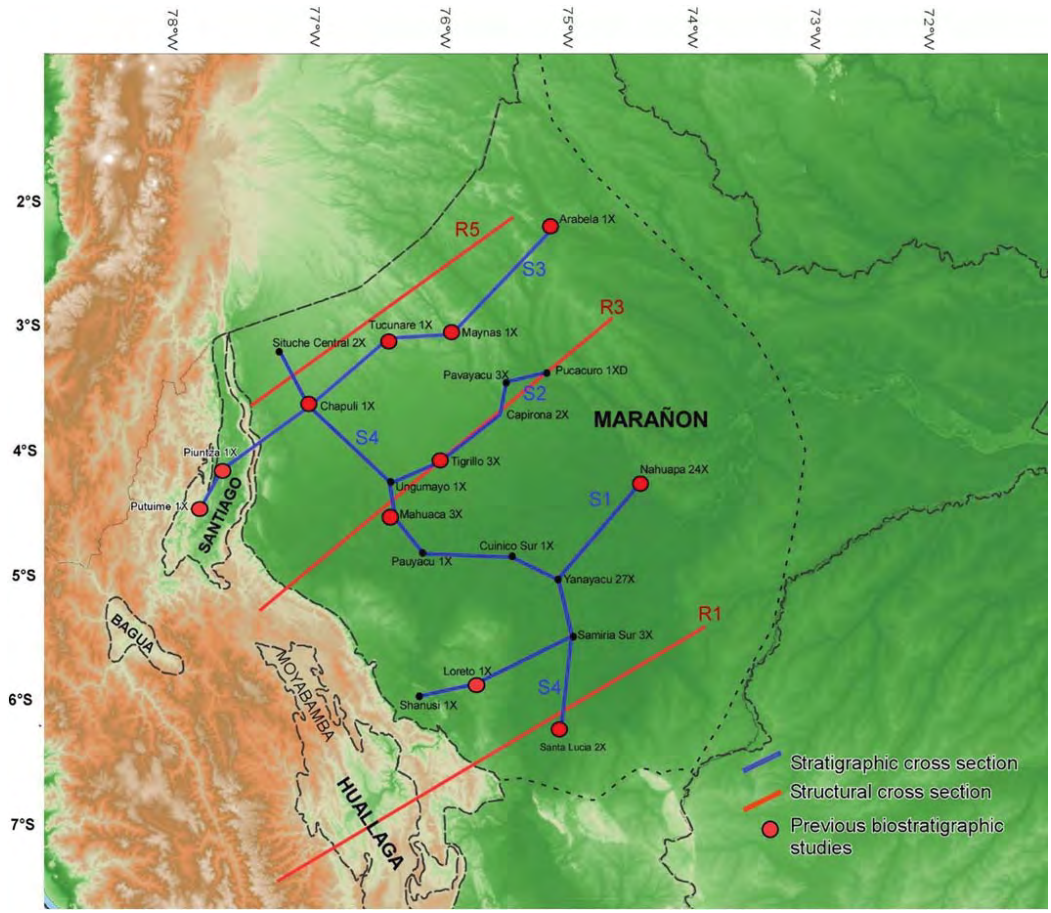

Figure 3.1. Digital Elevation Map (DEM) map with stratigraphic and structural cross sections constructed for this study. Dotted lines represent the outline of the sedimentary basins: Marañón, Santiago, Huallaga and Bagua. Biostratigraphic studies from previous reports are showed in red dots (Talisman, 2011, Conoco, 2008).

3.2. Sequential restauration of the southern Marañón foreland basin system

The southern Marañón FBS is deformed by thrust tectonics and cannot be dissociated from the Huallaga basin. Both basins belong to a wedge-top depozone (see Chapter 2). In this section, the Huallaga-Marañón FBS evolution is reconstructed and described in terms of foreland basin depozones (*sensu* DeCelles & Giles, 1996) (see Figure 1.5).

The sequential restauration has been done (Figure 3.2) from the balanced cross-section R1 (see Figure 3.1 for location) presented in the Chapter 2. It has been constructed using the Midland Valley Move software based on the flexural-slip algorithm, assuming constant bed length and thickness and constant area for salt units and Neogene infill. The cross-section is ~ 420 km long from the Eastern Cordillera to the Marañón foreland (Figure 3.1). Surface data were obtained from our field surveys and 1:100,000 INGEMMET (Instituto Nacional Geológico, Minero y Metalúrgico del Perú) geologic maps. Seismic sections and wells (see at Chapter 2, Figure 2.2.4 for location) were provided by PERUPETRO S.A. The cross-section was restored at the base of the Pozo Formation, which sealed a regional erosive planar unconformity (Christophoul et al., 2002).

The seismic reflection sections used for the construction of the balanced cross-section were presented in detail in Chapter 2. Thicknesses and stratigraphy are constrained by the Ponasillo 1X, Loreto 1X, Santa Lucia 2X, La Frontera 3X and Tamanco 1X wells (see Chapter 2, Figure 2.2.4 for location). A total horizontal shortening of 70 km has been calculated.

Along the cross-section R1, new apatite fission-tracks (AFT) dating allowed to constrain the timing of exhumation of the main thrust structures. These AFT analyses are presented in detail in Chapter 4. The results are relative to three samples collected in the Eastern Cordillera-Huallaga basin transition, the Chazuta Thrust and the Callanayacu Diapir. The three youngest cooling events ages range from 23.2 Ma in the Eastern Cordillera-Huallaga basin transition to 5.8 Ma in the Callanayacu Diapir, and show a decrease towards the east. We interpret this phenomenon as a classic in-sequence propagation and exhumation of the thrusts system. The sample collected on the Chazuta thrust gave a youngest exhumation event of 16.4 Ma, which is consistent with the AFT age of one other Jurassic sample collected in the Biabo anticline (TRU70,

see Eude et al. 2015). This cooling event age has been also interpreted as thrust related uplift.

In the sequential restoration of Figure 3.2, the initial stage of the balanced cross-section corresponds to the Middle Eocene configuration during the Pozo deposits, which sealed a regional planar unconformity (Christophoul et al., 2002). It shows that the Biabo anticline and the Cushabatay High were weakly developed at this period. Growth strata observable on the seismic (see Figure 2.2.6) and thickness variations show this deformation is Senonian to early Eocene in age. The Cushabatay High can be interpreted as the forebulge depozone separating the Marañón back-bulge depozone from the western deeding Huallaga foredeep depozone.

The second stage has been chosen to illustrate the middle Miocene foreland basin configuration and thrusts exhumation event recorded by the AFT analysis of the Chazuta thrust sample and of the Biabo anticline sample (Eude et al., 2015). The foreland basin system depozones have migrated to the east: the Huallaga basin corresponds to the wedge-top and the Marañón basin to the foredeep. This stage recorded the strongest sedimentation and must be considerate as fundamental in the understanding of the petroleum systems evolution. In the restoration, according to the study of Eude et al. (2015), we consider that the closure temperature of AFT (~110°C) corresponds to a depth of approximately 4.3 km that we replaced in the intermediate stage. In this middle Miocene stage, the Triassic rift of the Eastern Cordillera was partly inverted and the Biabo and Chazuta structures well developed. Total horizontal shortening was 25 km. In the Chazuta thrust foot-wall, a west verging basement thrust structure was uplifted and interfered with the Chazuta thrust propagation. In the center of the Huallaga wedge-top depozone, the Cenozoic charge reached more than 8 km thickness.

In the present stage, the Huallaga basin as the Marañón basin constitute a wedge-top depozone.

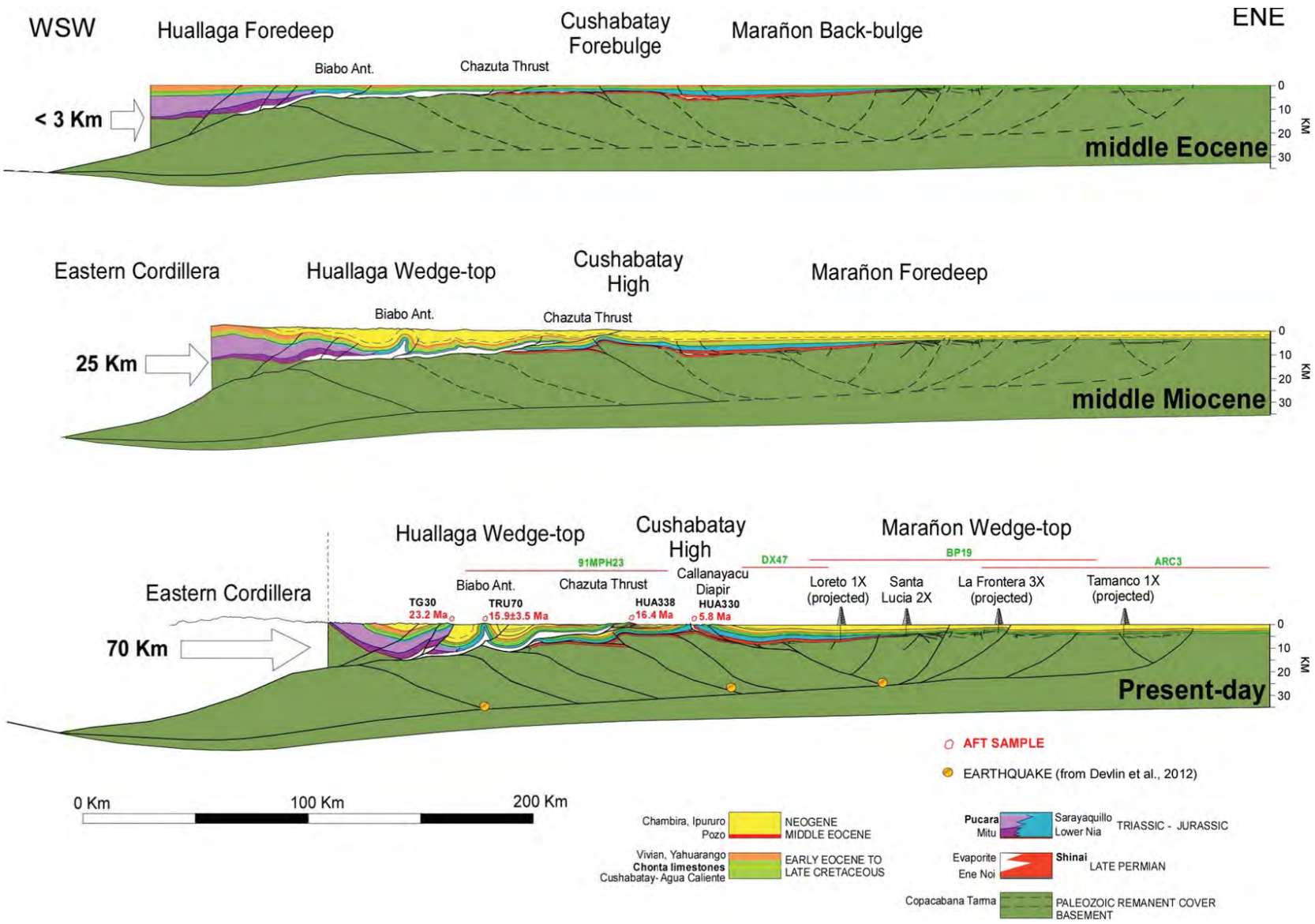

Figure 3.2. Huallaga-Marañón balanced cross-section (R1) and sequential restoration. Initial section (Middle Eocene) was obtained by flattening the base of the Pozo Formation (± 45Ma), which sealed previous deformation and configuration of the FBS. Intermediary stage corresponds to the Late Early Miocene stage and is calibrated by AFT dating in the Chazuta Thrust and Biabo Anticline. AFT samples are projected on present-day cross-section (see location on the map of Figures 3.1 and 2.2.2). AFT samples and analyses are described in the Chapter 4. CTFW: Chazuta Thrust Foot-Wall.

3.3. Stratigraphic architecture

3.3.1. Previous studies and definition of long term foreland basin sequences

We consider in this study the Albian, late Cretaceous and Cenozoic series deposited on the Andean Basal Foreland Unconformity (BFU; Figure 1.3). Albian and late Cretaceous series are formed by three fluvial to shallow marine cyclic transgressive sequences controlled by the tectonic loading of the incipient Andean orogenic wedge (Cushabatay-Raya; Agua Caliente-Chonta; Vivian-Cachiyacu-Huchpayacu; Mathalone & Montoya, 1995; PARSEP, 2001).

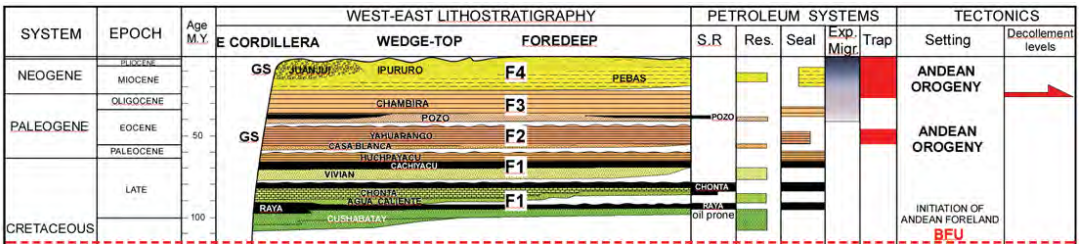

Figure 3.3. Late Cretaceous and Cenozoic sequences on the Andean Basal Foreland Unconformity (modified from Figure 1.3.). F1 to F4 appoint long term foreland basin sequences defined in this study (see below).

Main studies in the Marañón Basin have been focused in Cretaceous hydrocarbon reservoirs and source rocks, and conducted by the hydrocarbon industry. The stratigraphy in the Cretaceous sequences is therefore well defined in numerous and updated works (PARSEP, 2003; Conoco, 2008; Talisman, 2011). For the ages of the Cretaceous main sequences, we used the PARSEP synthesis updated by the biostratigraphic zones defined by Conoco (2008) and Talisman (2011) (see Annex 1).

To define the Cenozoic long term foreland basin sequences, we used the synthesis of Roddaz et al. (2010) on the Cenozoic sedimentary evolution of the Amazonian Foreland Basin System; it is illustrated by the Wheeler diagram of Figure 3.4.

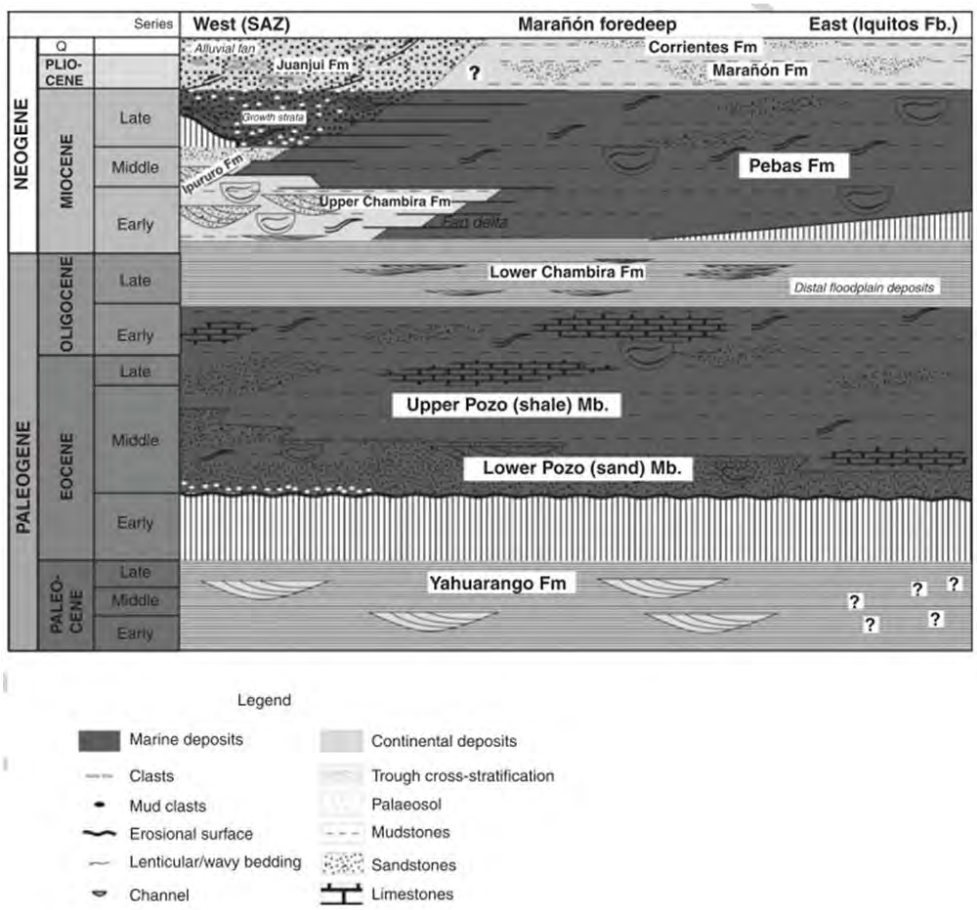

Figure 3.4. Stratigraphic overview (Wheeler diagram) of the Paleogene-Neogene northern Peruvian foreland basin (from Roddaz et al., 2010). Fm: formation; Mb: member; SAZ: sub-Andean zone.

Overall, we chose to define and quantify 4 long term sequences (see Figure 3.3):

F1 (Foreland sequence 1): Early Cretaceous (Albian) to late Cretaceous, 110-65 Ma; this is the first long term sequence on the Cushabatay Basal Foreland Unconformity; it includes the Cushabatay-Raya, Agua Caliente-Chonta and Vivian-Cachiyacu-Huchpayacu fluvial to shallow marine cyclic transgressive sequences and is capped by the basal regional unconformity of the Paleocene Casa Blanca sandstones; Albian and Maastrichtian sandstones of this first sequence have a cratonic provenance as shown by the presence of Precambrian-inherited zircon grains (Hurtado, 2017).

F2 (Foreland sequence 2): Paleocene-early Eocene, 65-45 Ma; this second long term sequence is characterized by continental environment; it recorded the first siliciclastic supply from the Andean uplift, and yield the first Cretaceous zircon grains (Hurtado et al., 2017); it corresponds probably to the distal foreland deposits of the

Marañón fold and thrust belt (presently preserved in the Western Cordillera uplift; see Mégard, 1984).

F3 (Foreland sequence 3): Middle Eocene-Oligocene, 45-23 Ma; this third long term sequence overlies the Basal Pozo regional erosional unconformity, interpreted as an unloading orogenic period (Christophoul et al., 2002). This stage of the FBS is represented in the sequential restauration of the Figure 3. 2.. The detrital zircon grains are sourced from the Cenozoic volcanism and the uplifting of the Western Cordillera (Hurtado et al., 2017) (see location of Western Cordillera in Figure 1.2).

F4 (Foreland sequence 4): Neogene, 23-0 Ma; this last long term sequence recorded an acceleration of the deformation and sedimentation represented in the sequential restauration of the Figure 3.2, and is contemporaneous with the uplift of the Eastern Cordillera as confirmed by zircon grains provenance (Hurtado, 2017). This period during the Miocene is characterized by lacustrine conditions alternating with episodes of fluvial drainage and marginal marine influence (Hoorn et al., 2010; Jaramillo et al., 2017), and finally by a complex deltaic to fluvial environment.

3.3.2 Wells stratigraphic correlations

The main objective of the stratigraphic correlations is to identify the boundaries of the regional sequences defined above (F1, F2, F3 and F4; Figure 3.3) that will then be carried over regional structural cross sections.

For the elaboration of the regional stratigraphic cross-sections (Figures 3.5 to 3.8), lithologic and stratigraphic logs of 21 wells have been constructed from the review of electric and mud logs, and lithologic and biostratigraphic information from the PERUPETRO data bank. We have used in particular the updated biostratigraphic zones defined by Conoco (2008) and Talisman (2011) (see Annex 1).

The four regional stratigraphic cross-sections presented allow to characterize the whole Marañón basin (see map of Figure 3.1). Each stratigraphic cross-section has been flattened at the regional Basal Pozo erosional unconformity, which constitutes the base of the long term sequence F3 and also the key horizon for the restoration of the balanced cross-sections (see Chapter 2). Furthermore, the Basal Pozo unconformity is easily identifiable in seismic sections and well logs.

The S1 wells stratigraphic cross-section (Figure 3.5) is located close to the R1 structural cross-section in the southern part of the Marañón basin. In our foreland basin structural model, this area is considered as part of a wedge-top depozone (see Chapter 2), particularly in the Loreto region where the Neogene F4 (Foreland sequence 4) has been uplifted and eroded. The Albian-late Cretaceous F1, which recorded the initiation of the foreland basin system (FBS), is formed by 3 fluvial to shallow marine transgressive sequences (described previously) that gradually thickens towards de SW. Total thickness of F1 varies between 900 and 1500 m. The Turonian carbonate succession of the Chonta Formation is missing in this part of the Marañón Basin. The base of the Vivian sandstones is clearly identified as an erosional unconformity that corresponds to a key reflector in seismic sections (see next section 3.3.3). The Paleocene-early Eocene F2 (Yahuarango Fm.) is poor developed in this part of the Marañón basin, which is probably due to a stronger erosion of the regional Basal Pozo unconformity. F2 is formed by siliciclastic continental sediments that recorded an important change in the foredeep environment. The middle Eocene to Oligocene F3 recorded the evolution of a second Marañón foreland basin system that installed on the Basal Pozo regional erosional unconformity. The Pozo Formation is characterized by a marine transgression. During the Chambira deposits, the Marañón basin seems to evolve to a typical foredeep depozone in a complex environment alternating between marginal marine and fluvial environments. F4 is only preserved east of the Loreto structure (more than 2000 m), where it is close to the current foredeep depozone. The presence of glauconite in F4 confirms Miocene marine incursions (Pebas Fm.) in this part of the Marañón basin.

The S2 stratigraphic cross-section (Figure 3.6) is located on the R2 structural cross-section in the center part of the Marañón Basin. The Albian-late Cretaceous F1 seems more developed with the apparition of the Chonta limestone in the center of the section. Thicknesses variation is difficult to evaluate because the western wells do not reach the base of F1 (BFU). The Basal Vivian erosional unconformity is still evident and overlain by fluvial sandstones. The F2 Paleocene-Lower Eocene continental series is more developed than in the S1 cross-section, and thickens toward the SW. It could characterize a distal foredeep. The middle Eocene to Oligocene F3 is comparable with that of S1. The Neogene F4 represents the depocenter of the current foredeep depozone. It evolved from lacustrine and marginal marine environments (Pebas Fm.) to fluvial deposits (Marañón Fm.). Maximum thickness (2600 m) is reached in the Tigrillo-3X well, in the central part of the basin.

The S3 wells stratigraphic correlations (Figure 3.7) cross the northern Marañón foredeep basin and the Santiago wedge-top basin (see Chapter 2), where part of the F4 has been uplifted and eroded. F1 shows an important development of the Chonta carbonates. The Cretaceous basal foreland unconformity has not been reached by the wells, except in the Santiago wedge-top, where F1 overlies directly late Permian evaporites (see structural cross-section of Figure 2.3.4). The Paleocene-early Eocene continental foredeep deposits of F2 are particularly developed in this cross-section. The depocenter is located in the current Santiago wedge-top basin, where some levels with glauconite show a marine influence. The eastern border of F2 is eroded by the Basal Pozo regional unconformity. F3 that overlies the Basal Pozo erosional event does not present important variations compared to others stratigraphic cross-sections S1 and S2. In this part of the basin, the Basal Pozo Formation includes tufaceous sands that have been dated at 43.0 ± 9.9 Ma and 35.1 ± 4.4 Ma (Hermoza, 2004). East to the Santiago wedge-top, F4 represents the current foredeep and reaches 2100 m of thickness. Marine incursions of the Pebas Fm. are still recorded in F4 infill.

The S4 (Figure 3.8) is a northwest to southeast stratigraphic cross-section showing lateral variations of the 4 foreland long term sequences in the Marañón Basin. It illustrates the transition from the current southern Marañón wedge-top to the northern Marañón foredeep also expressed in the structural cross-section R6 of the Figure 2.3.9. The Albian-late Cretaceous sequence F1 does not present lateral global thickness variation, but shows the development of the Chonta limestone towards the north. The Basal erosional unconformity of the fluvial Vivian sandstones is visible in all the cross-section. The Paleocene-early Eocene sequence F2 thickens towards the NW; it is probably eroded to the SE by the regional Basal Pozo unconformity. This regional erosional unconformity, already represented in the sequential restoration of Figure 3.2, seems to mark the end of the first Marañón Foreland Basin System (MFBS). The F3 and F4 sequences, influenced by marine incursions during a long period before to become exclusively fluvial, represents the second MFBS that is still active. F3 as F4 deposits are thickening toward the northern current foredeep depozone.

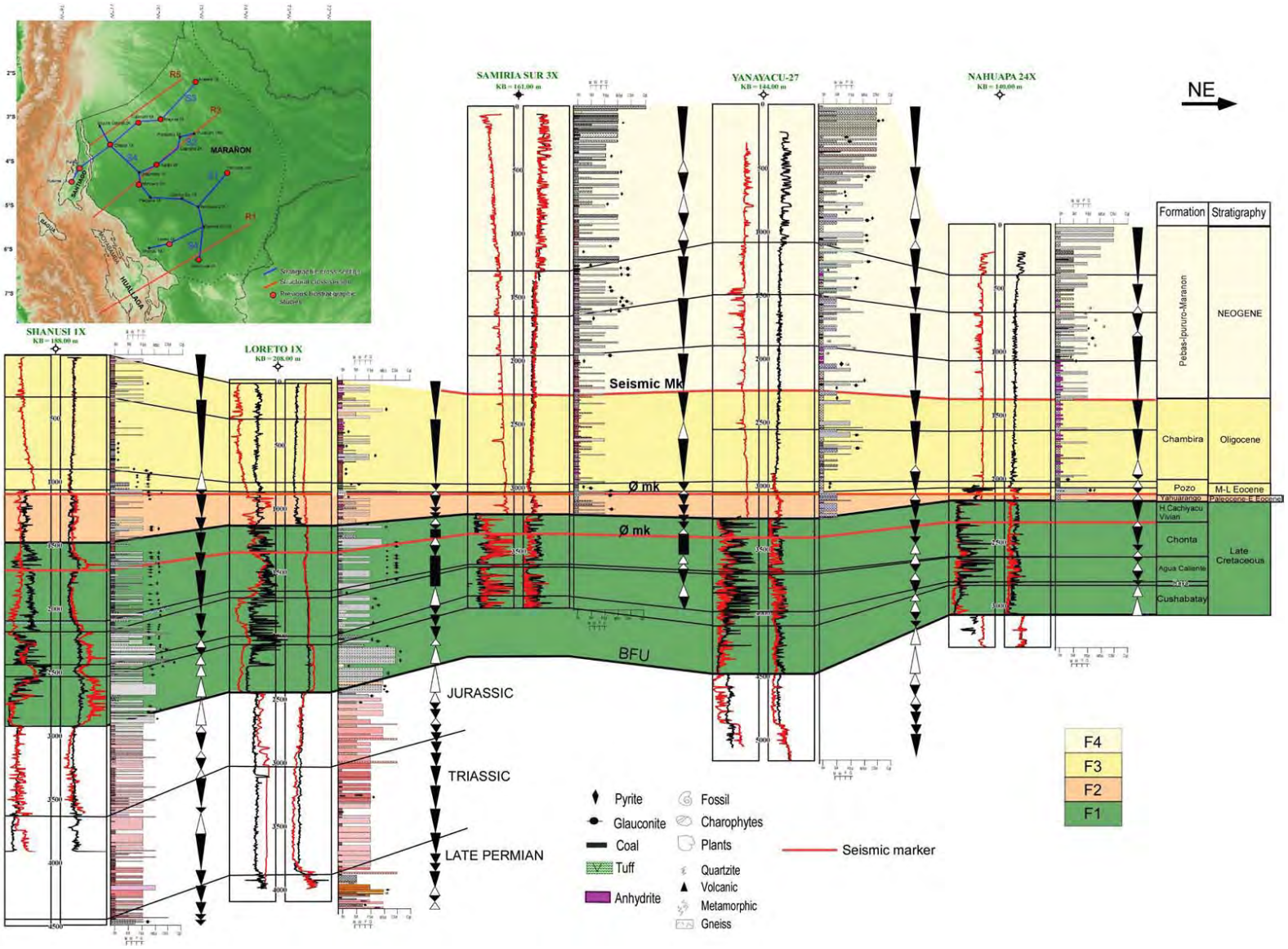

Figure 3.5. SW- NE wells stratigraphic correlation S1 (location on Fig. 3.1) crossing the southern Marañón basin, and flattened at the regional Basal Pozo erosional unconformity. BFU: Basal Foreland Unconformity. Depth is in meters.

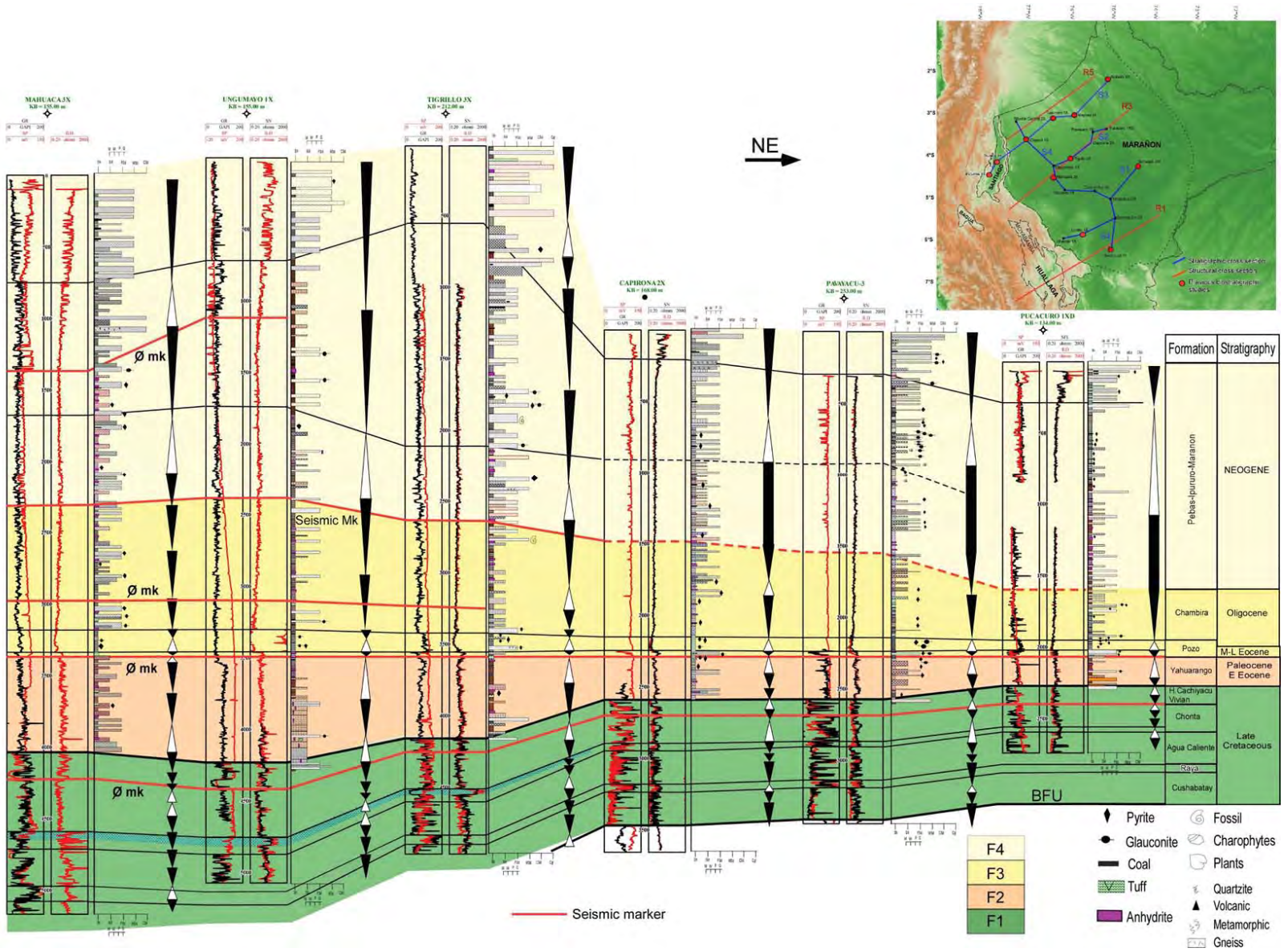

Figure 3.6. SW- NE wells stratigraphic correlation S2 (location on Fig. 3.1) crossing the Marañón basin, and flattened at the regional Basal Pozo erosional unconformity. BFU: Basal Foreland Unconformity. Depth is in meters.

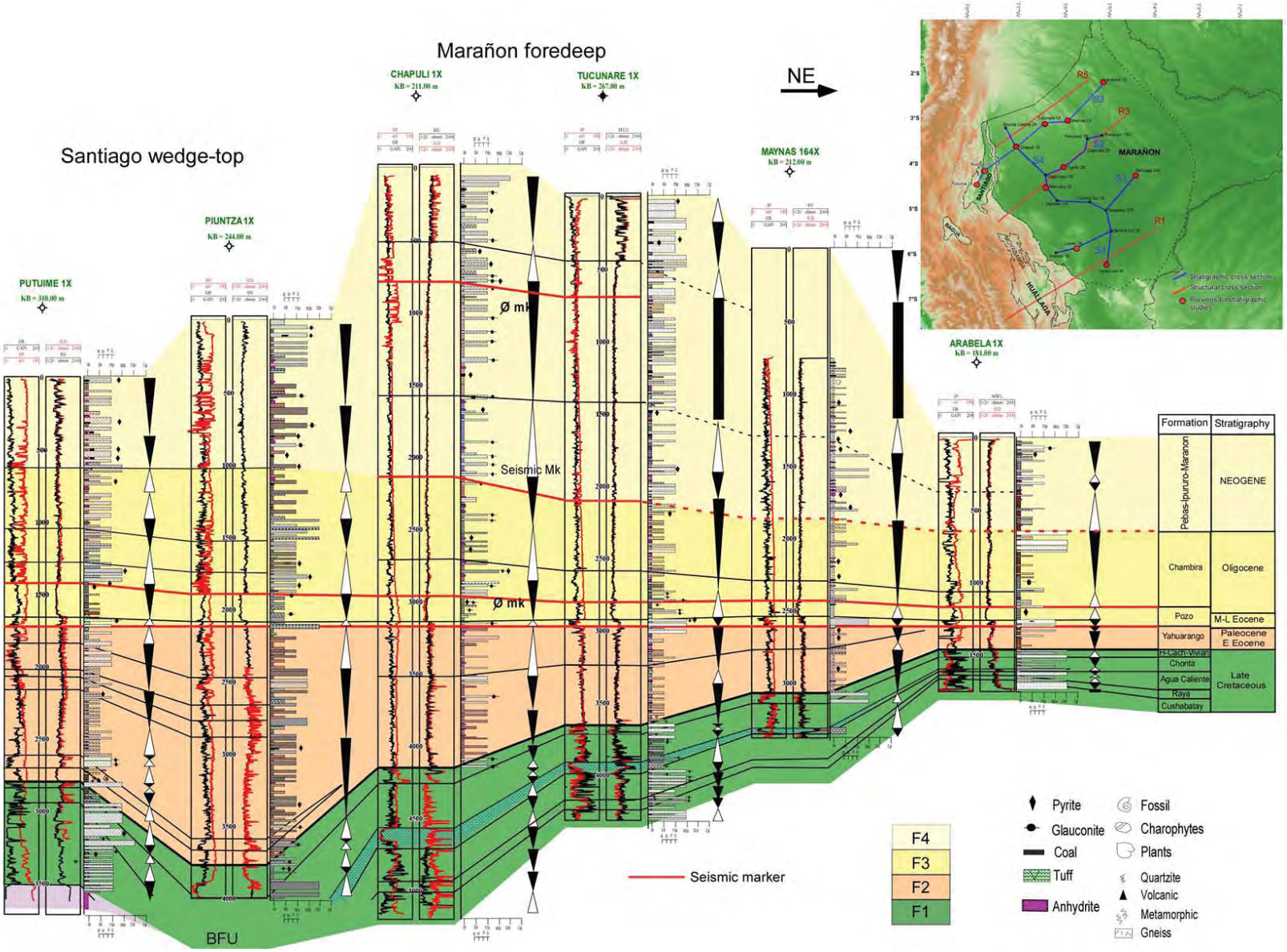

Figure 3.7. SW- NE wells stratigraphic correlation S3 (location on Fig. 3.1) in the Santiago and northern Marañón basin, and flattened at the regional Basal Pozo erosional unconformity. BFU: Basal Foreland Unconformity. Depth is in meters.

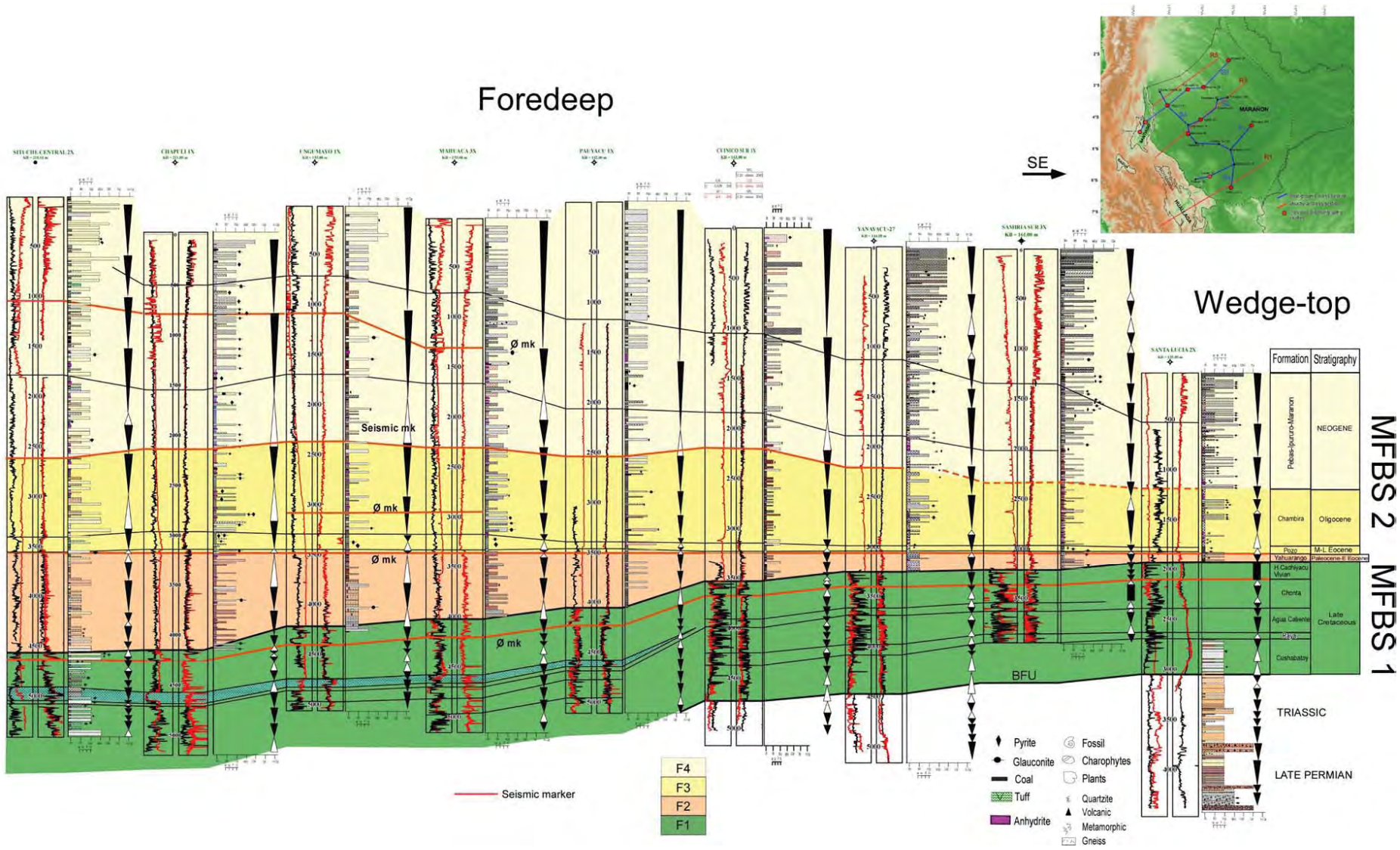

Figure 3.8. NW- SE wells stratigraphic correlation (S4, location on Fig. 3.1) crossing the Marañón basin, and flattened at the regional Basal Pozo erosional unconformity. BFU: Basal Foreland Unconformity. MFBS: Marañón Foreland Basin System. Depth is in meters.

3.3.3 Seismic and porosity logs calibration

Long term foreland basin sequences (F1 to F4, see above) boundaries need to be identified in seismic sections to be plotted in our structural regional cross-sections and then compute 2D sedimentation rates. For this purpose, we combine log porosity evolution of some key wells of the regional stratigraphic correlations (see above) with selected seismic sections. First, seismic sections were converted in depth using the process explains in method of Annex 2. Then, we calibrate seismic reflectors with log porosity discontinuities and stratigraphic boundaries of long term foreland sequence determined in the previous section 3.3.2. The porosity calculation for each well has been made using the method explains in Annex 2.

We present here some seismic examples calibrated by the more significant wells.

The seismic section DX-31 (Figure 3.9, see Figure 3.1 for location) is located in the southern part of the Marañón Basin. It shows the Loreto structure and is calibrated by the Loreto 1X well that crossed F2, F3, F4, and pre-cretaceous sequences. In the well, F4 is eroded due to the recent uplift of the Loreto basement mega-structure (wedge-top of southern Marañón Basin). Erosional unconformities of the base of F1 (Cushabatay BFU), Basal Vivian (last fluvial sequence of F1) and F3 (Basal Pozo) are clearly marked in porosity chart. The basal F4 sequence has been preserved in the Loreto flanks and can be correlated with seismic thanks to the INGEMMET geologic map. The limit between F2 and F3 is not clear in the porosity chart, but it is well defined in the stratigraphic log. The same is the case for all the seismic sections.

The seismic section Sun 16 (Figure 3.10, see Figure 3.1 for location) is located in the center part of the Marañón Basin (foredeep). It is calibrated by the Mahuaca-1X well that crossed the sequences F1, F2, F3 and F4. The Cushabatay BFU has not been reached by the well, but as in the southern part of the basin the Basal Vivian erosional unconformity in F1 is clearly evidenced in the porosity chart. The bases of F3 and F4 are also clearly evidenced both in seismic and porosity chart. Two new discontinuities appear in the porosity chart in F3 and F4. The intra-F3 discontinuity corresponds probably to the limit between the Pozo Fm. and the Chambira Fm. and can be identified in the seismic. The intra-F4 discontinuity, although strong in the porosity chart, does not appear in the seismic section and is difficult to track at regional scale due to highly discontinuous seismic facies.

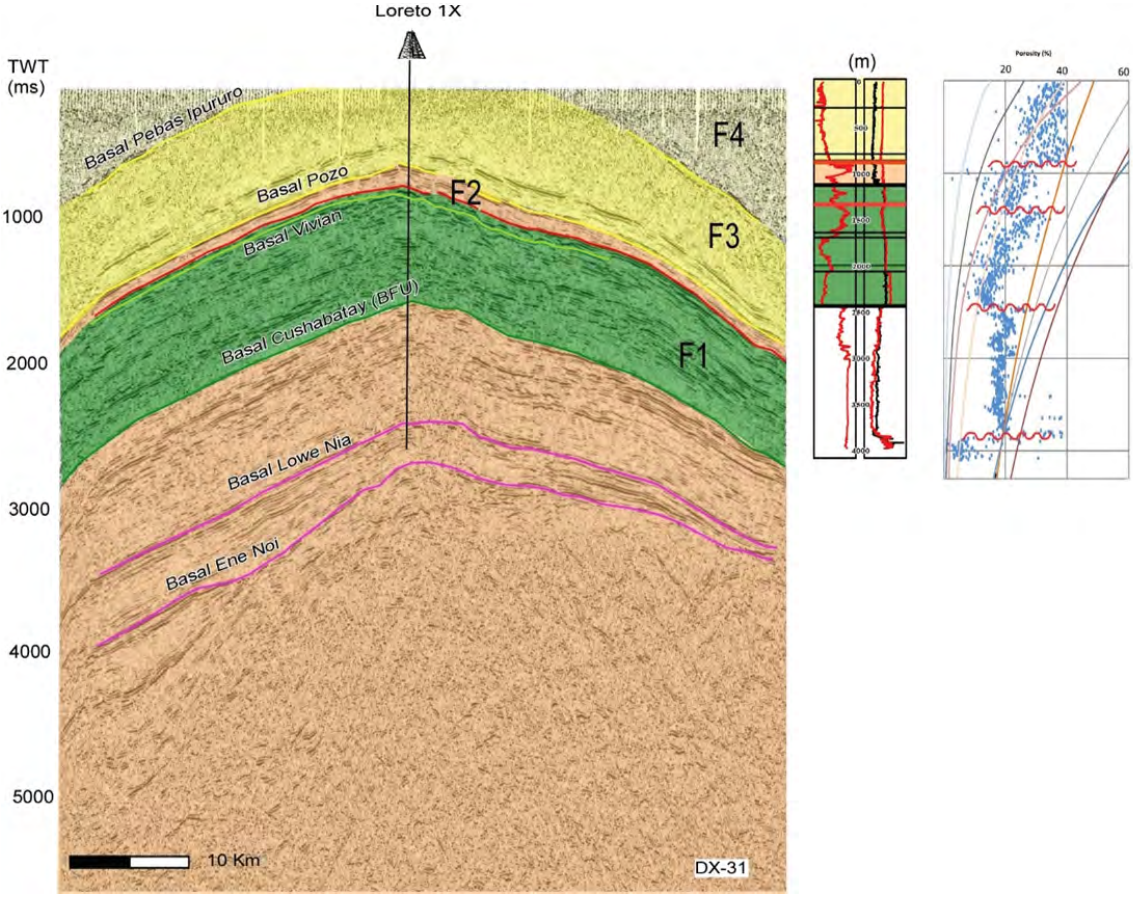

Figure 3.9. Seismic section DX-31 in the Loreto antiform (see Fig. 3.1 for location) and its correlation with well log and porosity chart showing mean unconformities and long-term foreland basin sequences (see Figure 3.3). BFU: Basal Foreland Unconformity.

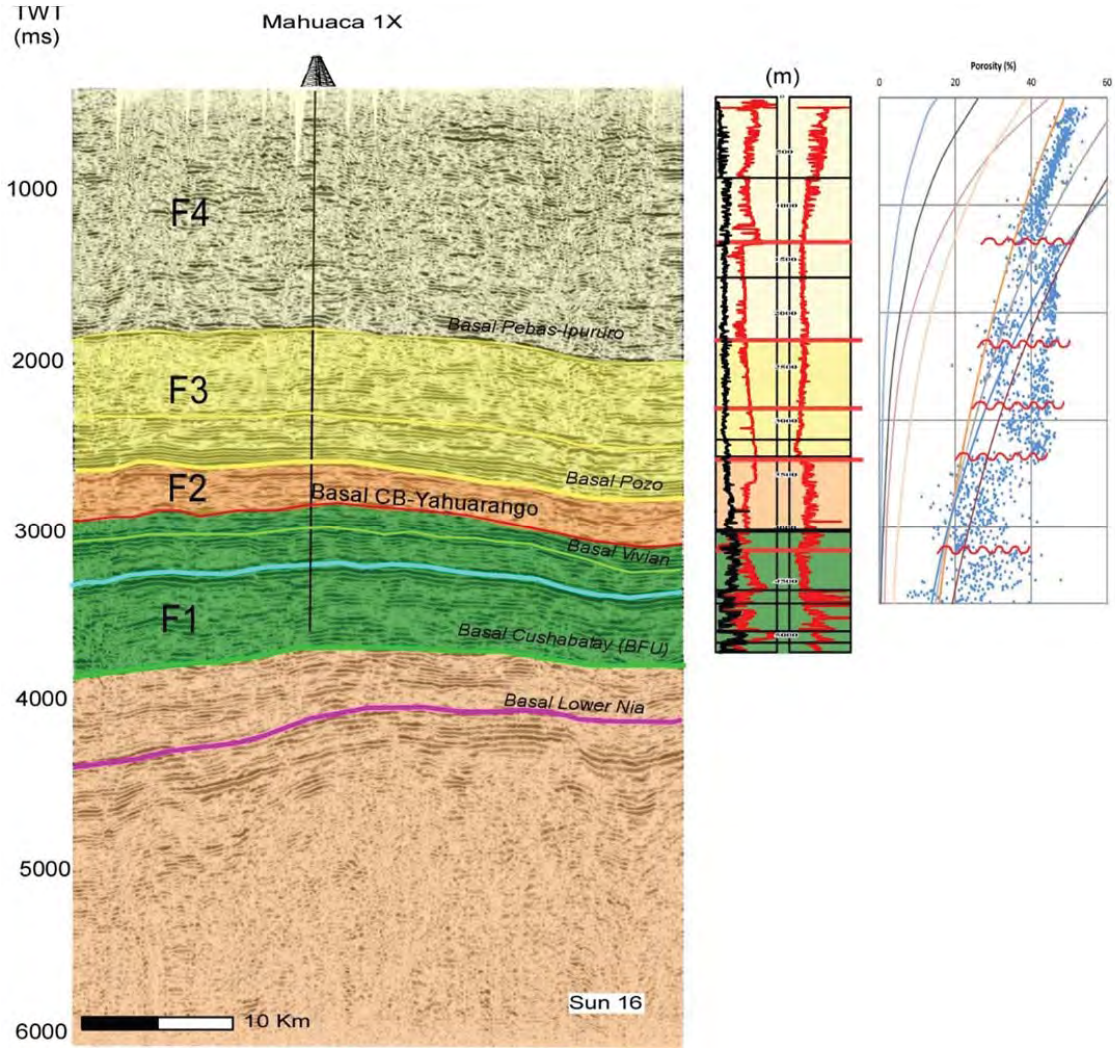

Figure 3.10. Seismic section Sun 16 in the Mahuaca area (see Fig. 3.1 for location) and its correlation with the well log and porosity chart showing mean unconformities and long-term foreland basin sequences (see Figure 3.3). BFU: Basal Foreland Unconformity.

The inline 194 section was obtained from the 3D seismic cube of the Tucunare area in the northern part of the basin (Figure 3.11, see Figure 3.1 for location). It is calibrated by the Tucunare-1X well that crossed sequences F1, F2, F3 and F4 without reaching the Cushabatay BFU. The high seismic resolution allows highlighting the stratigraphic long-term sequence discontinuities. The porosity chart shows the Basal Vivian and Basal Pozo erosional unconformities, the limit between the Pozo Fm. and the Chambira Fm., and the intra-F4 discontinuity always identified in the Mahuaca section. The limit between F1 and F2 is not clear in the porosity chart, but it is well defined in the stratigraphic log.

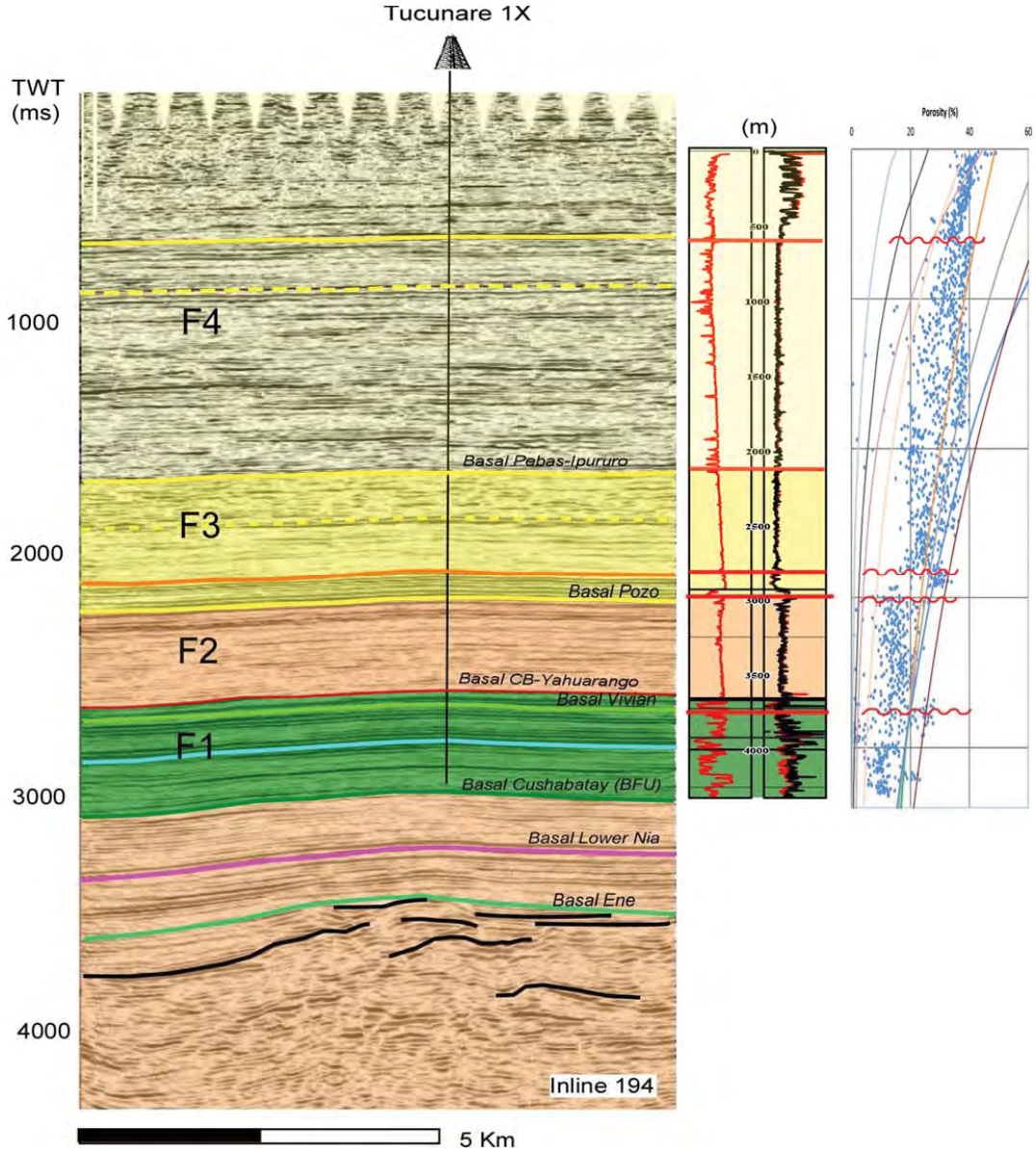

Figure 3.11. Inline 194 section from the 3D seismic cube of the Tucunare area (see Fig. 3.1 for location) and its correlation with well log and porosity chart showing mean unconformities and long term foreland basin sequences (see Figure 3.3). BFU: Basal Foreland Unconformity.

The Situche seismic section “Inline 173” is also extracted from a 3D seismic cube and presents high resolution (Figure 3.12, see Figure 3.1 for location). The porosity chart of the Situche C. 2X highlight the Vivian (intra-F1), Pozo (F3) and Pebas (F4) basal unconformities and the limit between the Pozo Fm. and the Chambira Fm. It also shows two intra-F4 discontinuities difficult to interpret at the stage of our study.

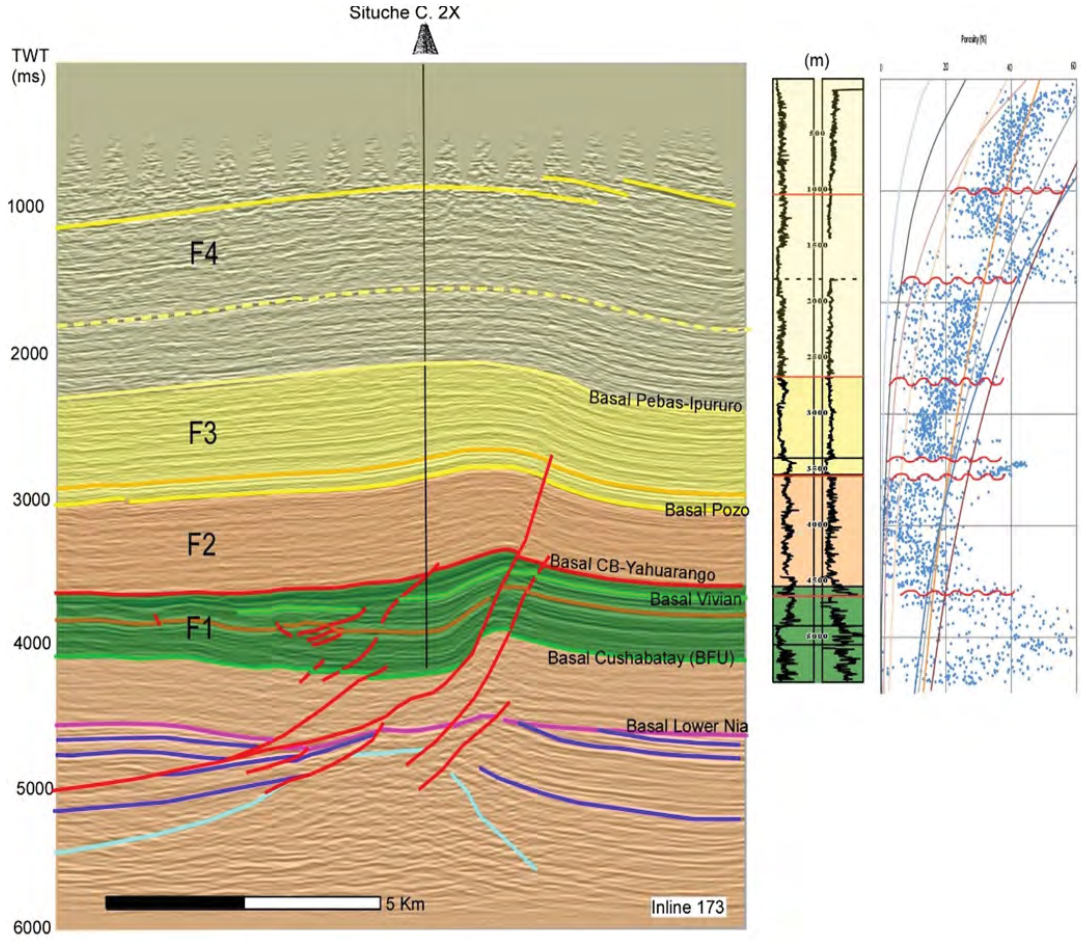

Figure 3.12. Inline 173 from the 3D seismic cube of the Situche area (see Fig. 3.1 for location) and its correlation with well log and porosity chart showing mean unconformities and long-term foreland basin sequences (see Figure 3.3). BFU: Basal Foreland Unconformity.

3.4. Quantification of sedimentation rates in the foreland basin system

3.4.1. Long term foreland basin sequences in structural cross-sections

The structural framework was analyzed using regional cross-sections that were described in Chapter 2. Here, the aim is to combine regional structural cross-sections and previous stratigraphic analysis to represent 2D long-term foreland basin sequences F1, F2, F3 and F4 that let us to quantify the flux of sediments since the late Cretaceous period to nowadays. We have selected the three most representative structural cross-sections R1, R3 and R5 (see location in Figure 3.1) to represent the distribution of the long-term

foreland sequences and compute 2D sedimentation rates. The cross-section R1 through the Huallaga-Marañón FBS shows that both basins correspond today to wedge-top depozones and have been submitted to strong erosion (Figure 3.2). This wedge-top eroded thickness will be taking into account in our sediment budget.

The first step was to delineate the 4 foreland basin long term sequences (see Figure 3.3) in the cross-sections R1, R3 and R5 using the boundaries defined with seismic and wells in the previous section 3.3.3. The delineation of these long-term sequences is represented in Figures 3.13 and 3.14, from the southern wedge-top to the northern foredeep of the Marañón Basin.

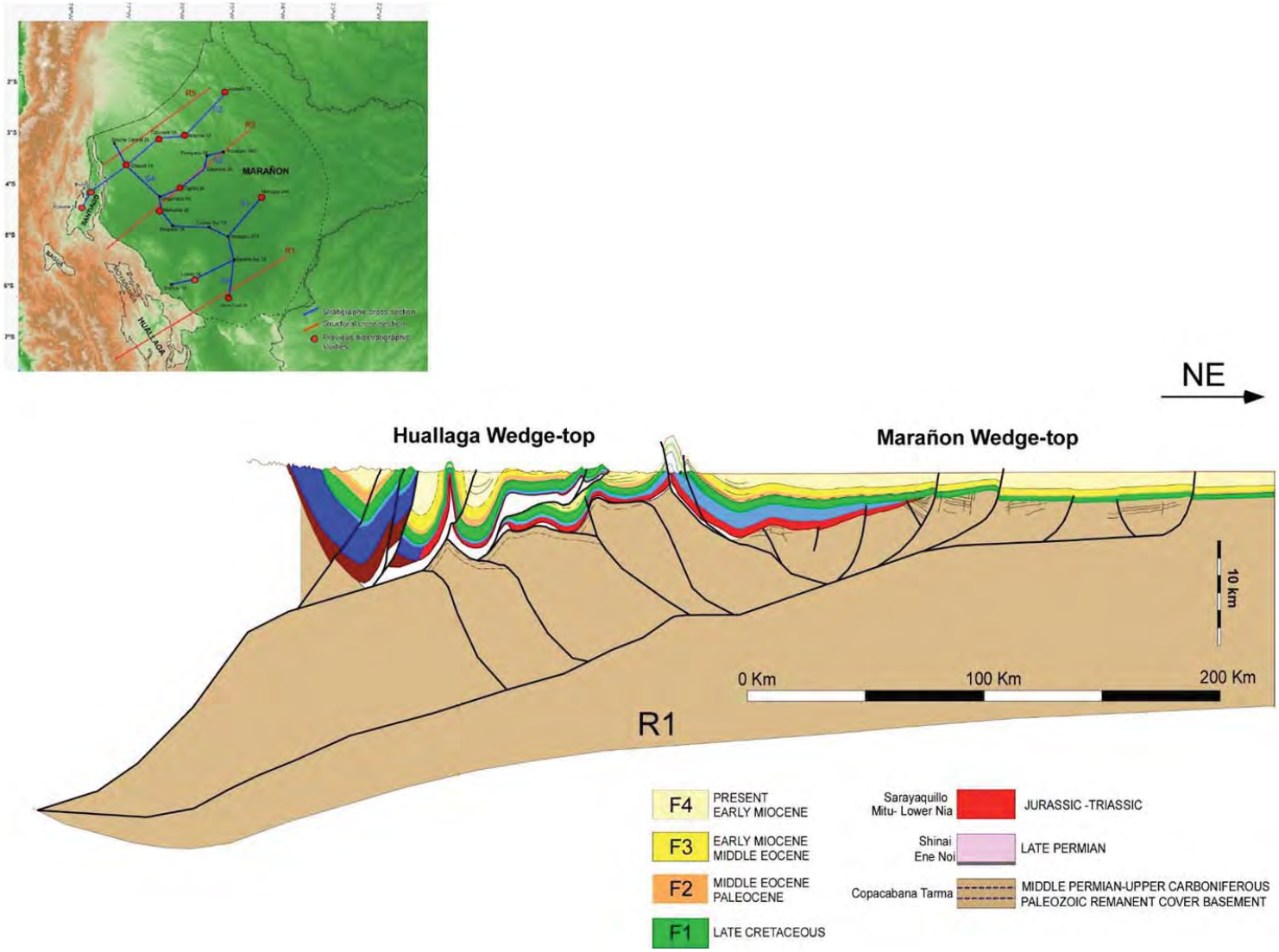

Figure 3.13. Regional structural cross sections R1 (location in Fig. 3.1) showing long term foreland basin sequences (F1, F2, F3 and F4). Vertical scale exaggeration

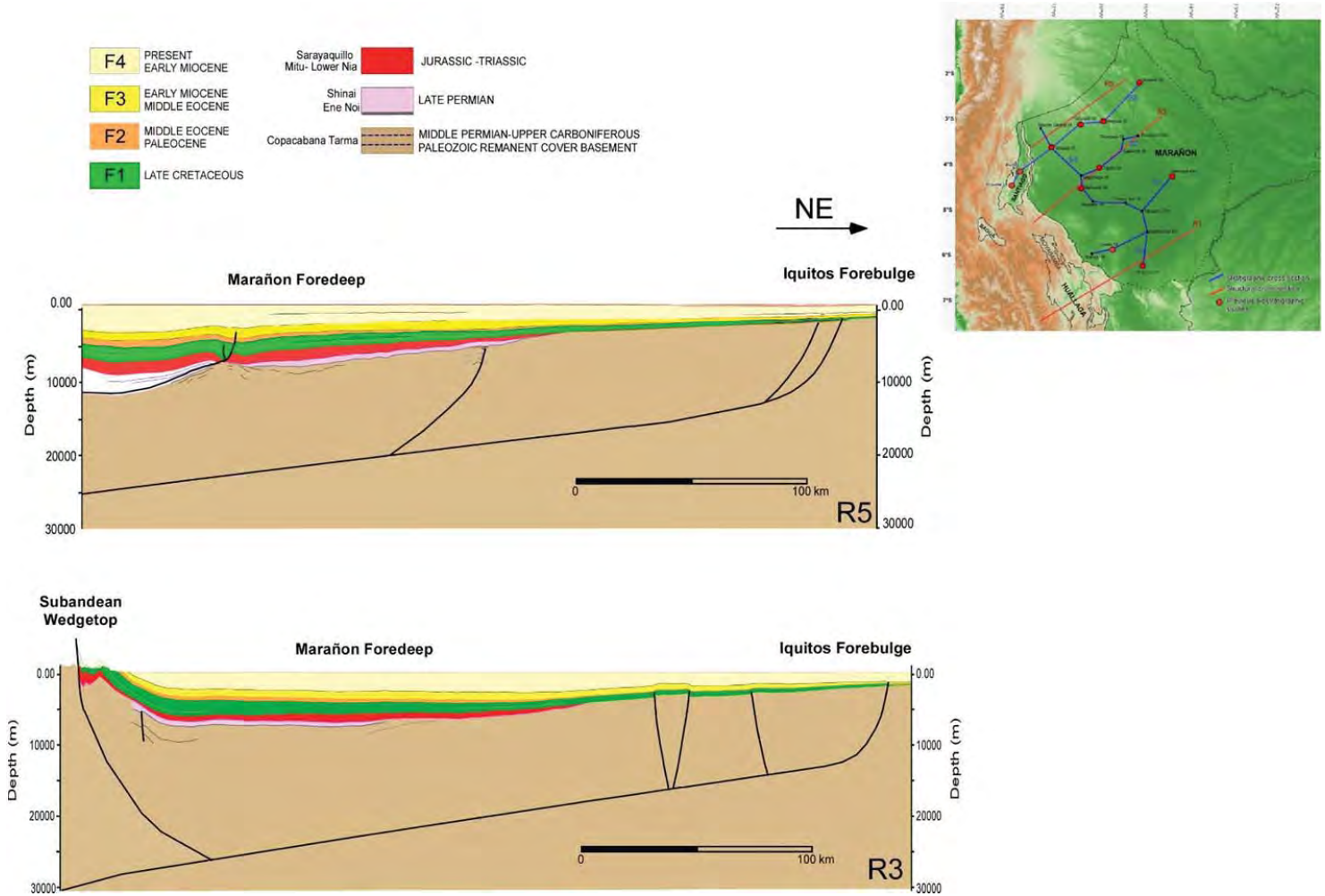

Figure 3.14. Regional structural cross sections R1 (location in Fig. 3.1) showing long term foreland basin sequences (F1, F2, F3 and F4). Vertical scale exaggeration.

3.4.2. Wedge-top eroded thicknesses

The wedgetop depozones are deformed and therefore subject to syn-orogenic erosion. To estimate cumulative wedge-top eroded thicknesses, especially in the southern Marañón-Huallaga FBS, we reconstructed the top Neogene paleosurface profiles using source rock maturity data as vitrinite reflectance (Ro). These erosional profiles have been computed in the three cross-sections R1, R3 and R5 by means of 1D thermal PetroMod (Schlumberger software) modeling in most of the wells along the studied cross-sections. A pseudo well (fictive) constructed from outcrops Ro analyses has been also computed in the Huallaga basin.

Vitrinite is one of the major elements of coal or organic matter in sedimentary rocks. The Ro (vitrinite reflectance) value is a sensitive geo-thermometer for sedimentary rocks used by the petroleum industry to study the maturity of the source rock, which is a function of the kinetic transformation of the organic matter, commonly associated with burial process. The Ro value depends on temperature and is irreversible (Sweeney and Burnham, 1990). The relation between Ro values and depth provides additional information about the thermal history of the basin and the history of the sedimentary burial. Ro values are converted in maximum reached temperature using the algorithm of Sweeney and Burnham (1990) using the software PetroMod of Schlumberger. For each well or fictive well, the maximum sedimentary burial can thus be computed in 1D thermal PetroMod modeling and an eventual eroded thickness reconstructed.

Vitrine Reflectance (Ro) data used for the 1D PetroMod modeling along R1, R3 and R5 are presented in Annex 3.

Along the R1 Huallaga-Marañón wedgetop cross-section (Figure 3.15), the PetroMod modeling allowed to reconstruct the top Neogene paleosurface profile, which shows that eroded thickness is significant and can reach 2 km. The maximum Cenozoic sedimentary burial reached 8 km in the deeper part of the Huallaga wedgetop depozone, and 4 km in Marañón. The top Neogene paleosurface profile shows that the southern part of the Marañón Basin is strongly uplifted and eroded. Wedgetop sediments are probably transported and deposited more to the north. According to the AFTA results and sequential restoration of Figure 3.2, this erosion could start around 6 My (Cushabatay High AFTA)

and is probably partly due to the eastwards thick-skinned deformation propagation combined with the Fitzcarrald Arch uplift (Espurt et al., 2007).

Along the cross-sections R3 and R5 (Figures 3.16 and 3.17), the top Neogene paleosurface has been only reconstructed in the eastern part of the Marañón Basin. In R3, the erosion thickness of the Neogene is negligible, which confirms that R3 represents in a large part the foredeep depozone of the Marañón Basin. In R5, the Neogene is weakly eroded due to the Iquitos forebulge uplift. The foredeep depozone is located in the western part in the Situche area.

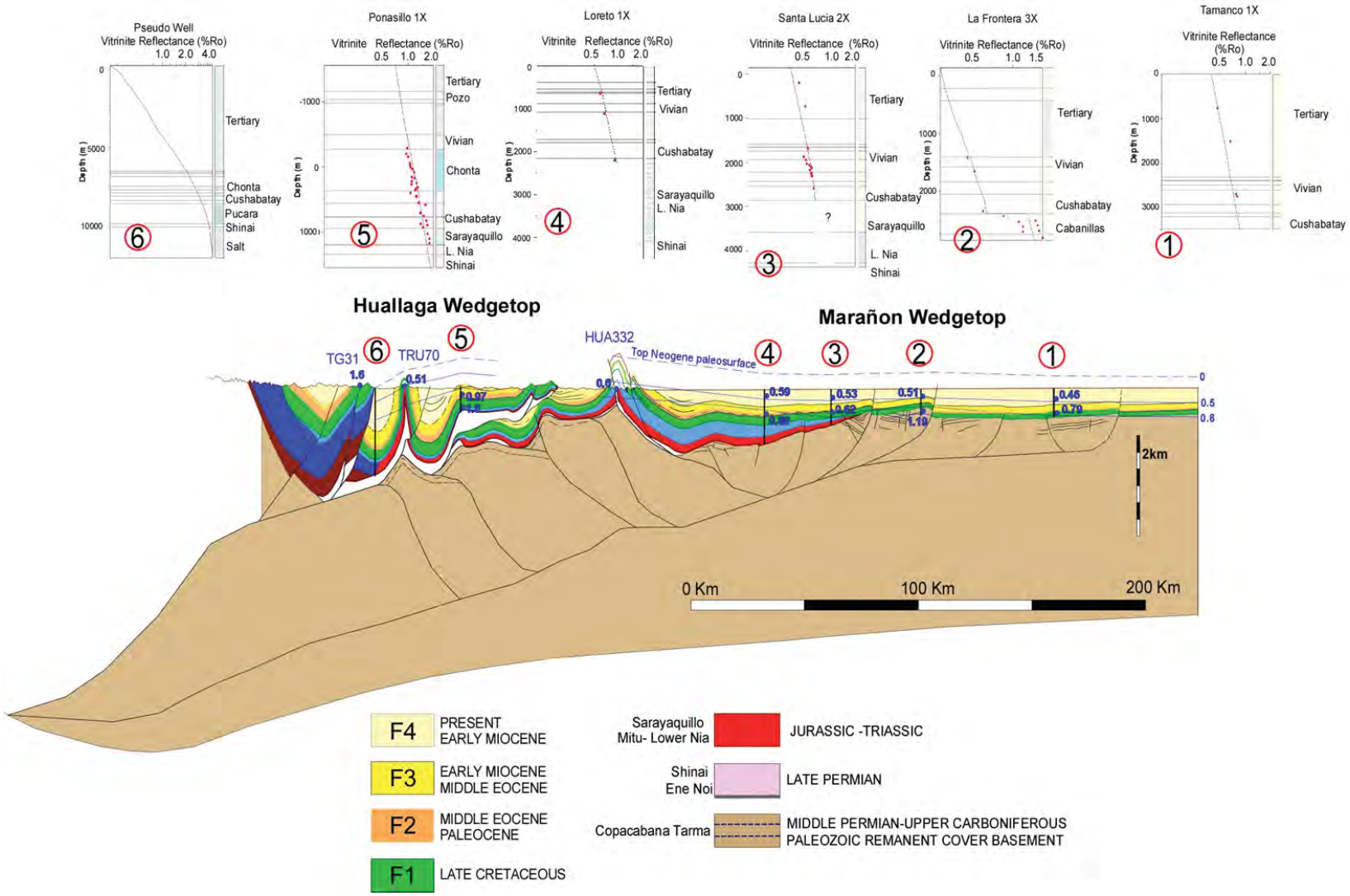

Figure 3.15. Regional structural cross sections R1 (location in Fig. 3.1) showing long term foreland basin sequences (F1, F2, F3 and F4) and the top Neogene paleosurface profile computed from 1D PetroMod modeling (see text). Vertical scale exaggeration.

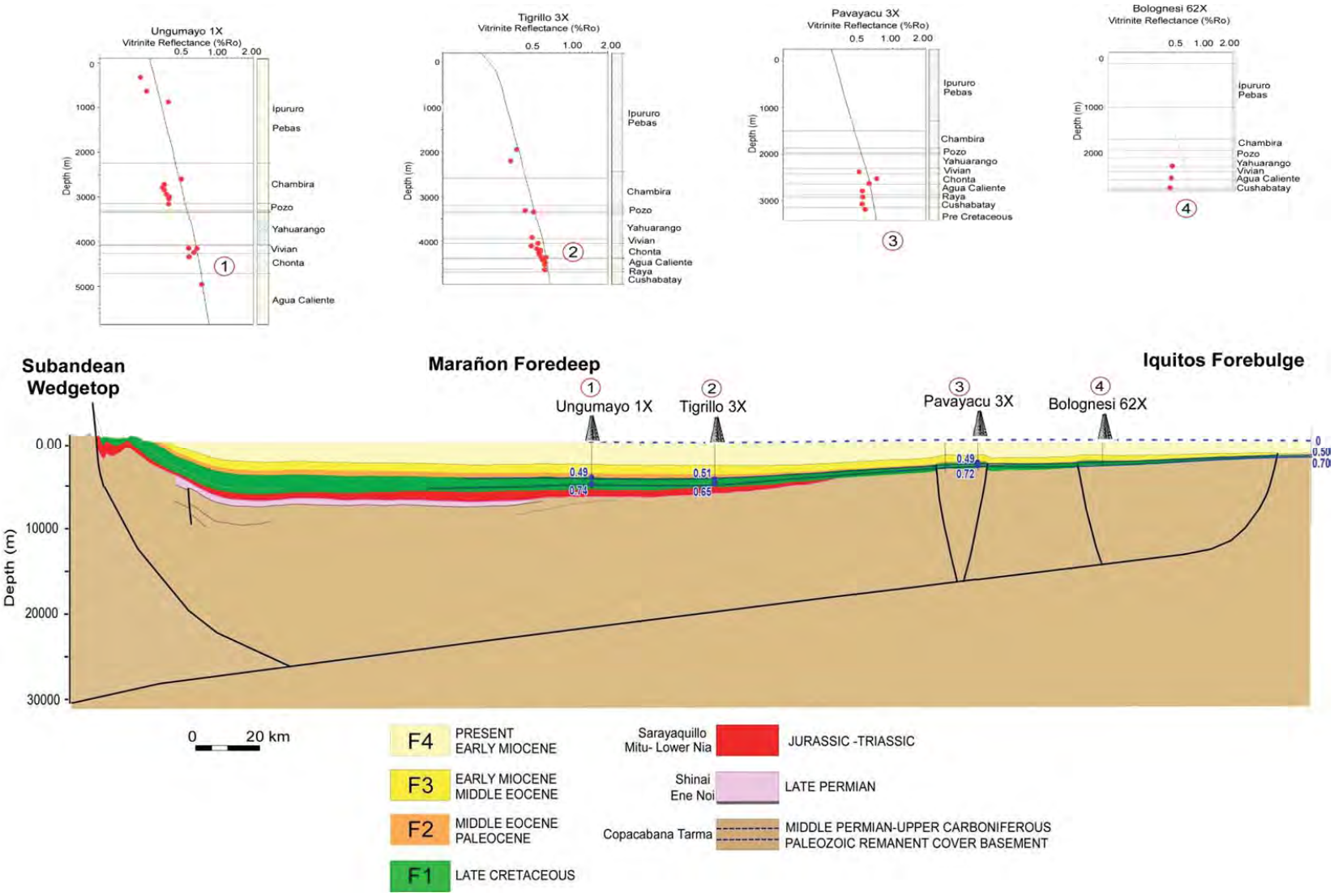

Figure 3.16. Regional structural cross sections R3 (location in Fig. 3.1) showing long term foreland basin sequences (F1, F2, F3 and F4) and the top Neogene surface profile computed from 1D PetroMod modeling (see text). Vertical scale exaggeration.

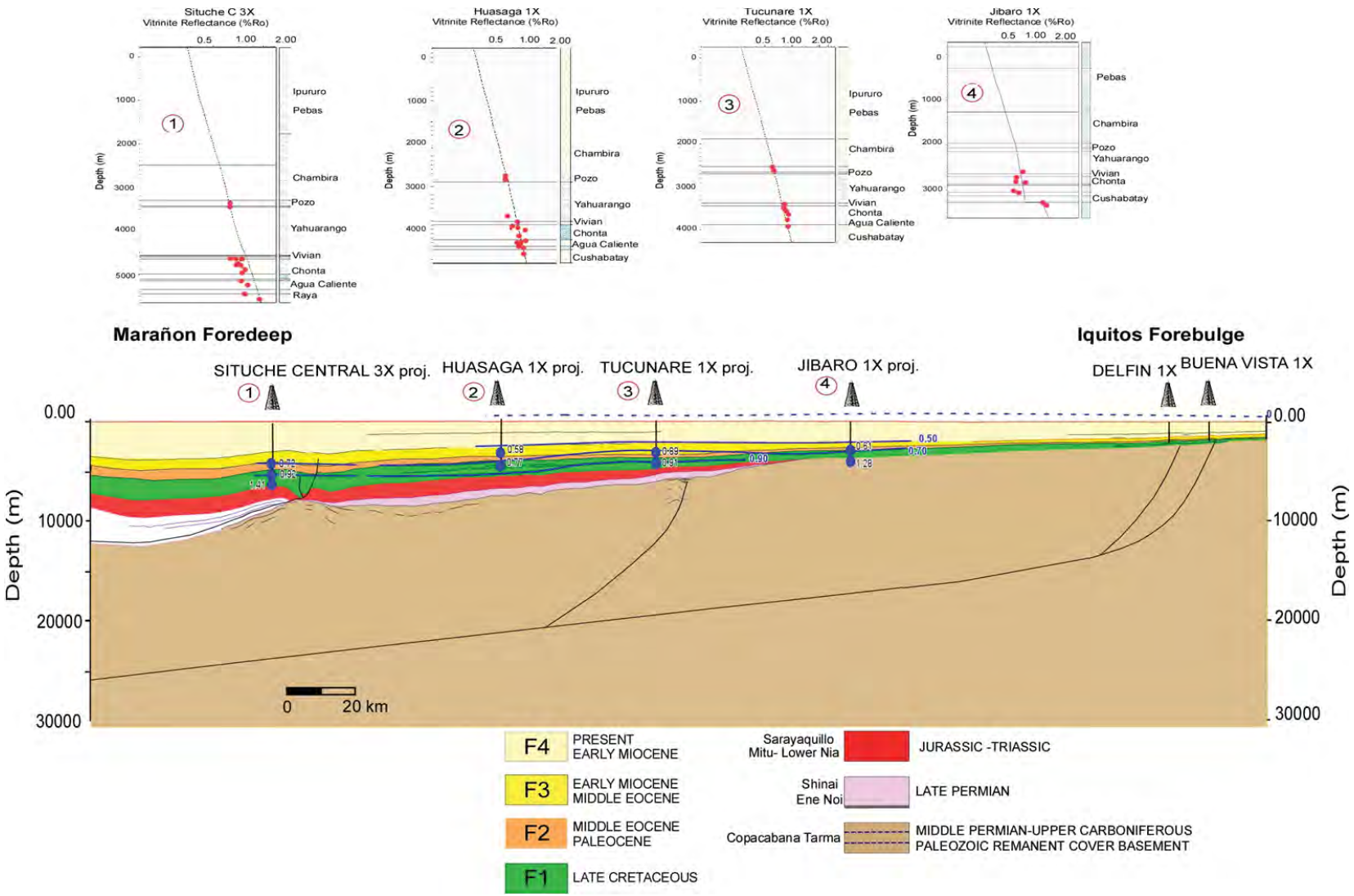

Figure 3.17. Regional structural cross sections R5 (location in Fig. 3.1) showing long term foreland basin sequences (F1, F2, F3 and F4) and the top Neogene surface profile computed from 1D PetroMod modeling (see text). Vertical scale exaggeration.

3.4.3. Sedimentation rates

The sedimentation rates along the cross-section R1, R3 and R5 (Figure 3.18) and the whole Marañón Basin (Figure 3.19) have been computed using the physical properties extracted from the subsurface data exposed above. The physical properties and the computed results are summarized in Table 3.1.

The methods used for time-depth conversion and compaction correction are presented in Annex 2. Foreland basin sequence areas have been computed with the software MOVE in the cross-sections. The sedimentation rates were calculated following standard methods (e.g. Métivier et al., 1999; Walford et al., 2005; Calvès et al., 2013).

The sedimentation rate since the early Cretaceous (Albian, 110 Ma) based on the sections R1, and R3 show a decrease at the transition with the Paleogene (Figure 3.18) followed by an increase until recent times. On section R5 the sedimentation rates have increased since the early Cretaceous (Figure 3.18). The amount of clastic deposited during the studied interval has been representing most of the fraction of the sedimentation with figure never lower than 75%. The carbonate or organics (coal, organic matter) do not represent a significant portion of the sediments that are preserved in the studied intervals (Table 3.1).

Section	Age		Sequence	Length	Area	Porosity		Lithology			Solid sediment sedimentation rates		Clastic sediment sedimentation rates
	Top	Bottom											
Unit	Ma	Ma		km	km²	%		%			km²/My		km²/My
						minimum	maximum	Carbonates	Organic matter	Clastics	minimum	maximum	average
R1	0	23	F4		5.9E+02	16	50	5	5	90	14.3	21.4	16.9
	23	45	F3		3.6E+02	20	40	0	5	95	9.8	13.0	10.1
	45	65	F2		1.5E+02	7.5	35	5	0	95	4.6	6.7	5.4
	65	110	F1	442	5.2E+02	12	40	15	10	75	7.5	10.2	7.0
R3	0	23	F4		8.9E+02	30	50	10	5	85	19.4	27.2	18.1
	23	45	F3		3.1E+02	25	50	5	0	95	7.1	10.7	7.4
	45	65	F2		1.4E+02	10	45	5	0	95	4.0	6.5	4.8
	65	110	F1	425	5.0E+02	10	40	10	5	85	6.7	10.0	7.1
R5	0	23	F4		6.8E+02	10	44	10	10	80	14.9	26.8	14.3
	23	45	F3		2.8E+02	10	40	5	0	95	7.6	11.3	9.6
	45	65	F2		2.2E+02	10	37	10	0	90	5.9	8.2	7.4
	65	110	F1	304	2.5E+02	10	36	10	5	85	3.8	5.8	4.9
				Surface	Volume								Qs (Clastics)
				km²	km^3						km^3/My		Mt/y
Marañón Basin	0	23	F4			10	50	10	5	85	6282	6520	12.1
	23	45	F3	3.3E+11	4.2E+05	10	40	5	0	95	2845	3084	5.2
	45	65	F2			7.5	35	5	0	95	1420	1479	2.5
	65	110	F1	3.6E+11	2.4E+05	10	40	10	5	85	2259	2317	3.3

Table 3.1. Marañón Basin volumetric, physical properties of sediments and sedimentation rates computed from regional cross sections R1, R3 and R5 and isopach map.

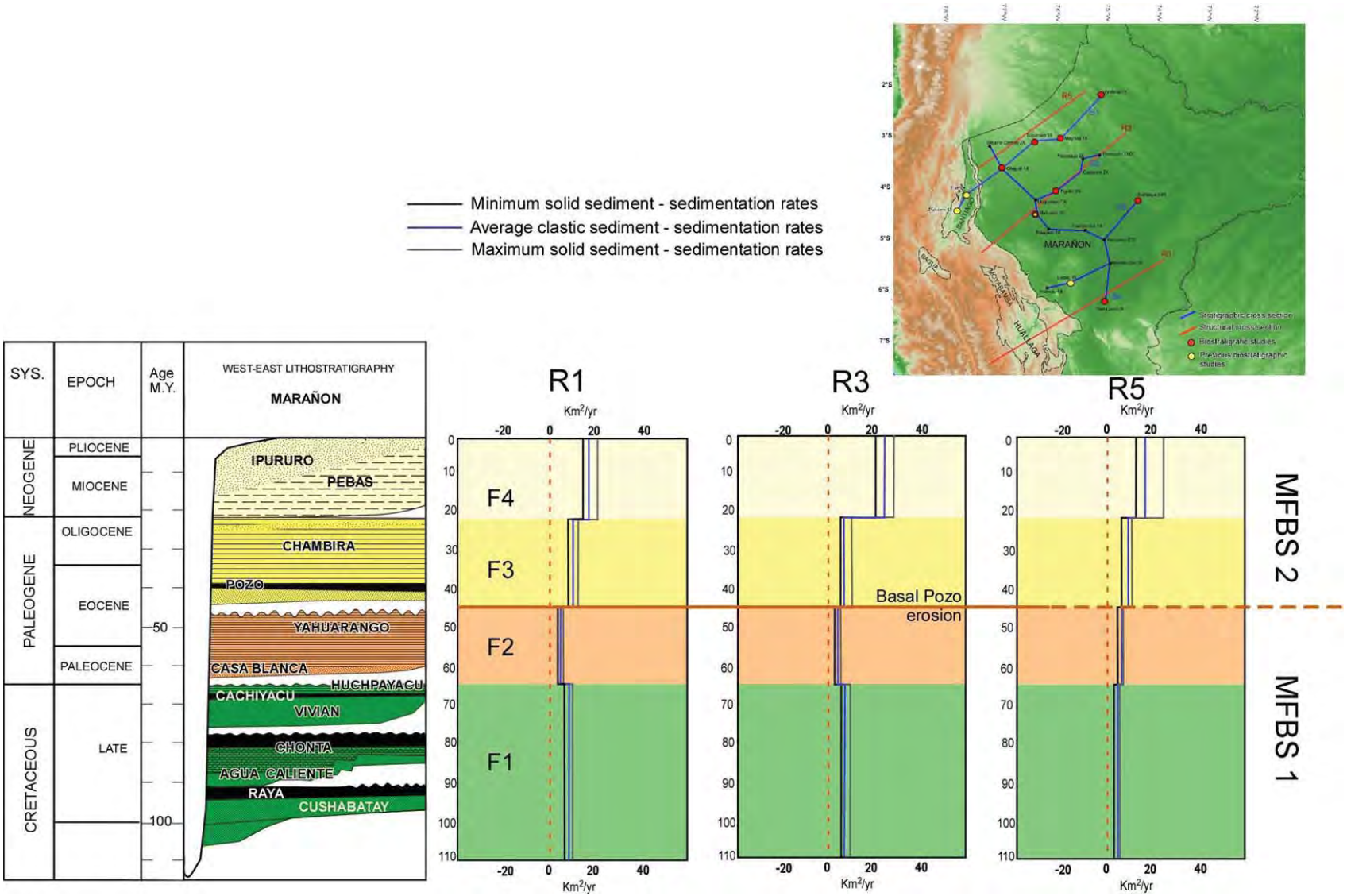

Figure 3.18. Computed sedimentation rates along regional cross sections R1, R3 and R5. MFBS: Marañón Foreland Basin System.

To the South of the Marañón Basin (R1, Figure 3.18), the computed sedimentation rates show a slight decrease less than two times from the late Cretaceous to the Paleogene. This is followed by an increase higher than twice from the middle Eocene to the late Oligocene for solid sediment and clastic rates of sedimentation. The highest figure of sedimentation, higher by two to three folds, is occurring from the late Oligocene to the Neogene to recent sequence. This despite the erosion observed in the section R1 (See Figure 3.15). Section R3 shows a stronger sedimentation rate during the Neogene. To the North of Marañón Basin, section R5 (Figure 3.18) and section R3 (Figure 3.18) mark a change with lower sedimentation rates compared to the section R1. Sedimentation rates trend and variation for R3 are equivalent to section R1, whereas section R5 show a progressive increase of sedimentation rates and no decrease during the Paleocene to middle Eocene sequence F2 (Figure 3.18). In the sections R1 and R3, the sedimentation rate calculation of F2 is probably biased by the Basal Pozo (base of F3) erosion that increases to the north as shown by the NW-SE wells stratigraphic correlation S4 (Figure 3.8). This may explain the sedimentation rates trend variation from R1 to R5 observed for the Paleogene.

Once these results on regional cross section are transferred to the whole Marañón Basin taking into account the isopach maps computed regionally (Annex 4). We can document the global evolution of flux of sediments and the Qs computed (Figure 3.19A). As a modern and a figure for sediment discharge based on observations of the river Amazon at Obidos (Brazil) and measurement using Doppler technology, we refer to the work of Filizola and Guyot (2014). The figure of modern sediment discharge project to a year is ranging from 884 to 1198 Mt/y. In the Subandean neighboring Ucayali Basin, the reference values are lower with 220 Mt/y (Santini et al., 2014), and represent the sediment flux deposited/preserved in the floodplain (Figure 3.19B).

The figures of sediment supply (Qs) since the Albian have been lower nx10 times than the modern estimated of sediment discharge (Figure 3.19). The Qs during the Cenozoic has been increasing by steps with two to three times the value of the previous sequence. The Neogene to recent show values 50 to 100 times lower than the present day observed sediment discharge of the River Amazon at Obidos, and 18 times lower than the modern sedimentation rates in the neighboring Ucayali Basin.

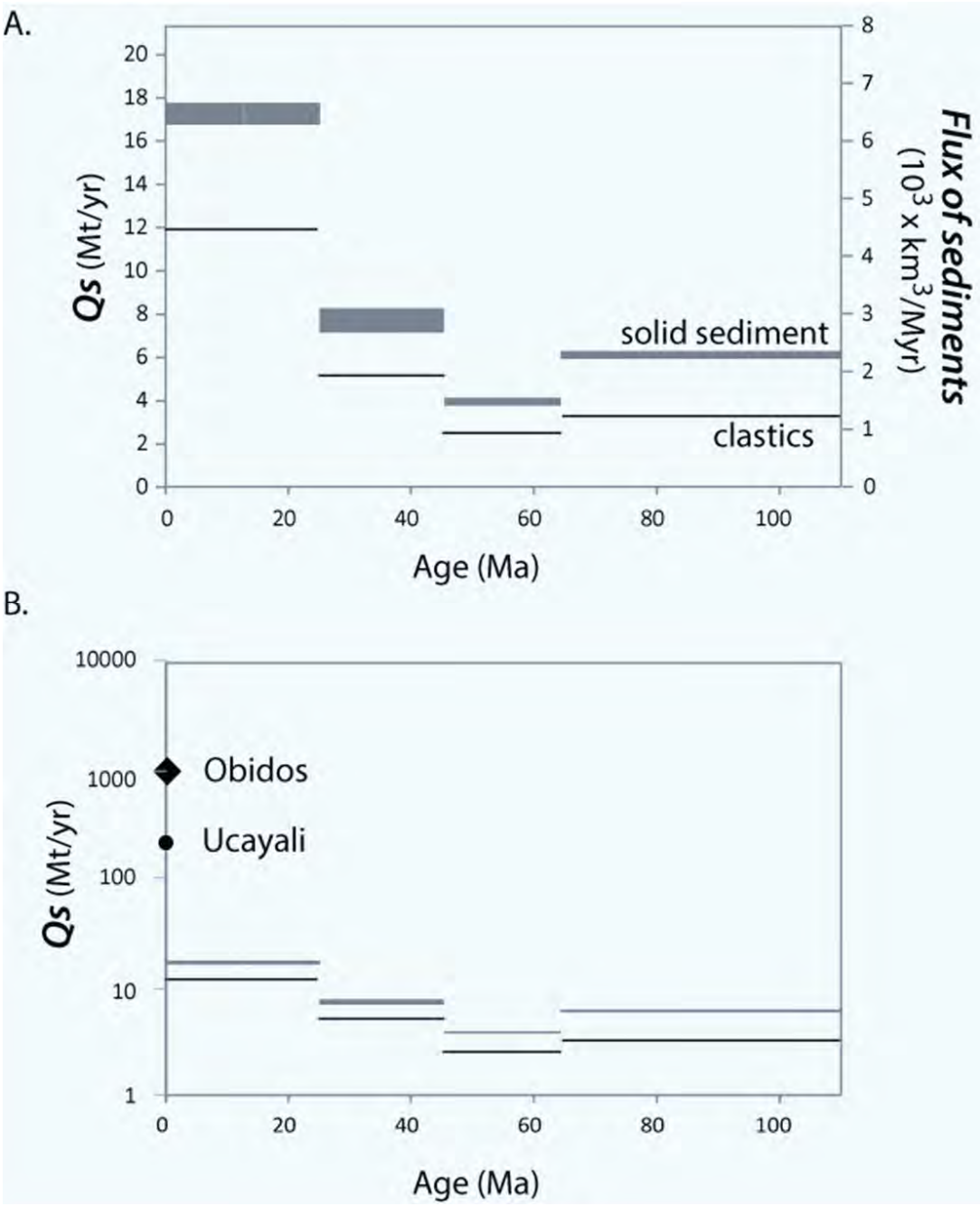

Figure 3.19. (A) Sediment supply and flux computed for the Marañón Basin over the last 110 Ma. (B) Modern sediment supply corresponds to the flux measured at Obidos (Filizola and Guyot 2014). In the Ucayali Basin, the modern sedimentation rates represent 220 Mt/y (Santini et al., 2014). Note the logarithmic scale to allow 'comparison' of the modern (high) and geological (low) rates.

3.5. Summary and conclusions

The Marañón FBS corresponds today to a transition zone, which evolves from a wedgetop depozone in the SE to a foredeep depozone towards the NW. In the south, the Huallaga and Marañón basins belong to the same FBS that could be studied in detail (see cross-section R1).

The Marañón FBS deposits can be divided into four foreland long term sequences (F1 to F4) defined from previous studies, wells stratigraphic correlations and regional unconformities identified on seismic data.

The first foreland sequence F1 is Albian and late Cretaceous in age and overlies the Andean basal foreland unconformity (Cushabatay BFU). It consists of three fluvial to shallow marine cyclic transgressive sequences that are probably deposited in a backbulge depozone. Albian and Maastrichtian sandstones have cratonic provenance (Hurtado, 2017).

The Paleocene-early Eocene long term sequence F2 recorded the first siliciclastic supply from the Andean uplift, and represents a continental distal foredeep to backbulge depozone (see R1 sequential restoration of Figure 3.2). The thickness of F2 decreases towards the south (Figure section S4 of Figure 3.8), which is probably due to a strongest erosion of the Basal Pozo erosional surface. This middle Eocene regional erosional surface sealed the deformation and configuration of the first stage of the Huallaga-Marañón FBS. It recorded a quiescence of thrust tectonics and an unloading orogenic period also described in Ecuador and Colombia (Christophoul et al., 2012).

The middle Eocene-Oligocene F3 long term sequence recorded the beginning of the second stage of the Huallaga-Marañón FBS, and the uplifting of the Western Cordillera (see location of Western Cordillera in Figure 1.2). The Marañón basin evolved in an environment from marginal marine to fluvial.

During the Neogene, the F4 sequence recorded the uplift of the Eastern Cordillera and an evolution of the Marañón Basin from distal to proximal foredeep depozone with increasing rate of sedimentation (Figure 3.18), contemporaneous with the formation of the Iquitos forebulge. The early and middle Miocene period is characterized by a complex environment alternating between marginal marine and fluvial environments (Hoorn et al., 2010; Jaramillo et al., 2017), due probably to global high sea level and fast subsidence. The transcontinental Amazon River drainage occurred in the late Miocene and provoked a radical change in the Marañón foredeep sedimentation that became exclusively fluvial (Roddaz et al., 2010). During the Pliocene, the eastward propagation of thrust tectonics combined the Fitzcarrald

Arch uplift (Espurt et al., 2007) led to the uplift and erosion of the southern part of the Marañón Basin. The strongest Neogene sedimentation rate is represented in the foredeep depozone of the section R3.

In the northern Marañón Basin, sedimentation rates computed from the regional cross-section R5 show a progressive increase from the Albian to the present that seems to represent a classic evolution of the FBS. To the south (sections R3 and R1), the sedimentation rate shows a decrease during the Paleocene to middle Eocene sequence due to the middle Eocene erosional basal surface of F3 (Basal Pozo) that recorded a period of orogenic unloading interrupting the foreland basin sedimentation. A second Marañón foreland basin system started in the late Eocene-Oligocene. Sedimentation rates significantly increase during the Neogene due to a fast subsidence associated to the orogenic loading of the uplifting Eastern Cordillera.

The sedimentation rates calculated for the Neogene is 18 times lower than the modern sedimentation rates measured in the Ucayali Basin (Figure 3.19B). This difference of values is probably due to the complex evolution of the Marañón FBS that we have not completely deciphered. The identified potential erosion and unconformities in the porosity and the thermal history (Ro) of the Marañón Basin show that numerous events have occurred with non-preserved sedimentary archive at the location of study area. Part of this record could have been displaced outside or recycled within the study area. It shows that it remains important periods of erosion and no sedimentation to be found.

Chapter 4: Petroleum systems restoration of the Huallaga-Marañón Andean retro-foreland basin, Peru

Introduction au chapitre

La ceinture de plis et chevauchements – ou zone de dépôt de wedgetop - du système de bassin d'avant-pays Huallaga-Marañón est la plus importante de la zone subandine péruvienne comme le montre la synthèse présentée en annexe 5 (Baby, Calderon et al., sous presse). Malgré un potentiel pétrolier avéré et la présence d'importants champs de gaz plus au sud dans les chevauchements subandins (Camisea), le système Huallaga-Marañón reste sous explorée à cause de sa complexité structurale et d'un calendrier de la déformation mal défini. Une analyse géométrique et cinématique appropriée ainsi qu'une modélisation pétrolière 2D sont donc nécessaires pour diminuer les risques d'exploration.

Ce chapitre présente une synthèse sur les structures et les systèmes pétroliers des bassins Huallaga et Marañón, en apportant de nouvelles données concernant l'âge des pièges structuraux (thermochronologie) et la géochimie de certaines roches mères. Pour la première fois, une modélisation pétrolière en 2D est réalisée grâce à la restauration séquentielle de la coupe structurale régionale R1 étudiée dans les chapitres 2 et 3. Ce type de modélisation pétrolière 2D est rare dans les systèmes de bassin d'avant-pays. Elle apporte indéniablement une plus-value pour l'exploration pétrolière de la région, et répond aux demandes de l'agence PERUPETRO chargée de mieux évaluer et promouvoir les bassins pétroliers péruviens.

La modélisation 2D proposée a été réalisée à l'aide du logiciel Petromod de Schlumberger. Elle reproduit les états de maturité et d'expulsion des systèmes pétroliers dans les trois stades de déformation de la restauration séquentielle de la coupe structurale R1. Elle modélise aussi les accumulations d'hydrocarbures possibles dans les pièges structuraux définies dans cette thèse. Elle montre l'intérêt d'explorer, comme dans d'autre région du monde, des structures de type « sub-trap » cachées sous les chevauchements.

Résumé en français

Le système de bassin d'avant-pays Huallaga-Marañón du nord-Pérou est déformé par une tectonique de socle et de couverture. Le système de chevauchements est complexe et résulte de la réactivation d'une chaîne plissée à vergence ouest d'âge permien, coiffée d'un important niveau de décollement de sel. Cet article présente une modélisation pétrolière 2D réalisée à partir d'une coupe équilibrée actualisée et d'une restauration séquentielle à travers le bassin « wedge-top » Huallaga-Marañón. La restauration séquentielle a été calibrée à partir de datations thermochronologiques et de variations d'épaisseur dans les sédiments synorogéniques cénozoïques. Elle montre deux importants stades de déformation (Eocène moyen, Miocène inférieur terminal). Les roches mères classiques du Trias supérieur/Jurassique inférieur et du Crétacé supérieur sont présentes dans le bassin d'avant-pays Huallaga-Marañón, mais la révision de la stratigraphie replacée dans son contexte structural actualisé conduit à mettre en évidence une nouvelle roche mère d'âge permien supérieur. La modélisation 2D de l'évolution de la maturité des kérogènes et des accumulations d'hydrocarbures dans la restauration séquentielle montre que des vieilles structures (Paléocène et Miocène Inférieur) pourraient préserver des accumulations d'hydrocarbures au mur du chevauchement de Chazuta. A l'est, dans le bassin Marañón, des structures plus jeunes comme Santa Lucia pourraient avoir aussi été chargées. Des structures profondes cachées sous les chevauchements restent inexplorées dans la chaîne plissée péruvienne. Le système d'avant-pays Huallaga-Marañón est probablement le meilleur exemple d'attractivité de « sub-trap » au Pérou.

Petroleum systems restoration of the Huallaga-Marañón Andean retro-foreland basin, Peru

(Published in *Mahdi A. AbuAli, Isabelle Moretti, and Hege M. Nordgård Bolås, eds.*, Petroleum Systems Analysis – Case studies: AAPG Memoir 114, p. 95–116, 2017)

Ysabel Calderon [a], Patrice Baby [b], Yessica Vela [a], Christian Hurtado [a], Adrien Eude [b], Martin Roddaz [b], Stéphane Brusset [b], Gérome Calvès [b], Rolando Bolaños [a]

[a] PERUPETRO S.A., Av. Luis Aldana 380, San Borja, Lima, Peru

[b] GET-UMR CNRS/IRD/Université Paul Sabatier, 13545, 14 Avenue Edouard Belin, 31400 Toulouse, France

Abstract

The Huallaga-Marañón retro-foreland basin system of northern Peru is deformed by both thick- and thin-skinned tectonics. The thrust system is complex and resulted from the reactivation of a west-verging Permian fold and thrust belt capped by an important salt detachment. This paper presents a 2D petroleum modeling from an updated balanced cross-section and sequential restoration through the Huallaga-Marañón wedge-top basin. The sequential restoration has been calibrated by thermochronological dating and thickness variations in Cenozoic synorogenic sediments. It shows two important stages of the deformation (Middle Eocene, Late Early Miocene). Late Triassic/Early Jurassic and Late Cretaceous classic source rocks are present in the Huallaga-Marañón foreland basin, but the revision of the stratigraphy replaced in its updated structural context allowed us to highlight a new Late Permian source rock (Shinai Formation). 2D modeling of kerogens maturity evolution and hydrocarbon (HC) accumulations in the sequential restoration shows that old structures (Paleocene and Early Miocene) could preserve HC accumulations in the Chazuta thrust sheet foot-wall. In the eastern Marañón basin, more recent structures as Santa Lucia could also have been charged. Deep sub-thrust structures stay unexplored in the Peruvian fold and thrust belts. The Huallaga-Marañón foreland system is probably the best example of sub-trap attractiveness in Peru.

4.1. Introduction

Among the 55 fold and thrust belts of the world (Cooper, 2007), only a few examples have been subject of 2D petroleum modeling. Such modeling needs well-constrained balanced cross-section, thrusts propagation dating and good information of the regional petroleum system. These conditions are met in the Subandean basins of Peru, in particular in the Huallaga-Marañón retro-foreland basin system (Figure 4.1), where the hydrocarbon potential is proven but poorly evaluated. The Huallaga-Marañón fold and thrust foreland basin contains Paleozoic and Mesozoic source rocks, Mesozoic reservoirs, sub-thrust traps, but remains in an immature exploration stage. From west to east, thick syn-orogenic Cenozoic sedimentation and thrust sheets propagation have controlled a complex burial and erosion history, which can be deciphered from an integrated geological study.

The object of this study is to present for the first time a 2D petroleum system modeling from an updated regional balanced cross-section through the Huallaga-Marañón retro-foreland basin system. A sequential restoration of the deformation, calibrated by thermochronological dating and thickness variations in Cenozoic synorogenic sediments, has been reconstituted and then used for the 2D petroleum systems modeling. Main structural results, kinematic and petroleum history evolution are presented. The oil and gas potential is re-assessed with a new vision of the stratigraphic and structural context.

4.2. Tectonic background

The Marañón and Huallaga Subandean sub-basins are located in the Andean-Amazonian transitional area, the so-called Northern Amazonian Foreland Basin (Espurt et al., 2007, 2011). They are classically interpreted as the components of a wide retro-foreland basin system, where the Huallaga Subandean area is conventionally correlated to the wedge-top depozone and the Marañón area to the foredeep depozone (Hermoza et al., 2005; Roddaz et al., 2005). Thermochronological dating shows that the North Amazonian Foreland Basin started to acquire its modern configuration between 30 and 24 Ma (Eude et al., 2015) with the development of the Huallaga syn-orogenic wedge-top basin (Hermoza et al., 2005). The Huallaga thrusts system is characterized by a strong horizontal shortening. To the west, the Andean Eastern Cordillera, which acted as the deformable backstop, corresponds to the tectonic inversion of the pre-Andean Triassic rift (Rosas et al., 2007; Eude et al., 2015). Several versions of balanced cross-sections have already been constructed in the Huallaga-

Marañón foreland basin system (Gil, 2001; Hermoza et al., 2005 and Eude et al., 2015). They show the importance of thin-skinned tectonics controlled by a regional evaporitic layer whose age is discussed below. A total horizontal shortening around 80-90 km has been calculated by these authors.

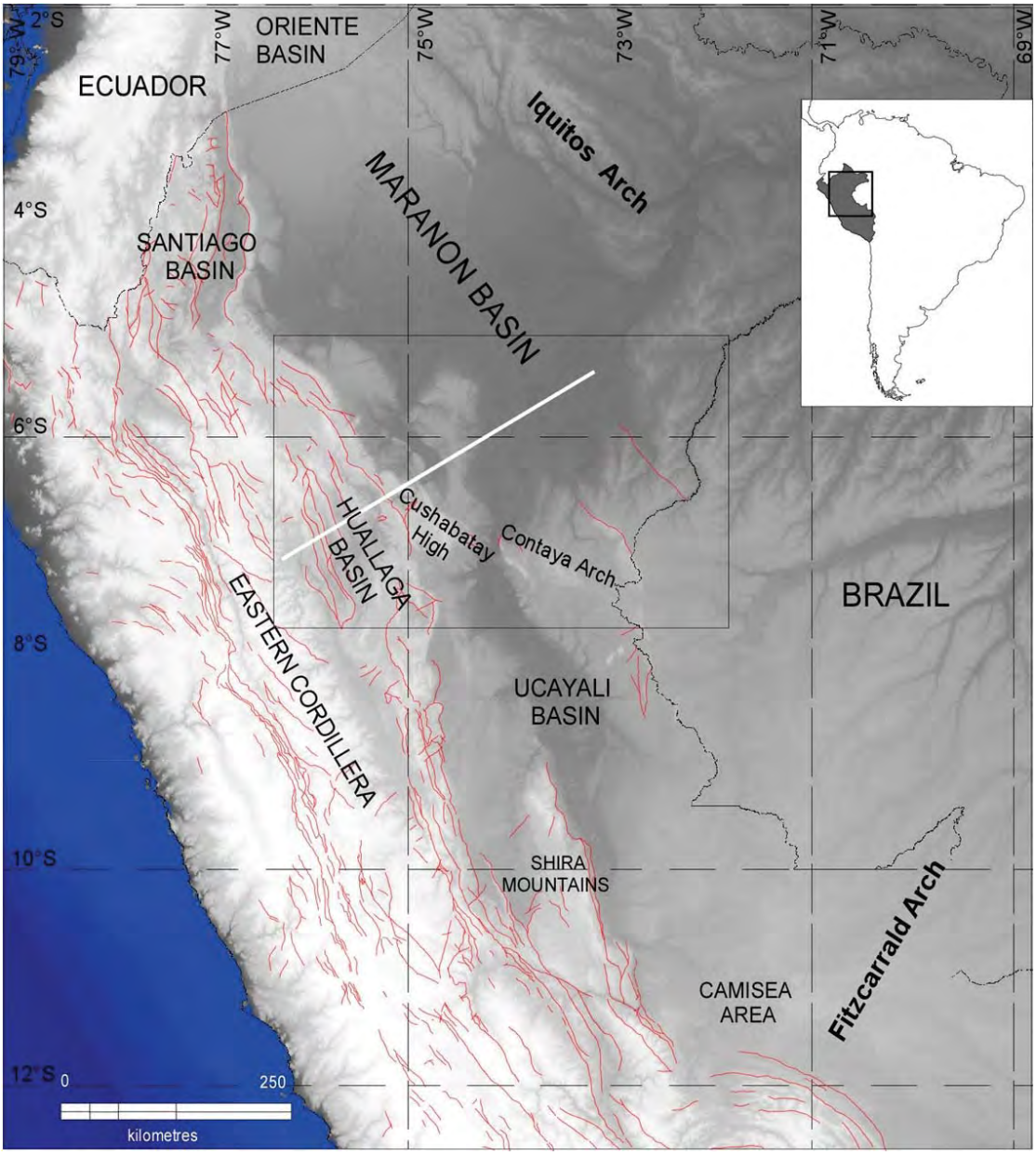

Figure 4.1. Tectonic map of the Subandean basins of northern and central Peru, showing the study area and the different morpho-tectonic units. The Huallaga-Marañón structural cross-section is located.

To the east of the Huallaga thrust front, the southern Marañón basin is deformed by a modern and still active thick-skinned tectonic, and should then be seen as the contemporaneous wedge-top rather than the foredeep of the foreland basin system. Seismic sections show east and west-verging basement thrusts, which branch on a deep detachment (Devlin et al., 2012; Eude et al., 2015). West verging thrusts are inherited from Permian thrusts of the Pan Gondwanian orogeny (Calderon et al., 2014). This basement thrusts system plunges to the west below the Huallaga piggyback basin and interferes with thin-skinned deformation of the sedimentary cover. The Cushabatay High, in the Huallaga-Marañón transition zone, is the geomorphologic expression of such structures (Figura 4.2). The complex Huallaga-Marañón orogenic wedge is illustrated and described later in our updated balanced cross-section.

North of the studied regional cross-section (Figure 4.1), the Marañón basin is progressively deepening and deformation is weaker. It constitutes a foredeep depozone limited in the west by the Santiago Subandean fold and thrust belt (PARSEP, 2001), and in the east by the Iquitos forebulge (Roddaz et al., 2005). To the north, it extends with the Oriente basin of Ecuador (Balkwill et al., 1995; Baby et al., 2013).

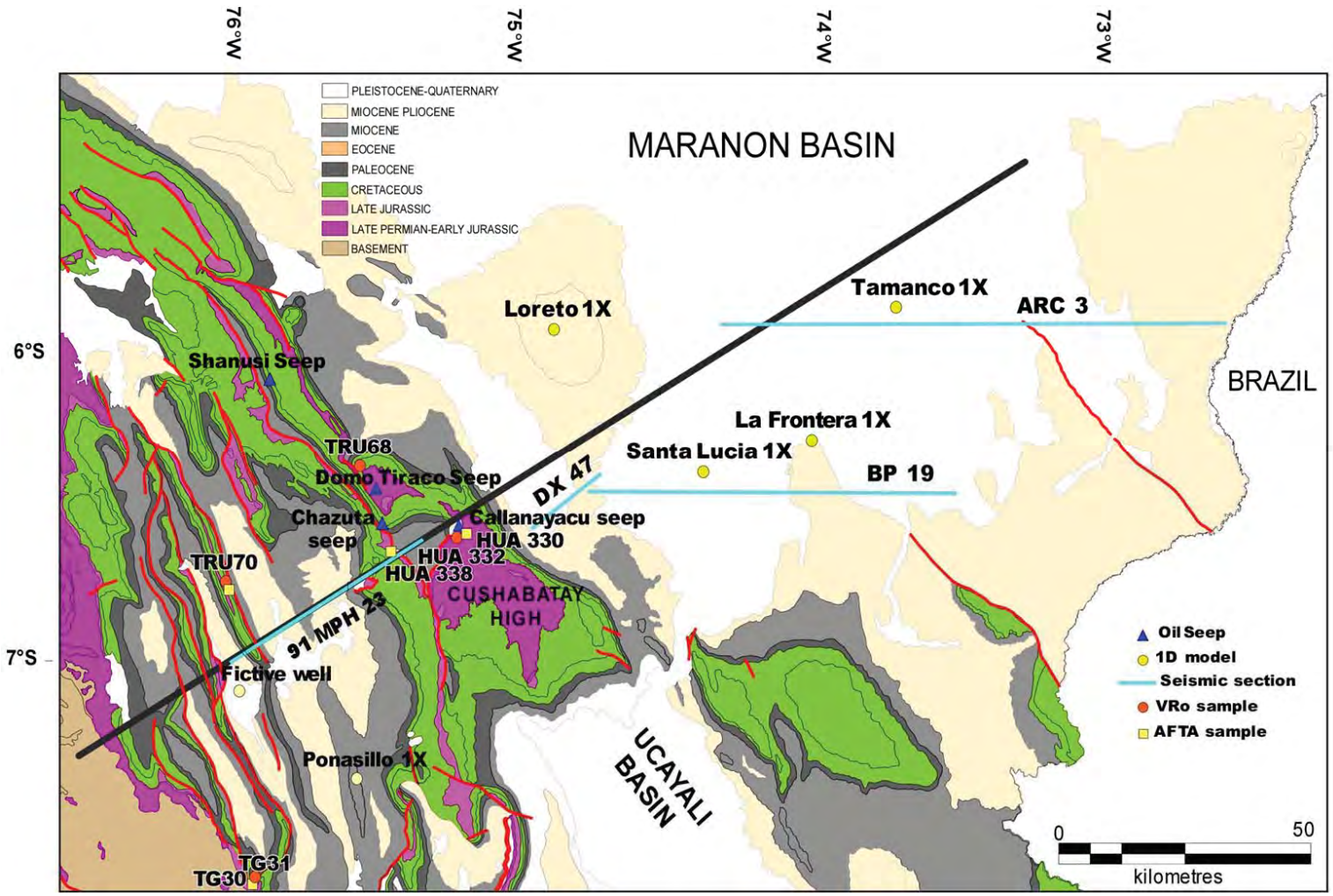

Figure 4.2. Geological map of the study area, with location of the Huallaga-Marañón balanced cross-section, subsurface data, AFT datings and Ro analyses.

4.3. Stratigraphy

The sedimentary cover involved in the deformation of the Huallaga-Marañón foreland basin system consists of a pre-Andean series, unconformably overlain by a marine to continental late Cretaceous sedimentary wedge thinning to the NE, and by a Cenozoic foreland continental and shallow marine infill. It is illustrated by the updated stratigraphic diagram of the Figure 4.3.

The pre-Andean series comprises remnants of Ordovician, Devonian, Carboniferous and Permian clastic and carbonated marine deposits, partly eroded below a Late Permian unconformity that marked the onset of a long period of rifting and post-rift regional sag (Rosas et al., 2007). This unconformity is overlain by a regional layer of evaporite, long regarded as Jurassic in age despite the absence of real dating (PARSEP, 2001; Moretti et al., 2013). Recent revisions of regional stratigraphy based on subsurface correlations, thanks to new seismic information (Perupetro S.A. database) and new field observations, allowed us to reconsider the stratigraphic position of this important regional layer of salt, which acted as the mean detachment of the Huallaga thrusts system (Baby et al., 2014; Hurtado et al., 2014). It outcrops on the Callanayacu Diapir, east of the Chazuta thrust (Huallaga thrust front; see Figure 4.2) along the Huallaga river, where evaporites are covered by marine black shales, limestones and dolomites. These marine deposits could never be dated. North-south seismic correlations from the South Marañón basin to the Ucayali basin show that they correspond to the Shinai Formation (Baby et al., 2014; Hurtado et al., 2014) defined and dated from the Late Permian in the Camisea area (Seminario et al., 2005 and reference therein). Along the Huallaga River, the Shinai Formation is overlain by approximately 2000 meters of aeolian and fluvial sandstones and silts, which can be correlated with the Lower Nia reservoir of the Camisea area (Seminario et al., 2005) and the overlaying Sarayaquillo Formation. These continental series are considered as Triassic and Jurassic in age (PARSEP, 2001; Seminario et al., 2005). To the west, the aeolian sandstones laterally pass to the continental Mitu rift and marine Pucara post-rift deposits outcropping in the Eastern Cordillera (Rosas et al., 2007), where they overlay directly the basement known as Marañón Complex (Wilson, 1985). This lateral change occurs apparently in the Huallaga basin-Eastern Cordillera transition zone and corresponds to the eastern Mitu rift border. The tectonic inversion of the Mitu rift has controlled the deformation and propagation of the Eastern Cordillera deformable backstop of the Subandean fold and thrust belt.

After a major sedimentary hiatus (110-120 Ma), corresponding probably to the Andean basal foreland unconformity, late Cretaceous sequences were deposited. They comprise Albian to Maastrichtian fluvial to shallow marine cyclic sequences of sandstones, shales and limestones (Cushabatay-Raya; Agua Caliente-Chonta; Vivian-Cachiyacu-Huchpayacu; see Figure 4.3). These eastward-thinning sequences were deposited in the Andean-Amazonian retro-foreland basin controlled by the tectonic loading of the incipient Andean orogenic wedge. They constitute today the main petroleum systems of the Oriente-Marañón prolific oil province (Marksteiner & Aleman, 1997; Barragan et al., 2008). Reservoirs corresponds to fluvio-deltaic and tide-dominated estuarine deposits of the Cushabatay, Agua Caliente and Vivian formations, and source rocks are constituted by shales and limestones of the Raya and Chonta formations (Mathalone & Montoya, 1995; PARSEP, 2001).

The Cenozoic foreland infill presents important lateral variations from the Huallaga hinterland to the Marañón foreland. It has been well described in terms of foreland system depositional environments controlled by thrusts propagation by Hermoza et al. (2005) and Roddaz et al. (2010). The Paleocene-Early Eocene sequence starts with the fluvial and tidal sandstones of the Casa Blanca Formation (Gil, 2001 and references therein), comparable to the Vivian reservoir. It passes gradually to red siltstones and mudstones forming distal fluvial deposits (Yahuarango Fm.). The Middle Eocene-Oligocene sequence overlies a regional erosional unconformity, which extends to the north in Ecuador and Colombia. This erosion has been interpreted as an unloading orogenic period (Christophoul et al., 2002). The Middle-Upper Pozo Formation developed in shallow marine environment and recorded a new orogenic loading period. It is overlaid by the Oligocene silts and sandstones of the Chambira Formation. The Neogene sequence recorded the development of the modern Huallaga wedge-top depozone and a strong subsidence in a deltaic environment evolving progressively to an alluvial system (Hermoza et al., 2005). This thick Neogene sequence corresponds to the main charge of the petroleum systems.

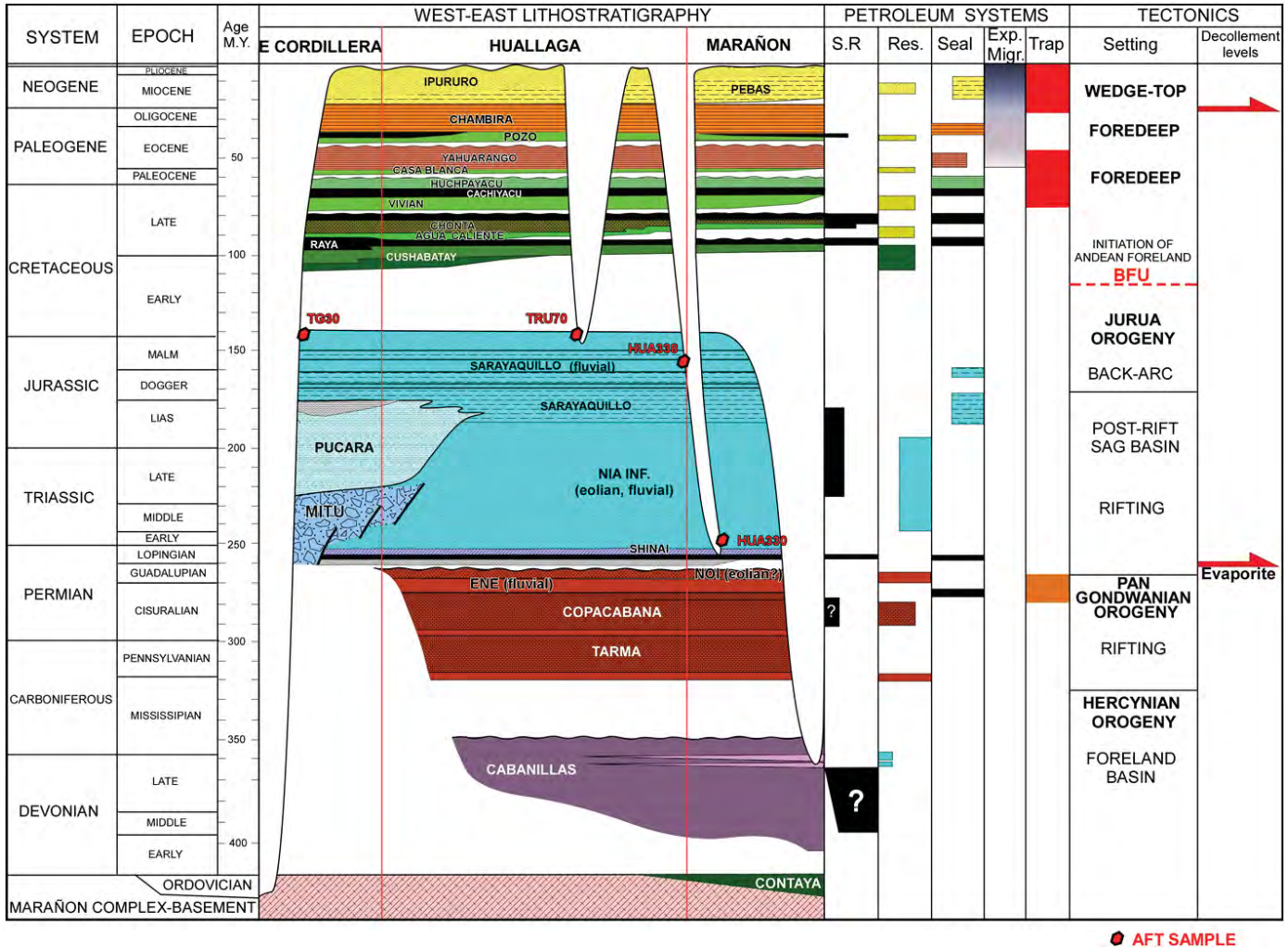

Figure 4.3. Stratigraphic diagram and petroleum systems along the Huallaga-Marañón cross-section.

4.4. Balanced cross-section, deformation timing and sequential restoration

The balanced cross-section (Figure 4.5) has been updated from previous versions (Gil, 2001; Hermoza et al., 2005; Eude et al., 2015) and news interpretations of some surface and sub-surface data. The differences from the Eude's version are the stratigraphic position of the salt detachment (Late Permian instead of Jurassic, see above and Figure 4.3) and the structural interpretation of the Eastern Cordillera-Huallaga basin transition. The balanced cross-section has been constructed using the Midland Valley Move 2015 software on the basis of the flexural-slip algorithm, assuming constant bed length and thickness and constant area for salt units and Neogene infill. The cross-section is ~ 420 km long from the Eastern Cordillera to the Marañón foreland (Figure 4.2). Its orientation is orthogonal to the arcuate shape of the Huallaga thrust front (Chazuta thrust) and is consistent with the thrust movement direction (bow-and-arrow rule). Surface data were obtained from our field surveys (see Eude et al., 2015) and 1:100,000 INGEMMET (Instituto Nacional Geológico, Minero y Metalúrgico del Perú) geologic maps. Seismic sections and wells (see Figure 4.2 for location) were provided by PERUPETRO S.A. The cross-section was restored at the base of the Pozo Formation which sealed a regional erosive planar unconformity (Christophoul et al., 2002).

The seismic reflection sections used for the construction of the balanced cross-section were presented in detail in Eude et al. (2015). In the Marañón basin, they show east-verging basement thrusts branched on an intra-basement detachment, which deform the entire Neogene series (Figure 4.4A). Thicknesses and stratigraphy are constrained by the Ponasillo 1X, Loreto 1X, Santa Lucia 1X, Floresta 1X and Tamanco 1X wells (location in Figure 4.2). West to the Loreto 1X well, seismic reflection shows west verging basement thrusts inherited from a Permian fold and thrust belt (Calderon et al., 2014). Below the Huallaga basin, this reactivated thrust system is evidenced by both seismic imagery (Figure 4.4B) and seismic activity (Devlin et al., 2012). The best topographic expression of this deep deformation coincides with the Cushabatay High, east of the Huallaga thrust front (Chazuta thrust), where merges the Callanayacu diapir structure (Figure 4.5). The Callanayacu structure is a diapir of Late Permian evaporite deformed at the top of the Cushabatay High mega-duplex, which developed between the intra-basement detachment and the salt detachment. In the Huallaga basin, the Mesozoic and Cenozoic cover is intensely deformed by thin-skinned tectonics, which propagated on the thick and continuous Late Permian evaporite layer at the top of the basement horses. The 91MPH23 seismic section (Figure 4.4B) clearly shows the large overthrusting of the Chazuta thrust sheet, whose eastward displacement is approximately 40

km. More to the west, the Biabo anticline is a major fault propagation fold that developed in the thick Neogene infill of the Huallaga wedge-top depozone. The Huallaga-Eastern Cordillera transition zone corresponds to a broad Neogene syncline transported on the inverted Triassic rift system. This inversion is well illustrated by the palinspastic restorations of the balanced cross-section (Figure 4.5). A total horizontal shortening of 70 km has been calculated.

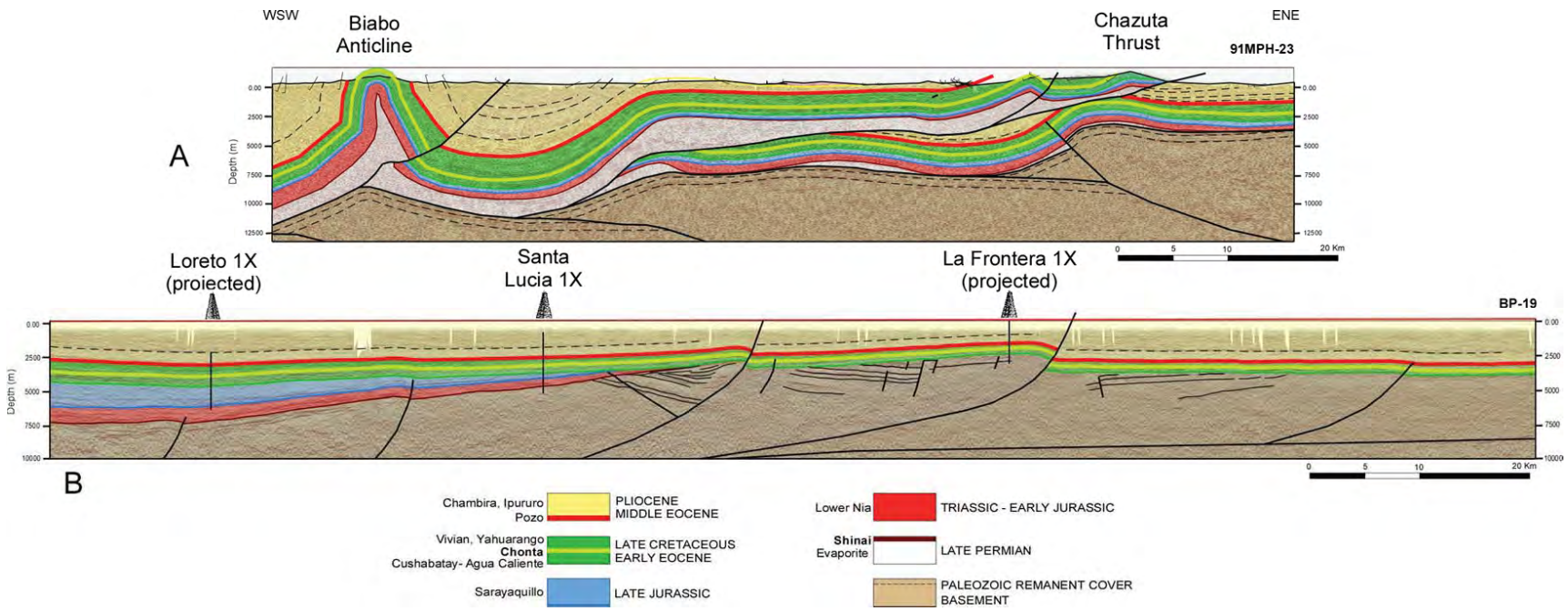

Figure 4.4. Interpreted seismic sections crossing the Huallaga and Marañón wedge-top basins and used for the balanced cross-section construction.

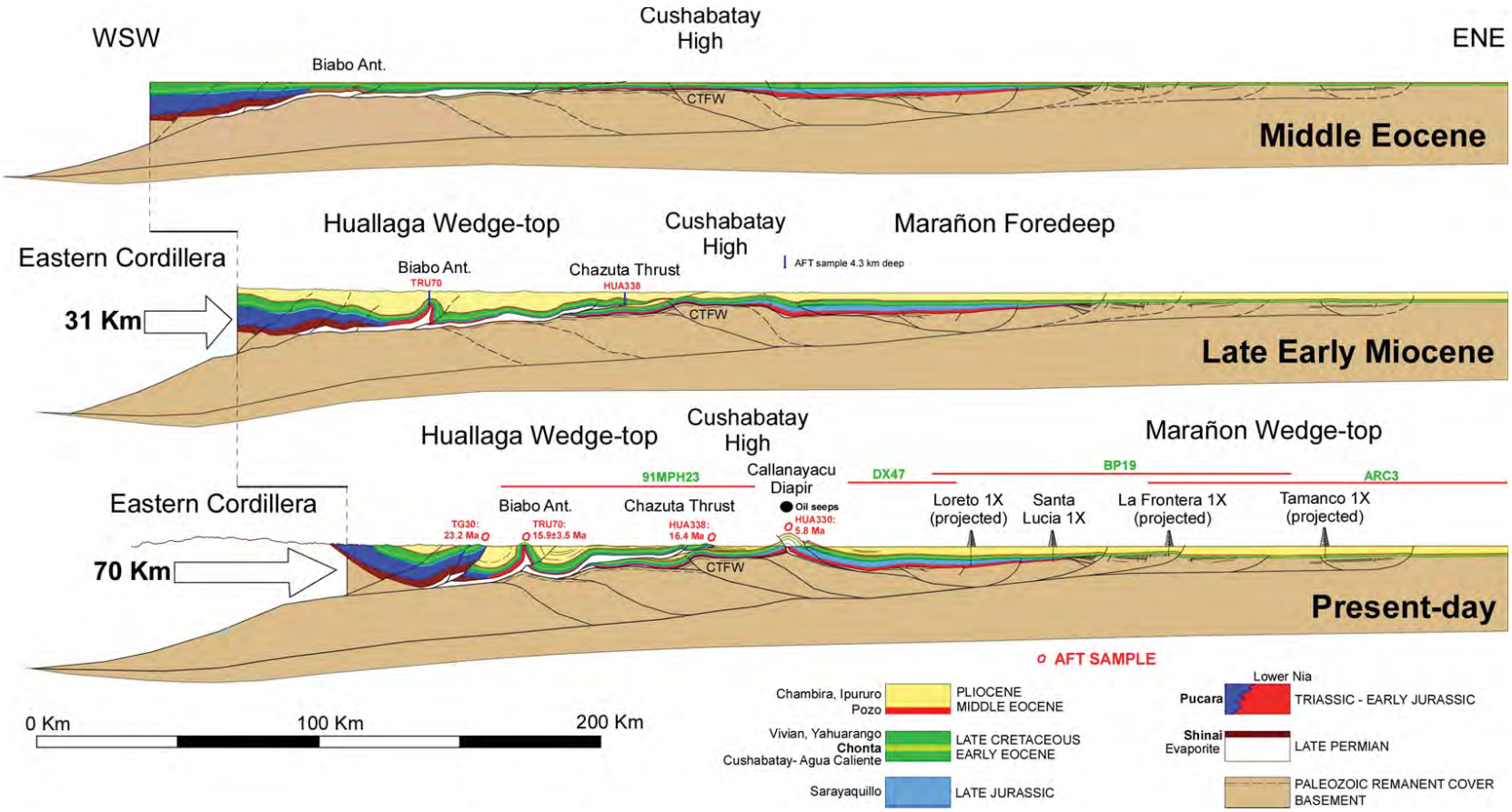

Figure 4.5. Huallaga-Marañón balanced cross-section and sequential restoration. Initial section was obtained by flattening the base of the Pozo Formation (± 45Ma). Intermediary stage corresponds to the Late Early Miocene stage and is calibrated by AFT dating in the Chazuta Thrust and Biabo Anticline. AFT samples are projected on the cross-section (see location on the map of Figure 4.2). TG30, HUA338 and HUA330 have been analyzed for this study (see Table 4.1); ages correspond to youngest cooling events. TRU70 has been published by Eude et al. (2015); the AFT age corresponds to the Central Age. CTFW: Chazuta Thrust Foot-Wall.

In the study area, new apatite fission-tracks (AFT) dating allowed to constrain the timing of exhumation of the main thrust structures. These AFT analyses were done at *Geotrack International Pty Ltd* in 2014. They are presented in the Table 4.1, and reported in the geological map of Figure 4.2 and on the cross-sections of Figure 4.5. They are relative to three samples collected in the Eastern Cordillera-Huallaga basin transition, the Chazuta Thrust and the Callanayacu Diapir. For each sample AFT analysis, we used the BinomFit software to statistically deconvolve grain-age distribution, and determine the youngest cooling event (Brandon, 1996; Brandon et al., 1998) (see Table 4.1). The three youngest cooling events ages range from 23.2 Ma in the Eastern Cordillera-Huallaga basin transition to 5.8 Ma in the Callanayacu Diapir, and show a decrease towards the east. We interpret this phenomenon as a classic in-sequence propagation and exhumation of the thrusts system. The sample collected on the Chazuta thrust gave a youngest exhumation event of 16.4 Ma, which is consistent with the AFT age of one other Jurassic sample collected in the Biabo anticline (TRU70, see Eude et al. 2015). This cooling event age has been also interpreted as thrust related uplift.

In the sequential restoration of Figure 4.5, the initial stage of the balanced cross-section corresponds to the Middle Eocene configuration during the Pozo deposits, which sealed a regional planar unconformity (Christophoul et al., 2002). It shows that weak thrust structures, as the Biabo anticline o the west-verging basement horse of the Chazuta thrust foot-wall (CTFW in the Figure 4.5), were partially developed at this period. Growth strata observable on the seismic show this weak deformation is Senonian and Paleocene in age. The second stage has been chosen to illustrate the Late Early Miocene thrusts exhumation event recorded by the AFT analysis of the Chazuta thrust sample (Table 4.1) and of the Biabo anticline sample (Eude et al., 2015). It also corresponds to a strong sedimentation stage that must be considerate as fundamental in the understanding of the petroleum systems evolution. In the restoration, according to the study of Eude et al. (2015), we consider that the closure temperature of AFT (~110°C) corresponds to a depth of approximately 4.3 km that we replaced in the intermediate stage. In this Late Early Miocene stage, the Triassic rift of the Eastern Cordillera was partly inverted and the Biabo and Chazuta structures well developed. Total horizontal shortening was 31 km. In the Chazuta thrust foot-wall, a west verging basement thrust structure was uplifted and interfered with the Chazuta thrust propagation. This basement uplift has been recorded by growth strata from Late Cretaceous to Miocene times. In the centre of the Huallaga wedge-top depozone, the Cenozoic charge reached more than 8 km thickness.

.

SAMPLE	STRATIGRAPHIC AGE/FORMATION	STRUCTURAL UNIT	LONGITUDE	LATITUDE	ELEVATION (M)	PS	NS	PI	NI	PD	ND	P(X2) (%)	U (PPM)	CL (WT %)	CENTRAL AGE (MA)	NG	COMPONENT AGES (MA)	CL (± 1б)
HUA330	Triassic Lower Nia	Callanayacu Dome	-75.962459	-6.574092	203	0.172	47	7.061	1933	1.408	2222	33	57	0.03	6.8 ± 1.0	20	**YP: 5.8**	-1.8 ± 2.7
																	OP: 15.6	-6.1 ± 10.1
HUA338	Jurassic Sarayaquillo	Chazuta Thrust	-76.162636	-6.613201	280	0.206	53	2.458	631	1.364	2148	1	21	0.22	21.8 ± 4.8	20	**YP: 16.4**	-2.8 ± 3.3
																	OP: 68.4	-20.0 ± 28.2
TG30	Jurassic Sarayaquillo	EC-Huallaga transition	-76.66421	-7.767454	596	0.233	85	2.433	888	1.367	2148	9	20	0.42	25.2 ± 3.1	20	**YP: 23.2**	-3.7 ± 4.4
																	OP: 66.8	-40.7 ± 103.2

Note: ρS density (cm -2) of spontaneous tracks; Ns— number of spontaneous tracks counted; Ni— number of induced tracks counted; ρi— density (cm–2) of induced tracks; ρd— density (cm -2) of tracks on the neutron fluence monitor (CN-1 glass); Nd— number of tracks counted in the dosimeter; P(X2)— probability (%) of greater chi-squared; central ages, reported for each sample with confidence interval (CI) of one sigma (±1б), were calculated using the zeta calibration method (Hurford and Green, 1982) with zeta of 380 ± 8; Ng— number of grains counted; Young population (YP) and old population (OP) were determined with the BinomFit software (Brandon, 1996; Brandon et al., 1998); the estimated 68% confidence interval (CI), which is approximately equal to ±1б, was calculated using precise algorithms (for details, see Brandon, 1996; Brandon et al., 1998)

Table 4.1. New apatite fission-tracks (AFT) data. Analyses were done at *Geotrack International Pty Ltd* in 2014.

Sample Code	Name	Laboratory	Latitude	Longitude	Average Depth (m [ft])	Formation	Structure	R_o	TOC	S1	S2	S3	T_{max}	HI	OI
MB01748R	Tamanco 1X	PSI	−5.8384	−74.3625	2842 [9324]	Chonta	Tamanco		2.62	0.53	12.00	1.58	426	458	60
MB01749R	Tamanco 1X	PSI	−5.8384	−74.3625	2876 [9436]	Chonta	Tamanco		1.20	0.11	1.73	0.60	428	144	50
MB01750R	Tamanco 1X	PSI	−5.8384	−74.3625	2900 [9500]	Chonta	Tamanco		1.18	0.22	1.94	0.65	428	164	55
MB01738R	Tamanco 1X	PSI	−5.8384	−74.3625	910 [2986]	Pebas	Tamanco	0.46	2.92		0.62		551	21	
MB01742R	Tamanco 1X	PSI	−5.8384	−74.3625	1669 [5476]	Chambira	Tamanco	0.66	2.00		6.56		423	328	
MB01748R	Tamanco 1X	PSI	−5.8384	−74.3625	2842 [9324]	Chonta	Tamanco	0.77	2.62		12		426	458	
MB01750R	Tamanco 1X	PSI	−5.8384	−74.3625	2900 [9500]	Chonta	Tamanco	0.79	1.18		1.94		428	164	
MB01963R	Loreto 1X	PSI	−5.9131	−75.5842	1372 [4501]	Chonta	Loreto		0.95	0.14	1.05	0.36	442	110	38
MB01964R	Loreto 1X	PSI	−5.9131	−75.5842	1402 [4600]	Chonta	Loreto		0.68	0.10	0.47	0.45	440	69	66
MB01968R	Loreto 1X	PSI	−5.9131	−75.5842	1492 [4895]	Chonta	Loreto		0.52	0.05	0.19	0.27	432	36	51
MB01972R	Loreto 1X	PSI	−5.9131	−75.5842	1612 [5289]	Chonta	Loreto		0.54	0.05	0.35	0.28	437	64	51
MB01067R	Loreto 1X	PSI	−5.9131	−75.5842	2024 [6640]	Raya	Loreto		0.61	0.02	0.61	0.37	436	100	61
MB01071R	Loreto 1X	PSI	−5.9131	−75.5842	2075 [6808]	Raya	Loreto		1.19	0.12	1.91	0.31	442	161	26
MB01983R	Loreto 1X	PSI	−5.9131	−75.5842	2031 [6663]	Raya	Loreto		2.32	0.22	2.97	0.21	438	128	9
MB01984R	Loreto 1X	PSI	−5.9131	−75.5842	2052 [6732]	Raya	Loreto		3.12	0.35	4.70	0.34	440	151	11
	Loreto 1X	SPT	−5.9131	−75.5842	873 [2864]	Pozo	Loreto	0.59							
	Loreto 1X	SPT	−5.9131	−75.5842	1355 [4446]	Chonta	Loreto	0.66							
	Loreto 1X	SPT	−5.9131	−75.5842	2452 [8045]	Cushabatay	Loreto	0.89							
MB03727R	Santa Lucia 1X	PSI	−6.3843	−75.0512	338 [1109]	Chambira	Santa Lucia	0.41	0.19						
MB03738R	Santa Lucia 1X	PSI	−6.3843	−75.0512	872 [2861]	Chambira	Santa Lucia	0.49	0.37						
MB03759R	Santa Lucia 1X	PSI	−6.3843	−75.0512	1826 [5991]	Pozo	Santa Lucia	0.53	0.31						
MB03764R	Santa Lucia 1X	PSI	−6.3843	−75.0512	2009 [6591]	Vivian	Santa Lucia	0.47	0.69						
MB03767R	Santa Lucia 1X	PSI	−6.3843	−75.0512	2079 [6821]	Vivian	Santa Lucia	0.50	0.55						
MB03769R	Santa Lucia 1X	PSI	−6.3843	−75.0512	2170 [7133]	Chonta	Santa Lucia	0.51	0.28						
MB03772R	Santa Lucia 1X	PSI	−6.3843	−75.0512	2198 [7211]	Chonta	Santa Lucia	0.55	0.44						
MB03774R	Santa Lucia 1X	PSI	−6.3843	−75.0512	2237 [7339]	Chonta	Santa Lucia	0.58	0.43						
MB03776R	Santa Lucia 1X	PSI	−6.3843	−75.0512	2265 [7431]	Chonta	Santa Lucia	0.59	0.38						
MB03778R	Santa Lucia 1X	PSI	−6.3843	−75.0512	2316 [7008]	Chonta	Santa Lucia	0.56	2.32	0.09	1.23	1.30	435	53	56
MB03779R	Santa Lucia 1X	PSI	−6.3843	−75.0512	2380 [7808]	Chonta	Santa Lucia	0.58	0.52						
MB03780R	Santa Lucia 1X	PSI	−6.3843	−75.0512	2390 [7841]	Chonta	Santa Lucia	0.58	0.38						

Table 4.2. Geochemical analyses of the PERUPETRO data bank (Petroleum System International, 2011; SPT Simon Petroleum, 1993) and new geochemical analyses done by Geo Lab Sur and Geotrack in new outcrop samples collected close to the regional cross-section.

MB03783R	Santa Lucia 1X	PSI	−6.3843	−75.0512	2444 [8018]	Agua Caliente	Santa Lucia	0.59	0.41						
MB03786R	Santa Lucia 1X	PSI	−6.3843	−75.0512	2716 [8911]	Agua Caliente	Santa Lucia	0.56							
MB03787R	Santa Lucia 1X	PSI	−6.3843	−75.0512	2728 [8950]	Agua Caliente	Santa Lucia	0.62	1.09						
MB03790R	Santa Lucia 1X	PSI	−6.3843	−75.0512	2761 [9058]	Cushabatay	Santa Lucia	0.66	1.64						
MB03793R	Santa Lucia 1X	PSI	−6.3843	−75.0512	2990 [9810]	Cushabatay	Santa Lucia	0.56	3.9						
MB03637R	La Frontera 3X	PSI	−6.2970	−74.6735	1771 [5810]	Chonta	La Frontera		0.75						
MB03638R	La Frontera 3X	PSI	−6.2970	−74.6735	1798 [5899]	Chonta	La Frontera	0.51	0.98	0.56	0.78	0.75	382	80	77
MB03639R	La Frontera 3X	PSI	−6.2970	−74.6735	1835 [6020]	Chonta	La Frontera		0.58						
MB03640R	La Frontera 3X	PSI	−6.2970	−74.6735	1890 [6201]	Chonta	La Frontera		0.93						
MB03641R	La Frontera 3X	PSI	−6.2970	−74.6735	1999 [6558]	Chonta	La Frontera		2.38	0.47	1.04	1.06	429	44	45
MB03642R	La Frontera 3X	PSI	−6.2970	−74.6735	2292 [7520]	Raya	La Frontera		0.82						
MB03643R	La Frontera 3X	PSI	−6.2970	−74.6735	2493 [8179]	Cushabatay	La Frontera	0.59	1.77		1.24		426	70	
MB03648R	La Frontera 3X	PSI	−6.2970	−74.6735	2576 [8451]	Cabanillas	La Frontera	0.85	1.05		1.56		341	149	
MB03654R	La Frontera 3X	PSI	−6.2970	−74.6735	2649 [8691]	Cabanillas	La Frontera	1.49	0.74		1.29		417	174	
MB03656R	La Frontera 3X	PSI	−6.2970	−74.6735	2676 [8780]	Cabanillas	La Frontera	1.11	1.26		1.83		340	145	
MB03660R	La Frontera 3X	PSI	−6.2970	−74.6735	2740 [8990]	Cabanillas	La Frontera	1.54	2.08		0.80		429	38	
MB03665R	La Frontera 3X	PSI	−6.2970	−74.6735	2758 [9049]	Cabanillas	La Frontera	1.19	2.00		0.65		394	33	
MB03671R	La Frontera 3X	PSI	−6.2970	−74.6735	2832 [9291]	Cabanillas	La Frontera	1.58	1.14		0.33		383	29	
MB03675R	La Frontera 3X	PSI	−6.2970	−74.6735	2850 [9350]	Cabanillas	La Frontera	1.19	1.00		0.26		357	26	
MB03685R	La Frontera 3X	PSI	−6.2970	−74.6735	2954 [9692]	Cabanillas	La Frontera	1.68	1.00		0.07			7	
MB01081R	Ponasillo 1X	PSI	−7.3980	−76.2972	1277 [4190]	Huchpayacu	Ponasillo	0.97							
MB01083R	Ponasillo 1X	PSI	−7.3980	−76.2972	1359 [4459]	Chonta	Ponasillo	0.95							
MB01085R	Ponasillo 1X	PSI	−7.3980	−76.2972	1407 [4616]	Chonta	Ponasillo	1.00							
MB01087R	Ponasillo 1X	PSI	−7.3980	−76.2972	1449 [4754]	Chonta	Ponasillo	1.48	0.94	0.38	0.97	0.34	432	103	36.00
MB01090R	Ponasillo 1X	PSI	−7.3980	−76.2972	1503 [4931]	Chonta	Ponasillo	1.05							
MB01091R	Ponasillo 1X	PSI	−7.3980	−76.2972	1530 [5020]	Chonta	Ponasillo	1.05							
MB01093R	Ponasillo 1X	PSI	−7.3980	−76.2972	1564 [5131]	Chonta	Ponasillo	1.06							
MB01094R	Ponasillo 1X	PSI	−7.3980	−76.2972	1593 [5226]	Chonta	Ponasillo	1.11							
MB01096R	Ponasillo 1X	PSI	−7.3980	−76.2972	1646 [5400]	Chonta	Ponasillo	1.17							
MB01100R	Ponasillo 1X	PSI	−7.3980	−76.2972	1737 [5699]	Chonta	Ponasillo	1.19							
MB01101R	Ponasillo 1X	PSI	−7.3980	−76.2972	1783 [5850]	Chonta	Ponasillo	1.10							
MB01102R	Ponasillo 1X	PSI	−7.3980	−76.2972	1811 [5942]	Chonta	Ponasillo	1.26							
MB01103R	Ponasillo 1X	PSI	−7.3980	−76.2972	1829 [6001]	Chonta	Ponasillo	1.09							

(*Continued*)

Sample Code	Name	Laboratory	Latitude	Longitude	Average Depth (m [ft])	Formation	Structure	R_o	TOC	S1	S2	S3	T_{max}	HI	OI
MB01105R	Ponasillo 1X	PSI	−7.3980	−76.2972	1875 [6152]	Chonta	Ponasillo	1.29							
MB01106R	Ponasillo 1X	PSI	−7.3980	−76.2972	1902 [6240]	Chonta	Ponasillo	1.23							
MB01108R	Ponasillo 1X	PSI	−7.3980	−76.2972	1920 [6299]	Chonta	Ponasillo	1.22							
MB01110R	Ponasillo 1X	PSI	−7.3980	−76.2972	1963 [6440]	Chonta	Ponasillo	1.06							
MB01113R	Ponasillo 1X	PSI	−7.3980	−76.2972	2014 [6608]	Agua Caliente	Ponasillo	1.24							
MB01114R	Ponasillo 1X	PSI	−7.3980	−76.2972	2014 [6608]	Agua Caliente	Ponasillo	1.28	1.81	0.18	1.29	0.31	498	71	17.00
MB01119R	Ponasillo 1X	PSI	−7.3980	−76.2972	2016 [6614]	Agua Caliente	Ponasillo	1.27							
MB01120R	Ponasillo 1X	PSI	−7.3980	−76.2972	2017 [6617]	Agua Caliente	Ponasillo	1.16	0.79	0.45	0.65	0.46	526	82	58.00
MB01123R	Ponasillo 1X	PSI	−7.3980	−76.2972	2115 [6939]	Agua Caliente	Ponasillo	1.33							
MB01124R	Ponasillo 1X	PSI	−7.3980	−76.2972	2143 [7031]	Agua Caliente	Ponasillo	1.60							
MB01125R	Ponasillo 1X	PSI	−7.3980	−76.2972	2271 [7451]	Agua Caliente	Ponasillo	1.40							
MB01126R	Ponasillo 1X	PSI	−7.3980	−76.2972	2275 [7464]	Agua Caliente	Ponasillo	1.59	1.59	0.14	1.26	2.15	435	79	135.00
MB01127R	Ponasillo 1X	PSI	−7.3980	−76.2972	2316 [7598]	Agua Caliente	Ponasillo	1.53							
MB01129R	Ponasillo 1X	PSI	−7.3980	−76.2972	2384 [7822]	Raya	Ponasillo	1.65							
MB01132R	Ponasillo 1X	PSI	−7.3980	−76.2972	2435 [7989]	Cushabatay	Ponasillo	1.41							
MB01133R	Ponasillo 1X	PSI	−7.3980	−76.2972	2457 [8061]	Cushabatay	Ponasillo	1.69							
MB01135R	Ponasillo 1X	PSI	−7.3980	−76.2972	2490 [8169]	Cushabatay	Ponasillo	1.50							
MB01139R	Ponasillo 1X	PSI	−7.3980	−76.2972	2594 [8510]	Cushabatay	Ponasillo	1.70							
MB01142R	Ponasillo 1X	PSI	−7.3980	−76.2972	2664 [8740]	Shinai	Ponasillo	1.80							
MB01144R	Ponasillo 1X	PSI	−7.3980	−76.2972	2737 [8980]	Shinai	Ponasillo	1.80							
MB05982R	Burlington OC 2-20	PSI	−5.7339	−77.7040	0	Pucara	Eastern Cordillera		2.07	0.08	0.11	0.27	575	5	13
MB05986R	Burlington OC 2-20	PSI	−5.7339	−77.7040	0	Pucara	Eastern Cordillera		1.07	0.04	0.03	0.71	343	3	66
MB05987R	Burlington OC 2-20	PSI	−5.7339	−77.7040	0	Pucara	Eastern Cordillera		1.60	0.02	0.08	2.21	477	5	138
MB05988R	Burlington OC 2-20	PSI	−5.7339	−77.7040	0	Pucara	Eastern Cordillera		2.15	0.03	0.07	2.93	479	3	136
MB05989R	Burlington OC 2-20	PSI	−5.7339	−77.7040	0	Pucara	Eastern Cordillera		2.31	0.12	0.51	4.30	467	22	186
MB05990R	Burlington OC 2-20	PSI	−5.7339	−77.7040	0	Pucara	Eastern Cordillera		3.56	0.09	0.13	0.65	581	4	18
MB05991R	Burlington OC 2-20	PSI	−5.7339	−77.7040	0	Pucara	Eastern Cordillera		0.54	0.03	0.07	0.64	360	13	119
MB05993R	Burlington OC 2-20	PSI	−5.7339	−77.7040	0	Pucara	Eastern Cordillera		0.88	0.01	0.03	0.60	360	3	68
MB05998R	Burlington OC 2-20	PSI	−5.7339	−77.7040	0	Pucara	Eastern Cordillera		1.29	0.16	0.15	0.31	572	12	24
MB05999R	Burlington OC 2-20	PSI	−5.7339	−77.7040	0	Pucara	Eastern Cordillera		3.06	0.07	0.13	1.31	576	4	43

MB06000R	Burlington OC 2-20	PSI	−5.7339	−77.7040	0	Pucara	Eastern Cordillera		1.54	0.03	0.10	1.21	390	7	79
MB06001R	Burlington OC 21-30	PSI	−5.7585	−77.8976	0	Pucara	Eastern Cordillera		2.07	0.02	0.10	3.65	490	5	176
MB06002R	Burlington OC 21-30	PSI	−5.7585	−77.8976	0	Pucara	Eastern Cordillera		1.71	0.12	0.13	1.15	547	8	67
MB06003R	Burlington OC 21-30	PSI	−5.7585	−77.8976	0	Pucara	Eastern Cordillera		2.41	0.10	0.31	0.17	565	13	7
MB06004R	Burlington OC 21-30	PSI	−5.7585	−77.8976	0	Pucara	Eastern Cordillera		3.93	0.08	0.35	3.11	562	9	79
MB06005R	Burlington OC 21-30	PSI	−5.7585	−77.8976	0	Pucara	Eastern Cordillera		4.42	0.23	0.17	0.52	575	4	12
MB06006R	Burlington OC 21-30	PSI	−5.7585	−77.8976	0	Pucara	Eastern Cordillera		3.44	0.18	0.47	0.59	565	14	17
MB06007R	Burlington OC 21-30	PSI	−5.7585	−77.8976	0	Pucara	Eastern Cordillera		4.89	0.27	0.58	0.24	562	12	5
MB06008R	Burlington OC 21-30	PSI	−5.7585	−77.8976	0	Pucara	Eastern Cordillera		5.15	0.68	0.90	0.99	555	17	19
MB06009R	Burlington OC 21-30	PSI	−5.7585	−77.8976	0	Pucara	Eastern Cordillera		4.80	0.29	0.50	0.30	540	10	6
MB06010R	Burlington OC 21-30	PSI	−5.7585	−77.8976	0	Pucara	Eastern Cordillera		1.87	0.10	0.08	0.28	445	4	15
MB06011R	Burlington OC 31-39	PSI	−5.8949	−77.9523	0	Pucara	Eastern Cordillera		1.08	0.13	0.13	0.12	424	12	11
MB06012R	Burlington OC 31-39	PSI	−5.8949	−77.9523	0	Pucara	Eastern Cordillera		3.21	0.22	0.26	0.41	500	8	13
MB06013R	Burlington OC 31-39	PSI	−5.8949	−77.9523	0	Pucara	Eastern Cordillera		3.14	0.09	0.10	0.33	542	3	11
MB06014R	Burlington OC 31-39	PSI	−5.8949	−77.9523	0	Pucara	Eastern Cordillera		1.24	0.01	0.01	1.17	396	1	94
MB06015R	Burlington OC 31-39	PSI	−5.8949	−77.9523	0	Pucara	Eastern Cordillera		2.21	0.08	0.16	1.07	479	7	48
MB06016R	Burlington OC 31-39	PSI	−5.8949	−77.9523	0	Pucara	Eastern Cordillera		2.51	0.03	0.22	2.01	459	9	80
MB06017R	Burlington OC 31-39	PSI	−5.8949	−77.9523	0	Pucara	Eastern Cordillera		1.41	0.02	0.02	1.53	379	1	109
MB06018R	Burlington OC 31-39	PSI	−5.8949	−77.9523	0	Pucara	Eastern Cordillera		3.50	0.32	0.12	0.20	398	3	6
MB06019R	Burlington OC 31-39	PSI	−5.8949	−77.9523	0	Pucara	Eastern Cordillera		1.78	0.28	0.26	0.22	518	15	12
MB06022R	Burlington OC 42	PSI	−5.7079	−77.5484	0	Pucara	Eastern Cordillera		2.24	0.05	0.07	1.79	394	3	80
IR12-0014	HUA332	Geo Lab Sur	−6.5726	−75.9254	0	Shinai	Cushabatay High	0.5−0.6	4.01	0.10	4.25	2.15	432	106	54
IR12-0015	TRU278	Geo Lab Sur	−6.3671	−77.9182	0	Pucara	Eastern Cordillera		2.17	0.78	0.81	0.71	422	37	33
IR12-0016	TRU048	Geo Lab Sur	−6.8466	−77.9722	0	Pucara	Eastern Cordillera		0.85	0.09	0.15	0.60	471	18	71
GC1169-28.1	TG031	Geotrack	−6.574092	−75.962459	0	Raya	Eastern Cordillera	1.6							
4H	GA-85-11	Corelab	−6.5359	−77.2335	0	Pucara	Eastern Cordillera		1.27	1.22	2.33	0.25	448	183	20
280-10	S-35A	Corelab	−6.5063	−75.0876	0	Shinai	Cushabatay High	0.53							
280-15	S-41	Corelab	−6.5063	−75.0876	0	Shinai	Cushabatay High		0.68	0.18	0.37	0.41	449	54	60
4L	58-273	Corelab	−7.1493	−76.0034	0	Shinai	Cushabatay High		6.06	1.49	5.21	3.24	427	86	53
B86209	M18	ELF96-02	−10.4124	−74.9823	0	Shinai	San Matías thrust	1.5	2.29	0.83	1.27		453	43	

Note: TOC - Total Organic Content, wt %, HI - Hydrogen index = S2*100/TOC, mg HC /g TOC, OI – Oxygen Index = S3*100/TOC, mg CO_2/g TOC.

4.5. Sources rocks

To describe the mean source rocks of the study area, geochemical analyses of the PERUPETRO data bank have been used and augmented with new data collected by sampling outcrops close to the regional cross-section (see Figure 4.2 and Table 4.2).

The Late Cretaceous Chonta and Raya Formations and the Late Triassic/Early Jurassic Pucara Group have always been considered as the classic source rocks of the hydrocarbons found in the Cretaceous Reservoirs of the Marañón Basin (Core laboratories, 1996, 1999; PARSEP, 2001). The PARSEP study concluded that these source rocks in the basin and neighboring areas are sufficiently rich enough to have generated the commercial amounts of hydrocarbons presently found in the oil fields of the Marañón Basin, and that such accumulations imply a long range remigration from these source rock kitchen areas to reservoir. While it is true that the Chonta and Raya source rocks have been proved to produce oil in the Huallaga and Marañón basins, the Pucara source rock geographic distribution is more controversial. As shown above in the stratigraphic discussion (Figure 4.3), the marine deposits considered as Pucara source rock in the Cushabatay High have been never dated, and can been interpreted as Late Permian (Shinai Fm.) thanks to north-south seismic and wells correlations. This new rethinking of the petroleum systems of the Huallaga and Southern Marañón basins appears in the Figure 4.3.

4.5.1. Late Cretaceous

Two Late Cretaceous black shale and limestone levels have been identified as source rocks in the Huallaga and Marañón basins (Core laboratories, 1996, 1999; PARSEP, 2001). They correspond to the Raya and Chonta shallow marine deposits (see stratigraphic diagram of Figure 4.3). Their regional distribution, TOC and maturity are showed on the maps of Figures 4.6 and 4.7.

The Chonta kerogens are Type III and Type II-III (Figure 4.8) with TOC values typically in the 2-3% range (Figure 4.6A). The Chonta source rock is well developed north of the study area where it constitutes the main source rock of the Oriente-Marañón prolific oil province (Marksteiner & Aleman, 1997; Barragan et al., 2008). Effective source rock thickness is estimated to 800 m in the Biabo foot-wall syncline and 60 m in the eastern Marañón depozone. Organic matter is more marine in the western Huallaga basin and becomes

terrestrial in the eastern Marañón. Vitrinite reflectance data reach 1.1% west of the Subandean thrust front and decrease to 0.45 % in the Marañón foreland (Figure 4.7A).

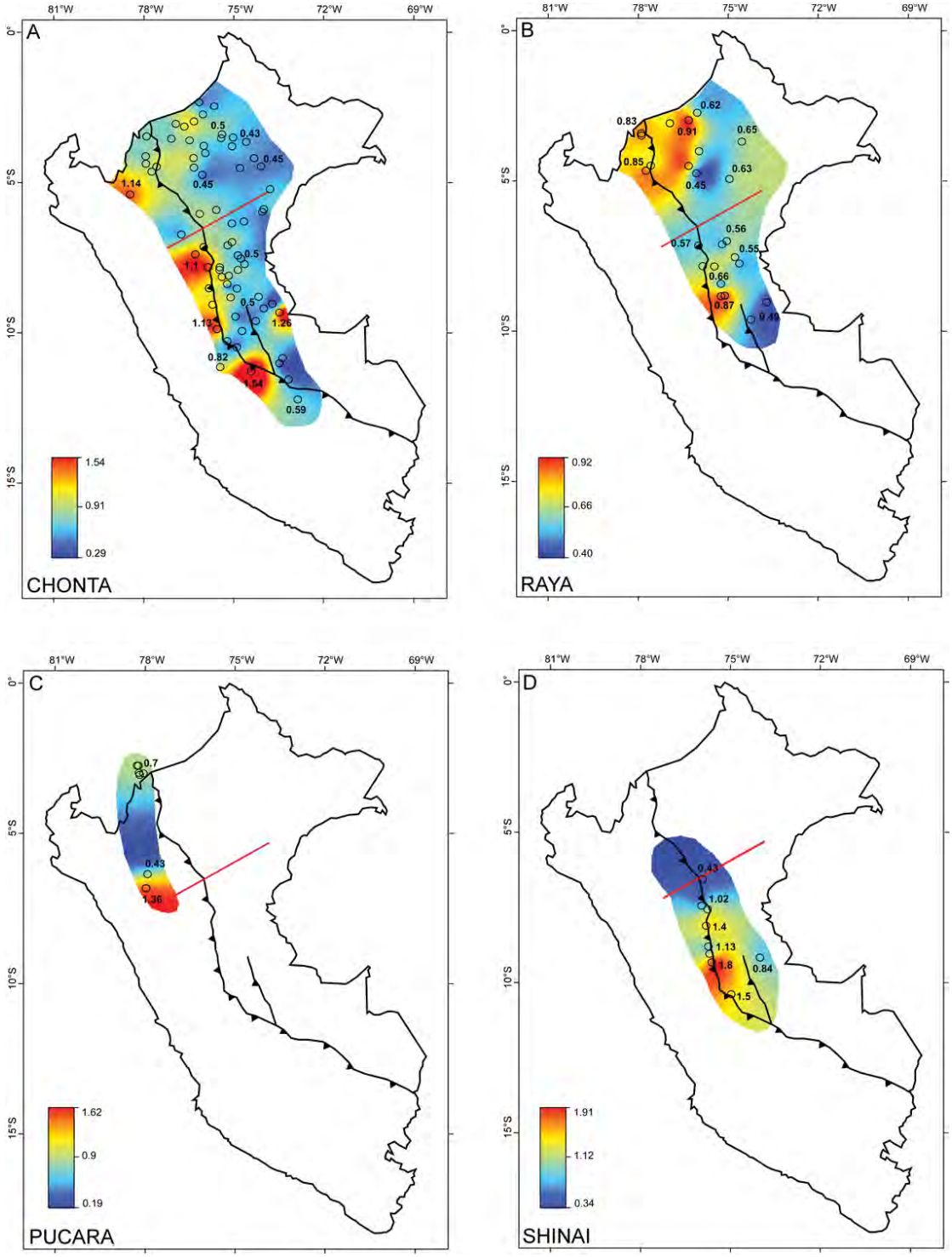

Figure 4.6. Geographic distribution and TOC of the four studied source rocks in the Peruvian Subandean basins. (A) Late Cretaceous (Chonta), (B) Late Cretaceous (Raya), (C) Triassic (Pucara), (D) Late Permian (Shinai).

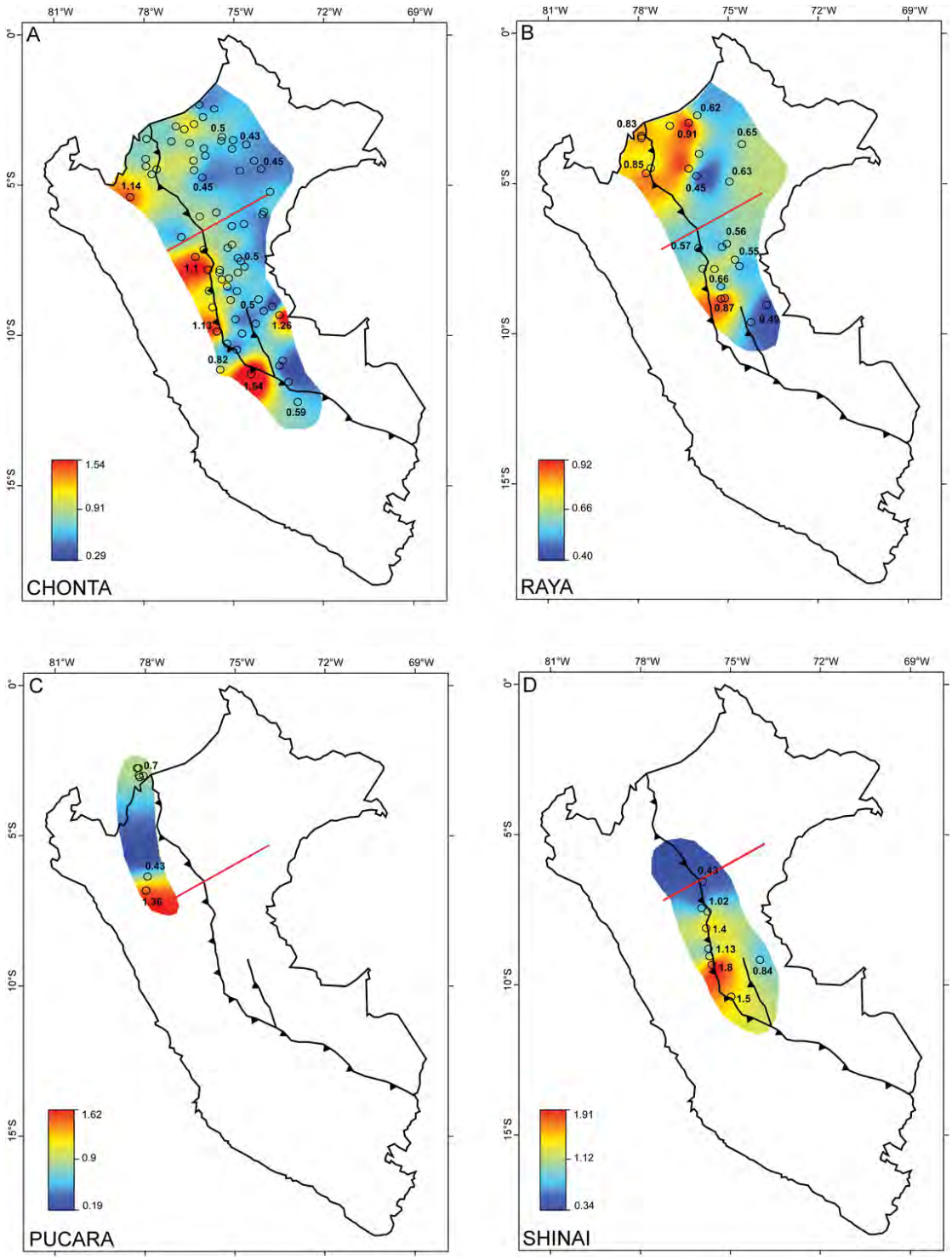

Figure 4.7. Geographic distribution and maturity of the four studied source rocks in the Peruvian Subandean basins. (A) Late Cretaceous (Chonta), (B) Late Cretaceous (Raya Fm.), (C) Triassic (Pucara), (D) Late Permian (Shinai).

The Raya source rocks are Type II and Type II-III (Figure 4.8). The TOC values are in the 1-2% range (Figure 4.6B), and vitrinite reflectance data are relatively constant between 0.5 and 0.6 %. The average effective source rock thickness is estimated to 160 m in the western region and 35 m in the eastern Marañón basin. As the Chonta source rock, it is more marine in the west and becomes terrestrial in the east.

The Cushabatay and Agua Caliente formation present some thin levels of potential source rocks (not proven) that seem negligible at the basin scale.

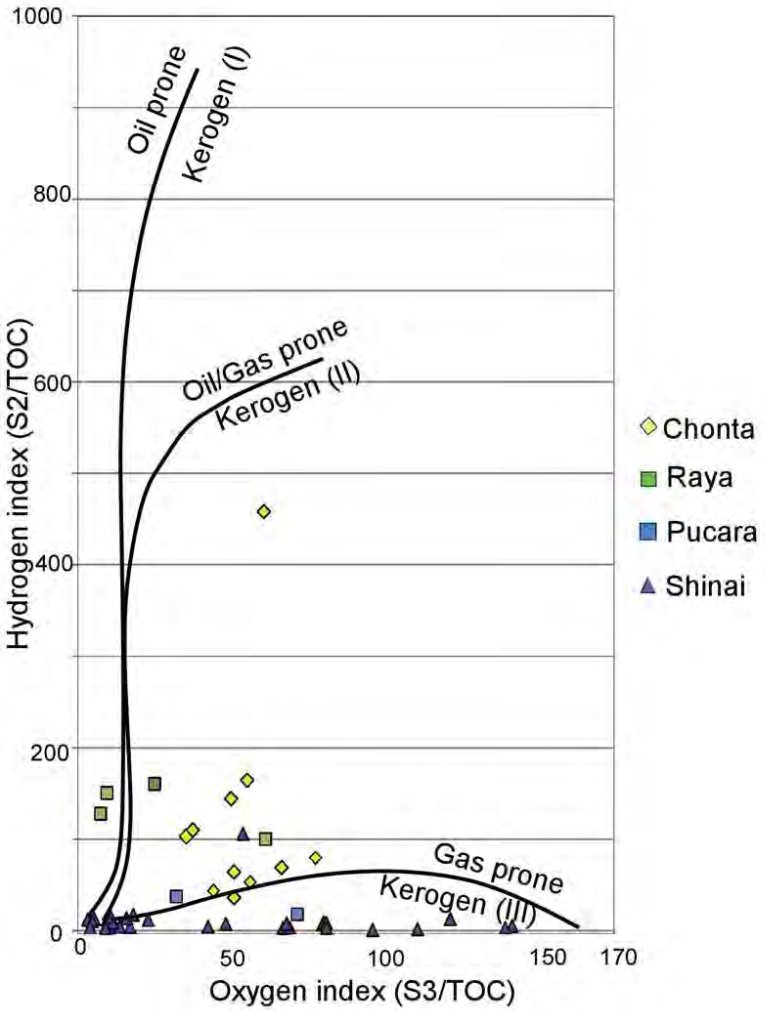

Figure 4.8. Van Krevelen plots of the pyrolysis results from the studied sources rocks (Chonta, Raya, Pucara, Shinai) in the Huallaga-Marañón foreland basin system.

4.5.2. Late Triassic/Lower Jurassic (Pucara)

The Pucara source rock interval corresponds to a bituminous carbonate with interbedded organic rich shale sections, known as Aramachay Fm. in the Peruvian stratigraphic nomenclature (Rosas et al., 2007 and reference therein). It is outcropping in the Eastern Cordillera and in the Huallaga-Eastern Cordillera transition zone (Figure 4.5). The Pucara Group deposits were controlled by post-rift regional subsidence and marine inundation during the Late Triassic and the Early Jurassic (Rosas et al., 2007). The main source rock sequence (Aramachay Fm.) was deposited during the period of maximum flooding. The Pucara marine deposits are confined to the western part of the studied regional cross-section (Figure 4.5), the Huallaga-Eastern Cordillera transition zone, which corresponds to the eastern border of the inverted Triassic rift system. They laterally grade to the continental sandstones and silts of the Lower Nia and Sarayaquillo formations (Figure 4.3). In fact, poor data are known about the oil potential of the Pucara source rock, and its geographic distribution is poorly constrained (Figure 4.6C). Analyses of two samples that we collected in the Eastern Cordillera (see Table 4.2) show that it contains Type III kerogens (Figure 4.8) with TOC values ranging between 1- 2 % (Figure 4.5C). One of these samples is thermally matures and the other overmature (Figure 4.7C). These data are consistent with the hydrocarbon source potential of the Santiago Fm. in the Cutucu Cordillera of Ecuador (Gaibor et al., 2008), which corresponds to the northern prolongation of the Peruvian Santiago basin (Figures 4.1, 4.6C, 4.7C). The Ecuadorian Santiago Formation is the temporal equivalent of the Peruvian Aramachay Formation.

4.5.3. Late Permian (Shinai)

East of the Chazuta thrust, in the Cushabatay High area (Figures 4.2, 4.5), the black shales of the Shinai Fm., previously considered as part of the Pucara Group, have been largely analysed (see Table 4.2). In fact, poor data are known about the oil potential of the Shinai source rock. It contains Type III kerogens (Figure 4.8) and the TOC value can reach 6%. In the outcrops of the Callanayacu Diapir, kerogen maturity is low (T= 432°C; Ro equivalent between 0.5 and 06) and recorded a weak sedimentary charge, which is consistent with the sequential restoration of the Figure 4.5. Thickness of the Shinai source rock varies between 60 and 200 m. Its geographic distribution is poorly constrained in the west and the north, but well identified in the south towards the Camisea gas field thanks to seismic and well correlations (Figures 4.6D, 4.7D).

4.5.4. Devonian Carboniferous (Cabanillas)

The only Devonian source rock known along our cross section is the Cabanillas Fromation (see Figure 3) reached by the La Frontera 3X well in the Marañón Basin (see Table 4.2). It is considered as a type III source rock (Baseline Geochemical Solutions, Infologic, 2006). Seismic sections (Figure 4.4) show that this Paleozoic series was strongly eroded prior to the Mesozoic rifting period. Its presence below the Huallaga basin is not proven and, probably, very hypothetical. In the La Frontera 3X well, the Cabanillas source rock is overmature, and the TOC values range between 0.7 and 2%.

4.5.5. Oil affinity background

Two oil seeps, Chazuta and Callanayacu, outcrop in the study area (Figure 4.2) and have been analysed (Jarvie and McCaffrey, 2001). These authors distinguished separate sources for each oil seep. They concluded that the Callanayacu oil was derived from a carbonate or marl, while the Chazuta oil was derived from shale. Mathalone and Montoya (1995) state that the northern Marañón basin oils originate from a Cretaceous source while the southern Marañón basin oils are likely derived from a Permian source. This is consistent with the geographic distribution of the Shinai source rock that we are proposing (Figures 4.6D, 4.7D). Idemitsu Oil & Gas Company Ltd. (2000) provided a detailed geochemical characterization of 42 crude oils and 11 condensates, and 73 extracts from source rocks of different ages from the different Subandean basins of Peru. In the Marañón basin, they correlated crude oils with Permian and Cretaceous sources rocks too (Figure 4.9).

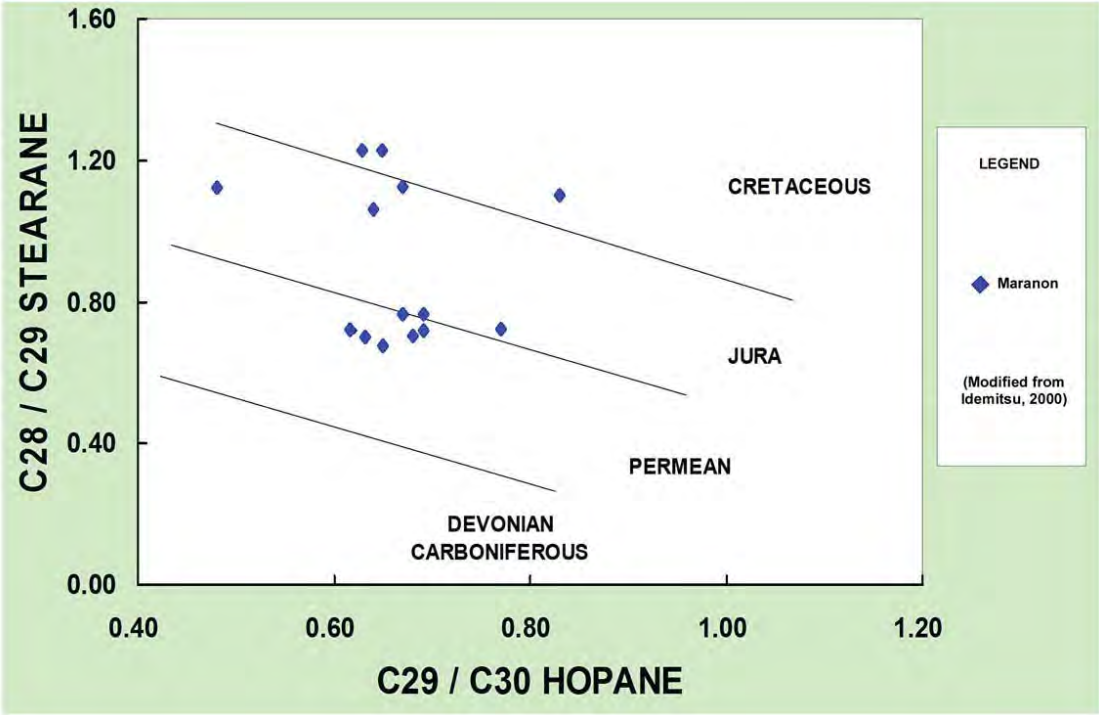

Figure 4.9. Oil to sources correlations in the Marañón basin from C28 / C29 Sterane Ratio versus C29 / C30 Hopane Ratio (modified from Idemitsu Oil & Gas Company Ltd., 2000).

4.6. Petroleum systems modeling

4.6.1. Method and data gathering

The basin analysis is a basic tool that let petroleum exploration to integrate the principles of maturity history, hydrocarbon generation, expulsion and migration in a dynamic setting in order to understand the petroleum system and to verify different exploration scenarios (Waples, 1980, 1994; Tissot et al., 1987; Hermanrud, 1993; Yalçin et al., 1997; Hantschel and Kauerauf, 2009). In fold and thrust belts, the key point is the relative timing between thrust emplacement and hydrocarbon migration (Baby et al., 1995; Moretti et al., 1996; Faure et al., 2004; Cooper, 2007). Petroleum modeling of balanced cross-section and respective sequential restoration is a necessary approach to deal with this problem.

In our study, we used the Schlumberger 1D and 2D Petromod software to model the burial history of the sequential restoration of the Huallaga-Marañón regional cross-section (Figure 4.5). In order to calibrate the thermal and petroleum system modeling, we compiled and used Rock-Eval-TOC and Vitrinite Reflectance (Ro) data of source rocks from the PERUPETRO databank. Some news outcrops analyses have also been performed (see Table 4.2). Subsurface temperature data of the Ponasillo 1X, Loreto 1X, Santa Lucia 1X, La Frontera 1X and Tamanco 1X wells were also considered for the calibration (see Figure 4.2 for location). The present crustal heat flow of the Huallaga-Marañón foreland system has been analysed by a few authors. There is a general agreement on the fact that it varies between 40 to 60 mW/m2 (Ocola, 1985; Hamza and Munoz, 1996). The heat-flow history of our modeling is based on source rock maturity and wells subsurface temperature data. Along our structural cross-section (Figure 4.5), we obtained a heat flow of 45mW/m2 in the western Huallaga area (Ponasillo 1X calibration) decreasing gradually to 35mW/m2 in the western Marañón basin (Santa Lucia 1X calibration) and increasing to 45mW/m2 in its eastern part (La Frontera 1X and Tamanco 1X calibrations). A value of 60mW/m2 has been assigned to the Triassic rifting period.

The stratigraphy and geohistory input corresponds to the stratigraphic diagram of Figure 4.3. The paleobathymetries for the sedimentary sequences involved in the Huallaga Marañón foreland system were assigned according to the sedimentary environments described more above in the stratigraphic framework. The sediment-water interface temperature was calculated from the paleobathymetry and the model loaded in Petromod and obtained from Global Mean Surface Temperature based on Wygrala (1994).

4.6.2. 1D modeling results

1D burial and thermal history models have been used to calibrate the subsidence, erosion and thermal evolution. We have done 1D modeling for 25 wells in the Marañón and Huallaga basins. However, we presented only the results of five wells close to the regional cross-section (Figures 4.2, 4.5). One fictive well (Biabo hanging-wall syncline) has been also modeled in the deepest part of the Huallaga wedge-top depozone to evaluate the charge history.

Generally, the major geologic events identified in basin modeling coincide with erosional events. In our case (see Figure 4.3), the most important is the pre-Cretaceous erosional event which sealed the Jurua Orogeny described in the Solimoes and Acre basins of northern Brazil (Caputo, 2014) and in the Ucayali basin (Baby et al., 2014; Hurtado et al., 2014). This erosion is strong towards the east and decreases rapidly towards the west. In the Marañón foreland basin, the La Frontera 3X vitrinite reflectance profile (Ro) versus depth (Figure 4.10) shows an important offset at the base of the Cretaceous Cushabatay Formation reflecting a difference of maturity on both sides of the pre-Cretaceous erosional surface. The 1D modeling (Figure 4.11) allowed us to compute that 2800 meters of erosion are necessary to fit with the onset of the Ro profile. The seismic section BP19 (Figure 4.4B) and the balanced cross-section (Figure 4.5) show this angular erosional unconformity disappears gradually towards the Cushabatay High. In the Huallaga wedge-top basin, the Ro profile versus depth of the Ponasillo 1X well confirms that the pre-Cretaceous erosional event is absent or insignificant. As regards intra-Cenozoic and intra-Cretaceous erosions, Ro profiles in all wells show they have been insignificant too. The Figure 4.10 underlines the iso-vitrinite reflectance curves in the regional cross-section and shows that a part of the Neogene charge is currently eroded. In the Marañón basin, the 1D modeling was used to estimate the amount of erosion which decreases from around 3000 m in the west to 1000 m in the east. This strong erosion started in the Early Pliocene as shown by the Apatite Fission Track dating of the exhumation of the Cushabatay High (see sample HUA330 in Figure 4.5 and Table 4.1). This is consistent with our sequential restoration (Figure 4.5) where, during the Pliocene, the southern part of the Marañón basin evolved from a foredeep depozone to a wedge-top depozone. During the Eocene, sedimentation rates were already controlled by thrust propagation and decreased from west to east. In the Biabo area, the entire Cenozoic series is currently preserved in the synclines where its thickness can reach 8000 m. From the Middle Eocene, in this part of the Huallaga basin, the foreland subsidence related to the tectonic loading of the Eastern Cordillera increased rapidly and was continuous as shown by the 1D fictive well modeling in the western

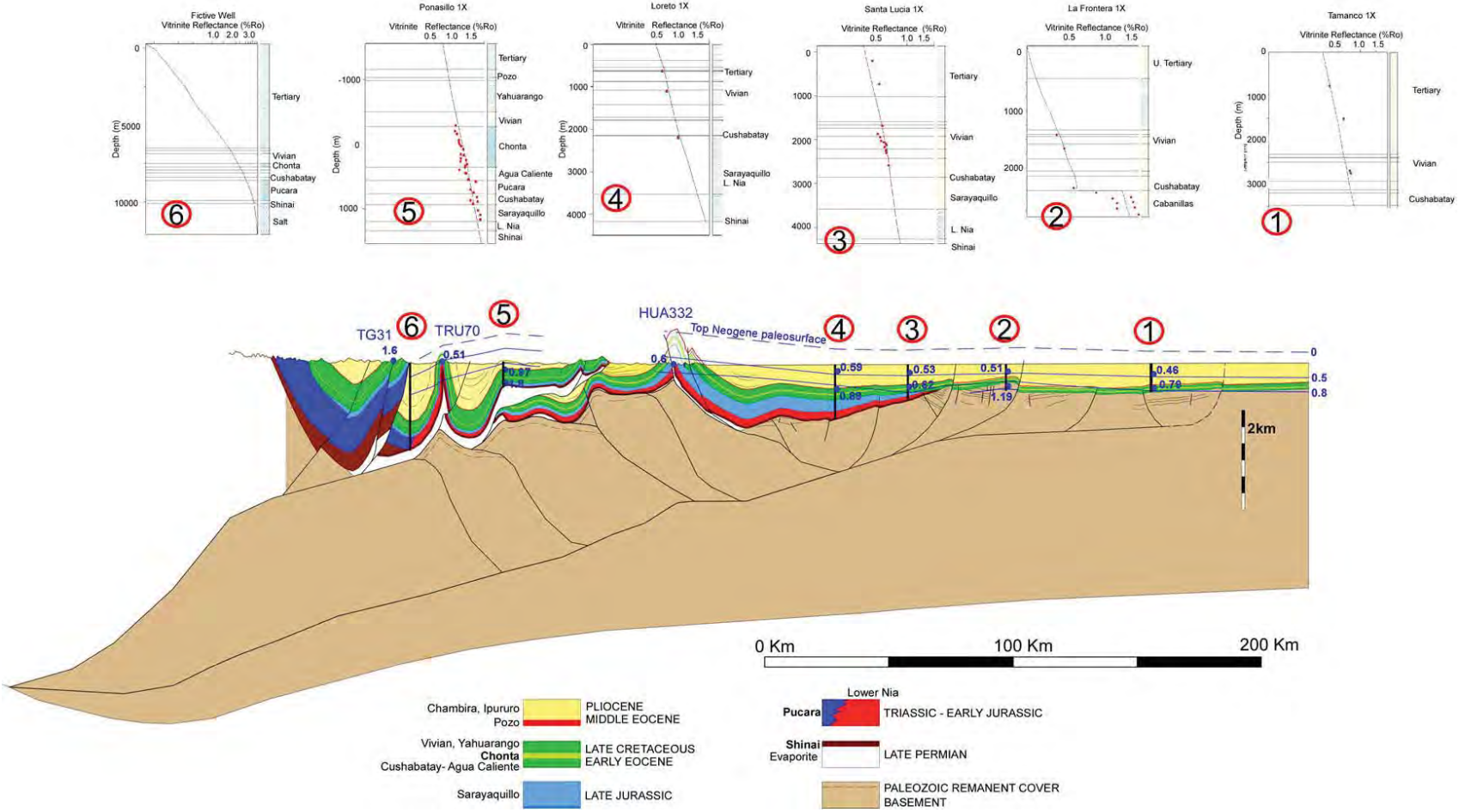

Figure 4.10. Maturity state on the present structural cross-section using 1D modeling and Ro calibration of Tamanco 1X, La Frontera 1X, Santa Lucia 1X, Loreto 1X, Ponasillo 1X and Biabo fictive well. Three outcrop analyses (TG32, TRU70 and HUA332) have been used too. Wells and outcrops are located on the map of Figure 4.2. TG32 and TRU70 are projected.

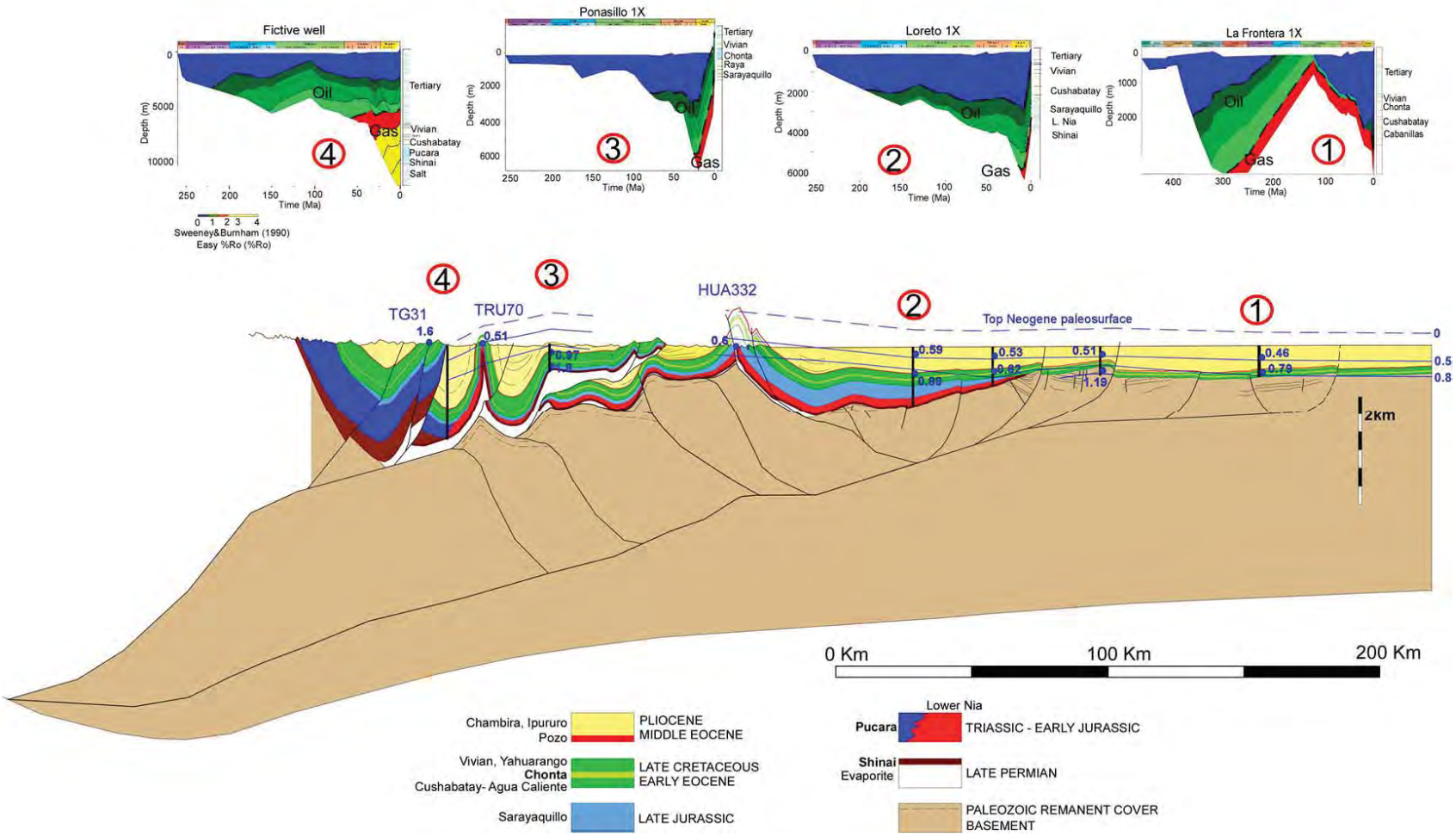

Figure 4.11. 1D burial and maturity modeling along the structural cross-section.

Biabo syncline (4 in Figure 4.11). Consequently, from the Middle Eocene, all sources rocks were progressively entering in gas window in the western Huallaga basin. More to the east, the subsidence stopped during the Miocene o Pliocene and source rocks maturity is lower (Figure 4.11).

4.6.3. 2D modeling results

The 2D modeling allows full integration of tectonic events, structural restoration, facies variation and source rock maturity through time. The project has been applied to the sequential restoration of the regional cross-section presented in Figure 4.5. The modeling was primarily based on 3 sets of input data: 1) structural analysis, facies definition and data that comprised balanced restoration, AFTA calibration; 2) heat flow history calibrated by the 1D modeling presented above; 3) stratigraphic and geohistory from the stratigraphic diagram of Figure 4.3.

The 2D modeling was conducted with the four source rocks presented above (Chonta, Raya, Pucara, Shinai). Their potential and characteristics have been yet discussed (Figures 4.6, 4.7, 4.8). Kinematic parameters Type III of Behar et al. (1997) have been applied for Chonta, Pucara and Shinai Formations and Type II of Behar et al. (1997) for Raya Formation. The model was simulated using the hybrid migration method in Petromod (combination of both Darcy and Flow path algorithms).

The Figure 4.12 represents the evolution of the maturity windows (Ro) through times for the four potential sources rocks and in the three stages of the sequential restoration of the regional cross-section. It shows a logic vertical and eastward migration of oil and gas kitchens through times. During the Middle Eocene, the Shinai source rock is in gas window or late oil window. To the west, in the kitchen of the Late Triassic/Lower Jurassic post-rift basin, a large proportion of the Pucara source rock is yet overmature and the rest is in gas window. The Cretaceous source rocks are in oil window or immature. In the intermediate stage of the Late Early Miocene, pre-Cretaceous source rocks are overmature, and Cretaceous source rocks are overmature or in oil and gas windows in the structural hights. In the current stage, a few parts of the Cushabatay Hyght and Marañón foreland stay in oil window. The Figure 4.13 reflects also the maturity evolution through times but in terms of transformation of the kerogens into hydrocarbons. It confirms that pre-Cretaceous kerogens were nearly fully transformed in the Middle Eocene stage. Cretaceous source rocks generation occurred essentially between Middle Eocene and Late Early Miocene. In the Figure 4.14, hydrocarbon saturation, vector of migration and accumulations computed by

Petromod are represented. The current stage shows attractive accumulations in sub-thrust structures below the large Chazuta thrust sheet. Two oil and gas accumulations (Vivian and Lower Nia reservoirs) appear in the big west-verging sub-thrust structure located in the foot-wall of the Chazuta front. Gas accumulations are also present in the deeper sub-thrust antiform. The modeling suggests oil and gas surface accumulations on the Callanayacu structure, which is consistent with the oil seeps outcropping in this area (see map of Figure 4.2 and cross-section of Figure 4.5). More to the east, oil accumulation is suggested in Cretaceous reservoir of the Santa Lucia basement thrust fold. The Santa Lucia 1 X exploration well, which has been drilled in the western flank of the structure, confirmed the presence of hydrocarbon traces (tar) in Cretaceous reservoirs. In the deeper part of the Santa Lucia structure, the petroleum simulation shows gas accumulation in the Triassic reservoir (Lower Nia) below the basal Cushabatay unconformity, in a probable stratigraphic trap.

4.7. Discussion and conclusion

The Huallaga-Marañón foreland basin shows both thick- and thin-skinned deformation. The thrust system is complex and resulted from the reactivation of a west-verging Permian fold and thrust belt capped by an important salt detachment. Stratigraphic correlations show that this salt must be considered as Late Permian in age. It apparently deposited during the early stage of the well-known Triassic Mitu rift event (Rosas et al., 2007). The inversion of the eastern border of this rift corresponds to the deformable back-stop of the Huallaga wedge-top basin. The construction of a balanced cross-section allowed us to calculate a total horizontal shortening of 70 km, whose 57% was accommodated in one single thrust sheet (Chazuta thrust). A three-stage sequential restoration of the balanced cross-section has been proposed thanks to kinematic constrains. New thermochronological dating confirmed a Late Oligocene age of the onset of the last phase of the deformation and an in-sequence thrust propagation. In the Marañón foreland, the younger structures started to uplift in the Pliocene. In the Late Early Miocene stage, the Huallaga wedge-top is well developed (50% of the total horizontal shortening) and the fold and thrust belt is buried by thick syn-depositional sediments. A pre-Middle Eocene compressive deformation is sealed by the shallow marine Pozo deposits in the Huallaga wedge-top basin. Growth strata show this weak deformation developed during the Senonian and Paleocene. It is well-known in the neighbouring Oriente basin of Ecuador, where the most productive oil fields have been structured during this period (Baby et al., 2013).

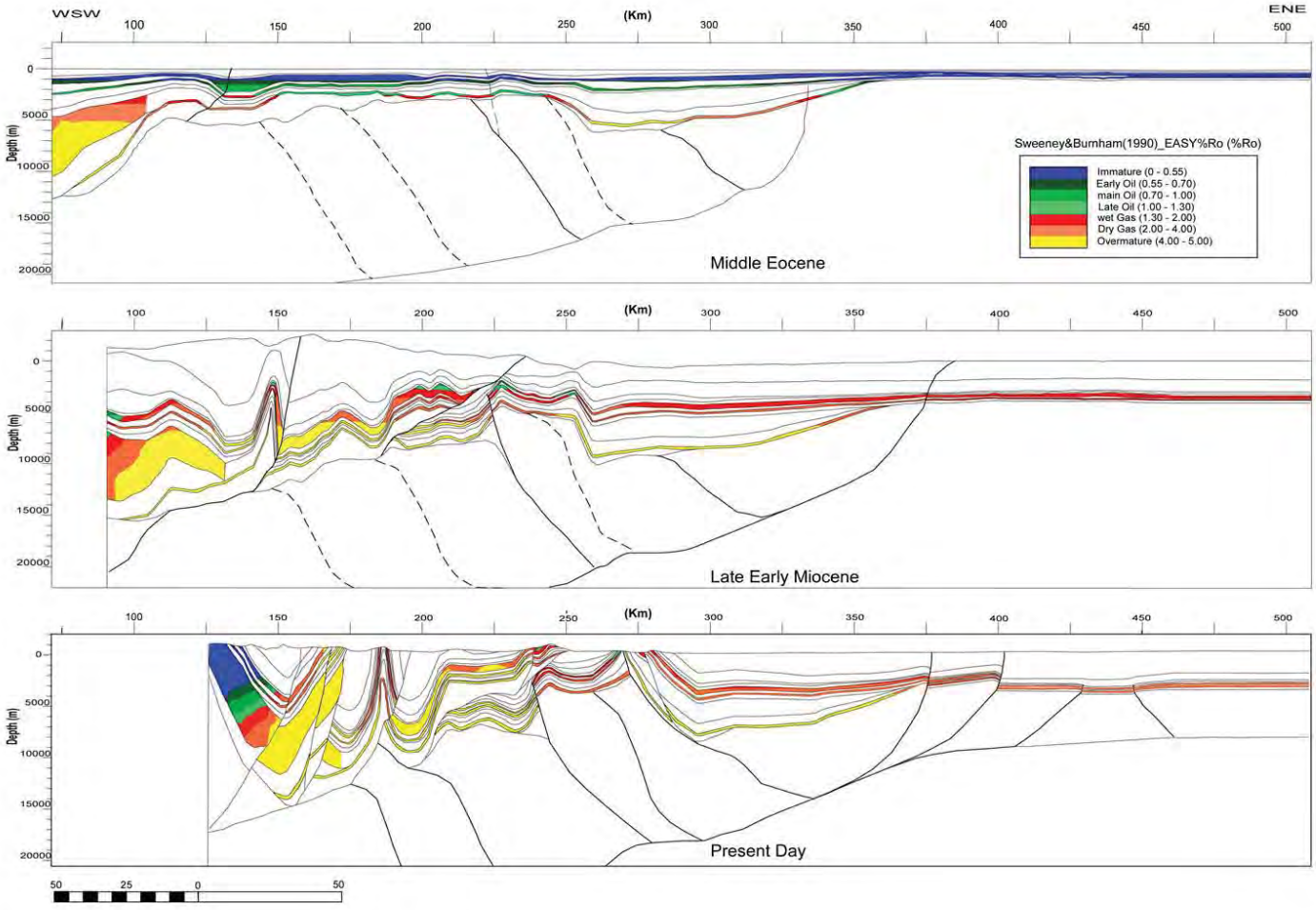

Figure 4.12. Evolution of the maturity windows (Ro) through times for the four potential sources rocks and in the three stages of the sequential restoration of the regional cross-section.

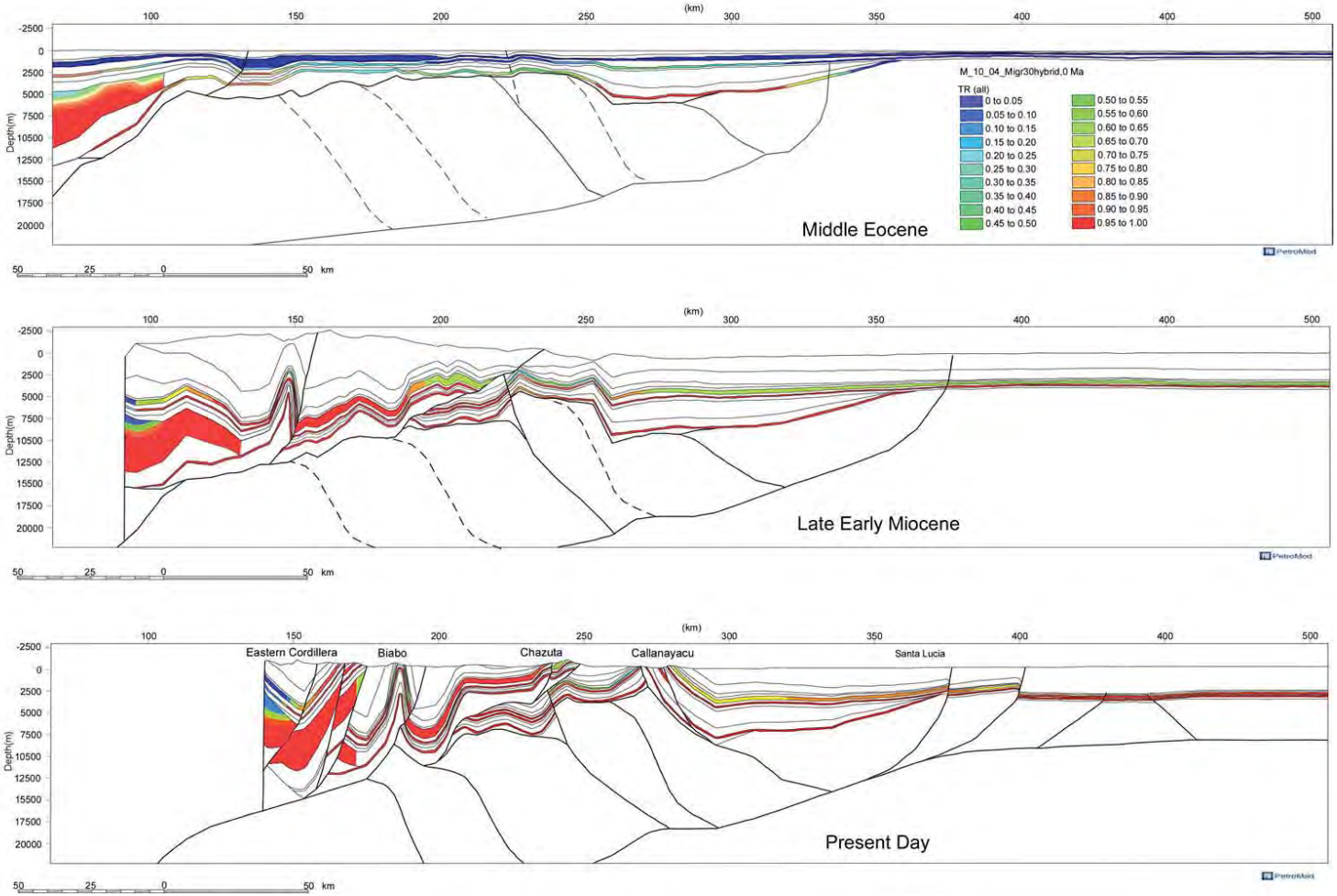

Figure 4.13. Evolution of the maturity showing the transformation ratio (TR) through times for the four potential sources rocks and in the three stages of the sequential restoration of the regional cross-section.

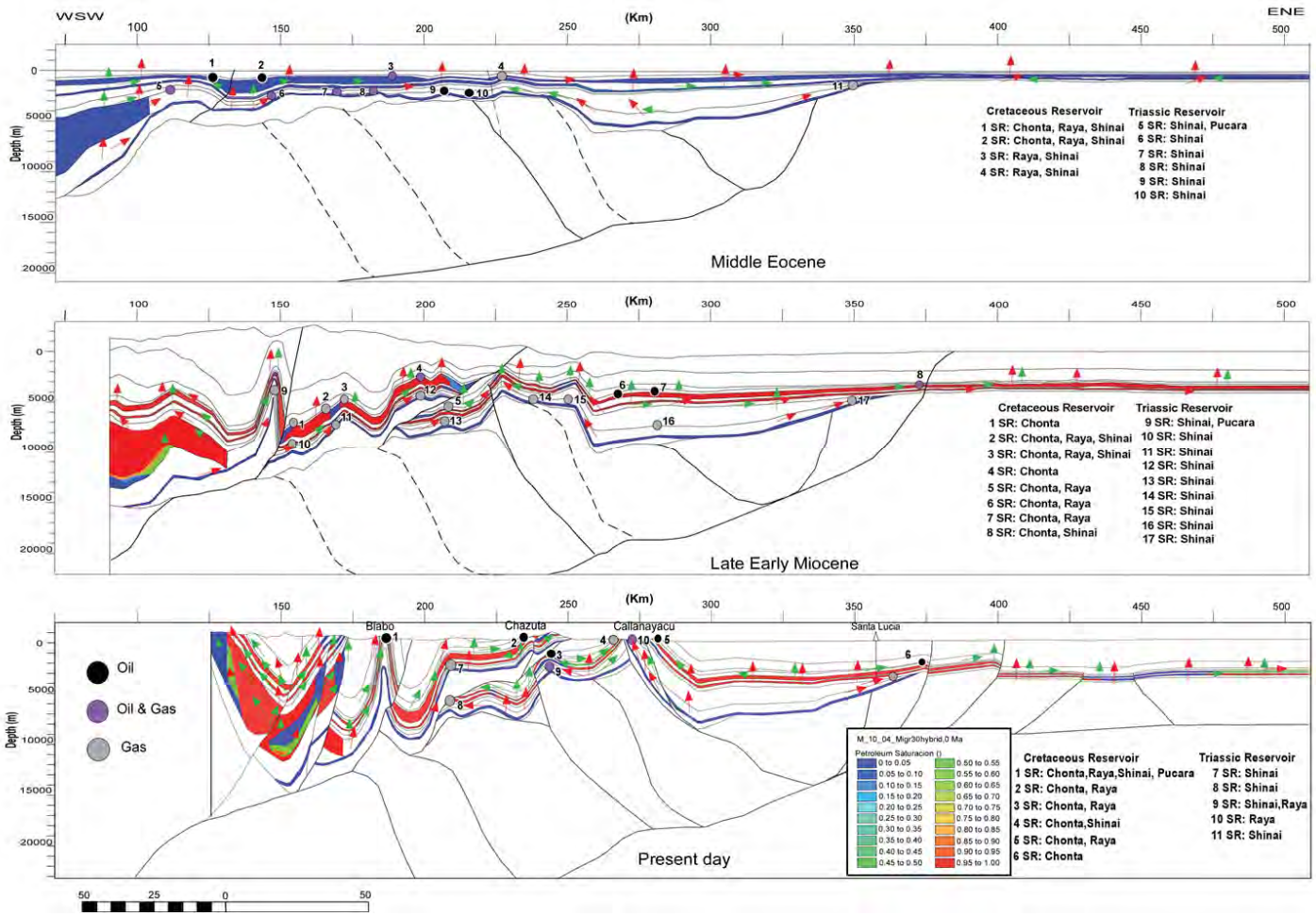

Figure 4.14. Hydrocarbon saturation and oil and gas migration vectors through time in the three stages of the sequential restoration of the regional cross section. Hydrocarbon accumulations computed by PetroMod ® are represented. Source rock (SR) and reservoir are indicated for each numbered accumulation

Late Cretaceous classic source rocks (Chonta, Raya) are present in the Huallaga-Marañón foreland basin system. The revision of the stratigraphy replaced in its updated structural context allowed us to highlight a new Late Permian source rock (Shinai). The Late Triassic/Early Jurassic Pucara source rock is confined to the Eastern Cordillera-Huallaga basin transition zone above the inverted Triassic rift, while the Shinai source rock seems represented in the rest of the study area. Oils-source rocks correlations in the Marañón basin are coherent with this new geographic distribution.

The 1 D Petromod modeling of 6 wells along the structural cross-section (Figures 4.10, 4.11) highlights the intensity of the pre-Cushabatay erosion in the Marañón foreland, which decreases progressively towards the west. This strong erosion postdated probably the Jurua Orogeny described in the Solimoes and Acre basins of northern Brazil (Caputo, 2014) and in the Ucayali basin (Baby et al., 2014; Hurtado et al., 2014). This 1D modeling also shows a strong erosion of the Marañón foreland during the Pliocene. Since 5 Ma, the southern Marañón basin evolved from a foredeep depozone to a wedge top depozone, which corresponds nowadays to the Andean orogenic front.

As in other fold and thrust belts, the expulsion timing versus thrusts emplacement timing is the key point for the exploration. Kerogens maturity evolution and HC accumulations in the sequential restoration (Figures 4.12, 4.13, 4.14) shows that old structures, Paleocene or Early Miocene in age, could preserve HC accumulations in the Chazuta thrust sheet foot-wall. In the eastern Marañón basin, more recent structures as Santa Lucia could also have been charged. Petroleum system, trap formation and expulsion-migration stages are resumed in the stratigraphic diagram of Figure 4.3.

Deep sub-thrust structures stay unexplored in the Peruvian fold and thrust belts. The Huallaga-Marañón foreland system is probably the best example of sub-trap attractiveness in Peru. The Chazuta thrust foot-wall comprises at least 3 potential sub-traps formed by a combination of salt pillows and basement horses. Such structural combination is outcropping in the Callanayacu diapir, which is well-known for its oil seeps (see Figure 4.5). In our case, the sub-traps are probably preserved since the Late Miocene. The 2D petroleum modeling shows that HC accumulations are present since the Early Miocene (Figure 4.13). The large thickness of salt transported on the Chazuta thrust sheet can constitute an excellent seal for these sub-traps. As in the Zagros fold and thrust belt, salt seals can help to maintain trap integrity over lengthy periods of geological time (Cooper, 2007).

Chapter 5: Conclusions

This thesis, through its multidisciplinary approach and the interpretation of a large amount of industrial data, provides new elements in the understanding of foreland basin systems, especially in the Andean-Amazonian domain of northern Peru. It proposes a new stratigraphic and structural model of this region and reconstructs and quantify the history of the deformation and sedimentation, which are essential data to model the petroleum systems and reduce the risks in exploration.

5.1. Structural Architecture

The Marañón Foreland Basin is the largest of the central Andes. The results of this thesis show that its structural architecture evolves laterally from a wedgetop depozone in the SE to a foredeep depozone in the NW.

In the SE, it forms a thrust wedge partly eroded, connected to the wedgetop basins of Huallaga and Moyabamba. The Huallaga, Moyabamba and Marañón basins form a single foreland system, deformed by the interference of an east-verging thin-skinned tectonics and a largely west-verging thick-skinned tectonics. The total horizontal shortening varies between 70 and 76 km. The thick-skinned tectonics is still active and propagates to the eastwards in the Marañón basin. It produces many crustal earthquakes that can be directly related to the thrusts faults. The west verging thick-skinned tectonics is controlled by the inheritance of the Middle Permian Gondwanide Orogeny that we have clearly identified for the first time in the subandean basins of northern Peru. The reactivation of the west-verging thrusts produces important structural reliefs such as the Loreto and Cushabatay highs. It also produces important crustal and destructive earthquakes in the Moyabamba basin. We could correlate these earthquakes with the activity of two major thrusts. The east-verging thin-skinned tectonics shows a strong shortening and is superimposed on the thick-skinned tectonics. It is limited to the Huallaga and Moyabamba wedgetop basins, where it is controlled by the geographical distribution of a large level of Late Permian evaporites that seals the structures of the Gondwanide Orogeny. This detachment allowed the development of the most important subandean thrust (Chazuta thrust, ± 40 km of horizontal shortening) at the front of the Huallaga and Moyabamba basins. To the west, the Eastern Cordillera, which constitutes the back-

stop of the Huallaga and Moyabamba thrusts wedge, corresponds to the inversion of the Triassic rift.

Towards the NW, the deformation of the Marañón basin is progressively attenuated, which is manifested by the transition to a foredeep depozone that extends to the southern part of the Ecuadorian Oriente Basin. It includes two depo-centers, where Cenozoic sediments can reach more than 4000 m thick. The deformation, although not very important, is still active and responsible for shallow earthquakes that are connected to the intra-basement detachment inherited from the Gondwanian fold and thrust belt. To the west, on the border of the Marañón basin, the Santiago wedgetop basin is also structured, as those for Huallaga and Moyabamba, by the interference of the inherited thick-skinned tectonics and a salt tectonics due to the presence of Late Permian evaporites that could reach here several thousand meters. Growth strata in the Santiago Basin recorded a first stage of deformation from the late Cretaceous to the early Eocene, the second stage being the most important and occurring during the Neogene. In the northern foredeep depozone of the Marañón Basin, the Situche structure, which corresponds to one of the most important oil fields, presents an atypical deformation. It corresponds to the Neogene inversion of a normal Campanian listric fault that controlled the sedimentation of the Vivian Formation sandstone reservoirs. This normal fault connects to Permian evaporites and are probably due to local salt and gravity tectonics during the Campanian period.

5.2. Stratigraphic Architecture and Evolution of the Foreland Basin System

This thesis let us to document four foreland mega-sequences in the Marañón basin. They were defined from well stratigraphic correlations and regional discontinuities identified in seismic and well porosity logs, based on the available data in the Perupetro databank. A structural cross-section through the Marañón-Huallaga system has been restored in three stages since the Middle Eocene to reconstruct and quantify the propagation of the foreland basin system.

The first foreland mega-sequence (F1) developed from the Albian to the late Cretaceous, and includes three transgressive series from fluvial to shallow marine sequences deposited in a back-bulge environment, as evidenced by the cratonic provenance of the main sandstone levels. It overlies a regional erosion surface that corresponds to the Basal Foreland Unconformity that extends over mesozoic, paleozoic or pre-cambrian strata. The second megasequence (F2) developed during the Paleocene and lower Eocene, and recorded the first Andean contribution of siliciclastic sediments in continental environment. It has been deposited in back-bulge and foredeep depozones, and shows an eastward propagation of the foreland basin system. This second mega-sequence is eroded and sealed by the base of the F3 (middle Eocene) mega-sequence, which marked a stop in the Andean tectonics and recorded an isostatic (orogenic unloading) rebound known regionally as far as in Ecuador and Colombia. The sequential

restoration of the Marañón-Huallaga structural cross-section (R1, Figure 3.2) reproduces this first stage of the deformation of the foreland basin system, showing that the Marañón basin was in a back-bulge position and the Huallaga basin in foredeep position at the time of the middle Eocene erosion. The mega-sequence F3 corresponds to the beginning of a second stage in the development of the Marañón-Huallaga foreland system, which recorded the uplift of the Western Cordillera of northern Peru. The Marañón basin developed at that time in an environment evolving from marginal marine to fluvial. During the Neogene, the mega-sequence F4 recorded the propagation of the Andean reliefs with the uplift of the Eastern Cordillera and high rates of sedimentation. The Marañón basin turned into foredeep depozone and the Huallaga basin into wedgetop zone. During the lower and middle Miocene, a complex environment that alternates between marginal marine and fluvial developed, probably due to a high global sea level and rapid subsidence. The transcontinental drainage of the Amazon is set up in the upper Miocene and causes a radical change in sedimentation that becomes exclusively fluvial. During the Pliocene, the acceleration of the thrusts propagation combined with the uplift of the Fitzcarrald Arch linked to the subduction of the Nazca Ridge controlled the uplift and erosion of the southern part of the Marañón basin.

From a quantitative point of view, the sedimentation rates calculated in 2D from the regional structural cross-sections constructed in this thesis show a gradual increase since the Albian, interrupted by the erosion of the middle Eocene, which limits two stages in the development of the foreland basin system. If we compare the Neogene sedimentation rates of the Marañón basin with the modern sedimentation rates measured in the neighboring Ucayali basin, they are at least 18 times lower. These results confirm that there are large and numerous periods of erosion and sedimentation gaps that are difficult to assess at the geological scale. Some of these discontinuities are illustrated by variations in sediment porosity.

5.3. Petroleum systems of the Huallaga-Marañón foreland basin

The 2D petroleum system modelings, carried out from a re-evaluation of petroleum systems and the sequential restoration of the regional structural cross-section R1, values a large part of the results obtained in this thesis by simulating the hydrocarbons expulsion during the different stages of deformation in the Huallaga-Marañón system and showing its potential hydrocarbon trapping areas. The revision of the stratigraphy in its structural context (Figure 4.3) has highlighted a new late Permian source rock (Shinai Formation) in addition to the upper Cretaceous source rocks long recognized in the region. The Shinai source rock has long been mistaken for the Pucara source rock (lower Triassic-Jurassic), which is in fact confined to the Huallaga basin-Eastern Cordillera transition zone on the eastern edge of the inverted Triassic rift.

In the Huallaga Basin, the study of deformation and sedimentary record shows that weakly developed Senonian and Paleocene structures are preserved below the middle Eocene erosional unconformity. This type of structural trap is well known in the neighboring Oriente basin of Ecuador where, when they are preserved, they constitute the main oil fields.

As in all fold and thrust belts, the key point of exploration lies in the relationship between the timing of the deformation and the timing of the expulsion of hydrocarbons. The 2D modelings carried out in this thesis show that there may be accumulations of hydrocarbons since the lower Miocene. Structures have been preserved under the giant Chazuta thrust at the front of the Huallaga wedgetop basin since that time, making this basin very attractive for future explorations.

Finally, this work has shown that the fossilized or partially reactivated middle Permian thrust structures (Gondwanide) constitute a new hydrocarbon play for the exploration of the Huallaga and Marañón basins. The anticlines associated with these thrusts are potential structural traps that can be fed by Paleozoic source rocks. Aeolian or Permian and Triassic fluvial sandstones can form excellent reservoirs as in the giant gas field of Camisea, and the late Permian evaporites an excellent seal.

5.4. The Huallaga-Marañón Foreland Basin System in the Subandean Basins of Peru

The synthesis on the Peruvian subandean basins presented in Appendix 5 shows that the Huallaga-Marañón foreland basin system is the largest and has the most significant shortening (70 km). This shortening decreases towards the south of Peru. The northern thick-skinned tectonics progressively decrease southward to give way to a thin-skinned tectonic that develops in the wedge of Paleozoic sediments better preserved. The best developed middle Permian structures of the Gondwanide orogeny are located in the Huallaga and Marañón basins. The structures hidden under the Chazuta thrust (40 km of cover) and the hydrocarbon systems of the Huallaga basin make it the most attractive basin of Peru for the exploration of fold and thrust belts.

Chapter 5: Conclusions en Français

Cette thèse, par son approche multidisciplinaire et l'interprétation d'une quantité importante de données industrielles, apporte de nouveaux éléments dans la compréhension des systèmes de bassin d'avant-pays, en particulier dans le domaine andino-amazonien du nord-Pérou. Elle propose un nouveau modèle stratigraphique et structural de cette région, et reconstitue l'histoire de la déformation et de la sédimentation tout en les quantifiant, données indispensables pour modéliser les systèmes pétroliers et réduire les risques en exploration.

5.1. Architecture structurale

Le bassin d'avant-pays de Marañón est le plus grand des Andes centrales. Les résultats de cette thèse montrent que son architecture structurale évolue latéralement d'une zone de wedgetop au SE à une zone de foredeep au NW.

Au SE, il forme un prisme de chevauchements en partie érodé, connecté aux bassins wedgetop de Huallaga et Moyabamba. L'ensemble Huallaga, Moyabamba et Marañón forme un seul système de bassin d'avant-pays, déformé par l'interférence d'une tectonique de couverture à vergence est et d'une tectonique de socle en grande partie à vergence ouest. Le raccourcissement horizontal total varie entre 70 et 76 km. La tectonique de socle est toujours active et se propage vers l'est dans le bassin Marañón. Elle produit de nombreux séismes crustaux que l'on peut relier directement aux chevauchements. La vergence ouest de cette tectonique de socle est contrôlée par l'héritage de l'orogénèse Gondwanide (Permien moyen) que nous avons clairement identifiée pour la première fois dans les bassins subandins du nord-Pérou. La réactivation de tels chevauchements à vergence ouest est à l'origine d'importants reliefs structuraux comme les antiformes de Loreto et Cushabatay. Elle produit aussi d'importants séismes crustaux et destructeurs dans le bassin de Moyabamba. Nous avons pu attribuer ces séismes à l'activité de deux chevauchements majeurs. La tectonique de couverture, à vergence Est, présente un fort raccourcissement et est superposée à la tectonique de socle. Elle est limitée aux bassins wedgetop de Huallaga et Moyabamba, où elle est contrôlée par la distribution géographique d'un important niveau d'évaporites d'âge permien terminal scellant les structures de l'orogénèse Gondwanide. Ce décollement a permis le développement du plus important chevauchement subandin (chevauchement de Chazuta, ± 40 km de raccourcissement horizontal) au front des bassins de Huallaga et Moyabamba. A l'ouest, la Cordillère Orientale qui constitue le

« back-stop » du prisme de chevauchements de Huallaga et Moyabamba correspond à l'inversion du rift triasique.

Vers le NW, la déformation du bassin Marañón s'amortit progressivement, ce qui se manifeste par la transition vers une zone de dépôt de type « foredeep » que l'on peut suivre jusqu'au sud du bassin Oriente d'Equateur. Elle comprend deux dépôt-centres où les sédiments cénozoïques peuvent atteindre plus de 4000 m d'épaisseur. La déformation, bien que peu importante, y est toujours active et responsable de séismes de faible profondeur à relier au décollement intra-socle hérité de la chaine Gondwanide. A l'ouest, en bordure du bassin de Marañón, le bassin wedgetop de Santiago est aussi structuré, comme ceux de Huallaga et Moyabamba, par l'interférence de la tectonique de socle héritée et d'une tectonique salifère due à la présence des évaporites du Permien terminal pouvant atteindre ici plusieurs milliers de mètres. Des strates de croissances ont enregistré dans le bassin de Santiago un premier stade de déformation allant du Crétacé supérieur à l'Eocène inférieur, la seconde étape et la plus importante se produisant durant le Néogène. Dans la zone de foredeep septentrionale du bassin Marañón, la structure de Situche, qui correspond à un des champs pétroliers les plus importants, présente une déformation atypique. Elle correspond à l'inversion néogène d'une faille listrique normale d'âge campanien qui a contrôlé la sédimentation des grès réservoirs de la Formation Vivian. Cette faille normale se branche sur les évaporites du Permien terminal et pourrait être due à une tectonique salifère et gravitaire locale durant le Campanien.

5.2. Architecture stratigraphique et évolution du système de bassin d'avant-pays

Cette thèse a permis de différencier quatre mégaséquences d'avant-pays dans le bassin de Marañón. Elles ont été définies à partir de corrélations stratigraphiques de puits et des discontinuités régionales identifiées en sismique et dans les logs de porosité de puits, en s'appuyant sur les datations disponibles dans la base de données de Perupetro. Une coupe structurale traversant le système Marañón-Huallaga a été restaurée en trois étapes depuis l'Eocène moyen pour reconstituer et quantifier la propagation du système de bassin d'avant-pays.

La première mégaséquence d'avant-pays (F1) s'est développée de l'Albien au Crétacé supérieur et comprend trois séquences transgressives fluviales à marines (peu profond) déposées dans un environnement de back-bulge, comme semble l'attester la provenance cratonique des principaux niveaux gréseux. Elle repose sur une surface d'érosion régionale qui correspond à la « Basal Foreland Unconformity » s'étalant sur des terrains mésozoiques, paléozoiques ou pré-cambriens. La deuxième mégaséquence (F2) s'est développée durant le Paléocène et l'Eocène inférieur, et a enregistré le premier apport de sédiments silicoclastiques en environnement continental provenant du soulèvement des Andes. Elle s'est déposée en zone de back-bulge et de foredeep, et montre une propagation vers l'est du système de bassin d'avant-pays. Cette

deuxième mégaséquence est érodée et scellée par la base de la mégaséquence F3 (Eocène moyen), qui marque un arrêt dans la tectonique de chevauchement andine et enregistre un réajustement isostatique (orogenic unloading) connu régionalement jusqu'en Equateur et Colombie. La restauration séquentielle de la coupe structurale Marañón-Huallaga (R1 ; Figure 3.2) reproduit ce premier état de la déformation du système de bassin d'avant-pays, où l'on montre que le bassin Marañón était en position de back-bulge et le bassin Huallaga en position de foredeep au moment de l'érosion de l'Eocène moyen. La mégaséquence F3 correspond au début d'une seconde étape dans le développement du système d'avant-pays Marañón-Huallaga, où est enregistrée le soulèvement de la Cordillère Occidentale du nord-Pérou. Le bassin Marañón se développe à cette époque dans un environnement évoluant de marin marginal à fluvial. Durant le Néogène, la mégaséquence F4 enregistre la propagation des reliefs andins avec le soulèvement de la Cordillère Orientale et de forts taux de sédimentation. Le bassin Marañón passe en zone de foredeep et le bassin Huallaga en zone de wedgetop. Durant le Miocène inférieur et moyen, s'installe un environnement complexe alternant entre marin marginal et fluvial, dû probablement à un niveau marin global élevé et à une subsidence rapide. Le drainage transcontinental de l'Amazone se met en place au Miocène supérieur et provoque un changement radical dans la sédimentation qui devient exclusivement fluviale. Durant le Pliocène, l'accélération de la propagation des chevauchements combinée au soulèvement de l'Arche de Fitzcarrald lié à la subduction de la ride de Nazca, conduit au soulèvement et à l'érosion de la partie sud du bassin Marañón.

D'un point de vue quantitatif, les taux de sédimentation calculés en 2D à partir des coupes structurales régionales construites dans cette thèse montrent une augmentation progressive depuis l'Albien, interrompue par l'érosion de l'Eocène moyen, qui limite deux étapes dans le développement du système de bassin d'avant-pays. Si l'on compare les taux de sédimentation néogènes du bassin Marañón aux taux de sédimentation actuels mesurés dans le bassin voisin d'Ucayali, ils sont au moins 18 fois inférieurs. Ces résultats confirment qu'il existe à l'échelle géologique d'importantes et nombreuses périodes d'érosion et de lacunes de sédimentation difficiles à évaluer. Certaines de ces discontinuités sont illustrées par les variations de porosité des sédiments.

5.3. Systèmes pétroliers du bassin d'avant-pays Huallaga-Marañón

Les modélisations pétrolières 2D, réalisées à partir d'une ré-évaluation des systèmes pétroliers et de la restauration séquentielle de la coupe structurale régionale R1, valorisent une grande partie des résultats obtenus dans cette thèse en simulant l'expulsion des hydrocarbures aux différentes étapes de la déformation du système Huallaga-Marañón et en montrant ses zones de piégeage potentielles. La révision de la stratigraphie replacée dans son contexte structural (Figure

4.3) a permis de mettre en évidence une nouvelle roche mère du Permien supérieur (Formation Shinai), venant s'ajouter aux roches mères crétacé supérieur reconnues depuis longtemps dans la région. La roche mère Shinai a été longtemps confondue avec la roche mère Pucara (Trias-Jurassique inférieur), qui est en fait confinée d'après nos travaux à la zone de transition Cordillère Orientale-bassin de Huallaga sur la bordure est du rift triasique inversé.

Dans le bassin de Huallaga, l'étude de la déformation et de l'enregistrement sédimentaire montre qu'il existe des structures faiblement développées d'âge sénonien et paléogène sous la discordance de l'Eocène moyen. Ce type de pièges structuraux est bien connu dans le bassin Oriente voisin d'Equateur où ils constituent, quand ils sont préservés, les principaux champs pétroliers.

Comme dans toutes les chaines plissées, le point clé de l'exploration réside dans les relations entre le calendrier de la déformation et le calendrier de l'expulsion des hydrocarbures. Les modélisations réalisées dans cette thèse montrent qu'il peut exister des accumulations d'hydrocarbures depuis le Miocène inférieur. Des structures sont préservées sous le chevauchement géant de Chazuta au front du bassin wedgetop de Huallaga depuis cette époque, ce qui rend ce bassin très attractif pour de futures explorations.

Enfin ce travail a permis de montrer que les structures chevauchantes fossilisées ou partiellement réactivées du Permien moyen (Gondwanide) constituent un nouveau « play » pétroliers pour l'exploration des bassins Huallaga et Marañón. Les anticlinaux associés à ces chevauchements sont des pièges structuraux potentiels pouvant être alimentés par les roches mères paléozoiques. Les grès éoliens ou fluviaux permiens et triasiques peuvent y former comme dans le champ géant de Camisea d'excellents réservoirs, et les évaporites du Permien terminal une excellente couverture.

5.4. Le système de bassin d'avant-pays Huallaga-Marañón dans les bassins subandins du Pérou

La synthèse sur les bassins subandins péruviens présentée en annexe 5 montre que le système de bassin d'avant-pays Huallaga-Marañón est le plus vaste et présente le raccourcissement le plus important (70 km). Ce raccourcissement diminue vers le sud du Pérou. La tectonique de socle qui le caractérise s'amortit progressivement vers le sud pour laisser place à une tectonique de couverture qui se développe dans le prisme de sédiments paléozoiques mieux préservé. Les structures du Permien moyen de l'orogénèse Gondwanide les mieux développées se situent dans les bassins Huallaga et Marañón. Les structures cachées sous le chevauchement de Chazuta (40 km de recouvrement) et les systèmes pétroliers du bassin de Huallaga en font le bassin le plus attractif du Pérou pour l'exploration des chaines plissées.

References cited

Alarcon and Borda, 2011. Evolución Tectónica de la Bahía de Sechura y su implicancia en la acumulación de hidrocarburos. VII INGEPET, Conference paper EXPR-3-PA-14-N, Lima.

Aleman A. M. & Marksteiner R., 1993. Structural styles in the Santiago fold and thrust belt, Peru: a salt related orogenic belt. Second ISAG, Oxford (UK), extended abstract, 147-153. http://horizon.documentation.ird.fr/exl-oc/pleins_textes/pleins_textes_6/colloques2/38392.pdf

Allen, P. A., Armitage, J. J., Carter, A., Duller, R. A., Michael, N. A., Sinclair, H. D., Whitchurch, A. L. and Whittaker, A. C., 2013. The Qs problem: Sediment volumetric balance of proximal foreland basin systems. Sedimentology, 60: 102–130.

Allen, P., 2017. Sediment Routing Systems: The Fate of Sediment from Source to Sink. Cambridge: Cambridge University Press. doi:10.1017/9781316135754

Baby P., I. Moretti, B. Guillier, J. Oller, R. Limachi, M. Specht, 1995. Petroleum System of the northern and central bolivian Sub-Andean Zone. In : Tankard A.J., Suárez S. R. et Welsink H.J., éd., Petroleum Basins of South America, AAPG Memoir 62, p. 445-458.

Baby P., M. Rivadeneira, R. Barragán, F. Christophoul, 2013. Thick-skinned tectonics in the Oriente foreland basin of Ecuador, In: Nemcˇok M., Mora A. R., Cosgrove J. W. (eds) Thick-Skin-Dominated Orogens: From Initial Inversion to Full Accretion, Geological Society, London, Special Publications, 377, p. 59-76, http://dx.doi.org/10.1144/SP377.1

Baby, P., Y. Calderon, M. Louterbach, A. Eude, N. Espurt, S. Brusset, M. Roddaz, S. Brichau, G. Calves, C. Hurtado, L. Ramirez, A. Quispe and R. Bolaños, 2014. Thrusts propagation and new geochronologic constraints in the Peruvian Subandean fold and thrust belt: VIII INGEPET 2014 (GEO-EX-PB-10-N).

Balkwill, H.R., Rodriguez, G. Paredes, F.I and J.P. Almeida, 1995. Northern part of Oriente Basin, Ecuador: reflection seismic expression of structures. In: Tankard, A.J., Suarez, S.R. and H. J. Welsink (eds) Petroleum Basins of South America, AAPG Memoir, 62, p. 559-571.

Barragan, R., P. Baby, W. Hermoza, and L. Navarro, 2008. The origin of the Marañón-Oriente basin cretaceous oils: the Santiago-Situche kitchens, a new alternative model: VI INGEPET (EXPR-3-RB-24).

Bayona, G., Cortés, M., Jaramillo, C., Ojeda, G., Aristizabal, J. J., & Reyes-Harker, A., 2008. An integrated analysis of an orogen–sedimentary basin pair: Latest Cretaceous–Cenozoic

evolution of the linked Eastern Cordillera orogen and the Llanos foreland basin of Colombia. Geological Society of America Bulletin, 120(9–10), 1171 LP-1197.

Behar, F., Vandenbroucke, M., Tang, Y., Marquis, F. & Espitalie, J., 1997. Thermal cracking of kerogen in open and closed systems: determination of kinetic parameters and stochiometric coefficients for oil and gas generation: Org. Geochem., 26(5/6), p. 321-339.

Brandon, M. T., 1996. Probability density plot for fission-track grain-age samples: Radiat. Meas., 26(5), p. 663-676, doi: 10.1016/S1350-4487(97)82880-6.

Brandon, M. T., M. K. Roden-Tice, and J. I. Garver, 1998. Late Cenozoic exhumation of the Cascadia accretionary wedge in the Olympic Mountains, northwest Washington State: Geol. Soc. Am. Bull., 110(8), 985-1009, doi: 10.1130/0016-7606(1998)110<0985:LCEOTC>2.3.CO;2.

Buchanan, P. G. & McClay, K. R., 1991. Sandbox experiments of inverted listric and planar fault systems. Tectonophysics, 188, 97-115.

Calderon, Y., P. Baby, A. Eude, G. Calves, R. Bolaños and E. Martínez, 2014. Pre-cretaceous structures in the Marañón and Huallaga basins and their petroleum implications: VIII INGEPET (GEO-EX-YC-15-N).

Calderón Y., P. Baby, Y. Vela, C. Hurtado, A. Eude, M. Roddaz, S. Brusset, G. Calvès and R. Bolaños, 2017b, Petroleum systems restoration of the Huallaga-Marañón Andean retro-foreland basin, Peru: In Mahdi A. AbuAli, Isabelle Moretti, and Hege M. Nordgård Bolås, eds., Petroleum Systems Analysis: American Association of Petroleum Geologists Memoir 114, p. 91–112.

Carlotto, V., J. Quispe, H. Acosta, R. Rodriguez, D. Romero, and Et.al (2009), Dominios geotectónicos y metalogénesis del Perú, *Bol. la Soc. Geolofgica del Peru*, *103*, 1–89.

Caputo M. V., 2014. Juruá Orogeny: Brazil and Andean Countries: Brazilian Journal of geology, 44(2), 181-190.

Calabro, R.A., Corrado, S., Di Bucci, D., Robustini, P., Tornaghi, M., 2003. Thin skinned vs. thick-skinned tectonics in the Matese Massif, Central–Southern Apennines (Italy), Tectonophysics 377, 269– 297.

Calvès, G., Toucanne, S., Jouet, G., Charrier, S., Thereau, E., Etoubleau, J., Lericolais, G. (2013). Inferring denudation variations from the sediment record; an example of the last glacial cycle record of the Golo Basin and watershed, East Corsica, western Mediterranean Sea. Basin Research, 25(2), 197–218. https://doi.org/10.1111/j.1365-2117.2012.00556.x

Catuneanu, O., 2004. Retroarc foreland systems—evolution through time. J. Afr. Earth Sci. 38, 225–242.

ConocoPhillips, (2008). Eastern Marañón Basin Petroleum Systems Evaluation. Block 123. First Exploration Period Commitment Report. ITP23296. Perupetros's archive.

Coward, M. P., 1983. Thrust tectonics, thin skinned or thick skinned, and the continuation of thrusts to deep in the crust, Journal of Structural Geology, 5, 113–123, 1983.

Chew, David M., Pedemonte, Giovanni, Corbett, Eoghan, 2016. Proto-Andean evolution of the Eastern Cordillera of Peru, *Gondwana Research*, doi: 10.1016/j.gr.2016.03.016

Christophoul F., P. Baby, C. Davila, 2002. Stratigraphic responses to a major tectonic event in a foreland basin: the Ecuadorian Oriente Basin from Eocene to Oligocene times: Tectonophysics, 345(1-4), 281-298.

Colletta B., Roure F., De Toni B., Loureiro D. and Passalacqua H., 1997. Tectonic inheritance, crustal architecture, and contrasting structural styles in the Venezuela Andes. Tectonics, 16, 5, 777-794.

Cooper, M., 2007, Structural style and hydrocarbon prospectivity in fold and thrust belts: a global review, In: Ries, A. C., Butler, R. W. H. & Graham, R. H. (eds), Deformation of the Continental Crust: The Legacy of Mike Coward. Geological Society, London, Special Publications, 272, p. 447–472.

Core Laboratories, 1996, Hydrocarbon Source Rocks of the Sub-andean Basins, Peru: vol. 3, Final Report, Interpretation and Synthesis, Perupetro´s catalog. ITP20004

Core Laboratories, Idemitsu Oil & Gas Company, 1999, Geochemical evaluation of oils and source rocks and oil-source rock correlations, Sub-Andean Basins, Peru: vol. 1, Perupetro´s catalog: ITP21239 @ ITP 21252.

Costa, E., Vendeville, B.B., 2002. Experimental insights on the geometry and kinematics of fold-and-thrust belt above weak, viscous evaporitic decollement. J. Struct. Geol. 24, 1729e1739. http://dx.doi.org/10.1016/S0191-8141(01)00169-9.

Dalmayrac B., Laubacher G. and Marocco R., 1988. Caracteres Generales de la Evolución Geológica de los Andes Peruanos. INSTITUTO GEOLOGICO MINERO Y METALURGICO, Bol. 12., Serie D. Estudios Especiales, 313 p.

Davis Dan M. and Engelder T., 1985. The role of salt in fold-and-thrust belts. Tectonophysics, 119, 67-88.

DeCelles, P.G., Giles, K.A. (1996) Foreland basin systems. Basin Res 8, 105-123.

Devlin, S., Isacks, B.L., Pritchard, M.E., Barnhart, W.D., and R.B. Lohman, 2012. Depths and focal mechanism of crustal earthquakes in the central Andes determined from teleseismic waveform analysis and InSAR.Tectonics, Vol. 31, TC2002.

DGSI Project, Murphy Oil Company, 1996, Geochemical, Analysis of Ten Crude Oils from the Ucayali Basin and Nine Outcrop samples from the Huallaga Basin, Peru. Final Report. Perupetro´s catalog: ITP20113.

EDCON Worldwide, 1997. Land Gravity Acquisition and Processing Report. Perú Project. Block 50.

Espurt N., P. Baby, S. Brusset, M. Roddaz, W. Hermoza, V. Regard, P.O. Antoine, R. Salas-Gismondi, R. Bolaños, 2007. Influence of the Nazca Ridge subduction on the modern Amazonian retro-foreland basin: Geology, 35(6), p. 515-518.

Espurt, N., J. Barbarand, M. Roddaz, S. Brusset, P. Baby, M. Saillard, and W. Hermoza, 2011. A scenario for late Neogene Andean shortening transfer in the Camisea Subandean zone (Peru, 12°S): Implications for growth of the northern Andean Plateau: Geol. Soc. Am. Bull., 123(9-10), p. 2050-2068, doi: 10.1130/B30165.1.

Eude, A., M. Roddaz, S. Brichau, S. Brusset, P. Baby, Y. Calderon and J.C. Soula, 2015. Timing of exhumation and deformation in the Northern Peruvian Eastern Andean Wedge (5 - 8 S) as inferred from Low Temperature Thermochronology and Balanced Cross Section: Tectonics, doi: 10.1002/2014TC003641.

Faure J.L., K. Osadetz, Z.N. Benaouali, F. Schneider and F. Roure, 2014, Kinematic and Petroleum Modeling of the Alberta Foothills and Adjacent Foreland - West of Calgary: Oil & Gas Science and Technology – Rev. IFP, Vol. 59, No. 1, pp. 81-108

Filizola, N., & Guyot, J. L. (2004). The use of Doppler technology for suspended sediment discharge determination in the River Amazon / L'utilisation des techniques Doppler pour la détermination du transport solide de l'Amazone. Hydrological Sciences Journal, 49(1), 143–153. https://doi.org/10.1623/hysj.49.1.143.53990

Gaibor, I., J.P.A. Hochuli, W. Winkler, & J. Toro, 2008 Hydrocarbon source potential of the Santiago Formation, Oriente Basin, SE of Ecuador: Journal of South American Earth Sciences, 25, p. 145-156.

Giambiagi, L., Mescua, J., Heredia, N., Farias, P., Garcia Sansegundo, J., Fernandez, C., Lossada, A., 2014. Reactivation of Paleozoic structures during Cenozoic deformation in the Cordon del Plata and Southern Precordillera ranges (Mendoza, Argentina). Journal of Iberian Geology, 40(2), 309–320. http://doi.org/10.5209/rev_JIGE.2014.v40.n2.45302

Gil Rodriguez, W., Baby, P. & Ballard, J. F., 2001. Structure et contrôle paléogéographique de la zone subandine péruvienne. Comptes Rendus de l'Académie des Sciences Paris, Série 2a: Sciences de la Terre et des Planètes, 333, 741–748.

Global Energy Development, Harken Del Peru LDT, 2002. Area III and Marañón Basin. Geochemical Interpretation and Geohistory/Maturation Modeling. Perupetros´s catalog: ITP22238.

Gutscher, M.-A., Spakman, W., Bijwaard, H., and Engdalh, E.R., 2000. Geodynamics of flat subduction: Seismicity and tomographic constraints from the Andean margin: Tectonics, v. 19, p. 814–833, doi: 10.1029/1999TC001152.

Hamza, V., and M. Munoz, 1996, Heat flow map of South America: Geothermics Vol. 25(6), p. 599-646.

Hantschel, T. and A.I. Kauerauf, 2009, Fundamentals of Basin and Petroleum Systems Modeling: Springer-Verlag, Berlin, Heidelberg.

Hermanrud, C., 1993, Basin modeling techniques-an overview: Basin modeling: advances and applications, 3, Norwegian Petroleum Society (NPF), Special Publication, p. 1-34.

Hermoza, W., 2004, Dynamique Tectono-Sédimentaire et Restauration Séquentielle du Retro-Bassin d'avant-pays des Andes Centrales: Thèse de doctorat de l'Université de Toulouse III, 296 p.

Hermoza, W., S. Brusset, P. Baby, W. Gil, M. Roddaz, N. Guerrero, and M. Bolaños, 2005, The Huallaga foreland basin evolution: Thrust propagation in a deltaic environment, northern Peruvian Andes: J. S. Am. Earth Sci., 19(1), 21-34, doi: 10.1016/j.jsames.2004.06.005.

Hillis, R. R., Thomson, K., & Underhill, J. R. (1994). Quantification of Tertiary erosion in the Inner Moray Firth using sonic velocity data from the Chalk and the Kimmeridge Clay. Marine and Petroleum Geology, 11(3), 283-293.

Hoorn, C., Wesselingh, F.P., ter Steege, H., Bermudez, M.A., Mora, A., Sevink, J., Sanmartin, I., Sanchez-Meseguer, A., Anderson, C.L., Figueiredo, J.P., Jaramillo, C., Riff, D., Negri, F.R., Hooghiemstra, H., Lundberg, J. Stadler, T., Sarkinen, T., Antonelli, A., (2010) Amazonian through time: Andean uplift, climate change, landscape evolution and biodiversity. Science 330, 927-931. 51-65.

Hoorn, C., Bogota-A, G., Romero-Baez, M., Lammertsma, E., Flantua, S., Dantas, E., Dino, R., do Carmo, D., Chemale Jr, F., (2017). The Amazon at sea: Onset and stages of the Amazon Rivers from a marine record, with special reference to Neogene plant turnover in the drainage basin. Global and Planetary Change 153,

Humble Geochemical Services, Burlington Resources, 2003. Peruvian Outcrops, Petroleum Geochemistry Report. Perupetro´s catalog: ITP20612.

Hurtado, C., P. Baby, Y. Calderon, R. Bolaños, H. Pelliza and C. Monges, 2014. Arquitectura estratigráfica y estructural con un nuevo sistema petrolero en la zona noroccidental de la cuenca Ucayali: VIII INGEPET (GEO-EX-CH-04-N).

Hurtado, C.A. 2017. Proveniência sedimentar do Mesozoico-Cenozoico da Bacia Andino-Amazônica de Huallaga, implicações geodinâmicas e paleogeográficas. (Dissertação de mestrado não publicada). Instituto de Geociências. Universidade de Brasilia.

Idemitsu Oil & Gas Company Ltd., 2000, SIGMA-2D Basin Modeling Study for the Evaluation of Oil and Gas Generation, Migration and Accumulation in the Sub-Andean Basins, Peru, Perupetro´s catalog: ITP21774 – ITP21775.

Jacques, J. M., 2004. The influence of intraplate structural accommodation zones on delineating petroleum provinces of the Sub-Andean foreland basins. *Petroleum Geoscience*, *10*(1), 1–19. http://doi.org/10.1144/1354-079303-582

Jaramillo, C., Romero, I., D'Apolito, C., Bayona, G., Duarte, E., Louwye, S., Escobar, J., Luque, J., Carillo-Briceno J., Zapata, V., Mora, A., Schouten, S., Zavada, M., Harrington, G., Ortiz, J., Wesselingh, F., (2017). Miocene flooding events of western Amazonia. Science Advances.

Jarvie, D. and M. McCaffrey, 2001, Geochemical Evaluation of Marañón Basin Oil and Seeps from Chazuta, Maquia, and Callanayacu, and Jurassic Rocks from the Pucara Formation, Humble Geochemical Services, Advantage Resources, Perupetros's catalog ITP 22782.

Kennan, L., 2008, Fission track ages and sedimentary provenance studies in Peru, and their implications for Andean paleogeographic evolution, stratigraphy and hydrocarbon systems, *in* VI INGEPET.

Kley, J., Monaldi, C. R. & Salfity, J. A., 1999. Along strike segmentation of the Andean foreland: causes and consequences. Tectonophysics, 301, 75–94.

Laubacher, G., 1978, Géologie de la Cordillère Orientale et de l'Altiplano au Nord et Nord-Ouest du lac Titicaca (Pérou): Travaux et Documents de l'Orstom, Paris, v. 95, 217 p.

Laubacher, G., Mégard, F., & Megard, F. 1985. The Hercynian basement: a review. In Pitcher, W.S., Atherton M; P., Cobbing E. J. and Beckinsale R. D. (eds): Magmatism at a Plate Edge, The Peruvian Andes, Halsted Press, 29–35.

Leturmy P., Mugnier J.L., Vinour P., Baby P., Colletta B., Chalaron E., 2000. Piggyback basin development above a thin-skinned thrust belt with two detachment levels as a function of interactions between tectonic and superficial mass transfer: the case of the Subandean Zone (Bolivia). Tectonophysics, Vol. 320 (1), 45-67.

Libro de Reservas, 2016. Published by the Minister of Energy and Mines of Peru.

Magoon, L.B., and Dow, W.G., 1994, The petroleum system, *in* Magoon, L.B., and Dow, W.G., eds., The Petroleum System—From source to trap: American Association of Petroleum Geologists Memoir 60, p. 3–23.

Mathalone, J. and M. Montoya, 1995. Petroleum Geology of the Sub-andean Basins of Peru, In: Tankard, A.J., Suarez, S.R. and H. J. Welsink (eds): Petroleum Basins of South America, AAPG Memoir, 62, p. 423-444.

Marksteiner, R. and A. M. Aleman, 1997. Petroleum systems along the fold belt associated to the Marañón Oriente – Putumayo (MOP) Foreland Basins: 6th Simposio Bolivariano Exploracion Petrolera en las Cuencas Subandinas, Tomo II, Asociacion Colombiana de Geologos y Geofisicos del Petroleo, Bogota, Colombia, p. 63-74.

McGroder, M.F., Lease, R.O., and Pearson, D.M., 2014. Along-strike variation in structural styles and hydrocarbon occurrences, Subandean fold-and-thrust belt and inner foreland, Colombia to Argentina, *in* DeCelles, P.G., Ducea, M.N., Carrapa, B., and Kapp, P.A., eds., Geodynamics of a Cordilleran Orogenic System: The Central Andes of Argentina and Northern Chile: Geological Society of America Memoir 212, doi:10.1130/2015.1212(05).

McClay, K.R., 1989. Analogue models of inversion tectonics. In: M.A. Cooper and G.D. Williams (Editors), Inversion Tectonics. Geol. Sot. London, Spec. Publ., 44: 41-59.

Mégard, F., 1984, The Andean orogenic period and its major structures in central and northern Peru: Journal of the Geological Society of London, v. 141, no. 5, p. 893–900, doi:10.1144/gsjgs.141.5.0893.

Metivier, F., Gaudemer, Y., Tapponnier, P. & Klein, M. (1999). Mass accumulation rates in Asia during the Cenozoic. Geophys J Int, 137(2), 280–318, doi:10.1046/j.1365-246X.1999.00802.x.

Mitouard, P.; JGssel, C.; and Laj C.; 1990, Post-Oligocene rotation in southern Ecuador and northern Peru and the formation of the Huancabamba deflection in the Andean Cordillera: Earth and Plan. Sc. Let. 98, p. 329-339.

Moretti I., P. Baby, E. Mendez, D. Zubieta, 1996, Hydrocarbon generation in relation to thrusting in the Sub Andean Zone from 18 to 22°S – Bolivia: Petroleum Geoscience, 2, p. 17-28.

Moretti, I., J.P. Callot, M. Principaud and D. Pillot, 2013. Salt pillows and localization of early structures: case study in the Ucayali Basin (Peru), In: Nemcˇok M., Mora A. R., Cosgrove J. W. (eds) Thick-Skin-Dominated Orogens: From Initial Inversion to Full Accretion, Geological Society, London, Special Publications, 377, doi 10.1144/SP377.8.

Mugnier J.L., Baby P., Colletta B., Vinour P., Bale P., Leturmy P., 1997. Thrust geometry controlled by erosion and sedimentation: a view from analogue models. Geology, 25, 5, 427-430.

Navarro, L., Baby, P., Bolaños, R., 2005. Structural style and hydrocarbon potential of the Santiago basin. INGEPET 2005 EXPR-3-LN-09.

Nocquet, J.-M. et al., 2014. Motion of continental slivers and creeping subduction in the northern Andes, *Nat. Geosci.*, *7*(March), 287–291, doi:10.1038/NGEO2099.

Ocola, L., 1985, Flujo calórico en el nor-oriente peruano: Cuenca Marañón: III Simposio Sudamericano de COGEODATA, Tema No. 20, Lima, Perú.

PARSEP, 2001. Final Report on the Huallaga basin and adjacent area. The hydrocarbon potential of NE Peru Huallaga, Santiago and Marañón Basins Study: Perupetro report, 74 pp, Lima.

Pelletier J. D., 2007. Erosion-rate determination from foreland basin geometry. Geology; 35 (1): 5–8. doi: https://doi.org/10.1130/G22651A.1

Petroleum Systems International, 2011, Marañón Basin Petroleum Systems FY2010. Prepared for Talisman Energy, Inc. Calgary, AB, Canada.

Poblet, J. & Lisle, R. J., 2011. Kinematic Evolution and Structural Styles of Fold-and-Thrust Belts.Geological Society, London, Special Publications, 349, 1–24.DOI: 10.1144/SP349.1

Prudhomme, A., Baby P., Robert A., Calderon Y., Ramirez L., Cuipa E., 2016, Cenozoic intramontane piggyback Calipuy basin: evidence of a major west verging thrusts system, north Peru.: In: Technical Papers (Geología Regional Peruana y Sudamericana), XVIII Congreso Peruano de Geología, Lima, Perú, Extended Abstracts CD.

Ramos, V.A., 1988. The tectonics of the Central Andes: 30° to 33°S latitude, *in* Clark, S., and Burchfiel, D., eds., Processes in Continental Lithospheric Deformation: Geological Society of America Special Paper 218, p. 31–54.

Roddaz M., P. Baby, S. Brusset, W. Hermoza, J. Darrozes, 2005. Forebulge dynamics and environmental control in Western Amazonia: the case study of the arch of Iquitos (Peru): Tectonophysics*,* 399, 87-108.

Roddaz, M., W. Hermoza, A. Mora, P. Baby, P. M., F. Christophoul, S. Brusset, and N. Espurt, 2010. Cenozoic sedimentary evolution of the Amazonian foreland basin system, in Amazonia, Landscape and Species Evolution: A look into the Past, 1st edition, edited by C. Hoorn and F. P. Wesselingh.

Rodriguez, A. & Chalco, A., 1975. Cuenca Huallaga, Reseña geológica y posibilidades petrolíferas. Bol. Soc. Geol. Perú, 45, 187-212 (in Spanish).

Rosas, S., L. Fontbote, and A. Tankard, 2007. Tectonic evolution and paleogeography of the Mesozoic Pucara Basin, central Peru: J. S. Am. Earth Sci., 24(1), p. 1-24, doi: 10.1016/j.jsames.2007.03.002.

Sassi, W., Colletta, B., Balé, P., Paquereau, T., 1993. Modelling of structural complexity in sedimentary basins: the role of pre-existing faults in thrust tectonics. Tectonophysics, 226, 97-112.

Seminario F., J. Luquez, S. Blanco, 2005. Las rocas reservorios del gran Camisea, Cuenca Ucayali-Peru: V INGEPET (EXPL-FS-208).

SPT Simon Petroleum, 1993, Geology - Hydrocarbon potential and prospect analyses, Ucayali basin – Peru.

Springer, M., A. Foster, 1997. Heat-flow density across the Central Andean subduction zone: Tectonophysics, 291, p. 123-139.

Sweeney, J. J., and Burnham, A. K., 1990. Evaluation of a Simple-Model of Vitrinite Reflectance Based on Chemical-Kinetics, AAPG Bull., 74, 1559-1570.

Talisman Energy, 2011. Marañón Regional Stratigraphic Study Perupetros's catalog.

Tavera, H., E. Buforn, I. Bernal, and Y. Antayhua, 2001. Analysis of the rupture processes of 1990 and 1991 Alto Mayo Valley earthquakes (Moyobamba, Peru). Bol. Soc. Geol. Perú, 91, 55–68 (in Spanish).

Tavera H., 2011. Mapa sísmico del Perú, periodo 1960-2011. Instituto Geofísico del Perú.

Teixell, A. and Koyi, H. A., 2003. Experimental and field study of the effects of lithological contrasts on thrust-related deformation, Tectonics, 22, 5, 1054, doi:10.1029/2002TC001407.

Timoteo, D., Romero, D., and Valencia, K., 2012. Posible existencia de la Faja Alleghanide? en el Noroeste del Perú: Recientes dataciones Ar/Ar y U-Pb, e implicancias en un Sistema Petrolero de la Cuenca Talara. Sociedad Geológica del Perú. XVI Congreso Peruano de Geología – Lima, Perú. DOI: 10.13140/RG.2.1.4571.1207.

Tissot, B., R. Pelet and P. Ungerer, 1987. Thermal history of sedimentary basins, maturation indices and kinetics of oil and gas generation: Am. Assoc. Petr. Geol., 71, p. 1445-1466.

Tozer, R.S.J., Butler, R.W.H. and Corrado, S., 2002. Comparing thin- and thick-skinned thrust tectonic models of the Central Apennines, Italy, EGU Stephan Mueller Special Publication Series, 1, 181–194.

Vergés, J., Marzo, M., Santaeulària, T., Serra-Kiel, J., Burbank, D. W., Muñoz, J. A., & Giménez-Montsant, J., 1998. Quantified vertical motions and tectonic evolution of the SE Pyrenean foreland basin. Geological Society, London, Special Publications, 134(1), 107 LP-134.

Walford, H. L., White, N. J. & Sydow, J. C., 2005. Solid sediment load history of the Zambezi Delta. Earth and Planetary Science Letters, 238(1–2), 49–63, doi:10.1016/j.epsl.2005.07.014.

Waples, D.W., 1980. Time and temperature in petroleum formation: application of Lopatin's method to petroleum exploration: Am. Assoc. Pet. Geol., 64, p. 916 – 926.

Waples, D.W., 1994. Maturity modeling: thermal indicators, hydrocarbon generation, and oil cracking. The Petroleum System from Source to Trap: Am. Assoc. Pet. Geol., 60, p. 285 - 306.

Williams, K. E., 1995. Tectonic subsidence analysis and Paleozoic paleogeography of Gondwana, *in* A. J. Tankard, R. Suárez S., and H. J. Welsink, Petroleum basins of South America: AAPG Memoir 62, p. 79–100.

Wilson, J. J., 1985. Geología de los cuadrangulos de Jayanca, Incahuasi, Cutervo, Chiclayo, Chongoyape, Chota, Celendin, Pacasmayo, Chepen: Bol. Inst. Geol. Miner. Metal., Ser. A: Carta Geológica Nacional, 38 INGEMMET, Lima, 104 pp.

Witte, J., B. Lemieux, and B. Veilleux, 2011. Regional structural styles in the Santiago and Marañón basins of northern peru : new implications for hydrocarbon trapping from interplay of thick-skin, thin-skin and salt tectonics, *in* VII INGEPET (EXPR-3-JW-11-E).

Wygrala, B., 1989. Integrated study of an oil field in the Southern Po Basin, Northern Italy: Berichte der forschungszentrum Julich 2313, p.1-217.

Wyllie, M. R. J., A. R. Gregory, and Gardner, L. W., 1956. “Elastic wave velocities in heterogeneous and porous media.” GEOPHYSICS, 21(1), 41-70. https://doi.org/10.1190/1.1438217

Yalçin, M.N., Littke, R., Sachsenhofer, R.F., 1997. Thermal History of Sedimentary Basins: Petroleum and Basin Evolution, p. 71-167.

Annex 1: Biostratigraphy

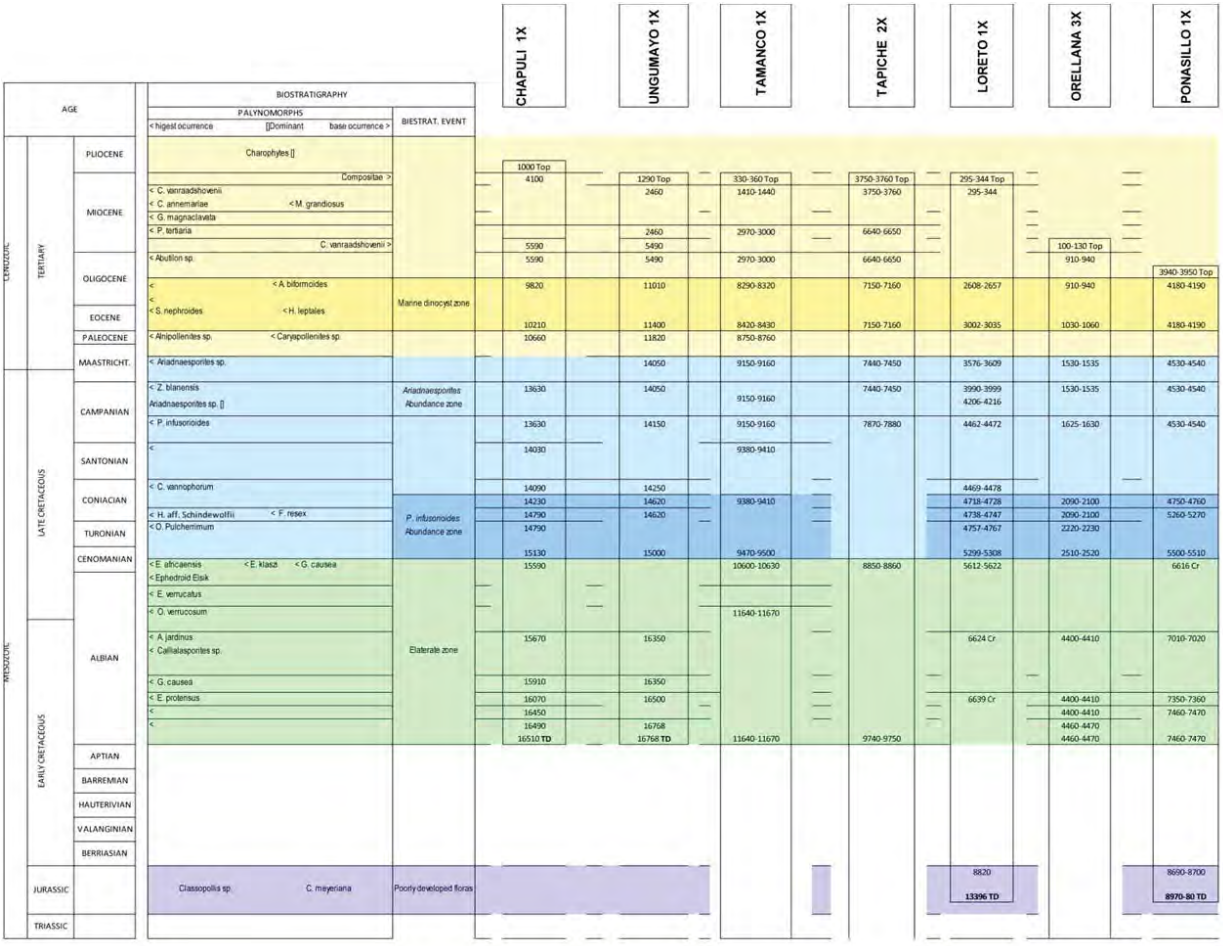

Figure A.1.1. Palynology study in the Marañón Basin from Talisman (2011). See location of the wells in Figure 3.1. This regional biostratigraphy study includes 7 wells prepared by Bert Van Helden. Key palynomorphs and biostratigraphic events are summarized.

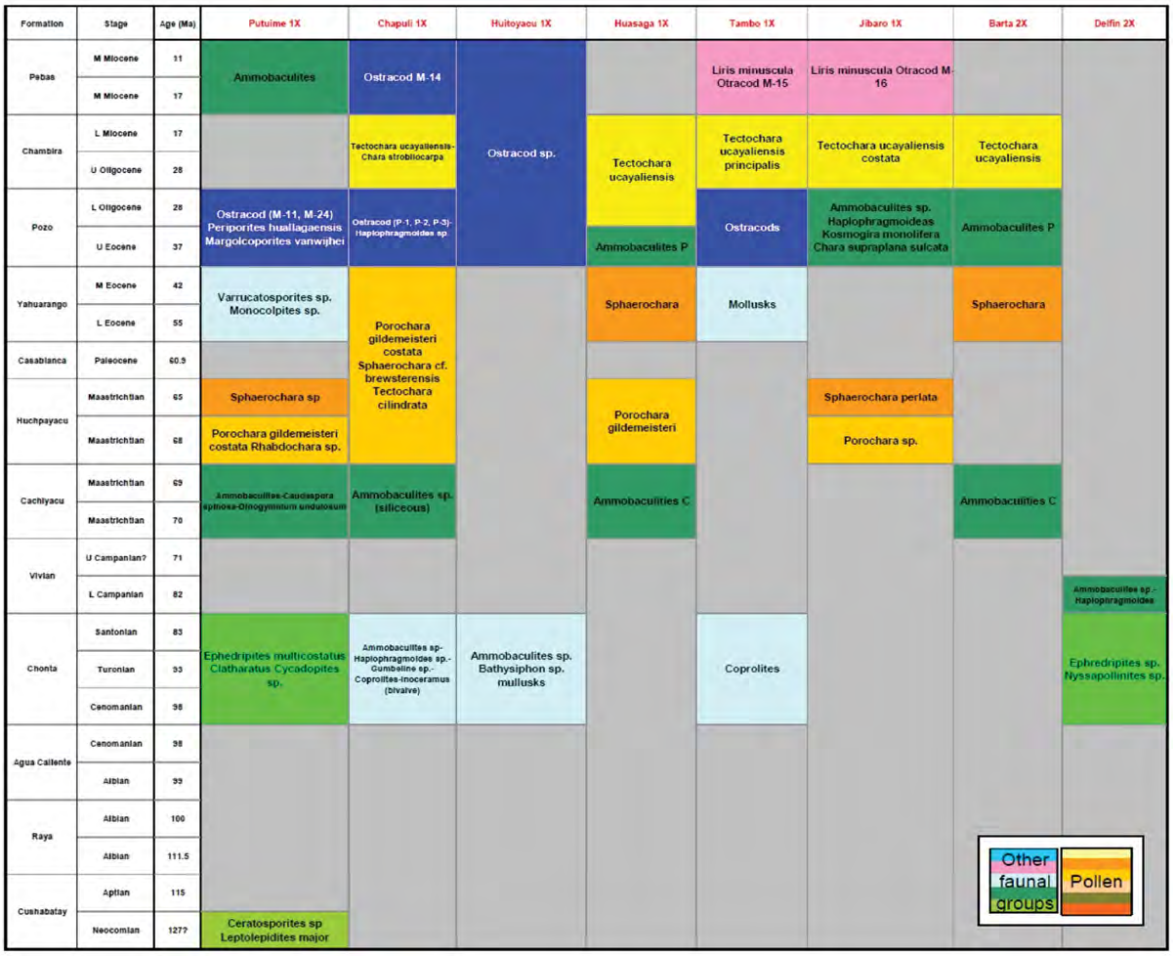

Figure A.1.2. Biostratigraphic zones in the Marañón Basin from Conoco, 2008. See location in Figure 3.1.1

Annex 2: Methods of time-depth conversion, porosity calculation, compaction correction and volume and rate estimation

Time-Depth conversion

From the seismic stratigraphic framework extracted in the Marañón Basin a transformation from time to depth domain has been computed using time-depth information in the study area. To convert the seismically-derived TWT values into depth we use a time-velocity charts extracted from the seismic sections where we use the rms velocity.

For this study, we have compiled a data base using the rms velocities derived from processed seismic reflection that we used in this project.

After that we have worked with the software Move from Midland Valley where we use a Depth Conversion tool that is accessed from Model Building tab and allows a surface to be converted from time to depth. We have use a fixed method where we assume that velocity increases linearly with depth. Our input parameters include an initial velocity (V_0) and the rate of velocity change with depth (k) and the depth conversion is carried out using the following function where:

$$Z= V_0 (e^{KT} -1)/k \ldots\ldots \text{(Eq. 1)}$$

Where

z = the thickness of the layer in meters.

V_0 = the initial velocity in meters per second.

k = the rate of velocity change with depth.

t = the one-way travel time (OWTT) in seconds.

e = the natural logarithm base.

Porosity Calculation

Porosities have been derived from sonic logs for the Cretaceous to Tertiary sequence of 15 hydrocarbon exploration wells in the Marañón Basin.

In the absence of core data for some wells, porosities in the Marañón Basin must be determined from wireline logs. Sonic logs were run in the Marañón of all the 15 wells available wells, and we used also 4 cores data from the northern region of Marañón for calibration.

The sonic tool measures the shortest time for a compressional wave to travel through the formation adjacent to the borehole wall. Sonic logs are generally presented in terms of traveling time, which is a velocity expressed in units of microseconds per foot (μs/ft).

Sonic logs are commonly used to estimate porosity, which is one of the rock parameters controlling sonic velocity. In this study, we have reviewed published articles in order to estimate porosity from sonic logs, and also we compare theses values with porosities that were obtained cores (Figure A.2.1).

Almost all the wells show porosity decreasing with depth throughout the Marañón Basin and also it is represented in the frequency analyses for the four long terms sequences (Figure A. 2. 2) which shows an average range of 38-43 % for the first sequence (Ipururo-Pebas), and porosity decay when it goes deeper.

One formula that have been used since 1956 was published by Wyllie et al. (1956), where time average equation is the most widely used sonic porosity transform:

$$\Delta t_{log} = \Delta t_{ma} (1 - \phi) + \phi \Delta t_{f},$$

$$\text{Whence } \phi = (\Delta t_{log} - \Delta t_{ma}) / (\Delta t_{f} - \Delta t_{ma}) \ldots \text{(Eq.1)}$$

Where ϕ is the porosity, and Δt_{log}, Δt_{ma}, and Δt_{f} are the sonic log, matrix, and interstitial fluid interval transit times (reciprocals of velocity) respectively.

Porosities that are above approximately 30% (Raymer et al., 1980), it is necessary to apply an empirical correction factor to the equation (1) because it over-estimates porosity (Schlumberger, 1987). In the range 5-25% (Raymer et at. 1980) the time average equation yields porosities which are too low.

Raymer-Clemenceau et al. (1988) introduced the concept of acoustic formation factor for more accurate porosity determination from sonic transit time data. The sandstone data provided by Raymer et al. (1980) augmented by data from carbonate reservoirs led them to propose that:

$$(1 - \phi)^{x} = F_{ac} = \Delta t_{log} / \Delta t_{ma},$$

$$\text{Whence } \phi = 1 - (\Delta t_{ma} / \Delta t_{log})^{1/x} \ldots\ldots \text{(Eq. 2)}$$

Where the symbols are as above, F_{ac} is the acoustic formation factor and the exponent *x* is specific to matrix lithology.

For this study interval transit times were converted to porosity using equation (2) with the appropriate calcite matrix transit time of 47.6 µs/ft, and exponent, *x* of 1.76 (Raiga-Clemenceau et al. 1988). Logs recorded in imperial units were resampled every 5 ft.

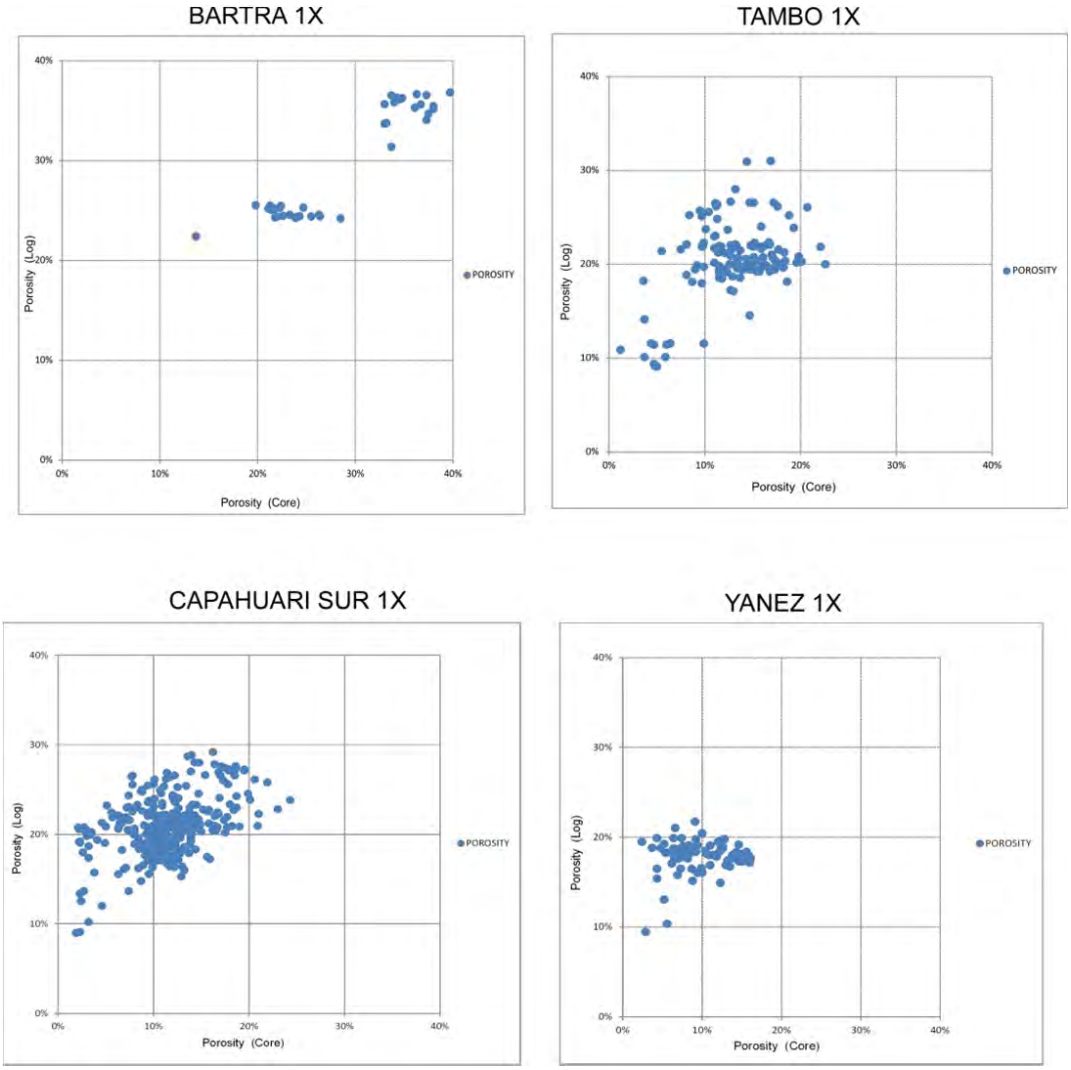

Figure A.2.1. Porosities values obtain from sonic logs vs. porosities data obtain from cores samples.

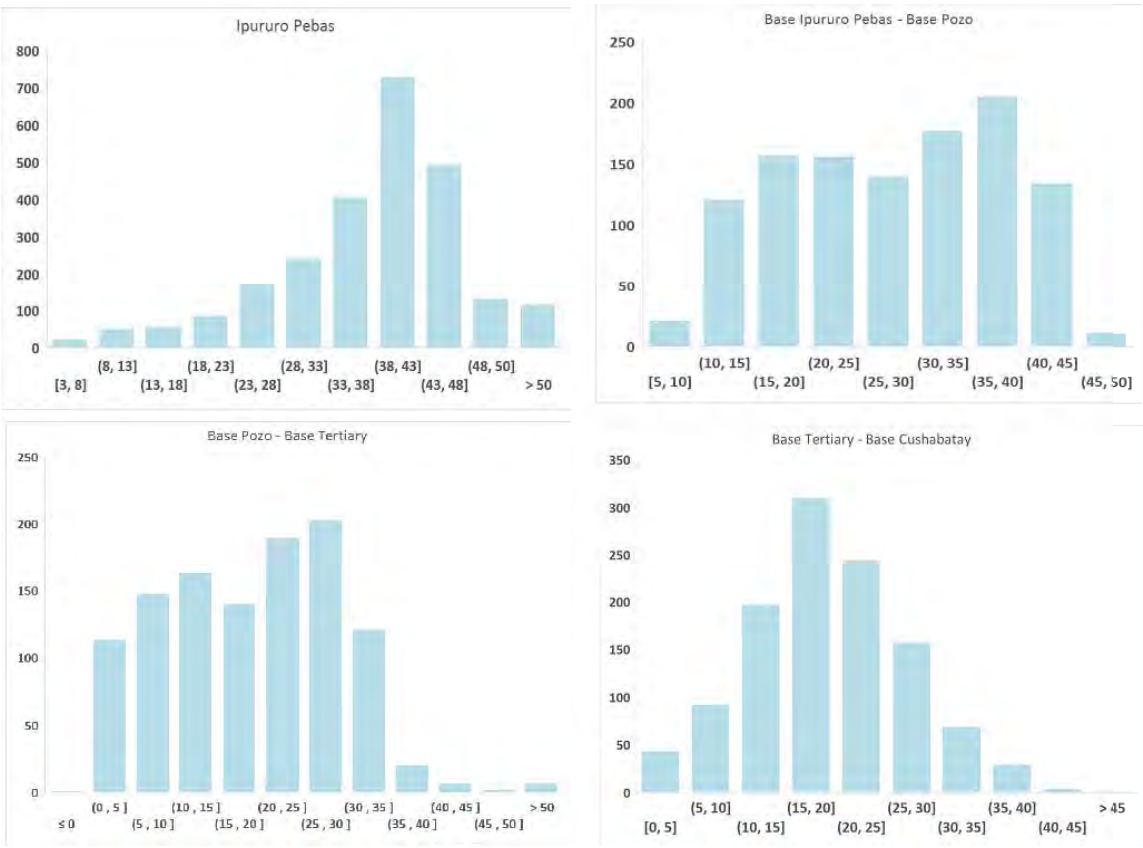

Figure A.2.2. Frequency analyses for the porosity values for the four long term sequence that were identified in the basin. A) Represent the frequency analyses for Ipururo Pebas. B) From Base Ipururo to Base Pozo. C) From Base Pozo to Base Tertiary. D) Base Tertiary to Base Cushabatay.

Compaction correction

Compaction (i.e. porosity decay) of recent soft sediment is an important source of uncertainty in quantifying the variation of sedimentary fluxes for different ages. We have estimated values of porosity from sample measurements on cores and used these to calibrate the porosity curves from wireline logging (Wyllie et al., 1956). The porosity evolution with depth can be then used to estimate uplifted and eroded section of a sedimentary basin (e.g. Hillis et al., 1994).

The solid sediment thickness estimate follows the methodology of many previous studies (e.g., Métivier et al., 1999; Walford et al., 2005). Knowing the carbonate, organic matter and volcaniclastics content of the different intervals we have removed these figures to each interval to obtain 'true' siliciclastic solid sediment. The porosity has been removed from the volume of each isopach to calculate solid sediment rock mass. Porosity, Φ, is assumed to vary exponentially with depth, z, according to:

$\Phi(z)= \Phi_o$ e-z/k …(Eq. 2)

where Φ_o is the initial porosity and k is the porosity decay length.

Using Eq. (2), the solid thickness, T_{sol}, of a unit is given by:

$T_{sol} = z_2 – z_1 + \Phi o$ k (e-z2/k – e-z1/k)… (Eq. 3)

where z_1 is the depth below the surface to the top of the unit and z_2 is the depth below surface to the bottom of the unit. Constant values of $k = 0.18$ and $\Phi_o = 45$ were determined from the measurements on samples from the Marañón Basin.

Volume and rate estimation

Volume where computed from the isopach maps sourced from the depth converted seismic and stratigraphic horizons. These volumes, the lithological information and physical properties, with age and duration of sequences have allowed us to compute the rates of sedimentation.

Annex 3: Vitrine Reflectance values used in the Basin Modeling

WELL NAME	LABORATORY	LATITUDE	LONGITUDE	AVE DEPTH (M)	FORMATION	VITRINITE REFLECTANCE (Ro)
Ungumayo 1X	ROBERTSON	-4.18330	-76.34995	470	Corrientes	0.22
Ungumayo 1X	ROBERTSON	-4.18330	-76.34995	780	Marañón	0.25
Ungumayo 1X	ROBERTSON	-4.18330	-76.34995	1015	Marañón	0.38
Ungumayo 1X	ROBERTSON	-4.18330	-76.34995	2750	Pebas	0.49
Ungumayo 1X	ROBERTSON	-4.18330	-76.34995	4280	Vivian	0.66
Ungumayo 1X	ROBERTSON	-4.18330	-76.34995	4315	Vivian	0.56
Ungumayo 1X	ROBERTSON	-4.18330	-76.34995	4490	Chonta	0.57
Ungumayo 1X	DGSI	-4.18330	-76.34995	4400	Vivian	0.62
Ungumayo 1X	DGSI	-4.18330	-76.34995	5110	Agua Caliente	0.74
Tigrillo 1X	PSI	-4.00684	-75.96303	2158	Pebas	0.38
Tigrillo 1X	PSI	-4.00684	-75.96303	2446	Pebas	0.34
Tigrillo 1X	PSI	-4.00684	-75.96303	3530	Pozo	0.45
Tigrillo 1X	PSI	-4.00684	-75.96303	3566	Pozo	0.52
Tigrillo 1X	PSI	-4.00684	-75.96303	4131	Yahuarango	0.51
Tigrillo 1X	PSI	-4.00684	-75.96303	4256	Chonta	0.55
Tigrillo 1X	PSI	-4.00684	-75.96303	4280	Chonta	0.57
Tigrillo 1X	PSI	-4.00684	-75.96303	4241	Chonta	0.57
Tigrillo 1X	PSI	-4.00684	-75.96303	4270	Chonta	0.57
Tigrillo 1X	PSI	-4.00684	-75.96303	4398	Chonta	0.59
Tigrillo 1X	PSI	-4.00684	-75.96303	4451	Chonta	0.6
Tigrillo 1X	PSI	-4.00684	-75.96303	4454	Chonta	0.59
Tigrillo 1X	PSI	-4.00684	-75.96303	4453	Chonta	0.6
Tigrillo 1X	PSI	-4.00684	-75.96303	4564	Chonta	0.65
Tigrillo 1X	PSI	-4.00684	-75.96303	4616	Agua Caliente	0.64
Tigrillo 1X	PSI	-4.00684	-75.96303	4631	Agua Caliente	0.61
Tigrillo 1X	PSI	-4.00684	-75.96303	4662	Agua Caliente	0.63
Tigrillo 1X	PSI	-4.00684	-75.96303	4677	Agua Caliente	0.65
Tigrillo 1X	PSI	-4.00684	-75.96303	4730	Agua Caliente	0.63
Tigrillo 1X	PSI	-4.00684	-75.96303	4308	Chonta	0.51
Tigrillo 1X	PSI	-4.00684	-75.96303	4314	Chonta	0.49
Tigrillo 1X	PSI	-4.00684	-75.96303	4388	Chonta	0.55
Tigrillo 1X	PSI	-4.00684	-75.96303	4421	Chonta	0.57
Tigrillo 1X	PSI	-4.00684	-75.96303	4473	Chonta	0.57
Tigrillo 1X	PSI	-4.00684	-75.96303	4479	Chonta	0.57
Tigrillo 1X	PSI	-4.00684	-75.96303	4558	Chonta	0.59
Tigrillo 1X	PSI	-4.00684	-75.96303	4561	Chonta	0.6
Tigrillo 1X	PSI	-4.00684	-75.96303	4574	Chonta	0.59
Tigrillo 1X	PSI	-4.00684	-75.96303	4836	Agua Caliente	0.64
Tigrillo 1X	PSI	-4.00684	-75.96303	4875	Raya	0.63

WELL NAME	LABORATORY	LATITUDE	LONGITUDE	AVE DEPTH (M)	FORMATION	VITRINITE REFLECTANCE (Ro)
Tigrillo 1X	PSI	-4.00684	-75.96303	4880	Raya	0.65
Pavayacu 3X	PSI	-3.38823	-75.40467	2640	Chonta	0.49
Pavayacu 3X	PSI	-3.38823	-75.40467	2755	Agua Caliente	0.72
Pavayacu 3X	PSI	-3.38823	-75.40467	2897	Raya	0.61
Pavayacu 3X	PSI	-3.38823	-75.40467	3053	Cushabatay	0.53
Pavayacu 3X	PSI	-3.38823	-75.40467	3193	Sarayaquillo	0.53
Pavayacu 3X	PSI	-3.38823	-75.40467	3333	Sarayaquillo	0.52
Pavayacu 3X	PSI	-3.38823	-75.40467	3406	Sarayaquillo	0.56
Huasaga 1X	PSI	-3.14223	-76.65998	2969	Pozo	0.58
Huasaga 1X	PSI	-3.14223	-76.65998	3020	Pozo	0.56
Huasaga 1X	PSI	-3.14223	-76.65998	3902	Yahuarango	0.62
Huasaga 1X	PSI	-3.14223	-76.65998	4067	Vivian	0.77
Huasaga 1X	PSI	-3.14223	-76.65998	4121	Chonta	0.67
Huasaga 1X	PSI	-3.14223	-76.65998	4136	Chonta	0.71
Huasaga 1X	PSI	-3.14223	-76.65998	4160	Chonta	0.77
Huasaga 1X	PSI	-3.14223	-76.65998	4194	Chonta	0.66
Huasaga 1X	PSI	-3.14223	-76.65998	4216	Chonta	0.93
Huasaga 1X	PSI	-3.14223	-76.65998	4373	Chonta	0.83
Huasaga 1X	PSI	-3.14223	-76.65998	4484	Agua Caliente	0.93
Huasaga 1X	PSI	-3.14223	-76.65998	4513	Agua Caliente	0.82
Huasaga 1X	PSI	-3.14223	-76.65998	4525	Agua Caliente	0.77
Huasaga 1X	PSI	-3.14223	-76.65998	4557	Agua Caliente	0.86
Huasaga 1X	PSI	-3.14223	-76.65998	4583	Agua Caliente	0.83
Huasaga 1X	PSI	-3.14223	-76.65998	4607	Agua Caliente	0.82
Huasaga 1X	PSI	-3.14223	-76.65998	4643	Raya	0.9
Huasaga 1X	PSI	-3.14223	-76.65998	4760	Cushabatay	0.92
Huasaga 1X	PSI	-3.14223	-76.65998	4194	Chonta	0.66
Huasaga 1X	PSI	-3.14223	-76.65998	4524	Agua Caliente	0.77
Tucunare 1X	PSI	-2.98469	-76.32691	2807	Yahuarango	0.62
Tucunare 1X	PSI	-2.98469	-76.32691	2850	Yahuarango	0.63
Tucunare 1X	PSI	-2.98469	-76.32691	3677	Chonta	0.83
Tucunare 1X	PSI	-2.98469	-76.32691	3693	Chonta	0.81
Tucunare 1X	PSI	-2.98469	-76.32691	3754	Agua Caliente	0.81
Tucunare 1X	PSI	-2.98469	-76.32691	3824	Agua Caliente	0.86
Tucunare 1X	PSI	-2.98469	-76.32691	3906	Raya	0.89
Tucunare 1X	PSI	-2.98469	-76.32691	4028	Cushabatay	0.89
Tucunare 1X	PSI	-2.98469	-76.32691	4171	Cushabatay	0.91
Tucunare 1X	PSI	-2.98469	-76.32691	4191	Cushabatay	0.91
Tucunare 1X	PSI	-2.98469	-76.32691	4214	Cushabatay	0.91
Ponasillo 1X	PSI	-7.39399	-76.29467	588	Pozo	1
Ponasillo 1X	PSI	-7.39399	-76.29467	604	Pozo	0.99
Ponasillo 1X	PSI	-7.39399	-76.29467	619	Pozo	1.03
Ponasillo 1X	PSI	-7.39399	-76.29467	1277	Cachiyacu	1.1

WELL NAME	LABORATORY	LATITUDE	LONGITUDE	AVE DEPTH (M)	FORMATION	VITRINITE REFLECTANCE (Ro)
Ponasillo 1X	PSI	-7.39399	-76.29467	1277	Cachiyacu	0.97
Ponasillo 1X	PSI	-7.39399	-76.29467	1359	Chonta	0.95
Ponasillo 1X	PSI	-7.39399	-76.29467	1407	Chonta	1
Ponasillo 1X	PSI	-7.39399	-76.29467	1442	Chonta	1.26
Ponasillo 1X	PSI	-7.39399	-76.29467	1449	Chonta	1.48
Ponasillo 1X	PSI	-7.39399	-76.29467	1457	Chonta	1.05
Ponasillo 1X	PSI	-7.39399	-76.29467	1503	Chonta	1.2
Ponasillo 1X	PSI	-7.39399	-76.29467	1503	Chonta	1.05
Ponasillo 1X	PSI	-7.39399	-76.29467	1530	Chonta	1.05
Ponasillo 1X	PSI	-7.39399	-76.29467	1539	Chonta	1.23
Ponasillo 1X	PSI	-7.39399	-76.29467	1564	Chonta	1.06
Ponasillo 1X	PSI	-7.39399	-76.29467	1593	Chonta	1.11
Ponasillo 1X	PSI	-7.39399	-76.29467	1594	Chonta	1.2
Ponasillo 1X	PSI	-7.39399	-76.29467	1646	Chonta	1.17
Ponasillo 1X	PSI	-7.39399	-76.29467	1678	Chonta	1.33
Ponasillo 1X	PSI	-7.39399	-76.29467	1692	Chonta	1.15
Ponasillo 1X	PSI	-7.39399	-76.29467	1737	Chonta	1.19
Ponasillo 1X	PSI	-7.39399	-76.29467	1783	Chonta	1.1
Ponasillo 1X	PSI	-7.39399	-76.29467	1811	Chonta	1.26
Ponasillo 1X	PSI	-7.39399	-76.29467	1829	Chonta	1.09
Ponasillo 1X	PSI	-7.39399	-76.29467	1875	Chonta	1.29
Ponasillo 1X	PSI	-7.39399	-76.29467	1902	Chonta	1.23
Ponasillo 1X	PSI	-7.39399	-76.29467	1920	Chonta	1.22
Ponasillo 1X	PSI	-7.39399	-76.29467	1963	Chonta	1.06
Ponasillo 1X	PSI	-7.39399	-76.29467	1966	Chonta	1.22
Ponasillo 1X	PSI	-7.39399	-76.29467	2012	Agua Caliente	1.25
Ponasillo 1X	PSI	-7.39399	-76.29467	2014	Agua Caliente	1.24
Ponasillo 1X	PSI	-7.39399	-76.29467	2014	Agua Caliente	1.28
Ponasillo 1X	PSI	-7.39399	-76.29467	2014	Agua Caliente	1.24
Ponasillo 1X	PSI	-7.39399	-76.29467	2015	Agua Caliente	1.26
Ponasillo 1X	PSI	-7.39399	-76.29467	2015	Agua Caliente	1.24
Ponasillo 1X	PSI	-7.39399	-76.29467	2016	Agua Caliente	1.27
Ponasillo 1X	PSI	-7.39399	-76.29467	2017	Agua Caliente	1.16
Ponasillo 1X	PSI	-7.39399	-76.29467	2017	Agua Caliente	1.33
Ponasillo 1X	PSI	-7.39399	-76.29467	2115	Agua Caliente	1.33
Ponasillo 1X	PSI	-7.39399	-76.29467	2143	Agua Caliente	1.6
Ponasillo 1X	PSI	-7.39399	-76.29467	2271	Raya	1.4
Ponasillo 1X	PSI	-7.39399	-76.29467	2275	Raya	1.59
Ponasillo 1X	PSI	-7.39399	-76.29467	2316	Raya	1.53
Ponasillo 1X	PSI	-7.39399	-76.29467	2323	Raya	1.7
Ponasillo 1X	PSI	-7.39399	-76.29467	2384	Raya	1.65
Ponasillo 1X	PSI	-7.39399	-76.29467	2411	Raya	1.9
Ponasillo 1X	PSI	-7.39399	-76.29467	2435	Cushabatay	1.41

WELL NAME	LABORATORY	LATITUDE	LONGITUDE	AVE DEPTH (M)	FORMATION	VITRINITE REFLECTANCE (Ro)
Ponasillo 1X	PSI	-7.39399	-76.29467	2457	Cushabatay	1.69
Ponasillo 1X	PSI	-7.39399	-76.29467	2462	Cushabatay	1.89
Ponasillo 1X	PSI	-7.39399	-76.29467	2490	Cushabatay	1.5
Ponasillo 1X	PSI	-7.39399	-76.29467	2499	Cushabatay	1.99
Ponasillo 1X	PSI	-7.39399	-76.29467	2517	Cushabatay	1.7
Ponasillo 1X	PSI	-7.39399	-76.29467	2594	Cushabatay	1.7
Ponasillo 1X	PSI	-7.39399	-76.29467	2604	Pre Cretaceo	1.7
Ponasillo 1X	PSI	-7.39399	-76.29467	2664	Pre Cretaceo	1.8
Ponasillo 1X	PSI	-7.39399	-76.29467	10	Pebas	0.67
Ponasillo 1X	PSI	-7.39399	-76.29467	400	Chambira	0.6
Ponasillo 1X	PSI	-7.39399	-76.29467	950	Yahuarango	0.95
Ponasillo 1X	PSI	-7.39399	-76.29467	1719	Chonta	1.1
Ponasillo 1X	PSI	-7.39399	-76.29467	2590	Cushabatay	1.7
Ponasillo 1X	PSI	-7.39399	-76.29467	2737	Pre Cretaceo	1.8
Loreto 1X	SPT	-5.91310	-75.58420	873	Pozo	0.59
Loreto 1X	SPT	-5.91310	-75.58420	1355	Chonta	0.66
Loreto 1X	SPT	-5.91310	-75.58420	2452	Cushabatay	0.89
Santa Lucia 1X	PSI	-6.38430	-75.05120	338	Chambira	0.41
Santa Lucia 1X	PSI	-6.38430	-75.05120	872	Chambira	0.49
Santa Lucia 1X	PSI	-6.38430	-75.05120	1826	Pozo	0.53
Santa Lucia 1X	PSI	-6.38430	-75.05120	2009	Vivian	0.47
Santa Lucia 1X	PSI	-6.38430	-75.05120	2079	Vivian	0.5
Santa Lucia 1X	PSI	-6.38430	-75.05120	2170	Chonta	0.51
Santa Lucia 1X	PSI	-6.38430	-75.05120	2198	Chonta	0.55
Santa Lucia 1X	PSI	-6.38430	-75.05120	2237	Chonta	0.58
Santa Lucia 1X	PSI	-6.38430	-75.05120	2265	Chonta	0.59
Santa Lucia 1X	PSI	-6.38430	-75.05120	2316	Chonta	0.56
Santa Lucia 1X	PSI	-6.38430	-75.05120	2380	Chonta	0.58
Santa Lucia 1X	PSI	-6.38430	-75.05120	2390	Chonta	0.58
Santa Lucia 1X	PSI	-6.38430	-75.05120	2444	Agua Caliente	0.59
Santa Lucia 1X	PSI	-6.38430	-75.05120	2716	Agua Caliente	0.56
Santa Lucia 1X	PSI	-6.38430	-75.05120	2728	Agua Caliente	0.62
Santa Lucia 1X	PSI	-6.38430	-75.05120	2761	Cushabatay	0.66
Santa Lucia 1X	PSI	-6.38430	-75.05120	2990	Cushabatay	0.56
Bolognesi 1X	PSI	-3.03875	-75.19731	2483	Chonta	0.47
Bolognesi 1X	PSI	-3.03875	-75.19731	2723	Raya	0.47
Bolognesi 1X	PSI	-3.03875	-75.19731	2963	Raya	0.45
Situche Central 3X	PSI	-3.13858	-77.30137	4856	Vivian	0.96
Situche Central 3X	PSI	-3.13858	-77.30137	4860	Vivian	0.92
Situche Central 3X	PSI	-3.13858	-77.30137	4866	Vivian	0.74
Situche Central 3X	PSI	-3.13858	-77.30137	4867	Vivian	0.83
Situche Central 3X	PSI	-3.13858	-77.30137	4887	Vivian	0.91

WELL NAME	LABORATORY	LATITUDE	LONGITUDE	AVE DEPTH (M)	FORMATION	VITRINITE REFLECTANCE (Ro)
Situche Central 3X	PSI	-3.13858	-77.30137	5806	Cushabatay	1.41
Situche Central 3X	PSI	-3.13858	-77.30137	390	Ipururo	0.41
Situche Central 3X	PSI	-3.13858	-77.30137	646	Ipururo	0.55
Situche Central 3X	PSI	-3.13858	-77.30137	3597	Pozo	0.72
Situche Central 3X	PSI	-3.13858	-77.30137	3661	Pozo	0.72
Situche Central 3X	PSI	-3.13858	-77.30137	4950	Chonta	0.87
Situche Central 3X	PSI	-3.13858	-77.30137	4990	Chonta	0.91
Situche Central 3X	PSI	-3.13858	-77.30137	5005	Chonta	0.84
Situche Central 3X	PSI	-3.13858	-77.30137	5032	Chonta	0.91
Situche Central 3X	PSI	-3.13858	-77.30137	5093	Chonta	0.97
Situche Central 3X	PSI	-3.13858	-77.30137	5130	Chonta	1.01
Situche Central 3X	PSI	-3.13858	-77.30137	5179	Chonta	0.96
Situche Central 3X	PSI	-3.13858	-77.30137	5371	Chonta	0.92
Situche Central 3X	PSI	-3.13858	-77.30137	5465	Agua Caliente	1.08
Situche Central 3X	PSI	-3.13858	-77.30137	5654	Raya	0.99
Situche Central 3X	PSI	-3.13858	-77.30137	5685	Raya	1.03
Jibaro 1X	PSI	-2.72189	-76.03729	2870	Yahuarango	0.71
Jibaro 1X	PSI	-2.72189	-76.03729	3000	Chonta	0.61
Jibaro 1X	PSI	-2.72189	-76.03729	3080	Chonta	0.59
Jibaro 1X	PSI	-2.72189	-76.03729	3115	Chonta	0.76
Jibaro 1X	PSI	-2.72189	-76.03729	3300	Agua Caliente	0.56
Jibaro 1X	PSI	-2.72189	-76.03729	3350	Raya	0.62
Jibaro 1X	PSI	-2.72189	-76.03729	3550	Pre Cretaceo	1.17
Jibaro 1X	PSI	-2.72189	-76.03729	3630	Pre Cretaceo	1.28
La Frontera 1X	PSI	-6.29700	-74.67350	1561	Pozo	0.45
La Frontera 1X	PSI	-6.29700	-74.67350	1798	Chonta	0.51
La Frontera 1X	PSI	-6.29700	-74.67350	2493	Cushabatay	0.59
La Frontera 1X	PSI	-6.29700	-74.67350	2576	Cabanillas	0.85
La Frontera 1X	PSI	-6.29700	-74.67350	2649	Cabanillas	1.49
La Frontera 1X	PSI	-6.29700	-74.67350	2676	Cabanillas	1.11
La Frontera 1X	PSI	-6.29700	-74.67350	2740	Cabanillas	1.54
La Frontera 1X	PSI	-6.29700	-74.67350	2758	Cabanillas	1.19
La Frontera 1X	PSI	-6.29700	-74.67350	2832	Cabanillas	1.58
La Frontera 1X	PSI	-6.29700	-74.67350	2850	Cabanillas	1.19
La Frontera 1X	PSI	-6.29700	-74.67350	2954	Cabanillas	1.68
Tamanco 1X	PSI	-5.83840	-74.36250	910	Pebas	0.46
Tamanco 1X	PSI	-5.83840	-74.36250	1669	Chambira	0.66
Tamanco 1X	PSI	-5.83840	-74.36250	2842	Chonta	0.77
Tamanco 1X	PSI	-5.83840	-74.36250	2900	Chonta	0.79

Geochemical analyses of the PERUPETRO data bank (not exhaustive), SPT Simon Petroleum (1993) and Petroleum System International (2011), Robertson Research (1990) and DGSI

Annex 4: Structural maps in depth

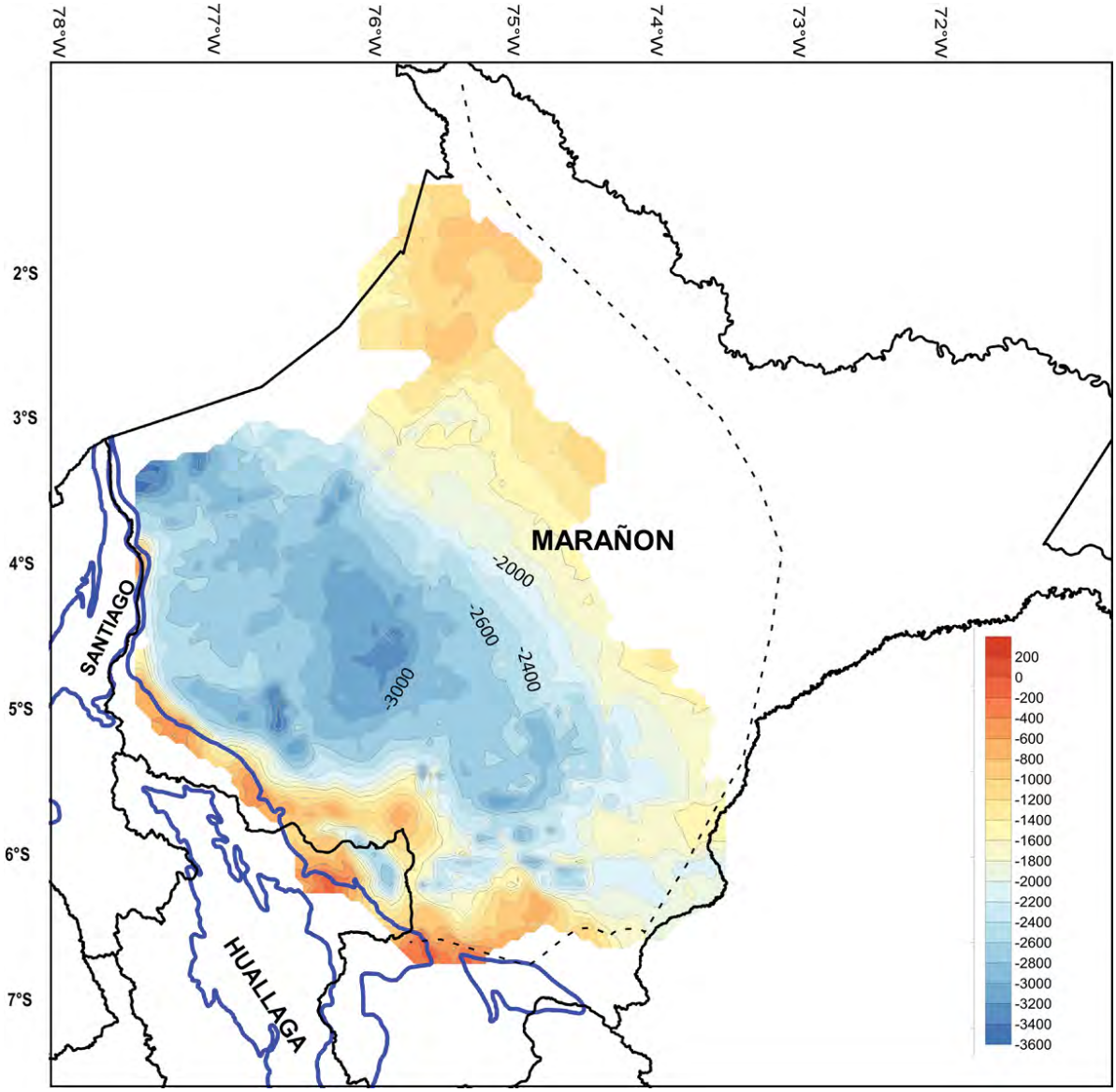

Figure A.4.1. Structural map (in meters) of the Base of Pozo Fm. in the Marañón Basin.

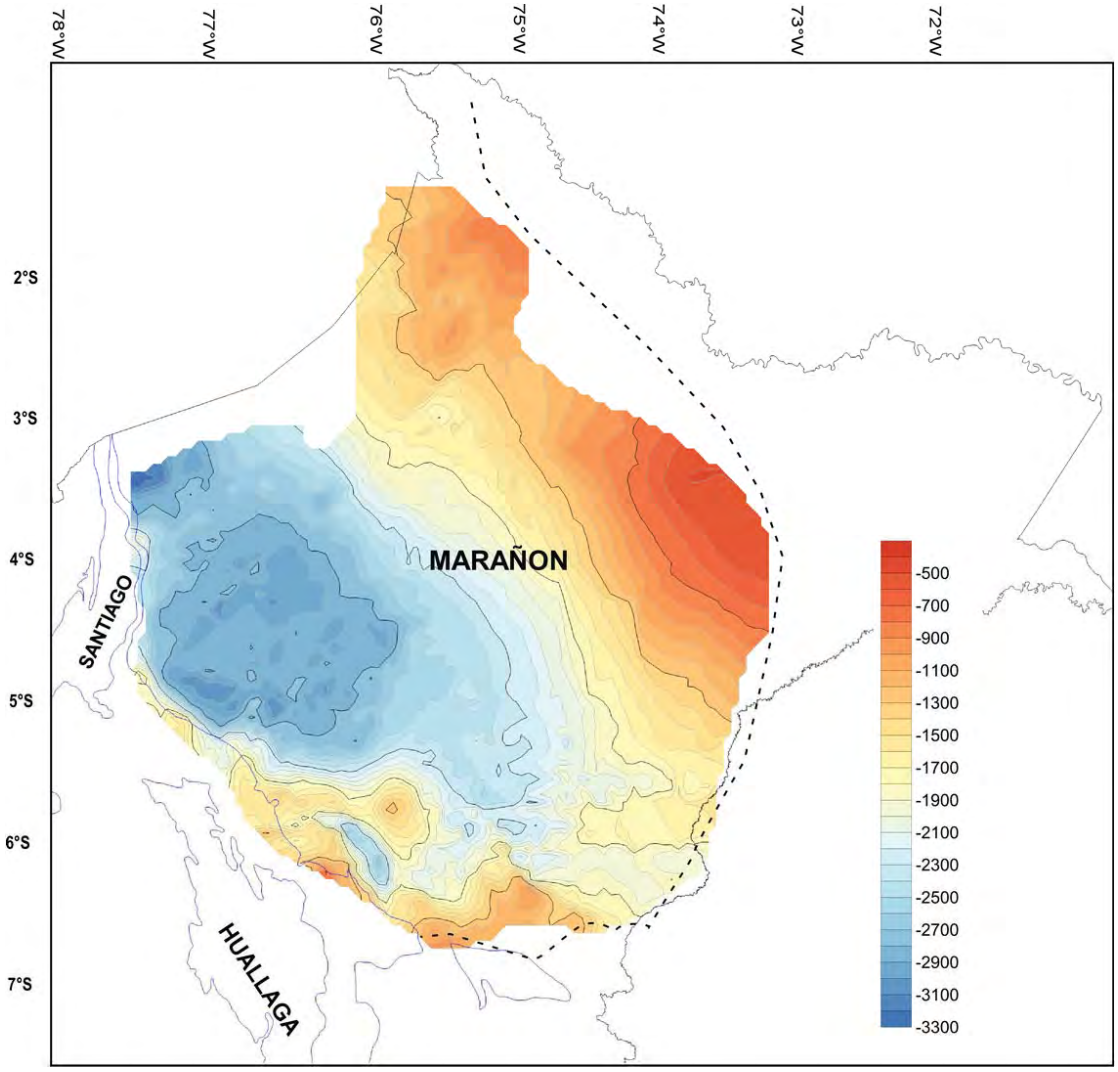

Figure A.4.2. Structural map (in meters) of the Base of Cretaceous in the Marañón Basin.

Annex 5: THE PERUVIAN SUBANDEAN FORELAND BASIN SYSTEM: STRUCTURAL OVERVIEW, GEOCHRONOLOGIC CONSTRAINTS, AND UNEXPLORED PLAYS *in Petroleum Basins and Hydrocarbon Potential of the Andes of Peru and Bolivia. AAPG Memoir 117*

Patrice Baby[1], Ysabel Calderón[1,2], Christian Hurtado[3], Mélanie Louterbach[4], Nicolas Espurt[5], Stéphane Brusset[1], Martin Roddaz[1], Stéphanie Brichau[1], Adrien Eude[1], Calves Gérome[1], Alejandro Quispe[2], Léonard Ramirez[2], Asaid Bandach[2], Rolando Bolaños[2].

1. Géosciences Environnement Toulouse (GET), Université de Toulouse, CNRS UMR 5563 / UR 234 IRD / UPS Toulouse / CNES, 14 Avenue Edouard Belin, 31400 Toulouse, France
2. PERUPETRO S.A., Avenida Luis Aldana No 320 San Borja, Lima 41, Perú
3. Instituto de Geociências, Universidade de Brasília, Campus Universitário Darcy Ribeiro ICC - Ala Central CEP 70.910-900 - Brasília DF
4. REPSOL Exploración S.A., Calle Méndez Álvaro 44, 28045 Madrid, Spain
5. CEREGE, UMR 7330, CNRS, Aix-Marseille Université, IRD, Aix-en-Provence, France

THE PERUVIAN SUBANDEAN FORELAND BASIN SYSTEM: STRUCTURAL OVERVIEW, GEOCHRONOLOGIC CONSTRAINTS, AND UNEXPLORED PLAYS

Patrice Baby[1], IRD FRANCE. patrice.baby@ird.fr

Ysabel Calderón[1,2], Christian Hurtado[3], Mélanie Louterbach[4], Nicolas Espurt[5], Stéphane Brusset[1], Martin Roddaz[1], Stéphanie Brichau[1], Adrien Eude[1], Calves Gérome[1], Alejandro Quispe[2], Léonardo Ramirez[2], Asaid Bandach[2], Rolando Bolaños[2].

1. Géosciences Environnement Toulouse (GET), Université de Toulouse, CNRS UMR 5563 / UR 234 IRD / UPS Toulouse / CNES, 14 Avenue Edouard Belin, 31400 Toulouse, France

2. PERUPETRO S.A., Avenida Luis Aldana No 320 San Borja, Lima 41, Perú

3. Instituto de Geociências, Universidade de Brasília, Campus Universitário Darcy Ribeiro ICC - Ala Central CEP 70.910-900 - Brasília DF

4. REPSOL Exploración S.A., Calle Méndez Álvaro 44, 28045 Madrid, Spain

5. CEREGE, UMR 7330, CNRS, Aix-Marseille Université, IRD, Aix-en-Provence, France

ABSTRACT

In the Peruvian Subandean foreland basin system, the construction of serial balanced cross-sections from a good set of structural data and an extensive knowledge of the stratigraphy and geodynamic evolution allow a more refined definition of the unexplored plays, as sub-thrusts, duplexes or pre-Andean structures. Sequential restorations are proposed by coupling thermochronologic analyses with growth strata studies. The results show significant north-south variations in geometry, timing and rates of deformation and foreland sedimentation. These latitudinal variations are related to the pre-Andean basins inheritance, but also to the interactions between thrusts propagation, erosion and sedimentation. Thermochronologic ages correspond to the most recent thrust-related uplifts and are supplemented by the study of stratigraphic foreland basin records that can bring to light oldest tectonic events. North of the Peruvian Subandean zone, thrusts propagation is controlled by thick-skinned and thin-skinned salt tectonics. Northern thick-skinned tectonics has westward vergence, and is inherited from a Middle Permian fold and thrust belt. To the south, thrusts deformation is largely controlled by the geometry of the preserved Paleozoic sedimentary wedge and becomes progressively thin-skinned. Total Subandean shortening varies between 70 km in the north to 47 km in the south. Subandean deformation started in the Late Cretaceous. After a period of quiescence during the Middle Eocene, it reactivates and is still active. Three stages of Subandean deformation are clearly identified and help to define the preservation time in the suggested petroleum plays.

INTRODUCTION

The Peruvian Subandean basins, which developed in a Foreland Basin System (FBS) (DeCelles and Giles, 1996) adjacent to the eastern side of the Central Andes (Figure 1), present a proven petroleum potential with a least two major petroleum systems (see Figure 2, 3 and 4). It stays poor explored in the wedge-top depozone (Subandean Fold and Thrust Belt *sensu stricto*), where some exploration wells have been drilled allowing the discoveries of giant gas fields in the Camisea Basin and the less significant Candamo gas field (Madre de Dios Basin). This Subandean Fold and Thrust Belt (FTB) presents apparently complex structural architecture and timing of deformation that can curb exploration. As in all the FTBs, this risk can be significantly reduced by an appropriate geometric and kinematic analysis.

Indeed, from north to south, the Peruvian Subandean FBS (Figure 1) shows a complex structural partitioning (McGroder et al., 2015) controlled by a Paleozoic and Mesozoic heritage, Andean slab geometry and probably climatic latitudinal variations. To illustrate and explain this lateral evolution, we present a structural synthesis and serial balanced cross-sections through the entire Subandean FBS. Balanced cross-sections have been constructed from a good set of structural data and an extensive knowledge of the stratigraphy, paleogeography and geodynamic evolution. The timing of the Subandean deformation was revised from thermochronologic ages and stratigraphic records of foreland deposits. For each serial cross-section, we propose a sequential restoration of the foreland basin system propagation. Finally, implications for the petroleum plays are discussed.

This work does not englobe the Santiago fold and thrust belt whose orientation changes to NNE-SSW and compromises the construction of appropriate balanced cross-sections. The Santiago and northern Marañón basins have to be considered as part to the Northern Andes retroarc foreland basin system. They belong to the large present-day Marañón–Oriente–Putumayo foreland system and oil province known as MOP (Marksteiner and Alemán, 1997), which developed from southern Colombia to northern Peru.

These results have been achieved thanks to the long-term researches carried out under the IRD-PERUPETRO S.A. cooperation and partnership agreement.

GEODYNAMIC SETTING

The Subandean basins of Peru (Figure 1) belongs to the Andean-Amazonian retroarc foreland basin system (Roddaz et al., 2010). They are classically interpreted as the components of a wide retroforeland basin system, where the Huallaga, Ucayali and Camisea sub-basins are correlated to wedge-top depozones (Hermoza et al., 2005), whereas the Marañón Basin is conventionally considered as a foredeep depozone limited to the NE by the Iquitos forebulge (Roddaz et al., 2005). To the south, the Madre de Dios Basin comprises the wedge-top and foredeep depozones.

The Central Andean slab geometry played an important role in the Peruvian Subandean FBS partitioning (Baudino and Hermoza, 2014). The long-wavelength Fitzcarrald Arch that separates the Ucayali Basin from the Madre de Dios Basin is the result of the subduction of the oceanic Nazca ridge (Figure 1; Espurt et al., 2007). Its tectonic uplift considerably affected the Subandean FBS propagation since the end of the Pliocene. It must be considered as a component of the petroleum systems that impacted the migration pathways.

The geometry of the pre-Andean Triassic-Jurassic rift controlled considerably the propagation of the Andean deformation (Rosas et al., 2007; Baby et al., 2013; McGroder et al., 2015). The balanced cross-sections of this paper will show that, in the Peruvian Subandean FBS, the Triassic-Jurassic rift inversion just concerns the western part of the northern FTB.

Heritages of old orogenies constitute other significant components that controlled the Andean deformation fabric (Laubacher et al., 1985; Dalmayrac et al., 1988; Ramos, 1988). Influence of Paleozoic and Late Jurassic orogenies have been yet discussed in the Peruvian Subandean basins (Bump et al., 2008; Espurt et al., 2008; Caputo, 2014; Calderón et al., 2017a).

STRATIGRAPHY, SOURCE ROCKS AND RESERVOIRS

The sedimentary cover involved in the deformation of the Peruvian Subandean FBS consists of a pre-Andean series, unconformably overlain by a marine to continental late Cretaceous sedimentary wedge thinning to the NE, and by a Cenozoic foreland continental and shallow marine infill (e.g. Mathalone and Montoya, 1995). The north-south evolution of this sedimentary cover is illustrated by the stratigraphic diagrams of the Figures 2, 3 and 4, which have been elaborated together with the regional balanced cross-sections. The Andean and pre-Andean series can be divided into long term sequences separated by regional

erosional unconformities clearly identified on seismic. The Paleozoic pre-Andean series comprises Ordovician, Devonian, Carboniferous and Permian clastic and carbonated marine sediments (Dunbar and Newell, 1946; Kummel, 1950; Newell et al., 1954; Mégard, 1978; Mathalone and Montaya, 1995; Gil, 2001; Wine et al., 2001; Alemán et al., 2003; Jacques, 2004; Haeberlin et al., 2004; Espurt et al., 2008; McGroder et al., 2015), deposited over a Cambrian o pre-Cambrian metamorphic complex (Chew et al., 2007; 2008). The marine clastic Paleozoic series, well preserved in the South (Madre de Dios and Camisea basins), are partly eroded in the North probably due to the Jurua orogeny (Caputo, 2014). They host good type III source rock levels as the Ambo Formation (Jacques, 2004). The long term Pennsylvanian to Middle Permian Tarma-Copacabana sequence starts with a regional erosional unconformity that sealed the Famatinian orogeny. The Middle Permian Copacabana Formation is partly eroded below a Late Permian erosional unconformity probably post Gondwanide orogeny (Ramos, 1988). This unconformity is overlain by Late Permian fluvial and aeolian reservoir sandstones – the famous Ene and Noi reservoirs of the Camisea Basin (Seminario et al., 2005) - and a regional layer of evaporites (see Figure 4), whose age has been recently revised and also considered as Late Permian (Calderón et al., 2017a). This evaporites layer acted as a major detachment in the Huallaga Basin. It is thinning eastward and southward in the Ucayali and Camisea basins, and disappears in the Madre de Dios and Marañón basins (Figure 4). At the top, it ends with marine black shales, limestones and dolomites, known as the Shinai Formation and also dated from the Late Permian in the Camisea Basin (Seminario et al., 2005 and references therein). The black shales of the Shinai Formation contain Type III kerogens and the TOC average value is 2.5% (Calderón et al., 2017b). It is partly eroded by a new erosional unconformity that marked the onset of a long period of rifting and post-rift regional sag (Sempere et al., 2002; Rosas et al., 2007). In the Subandean basins, this period is characterized by the deposition of thick Triassic and Jurassic aeolian and fluvial sandstones and silts that can reach 2,000 m of thickness in the Huallaga and Ucayali basins. This long term sequence, missing in the Madre de Dios Basin, corresponds to the Lower Nia and Sarayaquillo formations (Figures 2, 3 and 4). In the Camisea Basin, the Lower Nia aeolian sandstones constitute one of the best reservoirs of the giant gas field (Seminario et al., 2005; Grosso and Chung Ching, 2010). West of the Huallaga and Ucayali basins, these aeolian sandstones laterally pass to the continental Mitu rift and marine Pucará post-rift deposits outcropping in the Eastern Cordillera (Figure 2), where they overlay directly the basement known as Marañón Complex (Wilson, 1985). This lateral change occurs apparently in the Subandean-Eastern Cordillera transition zone and

corresponds to the eastern Mitu rift border. East of the Marañón Basin, the Triassic and Jurassic sediments pinch out below the Cretaceous deposits.

After a major sedimentary hiatus (110-120 Ma), corresponding probably to the Andean breakup foreland unconformity, late Cretaceous sequences were deposited. They comprise Albian to Maastrichtian fluvial to shallow marine cyclic sequences of sandstones, shales and limestones well defined in northern Peru (Figures 2, 3 and 4; Cushabatay-Raya; Agua Caliente-Chonta; Vivian-Cachiyacu-Huchpayacu). These eastward-thinning sequences were deposited in the Andean-proto-Amazonian retroforeland basin controlled by the tectonic loading of the incipient Andean orogenic wedge. They constitute today the main petroleum systems of the Oriente-Marañón prolific oil province (Marksteiner and Aleman, 1997; Barragan et al., 2008). Reservoir intervals correspond to fluvio-deltaic and tide-dominated estuarine deposits of the Cushabatay, Agua Caliente and Vivian formations, while source rocks are constituted by shales and limestones of the Raya and Chonta formations (Mathalone and Montoya, 1995; Wine et al., 2001, 2002). To the south (Camisea and Madre de Dios basins), the Cretaceous sequences become progressively more continental and it is difficult to differentiate the Cushabatay, Agua Caliente and Chonta formations. Therefore, the Cretaceous sources rocks well developed in the north become progressively sandier towards the south. The Campanian fluvial and tidal sandstones of the Vivian Formation fluvial and tidal sandstones remain good reservoirs in all the Subandean basins.

The Cenozoic foreland infill presents important lateral and longitudinal variations. It has been well described in terms of foreland system depositional environments controlled by thrusts propagation (Roddaz et al., 2010; DeCelles, 2012). The Paleocene-Early Eocene sequence starts with the fluvial and tidal sandstones of the Casa Blanca Formation (Figure 2; Gil, 2001 and references therein), comparable to the Vivian reservoir. It passes gradually to red siltstones and mudstones forming distal fluvial deposits (Yahuarango Formation). The Middle Eocene-Oligocene sequence overlies a regional erosional unconformity, which extends to the north in the Subandean FBS of Ecuador and Colombia. This erosion has been interpreted as an unloading orogenic period (Christophoul et al., 2002; Roddaz et al., 2010). In Northern Peru, the Middle Eocene Pozo Formation (Figures 2 and 4) recorded a shallow marine environment during a new orogenic loading period. It is overlain by the Oligocene silts and sandstones of the Chambira Formation (Figures 2 and 4). This Middle Eocene-Oligocene sequence is missing in the Madre de Dios Basin (Figures 3 and 4), where Miocene sediments overlay directly the Middle Eocene unconformity. The Neogene sequence recorded the

development of the modern Amazonian foreland basin system and a strong subsidence in a fluvio-estuarine environment (Pebas Mega-Wetland System) evolving progressively to an alluvial system (Hoorn et al., 2010; Roddaz et al., 2010; Boonstra et al., 2015). This thick Neogene sequence was responsible for the overburden that triggered hydrocarbon expulsion, migration and charge of the existing structures (Barragan et al., 2008; Calderón et al., 2017b).

According to the reserves and resources published by the Peruvian Energy and Mine Minister in 2014 and 2015, oil reported in the Marañón Basin is reservoired mainly in Cretaceous age rocks. These oils are usually in a range of gravities from 10° to 42° API. The remaining proven reserves are located in Vivian and Chonta sandstones (279.425 million bbl) and the prospective resources are quantified in 5,628 million bbl. The distribution of hydrocarbons in the Ucayali and Camisea basins is different from that of the Marañón Basin, being dominated by gas. The main production is coming from Camisea area, and the remaining proven reserves for the two basins are 720 million bbl (oil and condensate) and 13.7 trillion cubic feet (TCF) being reservoired in Cretaceous, Triassic and Paleozoic clastic rocks. The prospective resources are 1,156 million bbl (oil and condensate) and 14.2 TCF. Oil and gas seeps have been reported in the Madre de Dios fold and thrust belt, where the Candamo-X1 well found in 1998 hydrocarbon accumulation in Cretaceous reservoirs that were estimated in 1 TCF. The prospective resources are 44 million bbl and 8.7 TCF.

METHODOLOGY

Our structural analysis is based on 2D seismic interpretation, calibrated from the deepest wells of the Subandean basins, field data and the stratigraphic revision presented above (Figures 2, 3 and 4). Seismic sections and well data were provided by PERUPETRO S.A. Surface data were obtained from our field surveys and 1:100,000 INGEMMET (Instituto Nacional Geológico, Minero y Metalúrgico del Perú) geologic maps. Although our structural review is based on the interpretation of an exhaustive compilation of seismic data, only the most representative examples of seismic cross-sections have been choose to show the main tectonic Andean and pre-Andean features.

Balanced regional cross-sections have been constructed using the Midland Valley Move software on the basis of the flexural-slip algorithm, assuming constant bed length and thickness and constant area for salt units and Neogene infill. In their initial stage, they were restored at the base of the Pozo Formation, which

sealed a regional erosive planar unconformity (Christophoul et al., 2002), and/or at the base of the Late Cretaceous foreland deposits (basal foreland unconformity).

Sequential restorations have been constrained by thermochronologic ages derived in large part from published works, and stratigraphic records observed and analyzed in seismic sections and outcrops. Final and initial stages are taken from the balanced (final) and restored cross-section (initial). In the Huallaga-Marañón FBS, to constrain the restoration we used the AFT analyses published by Eude et al. (2015) and Calderón et al. (2017b). For the study of the Ucayali FBS, new apatite fission-tracks (AFT) analyses have been achieved and are detailed in this paper. These AFT analyses were conducted by Geotrack International Pty Ltd. and are presented in the Table 1. For each sample AFT analysis in the Ucayali FBS, we used the BinomFit software to statistically deconvolve grain-age distribution, and determine the youngest cooling event (Brandon, 1996; Brandon et al., 1998; Barnes et al., 2006). BinomFit results are shown with the presentation of the structural cross-section. In the Camisea FBS, our restoration is based on the works of Espurt et al. (2011) and Gautheron et al. (2013), and on new observations in the stratigraphic record. In the Madre the Dios Basin, our restoration is constrained by the AFT analyses published by Mora et al. (2011) and Louterbach (2014). All of the AFT analyses used are reported in the geological maps and structural cross-sections.

STRUCTURAL FABRIC AND TIMING OF DEFORMATION

In terms of thrust propagation in Foreland Basin System (DeCelles, 2012), we differentiate from north to south the Huallaga-Marañón, Ucayali, Camisea and Madre de Dios FBSs (Figure 1) to illustrate the lateral evolution of the Peruvian Subandean basins. For each FBS, we present one balanced cross-section (location in Figure 1) restored into two or three stages of deformation thanks to thermochronometric and stratigraphic ages.

Huallaga-Marañón Foreland Basin System

Structural fabric

In the Huallaga Basin (Figure 5), the seismic section *91MPH-23* (Figure 6) shows a perfect illustration of the interference between thick and thin-skinned tectonics in the Huallaga Basin. It shows how the 40 km overthrusting of the Chazuta thrust sheet (Hermoza et al., 2005; Eude et al., 2015) developed on the extensive and thick level of the Late Permian evaporites. This salt level is outcropping along some thrusts of

the Huallaga Basin (Figure 5) and pinched out to the east. Towards the west, it disappears in the Subandean-Eastern Cordillera transition zone, which corresponds to the inverted eastern border of the Triassic Mitu rift, preserved in the Eastern Cordillera (Sempere et al., 2002; Rosas et al., 2007; Perez et al., 2016a). Eastwards, in the Huallaga Basin, there is no evidence of the syn-rift Triassic Mitu infill and of the post-rift Triassic and Lower Jurassic Pucará cover (Calderón et al., 2017a, b). The western part of the Huallaga Basin is characterized by a major faulted detachment fold (Figures 5 and 6; Biabo Anticline) propagated into the thick almost continuous Neogene infill (Miocene and Pliocene). Further east, the Chazuta thrust sheet foot-wall consists of autochthonous Mesozoic and Lower Cenozoic sedimentary series and two Late Permian salt pillows (Figure 6a). It is deformed by an important west-verging basement thrusts system, which prolongs to the east in the Marañón Basin and should not be confused with inversion of previous extensional structures as suggested previously (Hermoza et al., 2005; McGroder et al., 2014). Seismic sections in the Marañón Basin show that this basement thrusts system is sealed by the erosional basal unconformity of the Late Permian Ene sandstones, and then partly reactivated during the Andean orogeny (Calderón et al., 2017a). These west-verging thick-skinned thrust structures belong to a reactivated Middle Permian fold and thrust belt (see Calderón et al., 2017a, and discussion) branched on an intra-basement detachment. The depth of this detachment (Figure 7) is constrained by the location of crustal earthquakes (Delvin et al., 2012). The best expression of this crustal deformation is the Cushabatay High, east of the Chazuta thrust front (Figures 5 and 7). Today, this west verging basement thrust system forms an active mega-duplex below the salt detachment (roof thrust) of the Huallaga Basin (Figure 7). Towards the north, in the Moyabamba Basin (Figure 5), one of these crustal west-verging thrusts is particularly active and responsible of the 1990-91 damaging earthquakes of Moyabamba city (Tavera et al., 2001). In the Marañón Basin, the seismic section BP-19 (Figure 6b) illustrates the recent Andean east-verging thick-skinned tectonics that deformed the entire Neogene cover.

Andean deformation ages

Thermochronometric ages of the deformation, used in the present study of the Huallaga-Marañon FBS, have been published and interpreted as thrust-related uplift by Eude et al. (2015) and Calderón et al. (2017b) (see Figure 7 for location). These ages ranging between 23.2 Ma and 5.8 Ma may suggest a classic in-sequence propagation and exhumation of the thin-skinned thrusts system, whose deformation history is described below in the sequential restoration in accordance with the observed thicknesses of foreland deposits.

Paleogene growth strata in the foot-wall of the Chazuta thrust, evidenced by seismic data and published by Eude et al. (2015), illustrate a previous stage of the Andean deformation and a first reactivation of the west-verging basement thrust structure.

Sequential restoration

The Huallaga-Marañon FBS sequential restoration (Figure 7) has been updated from previous versions (Eude et al., 2015; Calderón et al., 2017b) changing the structural geometry of the Cordillera Oriental-Subandean zone transition and the thick-skinned thrust system. The chronology is based on the deformation ages discussed above. The Andean FBS thrust propagation extends over 430 km and the total horizontal shortening measured is 70 km. It is related to the tectonic inversion of the Triassic Mitu rift that controlled the deformation and propagation of the Eastern Cordillera deformable backstop of the Huallaga wedge-top basin. The initial stage of the restoration (the restored cross-section) corresponds to the middle Eocene configuration during the Pozo Formation deposits, which sealed a regional planar erosional unconformity. This stage records the effect of a previous Andean deformation (Paleocene) in the Huallaga-Marañón FBS, with an estimated horizontal shortening less than 3 km. It shows that weak thrust structures, such as the Biabo Anticline or the west-verging basement horse of the Chazuta thrust foot-wall were partially developed (Figure 7). The second stage illustrates the middle Miocene thrusts system configuration recorded by AFT analysis (Eude et al., 2015; Calderón et al., 2017b). Total horizontal shortening measured for this stage is 25 km. The Triassic Mitu rift was partly inverted, the Eastern Cordillera was emerging and the Biabo Anticline and Chazuta thrust structures were largely developed (Figure 7). This stage shows that in the center of the Huallaga wedge-top depozone, the Cenozoic sedimentary charge has already reached more than 8 km of thickness. Therefore, it appears that between the middle Eocene and the late early Miocene the sedimentation rate has been strong, which is a key factor to understand the periods of petroleum systems generation and expulsion.

Ucayali Foreland Basin System

Structural fabric

As the Huallaga Basin, the Ucayali Basin (Figure 8) presents interactions between thin and thick-skinned tectonics. However, thin-skinned tectonics is much lesser developed due to the poor extension and thickness of the Late Permian salt layer. Figure 9 shows a seismic section where only some thick salt pillows are preserved. Such salt pillows have been also described in the same area (Moretti et al., 2013) and in the

southern Pachitea Basin (Witte et al., 2015). In addition, the same seismic section illuminates a remarkable fossilized duplex involving the Paleozoic series in its western margin (see also Hermoza et al., 2011). This duplex deformed the continental Triassic and Jurassic Lower Nia and Sarayaquillo formations and is eroded and sealed by the Late Cretaceous Cushabatay Formation (Figure 9). It is probably related to the Jurua orogeny described by Caputo (2014). This pre-Andean duplex had undeniably a buttress effect on the eastward propagation of the Andean thin-skinned tectonics as shown by the structural cross-section of Figure 10. Immediately to the west, in the Subandean wedge-top depozone, three imbricates involving the thick Triassic fluvial and aeolian sandstones are outcropping (Figure 8). They probably branch on the thin remnant Late Permian salt detachment. The Eastern Cordillera corresponds to the inverted Triassic rift system and its eastern border is emerging with the Pucará and Mitu deposits in the Tingo Maria area (Figure 10). It constitutes the deformable backstop of the Ucayali Subandean FTB. To the east, in the Ucayali foreland basin, east-verging thick-skinned tectonics predominates and deforms the entire Cenozoic cover. The present-day Subandean thrust front merges far to the east, in Brazil, with the Moa Divisor structures (Figure 8). In Peru, the San Alejandro and Agua Caliente oil fields are located in the northern termination of the Shira Mountain, a major basement uplift of the Peruvian Subandean basins (Espurt et al., 2008; Gautheron et al., 2013).

Andean deformation ages

We present here new apatite fission-track (AFT) dating (Table 1) essential to constrain the timing of exhumation of the main thrust structures. These AFT analyses were done at *Geotrack International Pty Ltd* in 2014. They are presented in the Table 1, and reported in the geological map of Figure 8 and on the cross-sections of Figure 10. Representative grain-age distributions are also shown for each AFT sample in Figure 10. Using the arguments of Espurt et al. (2011) in the neighboring Camisea Basin (see below), “we assume that cooling has been caused by the erosion of sedimentary rocks in response to thrust-related vertical motion”. For samples BOQ011, BOQ012 and TG03, $P[\chi 2\ ] > 5\%$ (see Table 1) and central ages were used to determine the last cooling; BinomFit results show one AFT component corresponding with these central ages (Figure 10). For samples BOQ007, BOQ010, BOQ015, BOQ020 and BOQ025, two AFT components have been identified (Figure 10) and the youngest components were used to determine the last cooling (Brandon et al., 1998). In the Subandean FTB, from west to east, ages range from 14 Ma to 3.3 Ma and may suggest, as in the Huallaga Basin, a classic in-sequence thrusts propagation of the thin-skinned system.

Exhumation age of the frontal imbricate of the Boquerón Padre de Abad is the best constrained. AFT samples have been collected in a 1600 m thick vertical stratigraphic section (Triassic-Jurassic), and AFT ages range from 4.8 to 3.5 Ma. Eastwards, in the Agua Caliente basement thrust structure, we projected the age of the Shira Mountain thrust-related exhumation onset (9+-2 Ma) obtained from the thermal inverse modelling of apatite (U-Th)/He age (Gautheron et al., 2013). Eastwards, late Neogene growth strata observed in the seismic section that cross the Tamaya structure (Figure 11) are consistent with this exhumation age.

Sequential restoration

The balanced cross-section encompasses all the Subandean FBS from Peru to the Acre Basin in Brazil (Figures 8 and 12). It has been constructed from seismic sections and wells in both countries, and structural data collected in our Peruvian field surveys and existing Perupetro S.A databases. The Subandean FBS thrust propagation extends over 395 km, with a total horizontal shortening of 69 km, which can be subdivided into thin-skinned (56 km) and thick-skinned (13 km) deformations (Figure 12). The initial stage of our restoration (full restored cross-section) corresponds to the middle Jurassic stage; it shows the eastern border of the Mitu rift in its original position sealed by the Pucará post rift deposits (Figure 12). The middle Eocene stage shows the importance of the pre-Cretaceous thrust deformation sealed by Andean breakup foreland unconformity at the base of the late Cretaceous Cushabatay Formation (Figures 3 and 12). The fossilized duplex of Paleozoic horses, evidenced by seismic (Figure 10), accommodated the first inversion of the Mitu rift and a minimum horizontal shortening of 16 km. This first inversion can be related to the Jurua Orogeny (Caputo, 2014) and will be discussed later. The middle Eocene stage, restored from subtle Paleogene regional thicknesses variations deduced from subsurface data, shows also the first Andean deformation that is manifested by a weak uplift of the San Alejandro and Agua Caliente thick-skinned structures (2 km of horizontal shortening). The third stage illustrates the late Miocene thrust systems configuration with an increase of thick-skinned thrusts shortening (see Figure 12), taking into account: 1) the exhumation AFT age of the sample TG-03 from the Mitu rift eastern border (14 Ma); 2) the exhumation onset (9+-2 Ma) of the Shira Mountain (Gautheron et al., 2013); and 3) the growth strata of the Tamaya structure (see Figure 11). Mean hinterland Subandean thrusts developed during the late Miocene and the Pliocene as shown by the AFT ages of samples collected in the Boquerón Padre Abad imbricates (see Figure 10). At present-day, deformation is still active and crustal earthquakes occur in the hinterland (Delvin et al.,

2012); they are apparently associated to the basement detachment, but also to more superficial inverted faults (Figure 12).

Camisea Foreland Basin System

Structural fabric

The Camisea Subandean basin (Figure 13) is the most prolific hydrocarbon province of Peru and therefore the most studied (Shaw et al., 1999; Gil et al., 2001; Disalvo et al., 2002; Seminario et al., 2005; Espurt et al., 2011; Gautheron et al., 2013). We used here the work from Espurt et al. (2011) to present the structural fabric of the Camisea FBS that is characterized by a change in shortening direction. The Camisea FBS is located on the E-W oriented Fitzcarrald Arch. Its propagation interfered with the Mio-Pliocene Fitzcarrald Arch uplift (Espurt et al., 2007). The balanced cross-section of Figure 14 shows that the Camisea FBS corresponds to a classic thin-skinned fold and thrust belt deforming the Paleozoic sedimentary wedge that pinches out to the east. The geometry and lithology of this preserved sedimentary wedge have exerted a strong control on the thrust propagation. Seismic data along the balanced cross-section do not reveal any basement thrust (Espurt et al., 2011). A series of four well-formed external thrust anticlines accommodated the shortening of a broad hinterland passive roof duplex modeled by three main horses in Ordovician and Silurian rocks (Figure 14a) (Espurt et al., 2011). Detachment levels are located at the interface between the basement and the Paleozoic sedimentary wedge (sole thrust of the hinterland duplex), at the base of the Devonian series (roof thrust of the hinterland duplex) and at the base of the Paleogene foredeep deposits. The Camisea anticlines are formed above north-verging thrust faults; from south to north, they correspond to the Timpia fault bend fold, the Armihuari and Cashiriari fault propagation folds, and the San Martin triangle zone that dies in the Paleogene infill of the Ucayali foreland (Figure 14a). All of them branched on the roof thrust (base of Devonian) of the hinterland duplex and accommodate part of its shortening (Figure 14a).

Andean deformation ages

Sequential restoration of Espurt et al. (2011) and the synthesis of thermochronometric ages of the central Peruvian Subandes published by Gautheron et al. (2013) give valuable information about the middle Miocene and Pliocene in-sequence Camisea thrusts propagation, that seems to start at ~14 Ma. (U-Th)/He thermochronometric age from a core (Triassic Lower Nia reservoir) of the San Martin well (Gautheron et al., 2013) shows that thrust uplift of the external San Martin triangle zone started at 4+-2 Ma.

With respect to the stratigraphic record, seismic data through the Cashiriari anticline (see, for example, Figure 14b) clearly show the presence of growth strata in the lower part of the Cenozoic infill that correspond, in the Camisea Basin, to the Paleogene Charophytes, Yahuarango Formation (Seminario et al., 2005). The upper part of this Cenozoic infill shows a constant thickness, and sealed the Paleogene Andean deformation before being reactivated by the Mio-Pliocene thrusts propagation.

Other growth strata have been observed and described in the Late Neogene conglomerate of the Shihuayro syncline (Espurt et al., 2011). They apparently recorded the Mio-Pliocene deformation.

Sequential restoration

The sequential restoration published by Espurt et al. (2011) is presented in Figure 15 and is updated by taking into account the Paleogene deformation evidenced in Figure 14b. Current horizontal shortening is 53 km and the extension of the thrusts system in the foreland is much less than in the Ucayali and Huallaga basins. No Triassic tectonic heritage appears in this part of the Subandean foreland basin system, and the Eastern Cordillera deformable backstop is composed of only basement and Lower Paleozoic cover. The initial stage of our restoration shows that in the middle Eocene some thrust anticlines, as the Cashiriari structure, might have already been developed and sealed. In this stage, we consider a minimum shortening of 2 km that is transferred from the incipient deformation of the hinterland duplex to the Cashiriari Anticline (Figure 15). Although the available seismic data did not allow to observe more growth strata in the section, it is not impossible that the entire thrust system has been partly formed in the Paleogene. The second stage corresponds to the middle Miocene period, when thrusts propagation restarted. New shortening of the hinterland duplex (8 km) is this time accommodated by the development of a passive roof back back-thrust (Figure 15). Such changes in the deformation location have been already described through a geometric and experimental study in the northern Subandean zone of Bolivia (Baby et al., 1995), where erosion and sedimentation process control thrusts propagation. In the early Pliocene stage (Figure 15; 45 km of horizontal shortening), vertical stacking of the hinterland passive roof duplex is well developed and the eastward accommodation of shortening is reflected by the propagation of the Timpia and Armihuari thrust anticlines. Between 5 Ma and the present day, the Cashiriari Anticline is weakly reactivated and the eastward thrust propagation is absorbed in the frontal San Martin triangle zone.

Madre de Dios Foreland Basin System

Structural fabric

The style of thrusts propagation presents a drastic change in the Madre de Dios FBS (Figure 16). Previous works on the structural fabric have been published by Gil et al. (2001) and Mora et al. (2011). We present a new balanced structural cross-section constructed from subsurface and field data (Figures 16, 17, 18 and 19), where horizontal shortening (47 km) is concentrated on less than 50 km. The Eastern Cordillera corresponds to a crustal ramp anticline, including 2nd order fold-thrusts. The eastward propagation of this mega basement ramp anticline is accommodated in the Madre de Dios fold and thrust belt by a vertical stacking of the thrust systems. This complex FTB is constituted by a hinterland dipping duplex developed in the Paleogene sedimentary infill, overthrusted by an imbricate system of Cretaceous strata (Figure 17a). Shortening of the duplex is accommodated partly by the Tambopata frontal thrust, which transported the Punquiri piggyback syncline that hosts more than 8 km of Cenozoic sediments (Figure 17a). This considerable sedimentary thickness – the most important of the Peruvian Subandean basins - implies a strong rate of Cenozoic sedimentation, which probably played an important role in the style of the thrust propagation as demonstrated by analogic experiments (Baby et al., 1995; Mugnier et al., 2007).

The foot-wall of the complex Madre de Dios thrust stacking systems is deformed by west-verging basement thrusts evidenced by seismic information (Figure 17b). These deep west-verging structures seem to be sealed by the basal erosional unconformity of the Ene sandstones (see Figure 3) and reactivated during the Andean orogeny. They coincide with the regional Madidi Arch (House et al., 2000; Alemán et al., 2003) that extends from the Bolivian Beni-Madre de Dios foredeep into the Peruvian Madre de Dios FTB (Figure 16).

Andean deformation ages

Apatite fission-track dating (AFT) projected in our balanced cross-section are those published and discussed by Mora et al. (2011) (MD 28, MD 29 and MD 30) and Louterbach (2014) (MD 216). They are located in the map of Figure 16 and the structural cross-section of Figure 17a. Globally, thermometric ages are younger than in the other cross-sections (5.5-2 Ma), and show a rapid exhumation cooling of the Eastern Cordillera deformable backstop and associated Subandean thrusts. These AFT ages recorded probably the more recent part of the orogenic event (Pliocene); they are consistent with the Apatite (U–Th)/He ages published recently by Lease and Ehlers (2013) in the “Eastern Andean Plateau” (Eastern Cordillera of our cross-section) and

Perez et al. (2016b) in the same area of the Subandean zone. Older Subandean deformations are identified through the sedimentary record observed in seismic data and outcrops.

The seismic section of the Figure 17b shows Paleogene growth strata in the Punquiri syncline sealed by an erosional unconformity located at the base of the Miocene deposits, and calibrated from field data and the Pariamanu-1X well. This Miocene erosion surface has been also evidenced by Louterbach et al. (2014) in the Madre de Dios Basin. Therefore, Paleogene growth strata of the Punquiri syncline are probably Paleocene and/or lower Eocene. They progressively sealed the intra-Paleogene duplex.

More to the west, outcrops of the Inambari imbricates show relevant growth strata in the Late Cretaceous Chonta Formation (Figure 18). They probably represent the starting point of the Andean compression in the Madre de Dios FBS.

Sequential restoration

The balanced cross-section (Figure 19) extends from the Eastern Cordillera to the Madre de Dios foredeep, whose geometry is well defined thanks to subsurface data. Total shortening is 47 km, and is concentrated in the western part of the cross-section, where the Eastern Cordillera basement ramp anticline displacement is absorbed into the Cenozoic foreland deposits by the intra-Paleogene duplex and its related Punquiri piggy-back and Tambopata thrust. The Eastern Cordillera basement ramp anticline provoked an important flexural loading on the foreland basin system that explains the strong thickness of Cenozoic sediments in the present wedge-top depozone.

The early Paleocene stage (Figure 19) shows west-verging basement thrusts that we interpret, as in northern Peru (Calderón et al., 2017a), as the reactivation of Middle Permian thrusts. Late Cretaceous growth strata observed in the field (Figure 18) probably recorded this first reactivation. The Madidi Arch was already formed since it is also eroded and sealed by the erosional unconformity of the base of the Ene sandstones (Late Permian). This is consistent with the Permian age proposed by Alemán et al. (2003) that consider this arch as related to the Late Hercynian orogeny (Gondwanide orogeny in our stratigraphic diagrams of Figures 2, 3 and 4).

The early Miocene stage (Figure 19) shows that the intra-Paleogene duplex was partly developed at the front of the Eastern Cordillera basement ramp anticline (14 km of shortening). It has been sealed by the lower Eocene growth strata and then partly eroded below the Miocene basal unconformity (see Figure 17). Upper

Eocene and Oligocene sediments are lacking in the Madre de Dios FBS (Louterbach et al., 2014), which seems to show a long period of no sedimentation or/and a regional uplift prior to the Neogene.

Between early Miocene and present-day, a new period of thrusts propagation occurs (Figure 19), and horizontal shortening increases considerably (33 km). This period of renewed tectonic activity could be correlated with the thermochronologic ages presented in the Figure 17, which suggest a Plio-Pleistocene rapid exhumation cooling of the Eastern Cordillera deformable backstop an associated Subandean thrusts.

DISCUSSION

Lateral structural evolution

Our balanced cross-sections show that total horizontal Subandean shortening in Peru decreases from north (70-69 km) to south (53-47 km) (Figure 20). The northern part (Huallaga-Marañón and Ucayali FBS) is characterized by interference of thick and thin-skinned tectonics, while the southern part (Camisea and Madre de Dios FBS) shows predominantly thin-skinned structures (Figure 20). This lateral evolution of thrusts propagation and shortening has been driven by inherited basement faults and thickness variations of pre-Andean sedimentary cover (see the updated stratigraphic diagram of Figure 4), but also by latitudinal changes in Cenozoic sedimentation rates. The presence of widespread Late Permian evaporites in the Huallaga Basin created an effective detachment level allowing the propagation of large overthrusts, which dies out towards the rapid thinning of the evaporites. Northern Subandean thick-skinned tectonics is seismically active; it is apparently related to the reactivation of a fossilized Middle Permian fold and thrust belt and not to the Triassic rift normal faults. The tectonic inversion of the Triassic Mitu rift occurred more to the west and forms the present-day Eastern Cordillera, which constitutes the deformable backstop of the Subandean fold and thrust belt. In the Huallaga and Ucayali basins, the eastern border of the Mitu rift is outcropping in the transition zone between the Eastern Cordillera and the Subandean FTB. Further south, the Andes are more developed toward the east and the NNE-SSW oriented eastern border of the Mitu rift prolongs in the central part of the mountain chain (Perez et al., 2016a) (see Figure 20), and does not control the eastward thrust propagation of the Eastern Cordillera. In the Ucayali and Camisea basins, the Paleozoic sedimentary wedge is well preserved allowing the development of shale detachments (frequently gas prone source rocks, see Figure 4) and important associated duplexes. Shortening is concentrated in antiformal stacks and accommodated in roof thrusts sequences. In the Madre de Dios Basin, these Paleozoic

detachments appears to be broken by the Madidi Arch and a contemporaneous Middle Permian west-verging fold and thrust belt. Cenozoic foreland infill thickness increases considerably in this part of the Subandean FBS (more than 8 km), where it controlled Subandean thrusts propagation and caused the development of an intra-Paleogene duplex. Such duplex propagation driven by sedimentation have has been already analyzed and modelled in analogic experiments in the neighbouring Bolivian Subandean Beni Basin (Baby et al., 1995; Mugnier et al., 2007).

Pre-Andean orogenies

Two pre-Andean orogenies have been identified in this study. In the Marañón-Huallaga FBS, a west-verging fossilized Middle Permian fold and thrust belt has been partly reactivated during Andean deformation (see also Calderón et al., 2017a). This FTB is part of the Gondwanide orogen described in Argentina by Ramos (1988). It developed along the southern margin of Gondwana, and it is now preserved in South America, South Africa, and Australia (Catuneanu, 2004). This Middle Permian FTB appears also in the foot-wall of the Madre de Dios wedge-top, where it can be assimilated to the Madidi Arch.

A second pre-Andean orogeny has been identified in the Ucayali FBS where an intra-Paleozoic and Mesozoic antiformal stack appears to be eroded and sealed by Late Cretaceous foreland basal unconformity. It is probably related to the Late Jurassic Jurua orogeny described by Caputo (2014) in Brazil in the Acre and Solimoes basins, where this compressive deformation occurs in the form of structural inversions. In the Ucayali FBS, the Eastern Cordillera rift inversion started during the Jurua orogeny and represented a minimum total horizontal shortening of 16 km accommodated in the intra-Paleozoic and Mesozoic antiformal stack (see second stage of Figure 12). Caputo (2014) proposes a Late Jurassic orogenic age associated to the initial opening of the Central Atlantic Ocean. In the Ucayali FBS, the Jurua deformation affects the Sarayaquillo Formation and is sealed by the sandstones of the Cushabatay Formation; therefore a Neocomian age seems more appropriate. In the Oriente Basin of Ecuador, such age of compressive deformation has been also described for the incipient tectonic inversion of the Sacha oil field graben (Baby et al., 2013). In our study of the Huallaga-Marañón and Madre de Dios FBS, it was not possible to identify the Jurua deformation probably hidden by the Andean reactivation.

Timing of deformation

The map of Figure 20 shows the north-south evolution of AFT ages that represent the more recent period of thrusts exhumation. These ages are younger in the south where the exhumation (tectonic uplift) of the Eastern Cordillera is faster and the associated foreland sedimentation far in excess (~ 8 km in the Madre de Dios wedge-top). This phenomenon could be related to the rainfall hotspot observed in the Eastern Cordillera-Subandean foothills transition of the Madre de Dios FBS (Quincemil hot spot; Espinoza et al., 2015), which could constitute a great factor in the erosion for several millions years.

Two older Subandean compressive deformations have been evidenced by growth strata, one in the late Cretaceous (Chonta Formation) and one in the lower Eocene (Yahuarango Formation) stratigraphic records. In Peru, the late Cretaceous compression, known as “Peruvian phase”, has long been described in the western and eastern cordilleras (Mégard, 1984). It is also identified as late Cretaceous inversion in the giant oil fields of the neighbouring Oriente Basin of Ecuador (Canfield et al., 1982; Balkwill et al., 1995; Baby et al., 2013). This long-term compressive deformation of the Andean retro-arc foreland system is probably controlled by the westward shift of the South American Plate initiated by the opening of the Equatorial Atlantic Ocean since Albian times (Pindell and Kennan, 2009). The lower Eocene compressive event corresponds to the major Andean orogenic period defined as the “Incaic phase“ in the Marañón fold and thrust belt of the western Cordillera of central and northern Peru (Mégard, 1984). It is also evidenced in the inverted structures of the Oriente Basin (Christophoul et al., 2002; Baby et al., 2013). It coincided with a change in convergence rate between the Farallon and South American plates (Jaillard and Soler, 1996).

Unexplored petroleum plays

Stratigraphic lateral evolution played a key role in the distribution of décollement levels, source rocks, reservoirs and charges; they are summarized in the Figure 4 and have been already described in the stratigraphic section. The matter of our paper is not to re-evaluate the petroleum systems, but to highlight unexplored petroleum plays thanks to our geometric and chronologic analysis of the Subandean deformation.

In the Huallaga Basin, a large sub-thrust unexplored domain is hidden under the Chazuta thrust. It comprises at least 3 potential sub-traps formed by a combination of salt pillows and thrust related anticlines, which belongs to a west-verging fossilized Middle Permian fold and thrust belts (Gondwanide orogeny, see above) partly reactivated during Andean deformation. Such structural combination is outcropping further east in the

Callanayacu diapir (Figure 5), which is well-known for its oil seeps (Calderón et al., 2017b). The late Cretaceous petroleum system has been amply described in the Huallaga Basin (Mathalone Montoya, 1995; Wine et al., 2001), while the late Permian petroleum system has been recently suggested thanks to a new vision of the stratigraphy (Calderón et al., 2017a, b). 2D petroleum modelling of both petroleum systems shows that hydrocarbon can be present since the early Miocene in the sub-thrust domain of the Huallaga Basin (Calderón et al., 2017b). Late Permian, Triassic and Cretaceous sand reservoirs could be also fed by hypothetic remnants of the classic Paleozoic Cabanillas and Ambo source rocks (Mathalone and Montaya, 1995; Jacques, 2004).

The Ucayali FBS is characterized by the preservation of the Jurua deformation in the Pachitea Sub-Basin as the intra-Paleozoic duplex illustrated by Figures 9 and 10. Such structures constitute a new unexplored play, and could have also a real petroleum potential when they are not deeply-buried. They host probably the Late Permian sandstones reservoirs (Ene-Noi) and Devonian and Carboniferous source rocks (Cabanillas-Ambo) of the neighbouring Camisea prolific gas basin. Petroleum modelling is needed to confirm generation and accumulation of hydrocarbons in these pre-Cretaceous compressive traps. Their extension are poorly known and must be investigated from new seismic acquisition.

The Camisea Basin is the most investigated of the Peruvian Subandean fold and thrust belt, but hinterland structures as the Timpia fault bend fold has been poorly explored and merits probably more attention. 2D petroleum modelling (Vela et al., 2016) shows that the Timpia Anticline has the best position with respect to the pod of active Paleozoic sources rocks. More seismic data are needed to define possible structural closures of the thrust-fold.

The poor explored Madre de Dios FBS presents a complex thrust system characterized by an intra-Paleogene duplex that increases exploration risks, as shown by the last exploratory well Dahuene-X1. The hanging-wall and foot-wall of this duplex are formed by imbricates involving the Devonian-Carboniferous sources rocks (Cabanillas-Ambo) and the late Cretaceous (Vivian) and probably late Permian (Ene-Noi) sand reservoirs. These imbricates form an important play that presents a clear potential already proved by the only successful exploratory well, the Candamo X-1, which found a gas accumulation estimated in more than 1 TCF.

CONCLUSIONS

1. The geometric and kinematic analyses realized in this work from seismic and surface data shows the complex lateral evolution of the Subandean foreland basin system of Peru. Total horizontal Subandean shortening decreases from the Huallaga-Marañón FBS (70 km) to the Madre de Dios FBS (47 km). The northern part is characterized by the interference of thick and thin-skinned tectonics inherited from middle Permian thrust structures and a widespread Late Permian evaporites level. The southern part shows predominantly thin-skinned structures controlled by a preserved Paleozoic sedimentary wedge.

2. Two pre-Andean orogeny have been identified. In the Marañón-Huallaga FBS, a west-verging fossilized Middle Permian fold and thrust belts has been partly reactivated during Andean deformation and is still seismically active. It is related to the Gondwanide orogeny that we also identified in the Madre de Dios FBS (Madidi Arch). In the Ucayali FBS, Neocomian horizontal shortening has been evidenced in an intra-Paleozoic duplex sealed by the Cushabatay sandstones. It is related to the Jurua orogeny defined in the neighbouring Brasilian Acre and Solimoes basins.

3. Thermochronologic ages (AFT) recorded the most recent periods of Subandean thrust exhumation from 23.2 Ma to 5.5 Ma. These ages are younger in the Madre de Dios FBS, where they could be related to an intense strong erosion due to the presence of a rainfall hotspot for several millions years.

4. Two older Subandean compressive deformation events have been evidenced in the stratigraphic record, and therefore led us confirm three Subandean stages of thrust propagation (Late Cretaceous, lower Eocene and Mio-Pliocene; see Figure 4), crucial to define the preservation time of some petroleum plays.

5. Our synthesis confirms the structural traps attractiveness of the Peruvian Subandean FBS. In the Huallaga Basin, the Chazuta overthrust preserves an unexplored large sub-thrust domain with Gondwanidian structures, Permian and Cretaceous petroleum systems, and salt cover. The Ucayali FBS contains pre-Cretaceous thin-skinned thrust structures developed in the preserved Paleozoic series that contains the prolongation of the Camisea petroleum system. The poor

explored and complex Madre de Dios fold and thrust belt includes imbricates, involving Paleozoic and Cretaceous petroleum systems, that show a clear potential proved by the Candamo gas field discovery. Exploration risks of this play is high due to the presence of an intra-Paleogene duplex that interfere with the Paleozoic-Cretaceous imbricates.

ACKNOWLEDGMENTS

This research project was conducted thanks to the IRD-PERUPETRO S.A. research agreement and the Institut Carnot ISIFoR. It received financial support from TOTAL and REPSOL for field surveys and laboratory analysis. Midland Valley is acknowledged for providing academic license of “Move” for structural modeling. We thank Pedro Kress, Gonzalo Zamora, Victor Ramos and an anonymous reviewer for their interesting comments that helped to improve the paper.

REFERENCES

Alemán, A. M., D. Valasek, C. Ardiles, G. D. Wood, G. P. Wahlman, and J. R. Groves, 2003, Petroleum systems and tectono-stratigraphic evolution of the Madre de Dios Basin and its associated thrustbelt in Peru and Bolivia, in 8th Simposio Bolivariano - exploración petrolera en las cuencas subandinas: p. 177–200.

Baby, P., B. Colletta, and D. Zubieta, 1995, Etude géométrique et expérimentale d’un bassin transporté: exemple du synclinorium de l’Alto Beni (Andes centrales): Bulletin de la Société Géologique de France, v. 166, no. 6200107, jv, p. 797–811.

Baby, P., M. Rivadeneira, R. Barragán, and F. Christophoul, 2013, Thick-skinned tectonics in the Oriente foreland basin of Ecuador: Geological Society, London, Special Publications, v. 377, no. 1, p. 59–76, doi:10.1144/sp377.1.

Balkwill, H., G. Rodriguez, F. Paredes, and J. Almeida, 1995, Northern part of Oriente Basin, Ecuador: reflection seismic expression of structures: In: Tankard, A. J., R. Suarez, S. and H. J. Welsink, eds., Petroleum Basins of South America. American Association of Petroleum Geologists, Memoir, 62, 559–571.

Barnes, J. B., T. A. Ehlers, N. McQuarrie, P. B. O’Sullivan, and J. D Pelletier, 2006, Eocene to Recent variations in erosion across the central Andean fold-thrust belt, northern Bolivia: Implications for plateau evolution: Earth and Planetary Science Letters, v. 248, p. 118–133, doi: 10.1016/j.epsl.2006.05.018.

Barragan, R., P. Baby, W. Hermoza, and L. Navarro, 2008, The origin of the Maranon-Oriente basin cretaceous oils: the Santiago-Situche kitchens, a new alternative model: VI INGEPET (EXPR-3-RB-24).

Baudino, R., and W. Hermoza, 2014, Subduction consequences along the Andean margin: Thermal and topographic signature of an ancient ridge subduction in the Marañon Basin of Peru: Geologica Acta, v. 12, no. 4, p. 287–306, doi:10.1344/GeologicaActa2014.12.4.2.

Boonstra, M., M. I. F. Ramos, E. I. Lammertsma, P. O. Antoine, and C. Hoorn, 2015, Marine connections of Amazonia: Evidence from foraminifera and dinoflagellate cysts (early to middle Miocene, Colombia/Peru): Palaeogeography, Palaeoclimatology, Palaeoecology, v. 417, p. 176–194, doi:10.1016/j.palaeo.2014.10.032.

Brandon, M. T., 1996, Probability density plot for fission-track grain-age samples: Radiation Measurements, v. 26(5), p. 663-676, doi: 10.1016/S1350-4487(97)82880-6.

Brandon, M. T., M. K. Roden-Tice, and J. I. Garver, 1998, Late Cenozoic exhumation of the Cascadia accretionary wedge in the Olympic Mountains, northwest Washington State: Bulletin of the Geological Society of America, 110(8), 985-1009, doi: 10.1130/0016-7606(1998)110<0985:LCEOTC>2.3.CO;2.

Bump, A., Kennan, L., and Fallon, J., 2008, Structural history of the Andean foreland, Peru, and its relation to subduction zone dynamics, in Ameri- can Association of Petroleum Geologists Annual Convention and Exhibi- tion: San Antonio, Texas, American Association of Petroleum Geologists, search and discovery article 30062.

Calderón, Y., P. Baby, C. Hurtado, and S. Brusset, 2017a, Thrust tectonics in the Andean retro-foreland basin of northern : Permian inheritances and petroleum implications: Marine and Petroleum Geology v. 82, p. 238–250, doi:10.1016/j.marpetgeo.2017.02.009.

Calderón Y., P. Baby, Y. Vela, C. Hurtado, A. Eude, M. Roddaz, S. Brusset, G. Calvès and R. Bolaños, 2017b, Petroleum systems restoration of the Huallaga-Marañon Andean retroforeland basin, Peru: In Mahdi A. AbuAli, Isabelle Moretti, and Hege M. Nordgård Bolås, eds., Petroleum Systems Analysis: American Association of Petroleum Geologists Memoir 114, p. 91–112.

Canfield, R. W., G. Bonilla, and R. K. Robbins, 1982, Sacha oilfield of Ecuadorian Oriente: American Association of Petroleum Geologists Bulletin, 66, 1076–1090.

Caputo, M. V., 2014, Juruá Orogeny: Brazil and Andean Countries: Brazilian Journal of Geology, v. 44, no. 2, p. 181–190, doi:10.5327/Z2317-4889201400020001.

Catuneanu, O., 2004, Retroarc foreland systems—evolution through time. Journal of African Earth Sciences, 38, 225–242.

Chew, D. M., U. Schaltegger, J. Košler, M. J. Whitehouse, M. Gutjahr, R. A. Spikings, and A. Miškovi´, 2007, U-Pb geochronologic evidence for the evolution of the Gondwanan margin of the north-central Andes: Bulletin of the Geological Society of America, v. 119, no. 5–6, p. 697–711, doi:10.1130/B26080.1.

Christophoul, F., P. Baby, and C. Davila, 2002, Stratigraphic responses to a major tectonic event in a foreland basin: the Ecuadorian Oriente Basin from Eocene to Oligocene times: Tectonophysics, 345(1-4), 281-298.

Dalmayrac, B., G. Laubacher, and R. Marocco, 1988, Caracteres Generales de la Evolución Geológica de los Andes Peruanos: INSTITUTO GEOLOGICO MINERO Y METALURGICO, Bol. 12., Serie D. Estudios Especiales, 313 p.

DeCelles, P. G., 2012, Foreland Basin Systems Revisited: Variations in Response to Tectonic Settings, in Tectonics of Sedimentary Basins: Recent Advances: p. 405–426, doi:10.1002/9781444347166.ch20.

Devlin, S., B. L. Isacks, M. E. Pritchard, W. D. Barnhart, and R. B. Lohman, 2012, Depths and focal mechanisms of crustal earthquakes in the central Andes determined from teleseismic waveform analysis and InSAR: Tectonics, v. 31, no. 2, p. 1–33, doi:10.1029/2011TC002914.

Disalvo A., M. Arteaga, and J. Chung Ching, 2002, Geometría de las trampas y análisis estructural en el área de Camisea y sus alrededores. Cuenca de Ucayali. Oriente de Perú: INGEPET (EXPR-3-AD-34).

Espinoza, J. C., S. Chavez, J. Ronchail, C. Junquas, K. Takahashi, and W. Lavado, 2015, Rainfall hotspots over the southern tropical Andes: Spatial distribution, rainfall intensity, and relations with large-scale atmospheric circulation: Water Resources Research, v. 51, no. 5, p. 3459–3475, doi:10.1002/2014WR016273.

Espurt, N., P. Baby, S. Brusset, M. Roddaz, W. Hermoza, V. Regard, P.-O. Antoine, R. Salas-Gismondi, and R. Bolaños, 2007, How does the Nazca Ridge subduction influence the modern Amazonian foreland basin? Geology, v. 35, no. 6, doi:10.1130/G23237A.1.

Espurt, N., S. Brusset, P. Baby, W. Hermoza, R. Bolaños, D. Uyen, and J. Déramond, 2008, Paleozoic structural controls on shortening transfer in the Subandean foreland thrust sytem, Ene and southern Ucayali basins, Peru: Tectonics, v. 27, no. 3, doi:10.1029/2007TC002238.

Espurt, N., J. Barbarand, M. Roddaz, S. Brusset, P. Baby, M. Saillard, and W. Hermoza, 2011, A scenario for late Neogene Andean shortening transfer in the Camisea Subandean zone (Peru, 12°S): Implications for growth of the northern Andean Plateau: Bulletin of the Geological Society of America, v. 123, no. 9–10, doi:10.1130/B30165.1.

Eude, A., M. Roddaz, S. Brichau, S. Brusset, Y. Calderón, P. Baby, and J.-C. Soula, 2015, Controls on timing of exhumation and deformation in the northern Peruvian eastern Andean wedge as inferred from low-temperature thermochronology and balanced cross section: Tectonics, v. 34, no. 4, doi:10.1002/2014TC003641.

Gautheron, C., N. Espurt, J. Barbarand, M. Roddaz, P. Baby, S. Brusset, L. Tassan-Got, and E. Douville, 2013, Direct dating of thick- and thin-skin thrusts in the Peruvian Subandean zone through apatite (U-Th)/He and fission track thermochronometry: Basin Research, v. 25, no. 4, doi:10.1111/bre.12012.

Gil, W., 2001, Evolution latérale de la déformation d'un front orogénique: exemple des bassins subandins entre entre 0° y 16°S, PhD. Thesis, Université Toulouse III, 137 pp.

Gil Rodríguez, W., P. Baby, and J.-F. Ballard, 2001, Structure and palaeogeographic control of the Peruvian Subandean zone: Comptes Rendus de l'Académie de Sciences - Serie IIa: Sciences de la Terre et des Planetes, v. 333, no. 11, doi:10.1016/S1251-8050(01)01693-7.

Grosso S.A. and J. F. Chung Ching, 2010, Caracterización estratigráfica de los depósitos eólicos pérmicos en los yacimientos delos bloques 56 y 88, Camisea, Cuenca Ucayali sur, Perú. XV Congreso Geologico del Perú, Cusco, Perú.

Haeberlin, Y., R. Moritz, L. Fontbote, and M. Cosca, 2004, Carboniferous orogenic gold deposits at Pataz, Eastern Andean Cordillera, Peru:Geological and structural framework, paragenesis, alteration, and Ar-40/Ar-39 geochronology: Economic Geology, v. 99, 73–112, doi:10.2113/gsecongeo.99.1.73.

Hermoza, W., S. Brusset, P. Baby, W. Gil, M. Roddaz, N. Guerrero, and M. Bolaños, 2005, The Huallaga foreland basin evolution: Thrust propagation in a deltaic environment, northern Peruvian Andes: Journal of South American Earth Sciences, v. 19, no. 1 SPEC. ISS., doi:10.1016/j.jsames.2004.06.005.

Hermoza, W., G. Zamora, C. Macellari, and R. Tocco, 2011, Paleozoic deformation and its hydrocarbon potential in the Northern Andean Foreland Basin: VII INGEPET (EXPR-3-WH-10-E).

Hoorn, C., F. P. Wesselingh, H. Ter Steege, M. A. Bermudez, A. Mora, J. Sevink, I. Sanmartín, A. Sanchez-Meseguer, C. L. Anderson, J. P. Figueiredo, C. Jaramillo, D. Riff, F. R. Negri, H. Hooghiemstra, J. Lundberg, T. Stadler, T. Sarkinen, and A. Antonelli, 2010, Amazonia through time: Andean uplift, climate change, landscape evolution, and biodiversity: Science, v. 330, no. 6006, p. 927–931, doi:10.1126/science.1194585.

House, N. J., D. G. Carpenter, P. S. Cunningham, and M. Berumen, 2000, Influence of Paleozoic Arches on Structural Style and Stratigraphy in the Madre de Dios Basin in Southern Peru and Northern Bolivia: SEG Technical Program Expanded Abstracts 2000, v. 19, no. 1, p. 672–676, doi:10.1190/1.1816156.

Hurford, A.J., and P.F. Green, 1982, A user's guide to fission track dating calibration: Earth and Planetary Science Letters, v. 59, p. 343–354, doi: 10.1016/0012-821X(82)90136-4.

Jacques, J. M., 2004, The influence of intraplate structural accommodation zones on delineating petroleum provinces of the Sub-Andean foreland basins. Petroleum Geoscience, 10(1), 1–19. http://doi.org/10.1144/1354-079303-582

Jaillard, E. And P. Soler, 1996, Cretaceous to early Paleogene tectonic evolution of the northern Central Andes (0–18 S) and its relations to geodynamics: Tectonophysics, 259, 41–53.

Jaillard, E., G. Hérail, T. Monfret, E. Díaz-Martínez, P. Baby, A. Lavenu, and J. F. Dumont, 2000, Tectonic Evolution of the Andes of Ecuador, , Bolivia and Northernmost Chile. in: U.G. Cordani, E.J.

Milani, A. Thomaz Filha and D.A. Campos, Tectonic Evolution of South America. 31st International Geological Congress, Rio de Janerio, pp. 481-559.

Kummel, B., 1950, Stratigraphic studies in Northern Peru: American Journal of Science, 248, 249–263, doi:10.2475/ajs.248.4.249.

Laubacher, G. and F. Mégard, 1985. The Hercynian basement : a review: In Pitcher, W.S., Atherton M; P., Cobbing E. J. and Beckinsale R. D. (eds): Magmatism at a Plate Edge, The Peruvian Andes, Halsted Press, 29–35.

Lease, R. O., and T. A. Ehlers, 2013, Incision into the eastern Andean Plateau during Pliocene cooling: Science (New York, N.Y.), v. 341, no. August, p. 774–6, doi:10.1126/science.1239132.

Louterbach, M. et al., 2014, Evidences for a Paleocene marine incursion in southern Amazonia (Madre de Dios Sub-Andean Zone, Peru): Palaeogeography, Palaeoclimatology, Palaeoecology, v. 414, p. 451–471, doi:10.1016/j.palaeo.2014.09.027.

Louterbach, M., 2014, Propagation du front orogénique Subandin et réponse sédimentaire associée dans le bassin d'avant-pays Amazonien (Madre de Dios, Pérou), PhD. Thesis, Université Toulouse III, 261 pp., http://thesesups.ups-tlse.fr/2530/

Marksteiner, R., and A. Alemán, 1997, Petroleum systems along the fold belt associated to the Marañon-Oriente-Putumayo (MOP) Foreland Basin. VI Simposio Bolivariano 'Exploración Petrolera en las Cuencas Subandinas', Memorias, Tomo II, 63– 74.

Mathalone, J. M. P., and Montoya R., M., 1995, Petroleum geology of the sub-Andean basins of Peru, in A. J. Tankard, R. Suárez S., and H. J. Welsink, Petroleum basins of South America: American Association of Petroleum Geologists Memoir 62, p. 423–444.

McGroder, M. F., R. O. Lease, and D. M. Pearson, 2015, Along-strike variation in structural styles and hydrocarbon occurrences, Subandean fold-and-thrust belt and inner foreland, Colombia to Argentina: Geological Society of America Memoirs , v. 212, p. 79–113, doi:10.1130/2015.1212(05).

Mégard, F., 1978, Etude Géologique du Pérou Central: Contribution à l'Etude Géologique des Andes: N°1, Mém. ORSTOM 86, p. 301, Office de la Recherche Scientifique et Technique Outre-mer, Paris.

Mégard, F., 1984, The Andean orogenic period and its major structures in central and northern Peru: Journal of the Geological Society of London, v. 141, no. 5, p. 893–900, doi:10.1144/gsjgs.141.5.0893.

Mora, A., P. Baby, M. Roddaz, M. Parra, S. Brusset, W. Hermoza, and N. Espurt, 2011, Tectonic History of the Andes and Sub-Andean Zones: Implications for the Development of the Amazon Drainage Basin: doi:10.1002/9781444306408.ch4.

Moretti, I., J. P. Callot, M. Principaud and D. Pillot, 2013, Salt pillows and localization of early structures: case study in the Ucayali Basin (Peru): In: Nemčok M., Mora A., Cosgrove J. W. eds., Thick-Skin-Dominated Orogens: From Initial Inversion to Full Accretion, Geological Society, London, Special Publications, 377, doi10.1144/SP377.8.

Mugnier, J. L., P. Baby, B. Colletta, P. Vinour, P. Bale, and P. Leturmy, 1997, Thrust geometry controlled by erosion and sedimentation: a view from analogue models: Geology, v. 25, no. 5.

Newell, N. D., J. Chronic, and T. G. Roberts, 1953, Upper Paleozoic of Peru: Geological Society of America Memoir, 58, pp. 1–315, Washington, D. C., doi:10.1130/MEM58-p1.

Perez, N. D., B. K. Horton, and V. Carlotto, 2016a, Structural inheritance and selective reactivation in the central Andes: Cenozoic deformation guided by pre-Andean structures in southern Peru: Tectonophysics, v. 671, no. February, p. 264–280, doi:10.1016/j.tecto.2015.12.031.

Perez, N. D., B. K. Horton, N. Mcquarrie, K. Stübner, And T. A. Ehlers, 2016b, Andean shortening, inversion and exhumation associated with thin- and thick-skinned deformation in southern Peru: Geological Magazine, v. 153, p. 1–29, doi:10.1017/S0016756816000121.

Pindell, J. L. and L. Kennan, L., 2009, Tectonic evolution of the Gulf of Mexico, Caribbean and northern South America in the mantle reference frame: an update: In: James, K., Lorente, M. A. & Pindell, J. (eds) The geology and evolution of the region between North and South America. Geological Society, London, Special Publications, 328, 1–55.

Ramos, V.A., 1988, The tectonics of the Central Andes: 30° to 33°S latitude, in Clark, S., and Burchfiel, D., eds., Processes in Continental Lithospheric Deformation: Geological Society of America Special Paper 218, p. 31–54.

Roddaz, M., P. Baby, S. Brusset, W. Hermoza, and J. M. Darrozes, 2005, Forebulge dynamics and environmental control in Western Amazonia: The case study of the Arch of Iquitos (Peru): Tectonophysics, v. 399, no. 1–4 SPEC. ISS., doi:10.1016/j.tecto.2004.12.017.

Roddaz, M., W. Hermoza, A. Mora, P. Baby, M. Parra, F. Christophoul, S. Brusset, and N. Espurt, 2010, Cenozoic Sedimentary Evolution of the Amazonian Foreland Basin System, in Amazonia: Landscape and Species Evolution: A look into the past: p. 61–88, doi:10.1002/9781444306408.ch5.

Rosas, S., L. Fontboté, and A. Tankard, 2007, Tectonic evolution and paleogeography of the Mesozoic Pucará Basin, central Peru: Journal of South American Earth Sciences, v. 24, no. 1, p. 1–24, doi:10.1016/j.jsames.2007.03.002.

Seminario F., J. Luques, and S. Blanco, 2005, Las rocas reservorio productivas del Gran Camisea, cuenca Ucayali, Perú: V INGEPET (EXPL-1-FS-208).

Sempere, T., G. Carlier, P. Soler, M. Fornari, V. Carlotto, J. Jacay, O. Arispe, D. Néraudeau, J. Cárdenas, S. Rosas, N. Jímenez, 2002, Late Permian-Middle Jurassic lithospheric thinning in Peru and Bolivia, and its bearing on Andean-age tectonics: Tectonophysics, v. 345, no. 1–4, p. 153–181, doi:10.1016/S0040-1951(01)00211-6.

Shaw, J. H., F. Bilotti, and P. A. Brennan, 1999, Patterns of imbricate thrusting: Bulletin of the Geological Society of America, v. 111, no. 8, p. 1140–1154, doi:10.1130/0016-7606(1999)111<1140:POIT>2.3.CO;2.

Tavera, H., E. Buforn, I. Bernal, and Y. Antayhua, 2001. Analysis of the rupture processes of 1990 and 1991 Alto Mayo Valley earthquakes (Moyobamba, Peru). Boletín de la Sociedad Geológica de Perú, 91, 55–68 (in Spanish).

Vela Y., P. Baby, Y. Calderón, N. Espurt, and S. Brusset, 2016, Modelización Petrolera 2D de una sección balanceada del Campo de Gas de Camisea: XVIII Congreso Peruano de Geología.

Wilson, J. J., 1985. Geología de los cuadrangulos de Jayanca, Incahuasi, Cutervo, Chiclayo, Chongoyape, Chota, Celendin, Pacasmayo, Chepen: Bol. Inst. Geol. Miner. Metal., Ser. A: Carta Geológica National, 38 INGEMMET, Lima, 104 pp.

Wine, G., J. Arcuri, E. Martínez J. Fernández, I. Calderón, C. Galdos, 2001, Huallaga Basin, Technical Report. The hydrocarbon potential of NE Perú Huallaga, Santiago and Marañon Basins Study: Proyecto de Asistencia para La Reglamentación del Sector Energético del Perú (PARSEP), Perupetro Final report, 74 pp, Lima.

Wine, G., J. Arcuri, E. Martínez J. Fernández, I. Calderón, C. Galdos, 2002, Marañón Basin Technical Report. The hydrocarbon potential of NE Perú Huallaga, Santiago and Marañon Basins Study: Proyecto de Asistencia para La Reglamentación del Sector Energético del Perú (PARSEP), Perupetro, 168 pp, Lima.

Witte, J., J. Rebaza, D. Westlund, M. Stratton, and C. Alegria, 2015, A new structural model of the Pachitea Basin, Peru: Interaction of thick-skinned tectonics and salt detached thrusting: Journal of South American Earth Sciences, v. 63, p. 400–416, doi:10.1016/j.jsames.2015.04.008.

FIGURE CAPTIONS

Figure 1: Central Andes, and Peruvian Subandean basins with location of the studied balanced cross-sections.

Figure 2: Stratigraphic diagram and petroleum systems along the Huallaga-Southern Marañon foreland basin system. The pre-Andean orogenic cycles names are those that are more commonly used in the Andes (see Ramos, 1988; Caputo, 2014; Chew et al., 2016).

Figure 3: Stratigraphic diagram and petroleum systems along the Madre de Dios foreland basin system. The pre-Andean orogenic cycles names are those that are more commonly used in the Andes (see Ramos, 1988; Caputo, 2014; Chew et al., 2016).

Figure 4: North-South evolution of the stratigraphic and petroleum systems along the Peruvian Subandean foreland basin system. The pre-Andean orogenic cycles names are those that are more commonly used in the Andes (see Ramos, 1988; Caputo, 2014; Chew et al., 2016).

Figure 5: Simplified geologic map of the Huallaga-Marañón foreland basin system with location of the balanced cross-section. Seismic sections and wells used for the construction of the balanced cross-section are also located.

Figure 6: Interpreted seismic sections crossing the Huallaga and Marañón wedge-top basins (location on Figure 5). These sections have been used for the balanced cross-section construction. Dashed lines highlight growth-strata.

Figure 7: Sequential restoration of the Huallaga-Marañón balanced cross-section (location on Figure 5). Ages of AFT samples HUA330, HUA338 and TG30 have been published by Calderón et al. (2017b) and TG30 by Eude et al. (2015).

Figure 8: Simplified geologic map of the Ucayali foreland basin system with location of the balanced cross-section. Seismic sections and wells used for the construction of the balanced cross-section are also located.

Figure 9: Seismic sections PP10707-12 and G35-604E through the Pachitea sub-basin (location on Figures 8 and 10) showing the structural architecture of the western Ucayali FBS.

Figure 10: Balanced cross-section through the western Ucayali FBS (location on Figure 8). The dashed rectangle shows the location of the seismic section of Figure 9. AFT samples and ages used for the

sequential restoration are located. Representative grain-age distributions are shown for each AFT sample. BinomFit results show grain- age histogram (bars), probability density function fit to grain-age distribution (gray dashed line), and binomially best-fit component (thick black lines labeled , with ages). For samples BOQ007, BOQ010, BOQ015, BOQ020 and BOQ025, two AFT components have been identified. Gray rectangle corresponds to young population used to determine the last cooling event (Brando et al., 1998). For samples BOQ011, BOQ012 and TG03, the P[$\chi 2$] > 5% and BinomFit results show one AFT component that corresponds with central age. In the eastern Agua Caliente structure, we project the exhumation age obtained for the Shira Mountain by Gautheron et al. (2013).

Figure 11: Seismic sections W74-27 and G97W84-7 (location on figures 8 and 12) showing the structural architecture of the eastern Ucayali FBS, and Neogene growth strata.

Figure 12: Sequential restoration of the Ucayali balanced cross-section (location on Figure 8).

Figure 13: Simplified geologic map of the Camisea foreland basin system with location of the balanced cross-section. Seismic sections and wells used for the construction of the balanced cross-section are also located.

Figure 14: Structural architecture of the Camisea FBS. A: balanced cross-section (modified from Espurt et al. (2011) (location on Figure 13). B: seismic section crossing the Cashiriari structure (location on Figure 13). AFT and AHe ages from Espurt et al. (2011) and Gautheron et al. (2013) are located.

Figure 15: Sequential restoration of the Camisea balanced cross-section modified from Espurt et al. (2011) (location on Figure 13).

Figure 16: Simplified geologic map of the Madre de Dios foreland basin system with location of the balanced cross-section. Seismic sections used for the construction of the balanced cross-section and exploration wells of the Madre de Dios FBS are also located.

Figure 17: Structural architecture of the western Madre de Dios FBS. A: balanced cross-section (location on Figure 16). AFT ages used for the sequential restoration (Figure 19) are located. They have been published and interpreted as thrust related by Mora et al. (2011) and Louterbach (2014). B: seismic section 97-MCT-109 through the Inambari imbricates and Punquiri piggy-back syncline (location on Figure 16).

Figure 18: Photo of growth strata in the clastic deposits (fluvial and tidal) of the Late Cretaceous Chonta Formation in the Inambari imbricates (Madre de Dios, see Figure 17) (coord: X= -70.606705°, Y= -13.182472°).

Figure 19: Sequential restoration of the Madre de Dios balanced cross-section (location on Figure 16).

Figure 20: North-South evolution of total shortening and timing of Andean deformation (AFT ages) from the studied balanced cross-sections.

TABLE CAPTION

Table 1: Apatite fission-tracks (AFT) data in the Ucayali FBS. Analyses were done at Geotrack International Pty Ltd.

Note: Abbreviations are as follows; ρs—density (cm–2) of spontaneous tracks; Ns—number of spontaneous tracks counted; Ni—number of induced tracks counted; ρi—density (cm–2) of induced tracks; ρd—density (cm–2) of tracks on the neutron fluence monitor (CN-5 glass); Nd—number of tracks counted in the dosimeter; P(X2)—probability (%) of greater chi-squared (Galbraith, 1981; Green, 1981); central ages, reported for each sample with confidence interval (CI) of one sigma (±1б), were calculated using the zeta calibration method (Hurford and Green, 1982) with zeta of 392.9 ± 7.4; Ng—number of grains counted; Young population (YP) and old population (OP) were determined with the BinomFit software (Brandon, 1996; Brandon et al., 1998); the estimated 68% confidence interval (CI), which is approximately equal to ±1, was calculated using precise algorithms (for details, see Brandon, 1996; Brandon et al., 1998). For this case we do not use Dpar, the kinetics be controlled properly using the apatite chlorine content (Cl wt%).

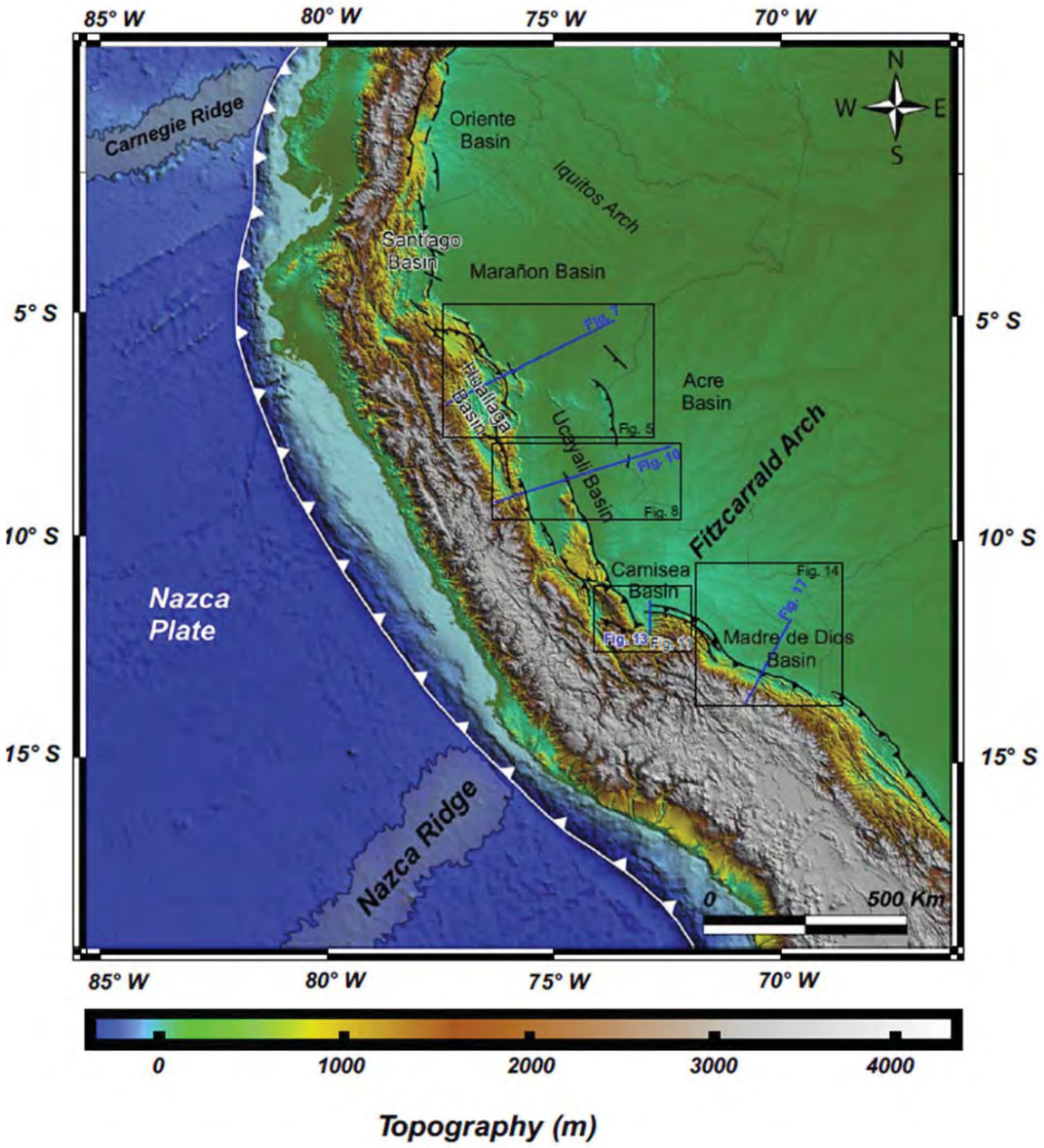
85° W
80° W
75° W
70° W
5° S
10° S
15° S
N
W
E
S
Carnegie Ridge
Oriente Basin
Iquitos Arch
Santiago Basin
Marañon Basin
Fig. 7
Huallaga Basin
Acre Basin
Fig. 5
Ucayali Basin
Fig. 10
Fig. 8
Fitzcarrald Arch
Camisea Basin
Fig. 14
Fig. 12
Fig. 13
Fig. 11
Madre de Dios Basin
Nazca Plate
Nazca Ridge
0
500 Km
0
1000
2000
3000
4000
Topography (m)

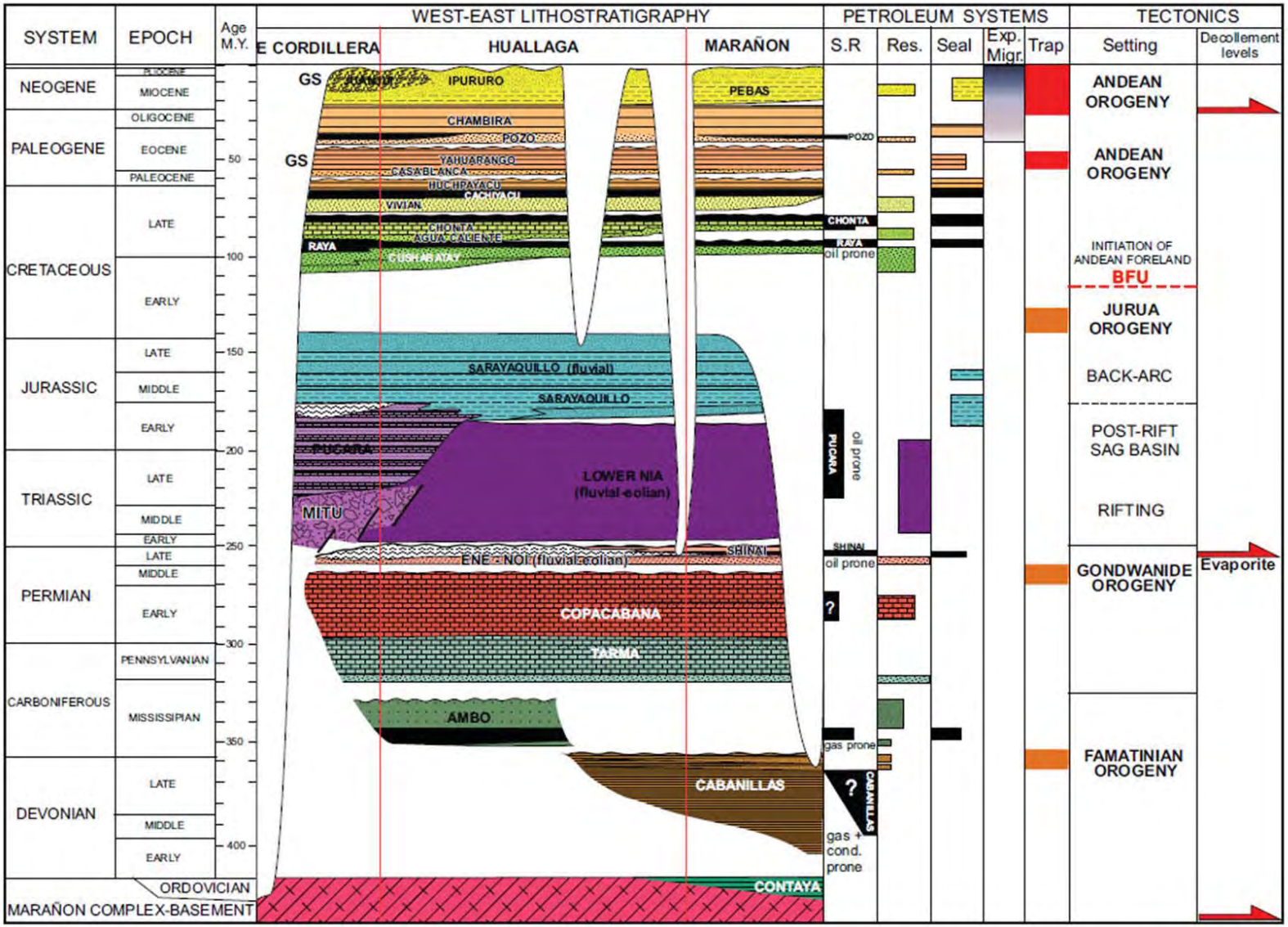
SYSTEM
EPOCH
Age M.Y.
WEST-EAST LITHOSTRATIGRAPHY
E CORDILLERA
HUALLAGA
MARAÑON
PETROLEUM SYSTEMS
S.R
Res.
Seal
Exp. Migr.
Trap
TECTONICS
Setting
Decollement levels
NEOGENE
MIOCENE
PALEOGENE
OLIGOCENE
EOCENE
PALEOCENE
CRETACEOUS
LATE
EARLY
JURASSIC
LATE
MIDDLE
EARLY
TRIASSIC
LATE
MIDDLE
EARLY
PERMIAN
LATE
MIDDLE
EARLY
CARBONIFEROUS
PENNSYLVANIAN
MISSISSIPIAN
DEVONIAN
LATE
MIDDLE
EARLY
ORDOVICIAN
MARAÑON COMPLEX-BASEMENT
50
100
150
200
250
300
350
400
GS
GS
IPURURO
CHAMBIRA
POZO
YAHUARANGO
CASABLANCA
HUCHPAYACU
CACHIYACU
VIVIAN
CHONTA
AGUA CALIENTE
RAYA
CUSHABATAY
SARAYAQUILLO (fluvial)
SARAYAQUILLO
PUCARA
LOWER NIA
(fluvial-eolian)
MITU
ENE - NOI (fluvial-eolian)
COPACABANA
TARMA
AMBO
CABANILLAS
CONTAYA
PEBAS
POZO
CHONTA
RAYA
oil prone
PUCARA
oil prone
SHINAI
oil prone
?
gas prone
?
CABANILLAS
gas + cond. prone
ANDEAN OROGENY
ANDEAN OROGENY
INITIATION OF ANDEAN FORELAND
BFU
JURUA OROGENY
BACK-ARC
POST-RIFT SAG BASIN
RIFTING
GONDWANIDE OROGENY
FAMATINIAN OROGENY
Evaporite

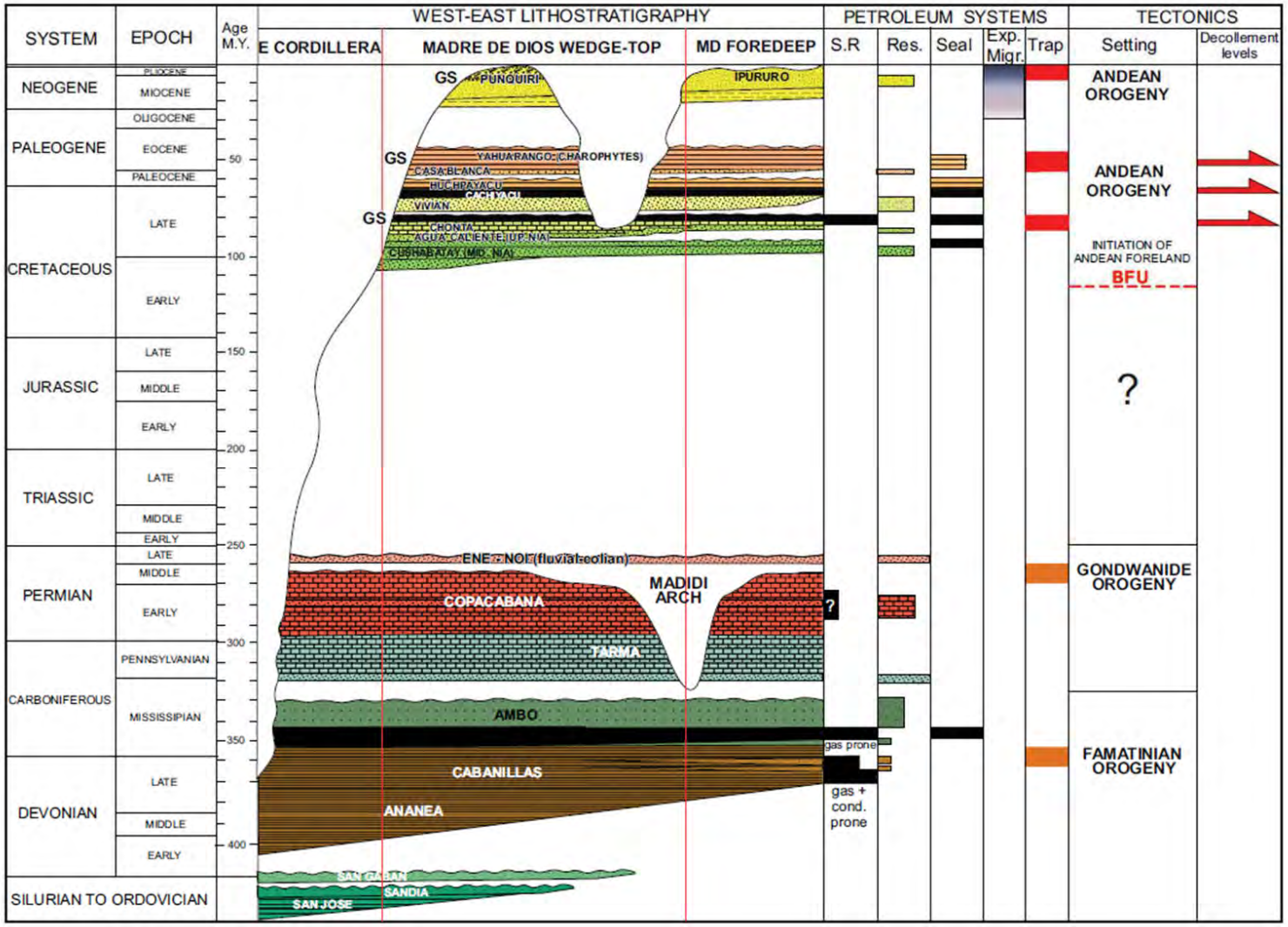
SYSTEM
EPOCH
Age M.Y.
WEST-EAST LITHOSTRATIGRAPHY
E CORDILLERA
MADRE DE DIOS WEDGE-TOP
MD FOREDEEP
PETROLEUM SYSTEMS
S.R
Res.
Seal
Exp. Migr.
Trap
TECTONICS
Setting
Decollement levels
NEOGENE
PLIOCENE
MIOCENE
PALEOGENE
OLIGOCENE
EOCENE
PALEOCENE
CRETACEOUS
LATE
EARLY
JURASSIC
LATE
MIDDLE
EARLY
TRIASSIC
LATE
MIDDLE
EARLY
PERMIAN
LATE
MIDDLE
EARLY
CARBONIFEROUS
PENNSYLVANIAN
MISSISSIPIAN
DEVONIAN
LATE
MIDDLE
EARLY
SILURIAN TO ORDOVICIAN
50
100
150
200
250
300
350
400
GS
PUNQUIRI
IPURURO
YAHUARANGO (CHAROPHYTES)
CASA BLANCA
HUCHPAYACU
CACHYACU
VIVIAN
CHONTA
AGUA CALIENTE (UP. NIA)
CUSHABATAY (MID. NIA)
ENE ? NOI (fluvial-eolian)
MADIDI ARCH
COPACABANA
TARMA
AMBO
CABANILLAS
ANANEA
SAN GABAN
SANDIA
SAN JOSE
?
gas prone
gas + cond. prone
ANDEAN OROGENY
ANDEAN OROGENY
INITIATION OF ANDEAN FORELAND
BFU
?
GONDWANIDE OROGENY
FAMATINIAN OROGENY

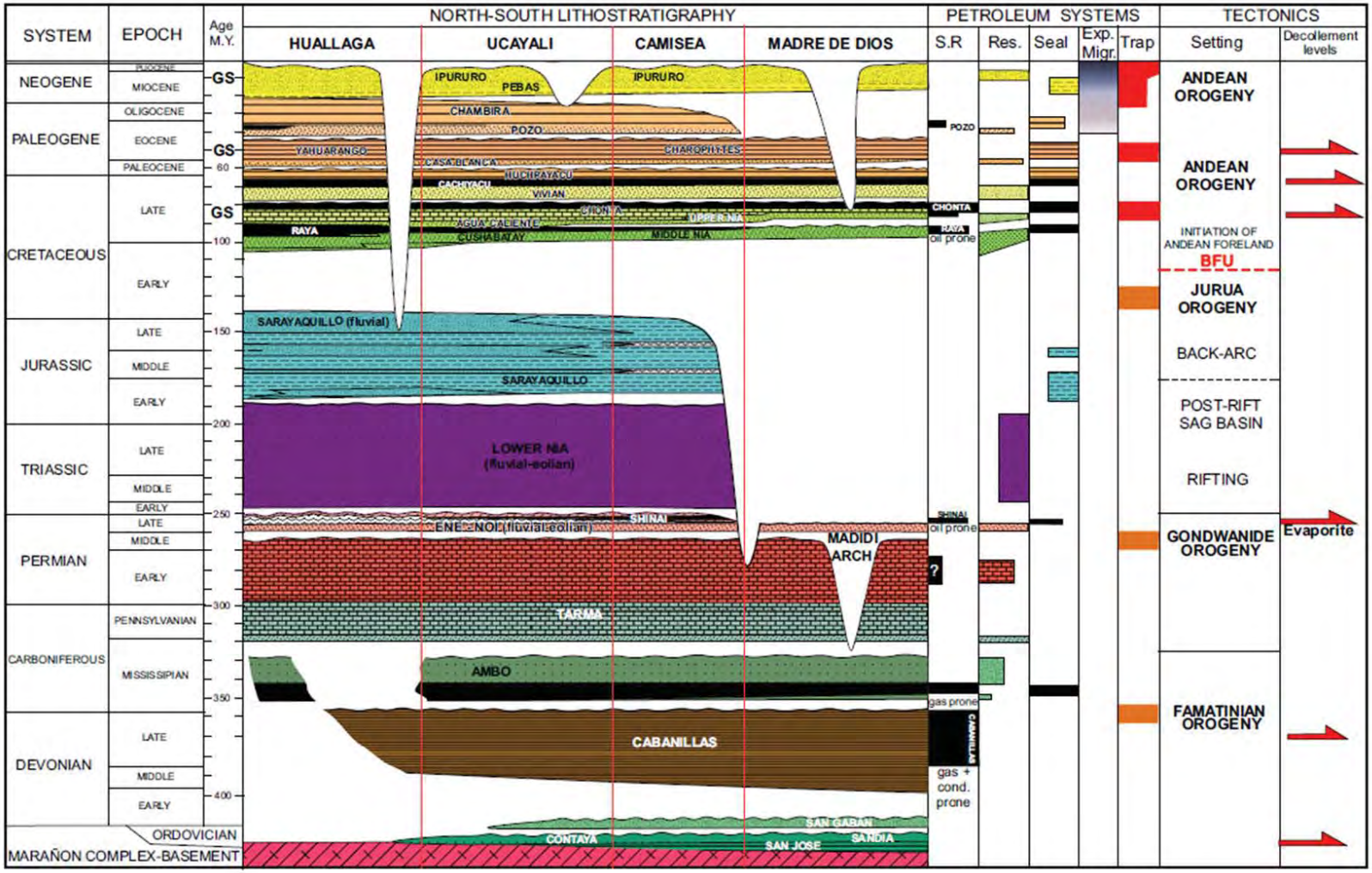
SYSTEM
EPOCH
Age M.Y.
NORTH-SOUTH LITHOSTRATIGRAPHY
HUALLAGA
UCAYALI
CAMISEA
MADRE DE DIOS
PETROLEUM SYSTEMS
S.R
Res.
Seal
Exp. Migr.
Trap
TECTONICS
Setting
Decollement levels
NEOGENE
PALEOGENE
CRETACEOUS
JURASSIC
TRIASSIC
PERMIAN
CARBONIFEROUS
DEVONIAN
MIOCENE
OLIGOCENE
EOCENE
PALEOCENE
LATE
EARLY
MIDDLE
PENNSYLVANIAN
MISSISSIPIAN
ORDOVICIAN
MARAÑON COMPLEX-BASEMENT
GS
60
100
150
200
250
300
350
400
IPURURO
PEBAS
CHAMBIRA
POZO
YAHUARANGO
CHAROPHYTES
CASA BLANCA
HUCHIRAYACU
CACHIYACU
VIVIAN
CHONTA
UPPER NIA
AGUA CALIENTE
RAYA
CUSHABATAY
MIDDLE NIA
SARAYAQUILLO (fluvial)
SARAYAQUILLO
LOWER NIA
(fluvial-eolian)
SHINAI
ENE - NOI (fluvial-eolian)
MADIDI ARCH
TARMA
AMBO
CABANILLAS
SAN GABAN
CONTAYA
SAN JOSE
SANDIA
oil prone
gas prone
gas + cond. prone
?
ANDEAN OROGENY
INITIATION OF ANDEAN FORELAND
BFU
JURUA OROGENY
BACK-ARC
POST-RIFT SAG BASIN
RIFTING
GONDWANIDE OROGENY
FAMATINIAN OROGENY
Evaporite

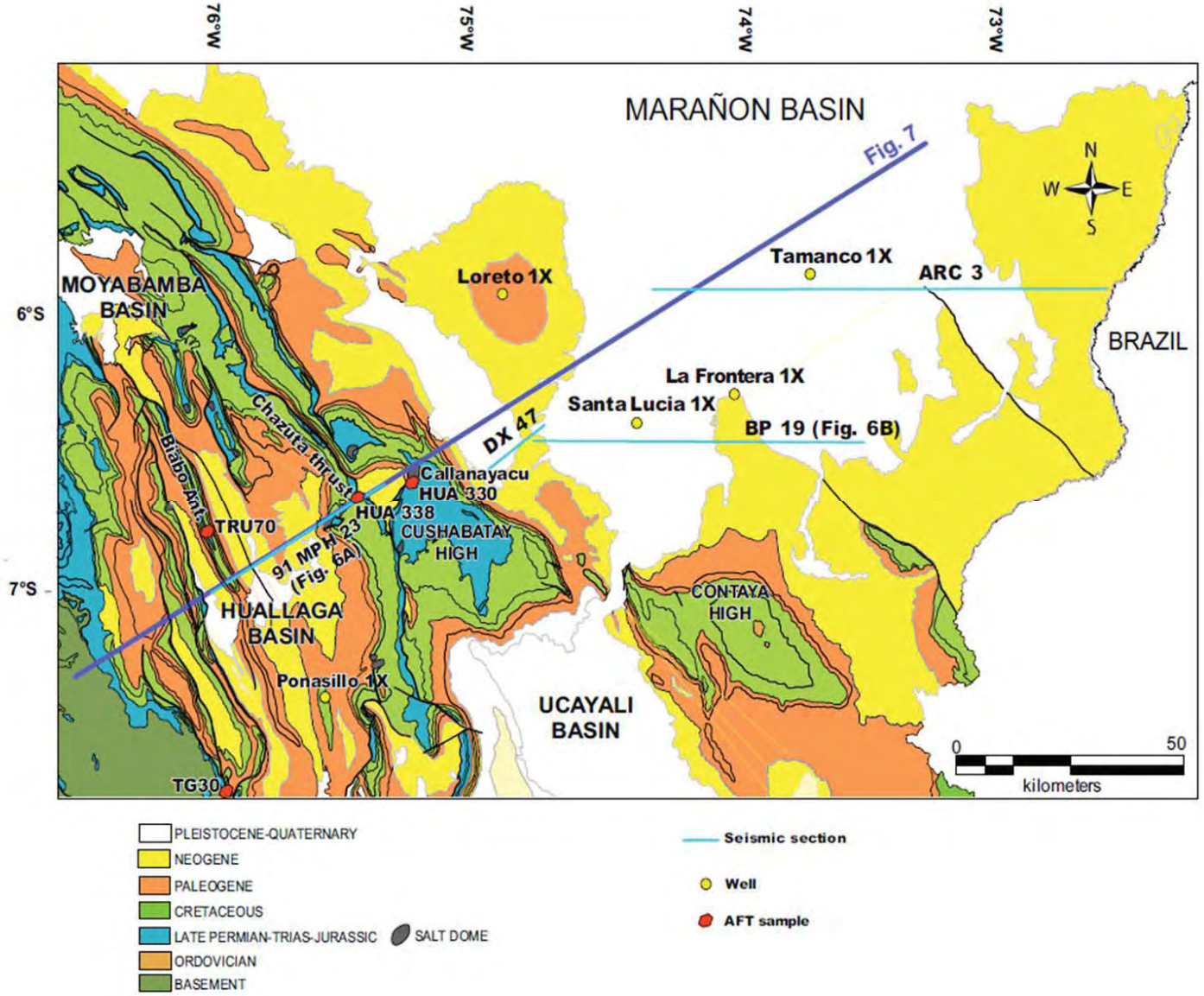
76°W
75°W
74°W
73°W
6°S
7°S
MARAÑON BASIN
Fig. 7
N
W
E
S
Tamanco 1X
ARC 3
Loreto 1X
MOYABAMBA BASIN
BRAZIL
La Frontera 1X
Santa Lucia 1X
BP 19 (Fig. 6B)
DX 47
Chazuta thrust
Biabo Ant.
Callanayacu
HUA 330
HUA 338
TRU70
91 MPH 23 (Fig. 6A)
CUSHABATAY HIGH
CONTAYA HIGH
HUALLAGA BASIN
Ponasillo 1X
UCAYALI BASIN
TG30
0
50
kilometers
PLEISTOCENE-QUATERNARY
NEOGENE
PALEOGENE
CRETACEOUS
LATE PERMIAN-TRIAS-JURASSIC
SALT DOME
ORDOVICIAN
BASEMENT
Seismic section
Well
AFT sample

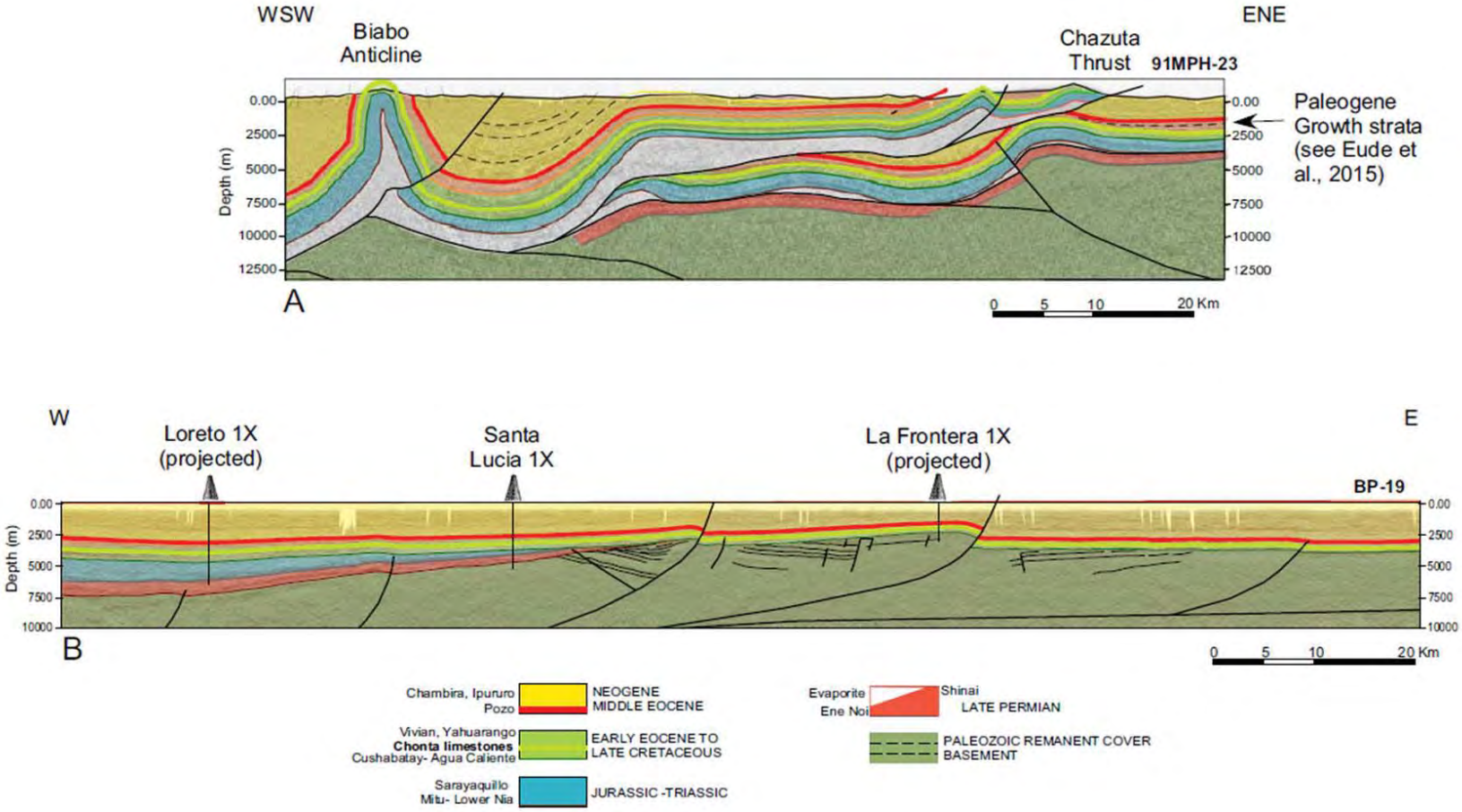
WSW
ENE
Biabo Anticline
Chazuta Thrust
91MPH-23
Paleogene Growth strata (see Eude et al., 2015)
Depth (m)
0.00
2500
5000
7500
10000
12500
A
0 5 10 20 Km
W
E
Loreto 1X (projected)
Santa Lucia 1X
La Frontera 1X (projected)
BP-19
B
Chambira, Ipururo
Pozo
NEOGENE
MIDDLE EOCENE
Vivian, Yahuarango
Chonta limestones
Cushabatay- Agua Caliente
EARLY EOCENE TO LATE CRETACEOUS
Sarayaquillo
Mitu- Lower Nia
JURASSIC -TRIASSIC
Evaporite
Ene Noi
Shinai
LATE PERMIAN
PALEOZOIC REMANENT COVER
BASEMENT

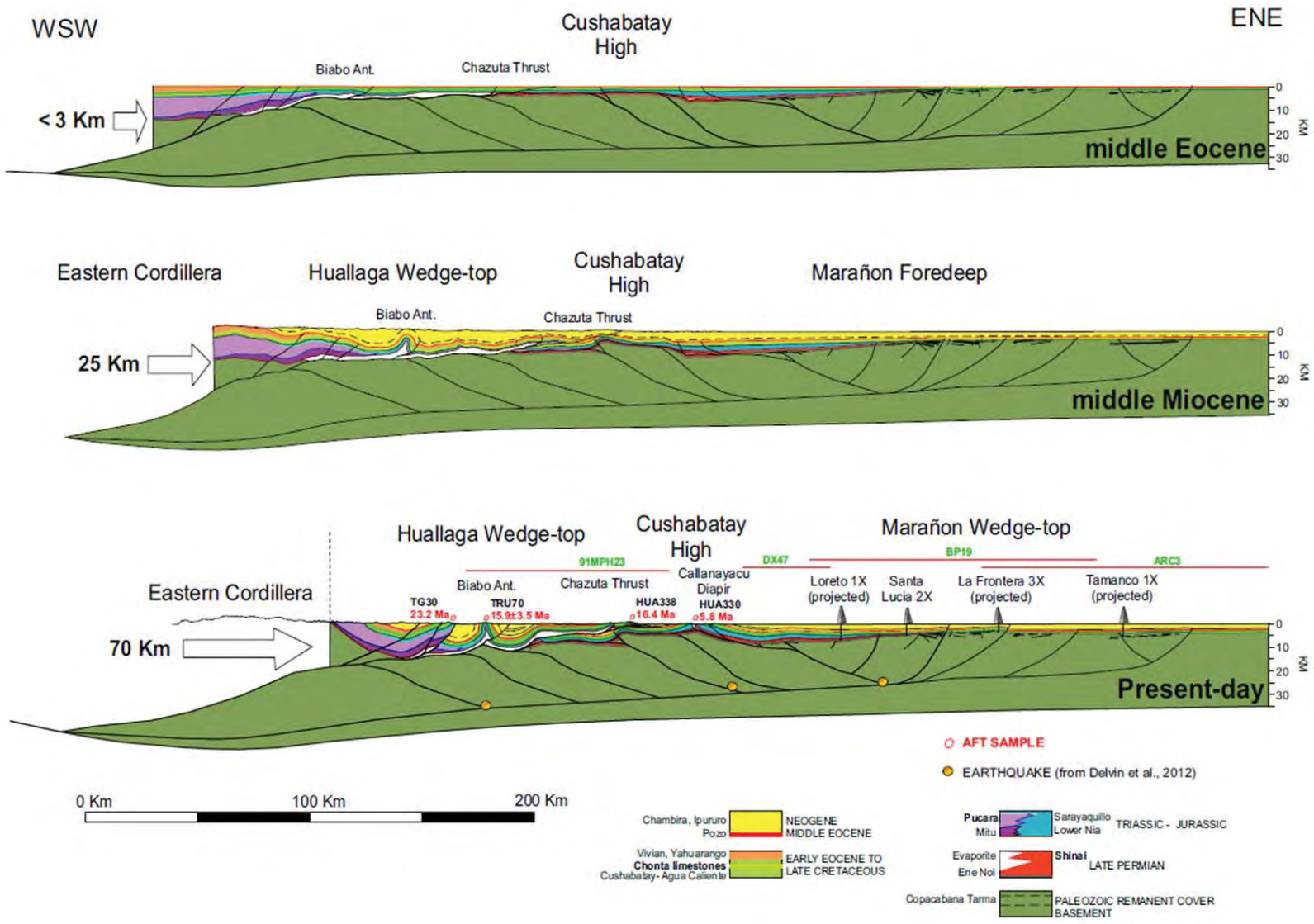
WSW
ENE
Cushabatay High
Biabo Ant.
Chazuta Thrust
< 3 Km
middle Eocene
Eastern Cordillera
Huallaga Wedge-top
Cushabatay High
Marañon Foredeep
Biabo Ant.
Chazuta Thrust
25 Km
middle Miocene
Huallaga Wedge-top
Cushabatay High
Marañon Wedge-top
91MPH23
DX47
BP19
ARC3
Eastern Cordillera
Biabo Ant.
Chazuta Thrust
Callanayacu Diapir
Loreto 1X (projected)
Santa Lucia 2X
La Frontera 3X (projected)
Tamanco 1X (projected)
TG30
23.2 Ma
TRU70
15.9±3.5 Ma
HUA338
16.4 Ma
HUA330
5.8 Ma
70 Km
Present-day
KM
AFT SAMPLE
EARTHQUAKE (from Delvin et al., 2012)
0 Km
100 Km
200 Km
Chambira, Ipururo
Pozo
NEOGENE
MIDDLE EOCENE
Vivian, Yahuarango
Chonta limestones
Cushabatay-Agua Caliente
EARLY EOCENE TO LATE CRETACEOUS
Pucara
Mitu
Sarayaquillo
Lower Nia
TRIASSIC - JURASSIC
Evaporite
Ene Noi
Shinai
LATE PERMIAN
Copacabana Tarma
PALEOZOIC REMANENT COVER BASEMENT

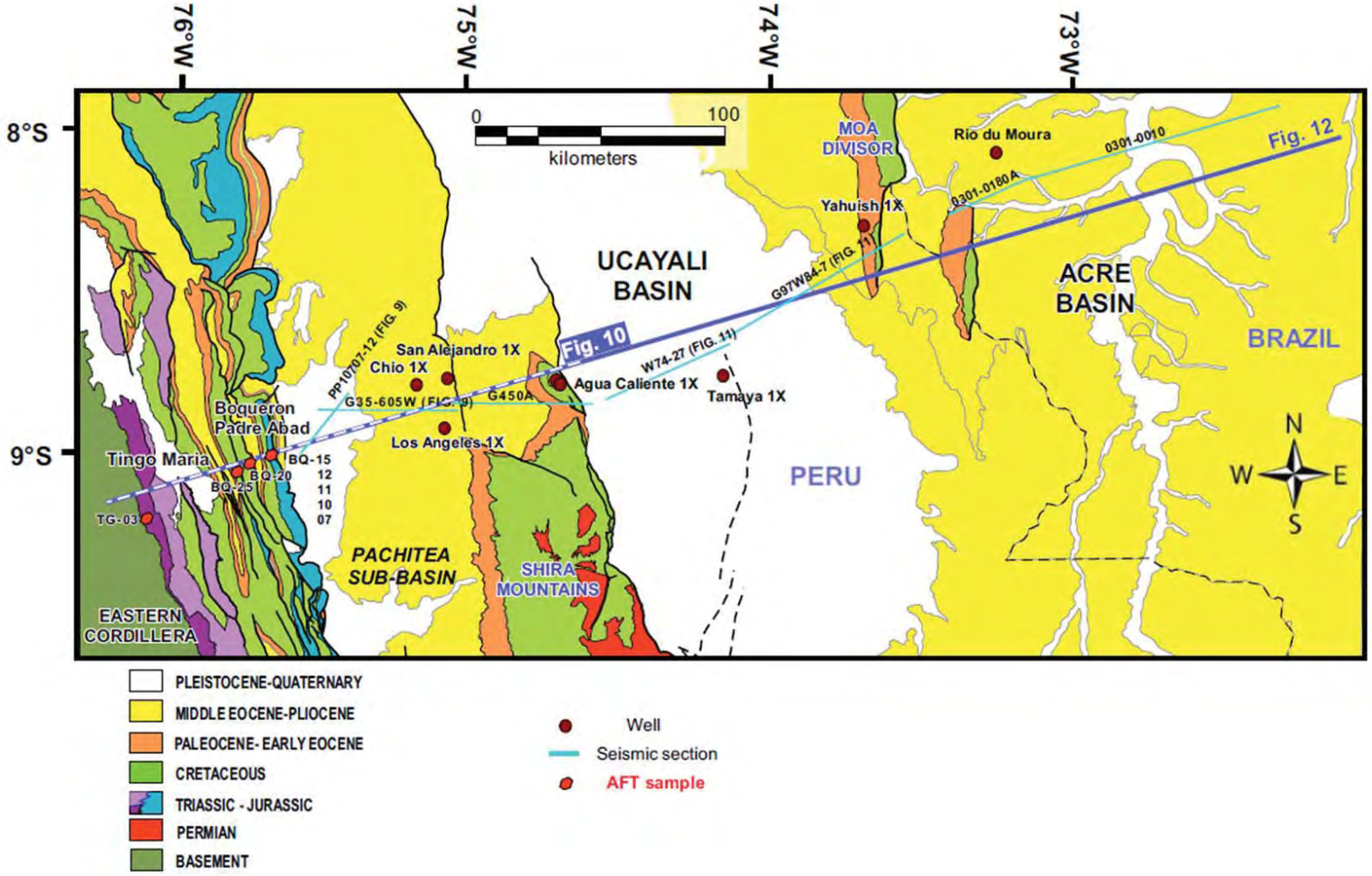
76°W
75°W
74°W
73°W
8°S
9°S
0
100
kilometers
MOA DIVISOR
Rio du Moura
0301-0010
Fig. 12
0301-0180A
Yahuish 1X
G97W84-7 (FIG. 11)
UCAYALI BASIN
ACRE BASIN
BRAZIL
PP10707-12 (FIG. 9)
San Alejandro 1X
Chio 1X
Fig. 10
W74-27 (FIG. 11)
Agua Caliente 1X
Tamaya 1X
G35-605W (FIG. 9)
G450A
Boqueron Padre Abad
Los Angeles 1X
Tingo Maria
BQ-15
BQ-20
BQ-25
12
11
10
07
TG-03
PERU
N
W
E
S
PACHITEA SUB-BASIN
SHIRA MOUNTAINS
EASTERN CORDILLERA
PLEISTOCENE-QUATERNARY
MIDDLE EOCENE-PLIOCENE
PALEOCENE- EARLY EOCENE
CRETACEOUS
TRIASSIC - JURASSIC
PERMIAN
BASEMENT
Well
Seismic section
AFT sample

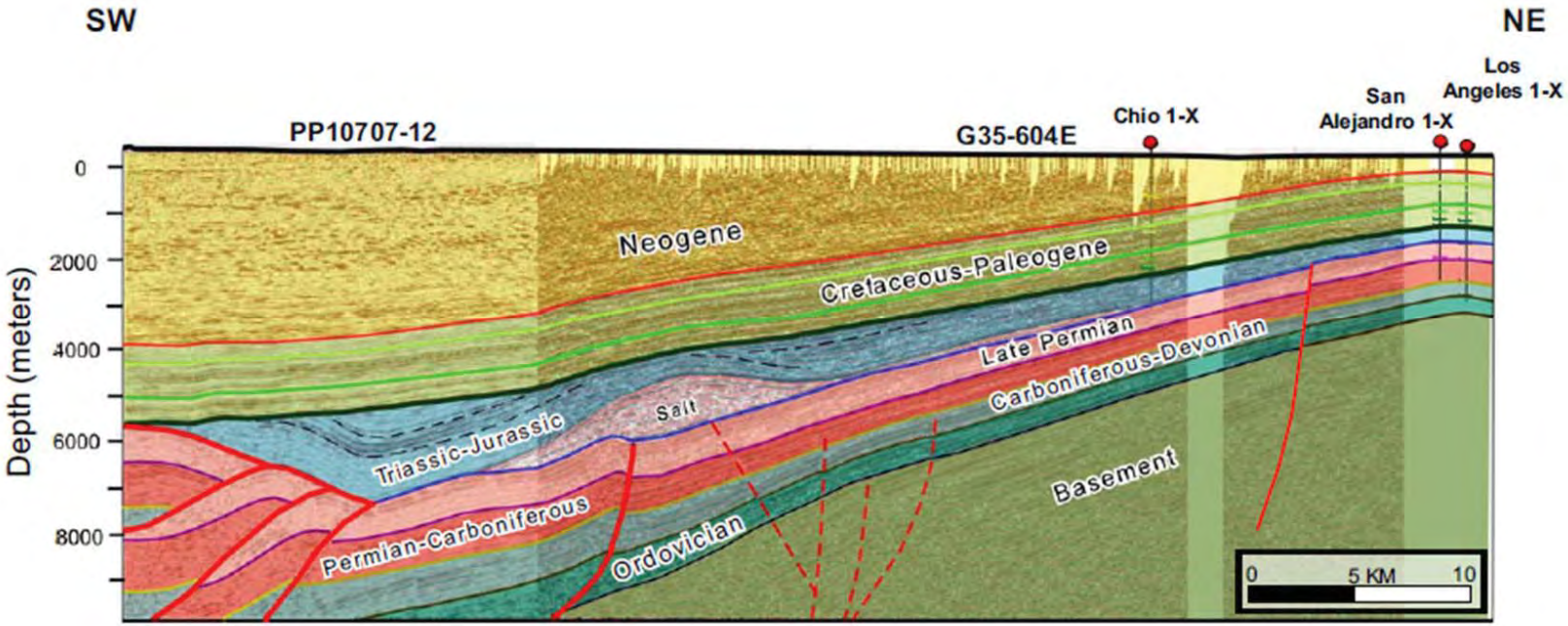
SW
NE
PP10707-12
G35-604E
Chio 1-X
San Alejandro 1-X
Los Angeles 1-X
Depth (meters)
0
2000
4000
6000
8000
Neogene
Cretaceous-Paleogene
Late Permian
Carboniferous-Devonian
Salt
Triassic-Jurassic
Permian-Carboniferous
Ordovician
Basement
0
5 KM
10

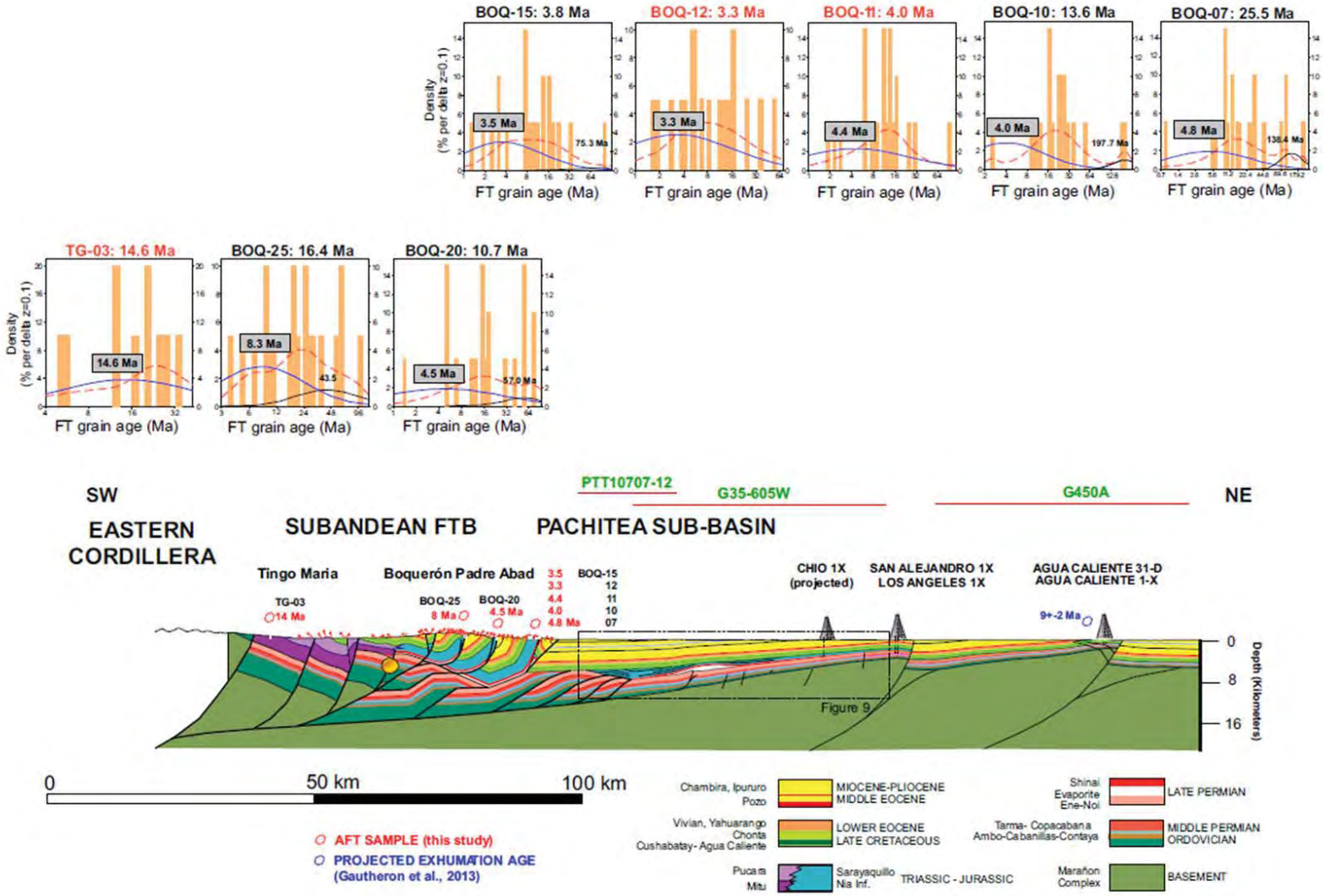
BOQ-15: 3.8 Ma
BOQ-12: 3.3 Ma
BOQ-11: 4.0 Ma
BOQ-10: 13.6 Ma
BOQ-07: 25.5 Ma
Density (% per delta z=0.1)
3.5 Ma
3.3 Ma
4.4 Ma
4.0 Ma
4.8 Ma
FT grain age (Ma)
TG-03: 14.6 Ma
BOQ-25: 16.4 Ma
BOQ-20: 10.7 Ma
14.6 Ma
8.3 Ma
4.5 Ma
SW
NE
EASTERN CORDILLERA
SUBANDEAN FTB
PACHITEA SUB-BASIN
PTT10707-12
G35-605W
G450A
Tingo María
Boquerón Padre Abad
CHIO 1X (projected)
SAN ALEJANDRO 1X
LOS ANGELES 1X
AGUA CALIENTE 31-D
AGUA CALIENTE 1-X
Figure 9
Depth (Kilometers)
0
8
16
0
50 km
100 km
AFT SAMPLE (this study)
PROJECTED EXHUMATION AGE (Gautheron et al., 2013)
MIOCENE-PLIOCENE
MIDDLE EOCENE
LOWER EOCENE
LATE CRETACEOUS
TRIASSIC - JURASSIC
LATE PERMIAN
MIDDLE PERMIAN
ORDOVICIAN
BASEMENT

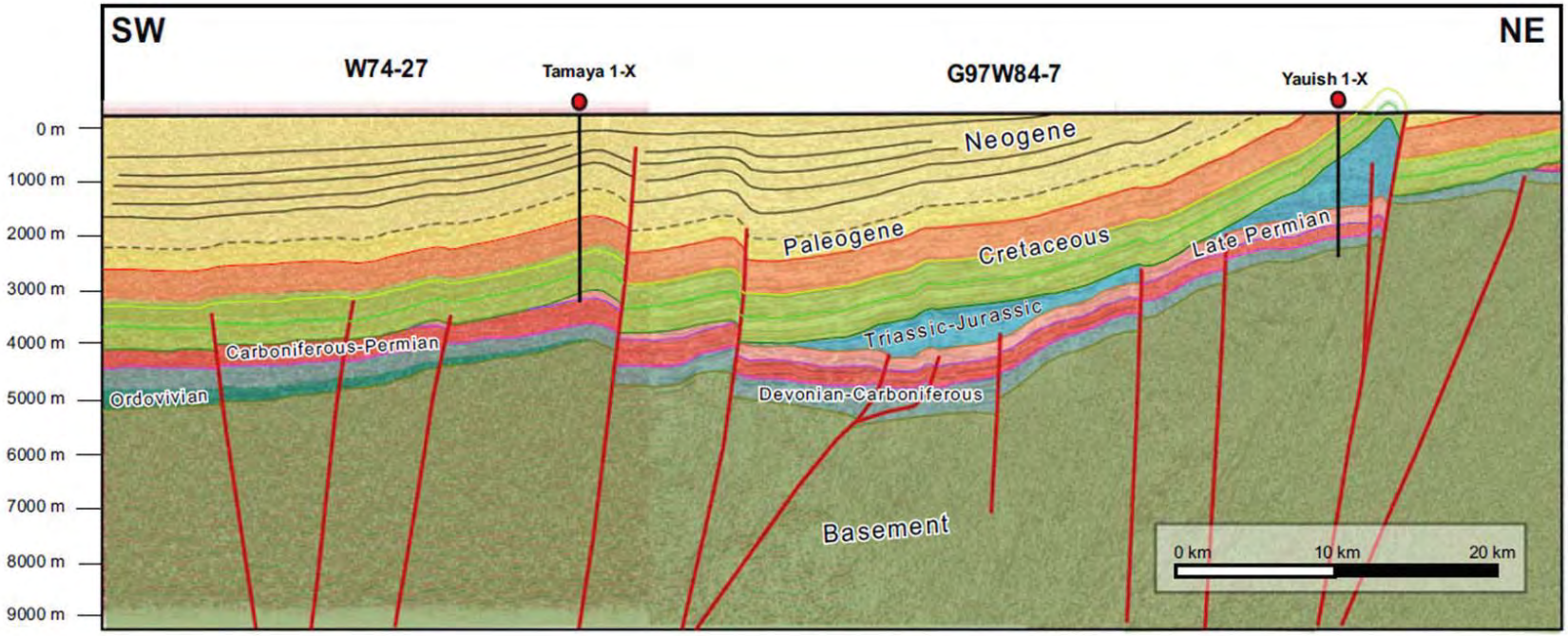
SW
NE
W74-27
Tamaya 1-X
G97W84-7
Yauish 1-X
0 m
1000 m
2000 m
3000 m
4000 m
5000 m
6000 m
7000 m
8000 m
9000 m
Neogene
Paleogene
Cretaceous
Late Permian
Triassic-Jurassic
Carboniferous-Permian
Ordovivian
Devonian-Carboniferous
Basement
0 km
10 km
20 km

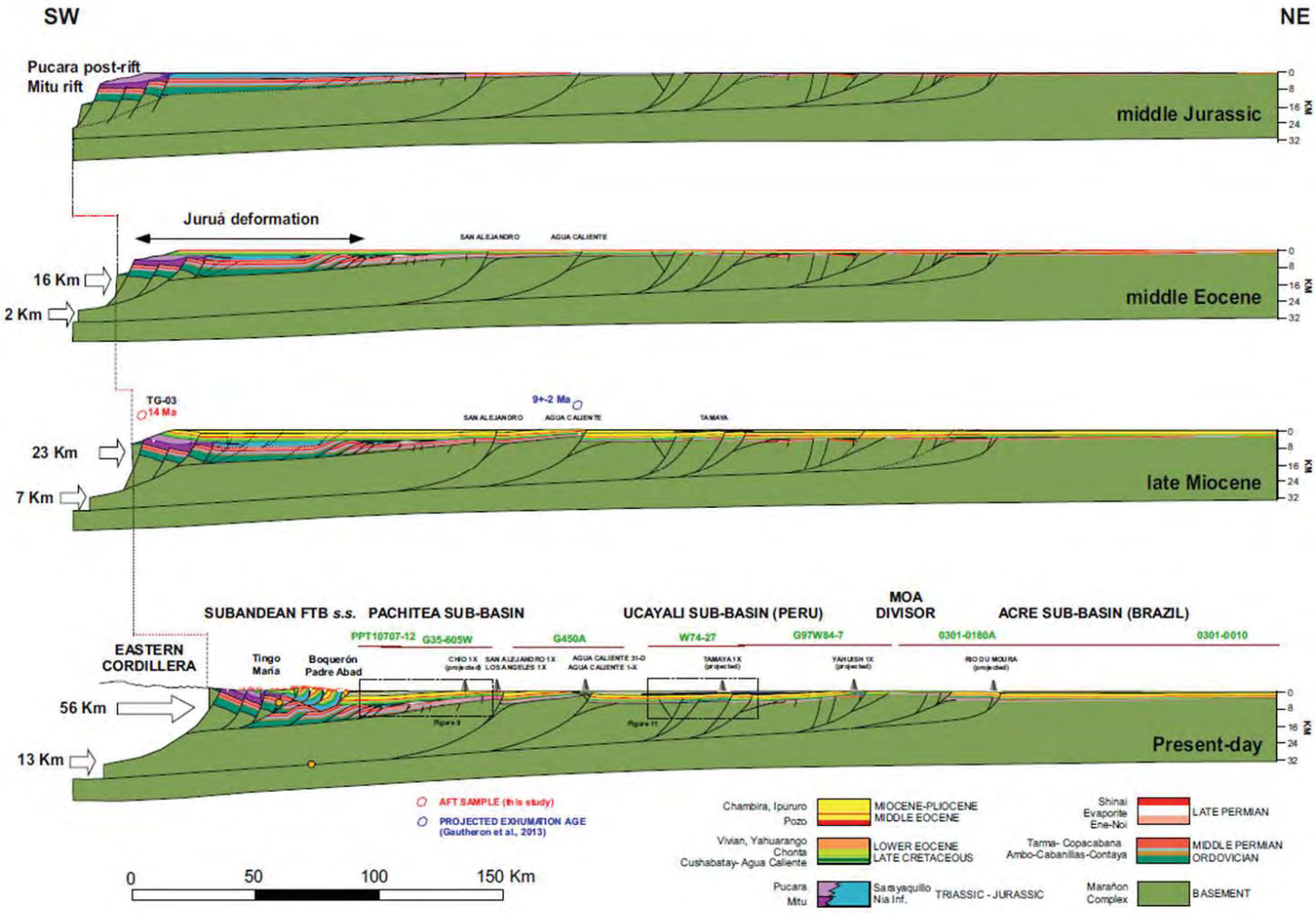
SW
NE
Pucara post-rift
Mitu rift
middle Jurassic
Juruá deformation
SAN ALEJANDRO
AGUA CALIENTE
16 Km
2 Km
middle Eocene
TG-03
14 Ma
9+-2 Ma
SAN ALEJANDRO
AGUA CALIENTE
TAMAYA
23 Km
7 Km
late Miocene
SUBANDEAN FTB s.s.
PACHITEA SUB-BASIN
UCAYALI SUB-BASIN (PERU)
MOA DIVISOR
ACRE SUB-BASIN (BRAZIL)
PPT10707-12
G35-605W
G450A
W74-27
G97W84-7
0301-0180A
0301-0010
EASTERN CORDILLERA
Tingo María
Boquerón Padre Abad
CHIO 1X
SAN ALEJANDRO 1X
LOS ANGELES 1X
AGUA CALIENTE 31-D
AGUA CALIENTE 1-X
TAMAYA 1X
YAHUESH 1X
RIO DO MOURA
56 Km
13 Km
Present-day
AFT SAMPLE (this study)
PROJECTED EXHUMATION AGE (Gautheron et al., 2013)
0
50
100
150 Km
Chambira, Ipururo
Pozo
MIOCENE-PLIOCENE
MIDDLE EOCENE
Vivian, Yahuarango
Chonta
Cushabatay- Agua Caliente
LOWER EOCENE
LATE CRETACEOUS
Pucara
Mitu
Sarayaquillo
Nia Inf.
TRIASSIC - JURASSIC
Shinai
Evaporite
Ene-Noi
LATE PERMIAN
Tarma- Copacabana
Ambo-Cabanillas-Contaya
MIDDLE PERMIAN
ORDOVICIAN
Marañon
Complex
BASEMENT

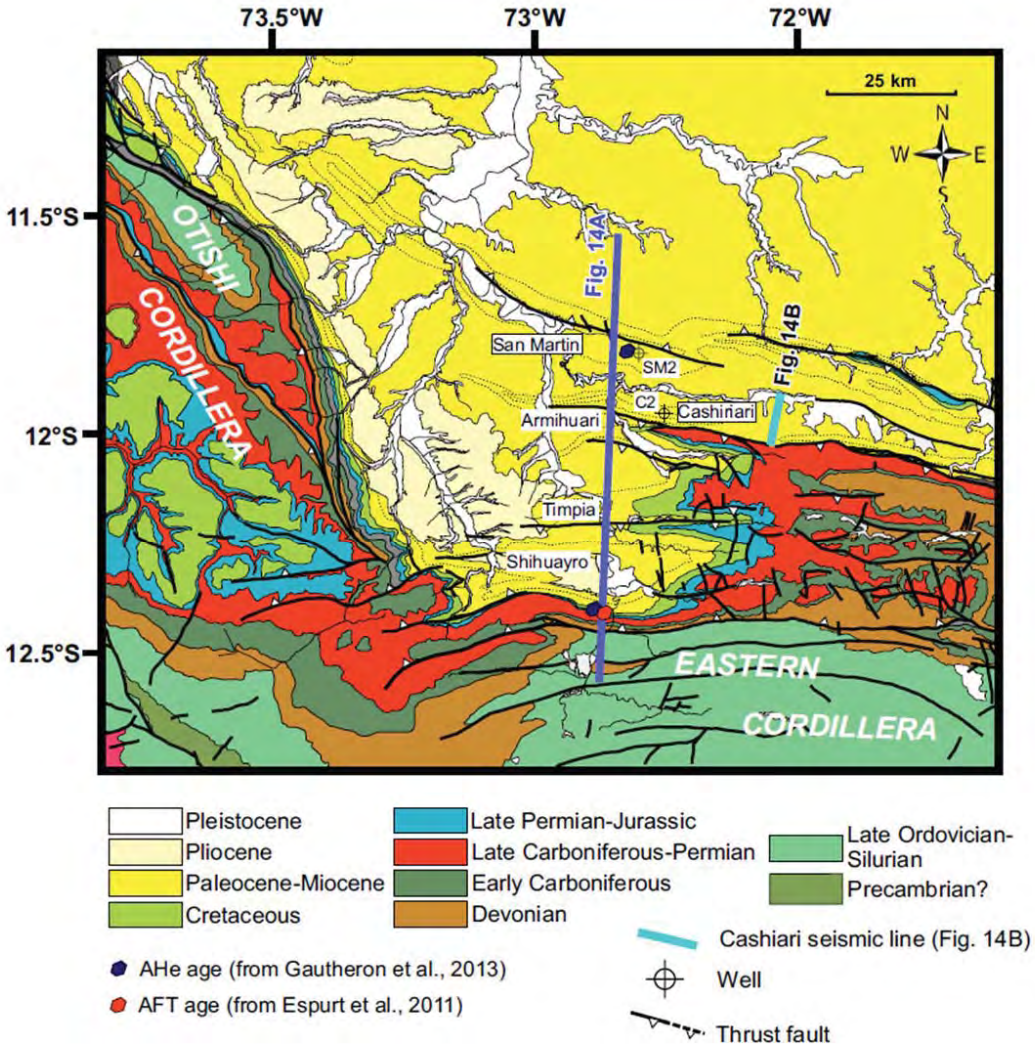
73.5°W
73°W
72°W
11.5°S
12°S
12.5°S
25 km
N
W
E
S
OTISHI
CORDILLERA
Fig. 14A
Fig. 14B
San Martin
SM2
C2
Cashiari
Armihuari
Timpia
Shihuayro
EASTERN
CORDILLERA
Pleistocene
Pliocene
Paleocene-Miocene
Cretaceous
Late Permian-Jurassic
Late Carboniferous-Permian
Early Carboniferous
Devonian
Late Ordovician-Silurian
Precambrian?
Cashiari seismic line (Fig. 14B)
AHe age (from Gautheron et al., 2013)
AFT age (from Espurt et al., 2011)
Well
Thrust fault

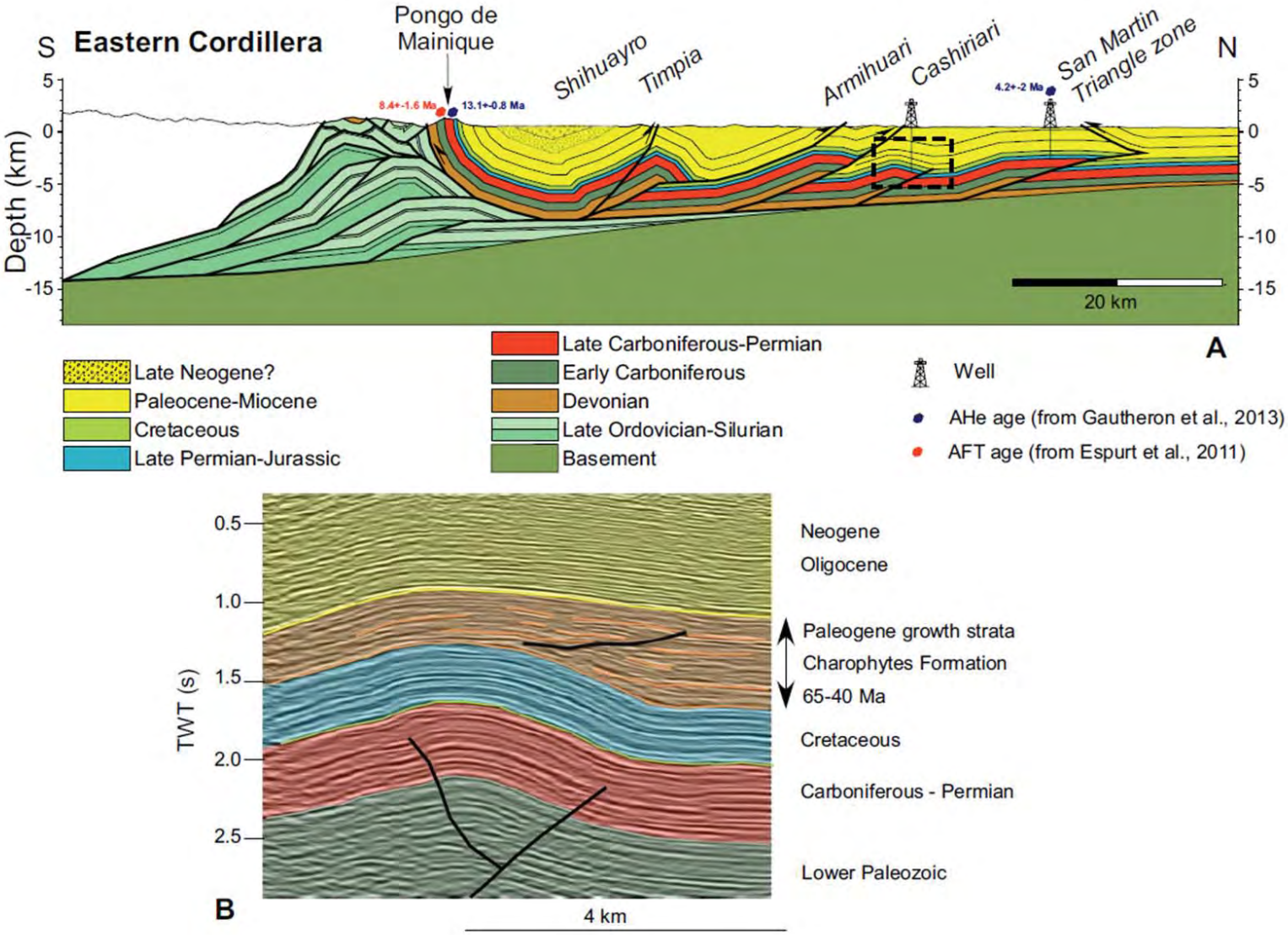
S
Eastern Cordillera
Pongo de Mainique
Shihuayro
Timpia
Armihuari
Cashiriari
San Martin Triangle zone
N
8.4+-1.6 Ma
13.1+-0.8 Ma
4.2+-2 Ma
Depth (km)
5
0
-5
-10
-15
20 km
A
Late Neogene?
Paleocene-Miocene
Cretaceous
Late Permian-Jurassic
Late Carboniferous-Permian
Early Carboniferous
Devonian
Late Ordovician-Silurian
Basement
Well
AHe age (from Gautheron et al., 2013)
AFT age (from Espurt et al., 2011)
TWT (s)
0.5
1.0
1.5
2.0
2.5
Neogene
Oligocene
Paleogene growth strata
Charophytes Formation
65-40 Ma
Cretaceous
Carboniferous - Permian
Lower Paleozoic
B
4 km

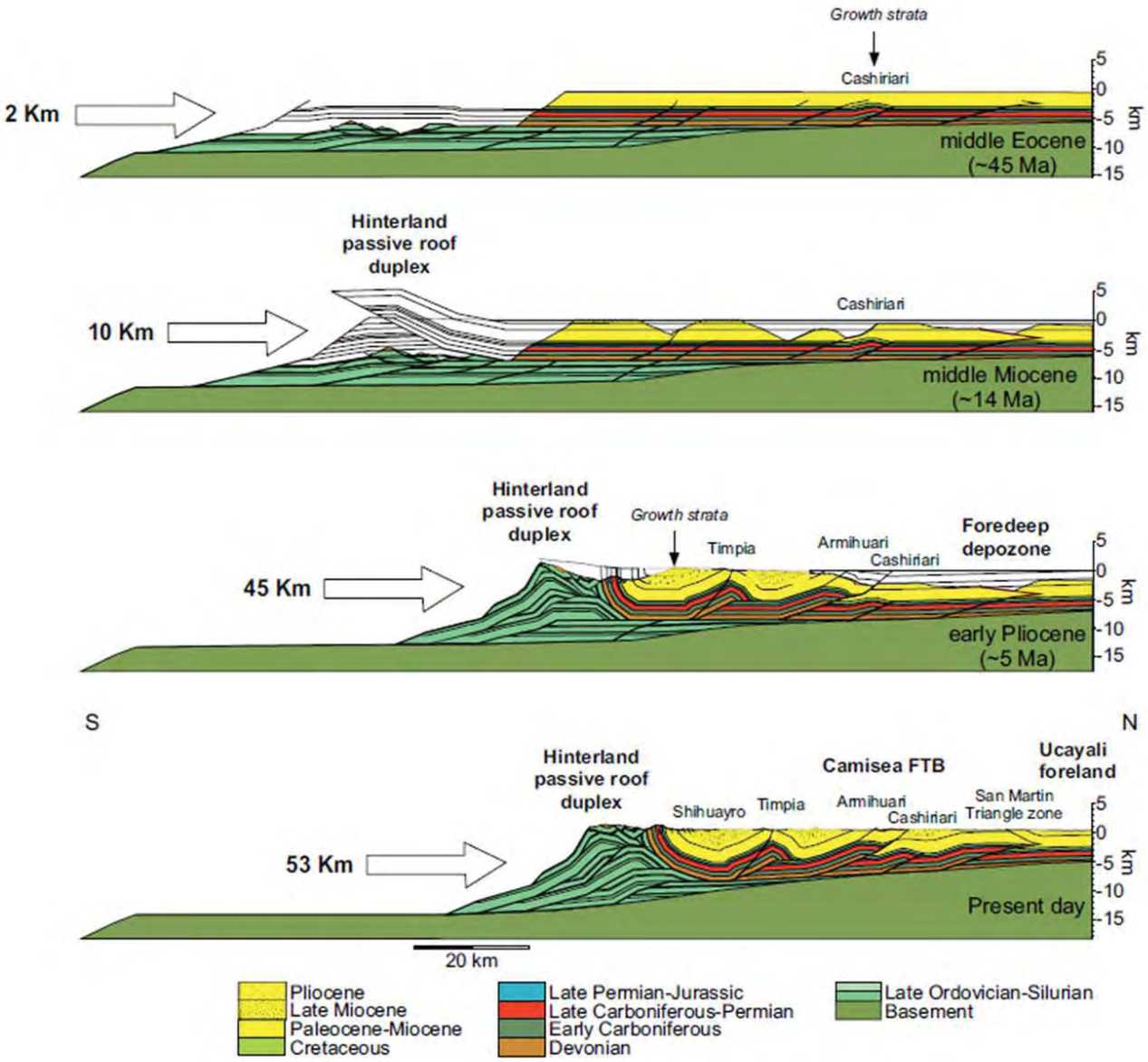
Growth strata
Cashiriari
2 Km
middle Eocene
(~45 Ma)
Hinterland
passive roof
duplex
10 Km
Cashiriari
middle Miocene
(~14 Ma)
Hinterland
passive roof
duplex
Growth strata
Timpia
Armihuari
Cashiriari
Foredeep
depozone
45 Km
early Pliocene
(~5 Ma)
S
N
Hinterland
passive roof
duplex
Camisea FTB
Ucayali
foreland
Shihuayro
Timpia
Armihuari
Cashiriari
San Martin
Triangle zone
53 Km
Present day
5
0
-5
-10
-15
km
20 km
Pliocene
Late Miocene
Paleocene-Miocene
Cretaceous
Late Permian-Jurassic
Late Carboniferous-Permian
Early Carboniferous
Devonian
Late Ordovician-Silurian
Basement

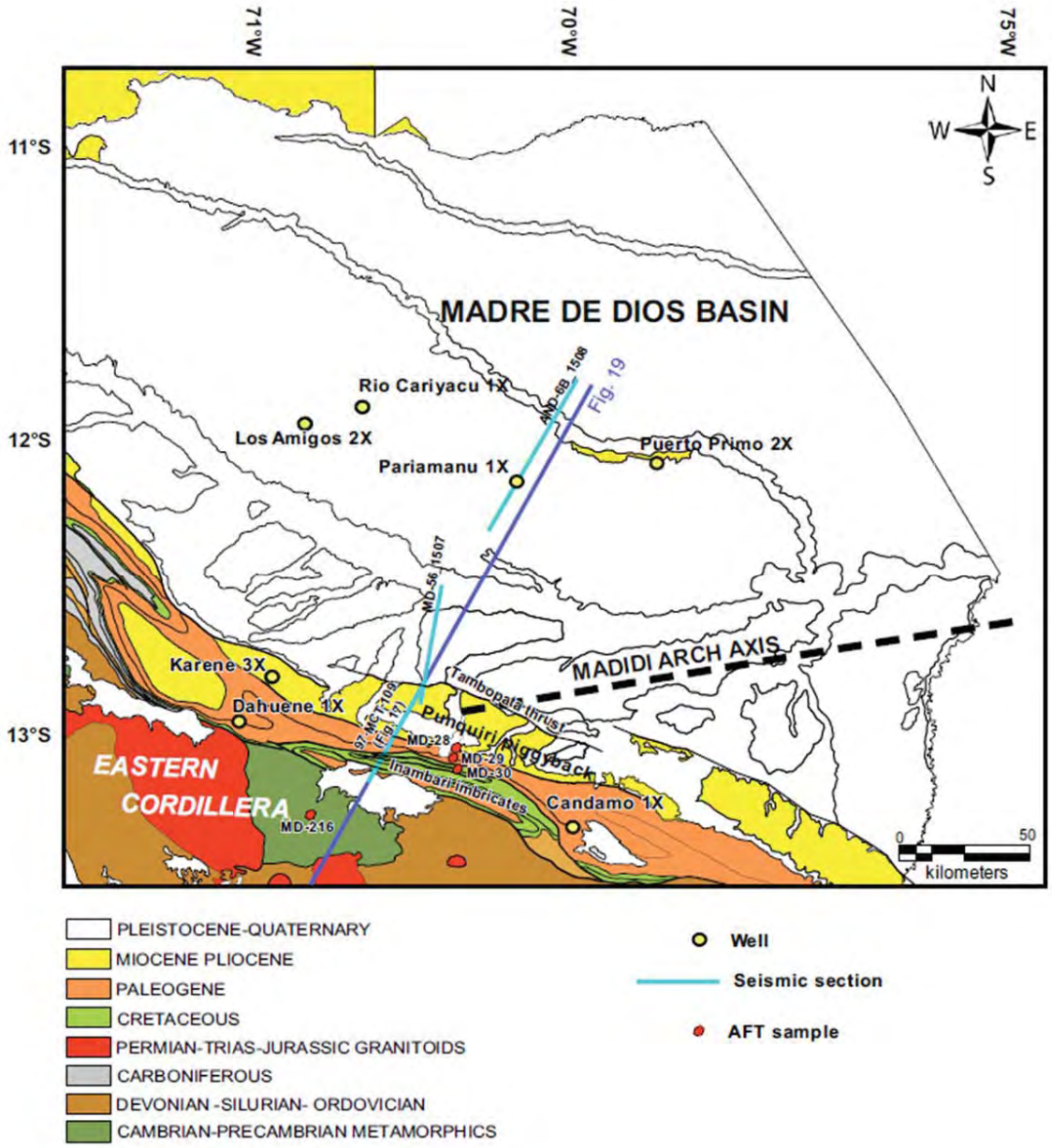
71°W
70°W
75°W
11°S
12°S
13°S
N
W
E
S
MADRE DE DIOS BASIN
Rio Cariyacu 1X
Los Amigos 2X
Pariamanu 1X
Puerto Primo 2X
AND-6B_1506
Fig. 19
MD-56_1507
MADIDI ARCH AXIS
Karene 3X
Dahuene 1X
Tambopata thrust
Punquiri Piggyback
MD-28
MD-29
MD-30
Inambari imbricates
Candamo 1X
EASTERN CORDILLERA
MD-216
0
50
kilometers
PLEISTOCENE-QUATERNARY
MIOCENE PLIOCENE
PALEOGENE
CRETACEOUS
PERMIAN-TRIAS-JURASSIC GRANITOIDS
CARBONIFEROUS
DEVONIAN -SILURIAN- ORDOVICIAN
CAMBRIAN-PRECAMBRIAN METAMORPHICS
Well
Seismic section
AFT sample

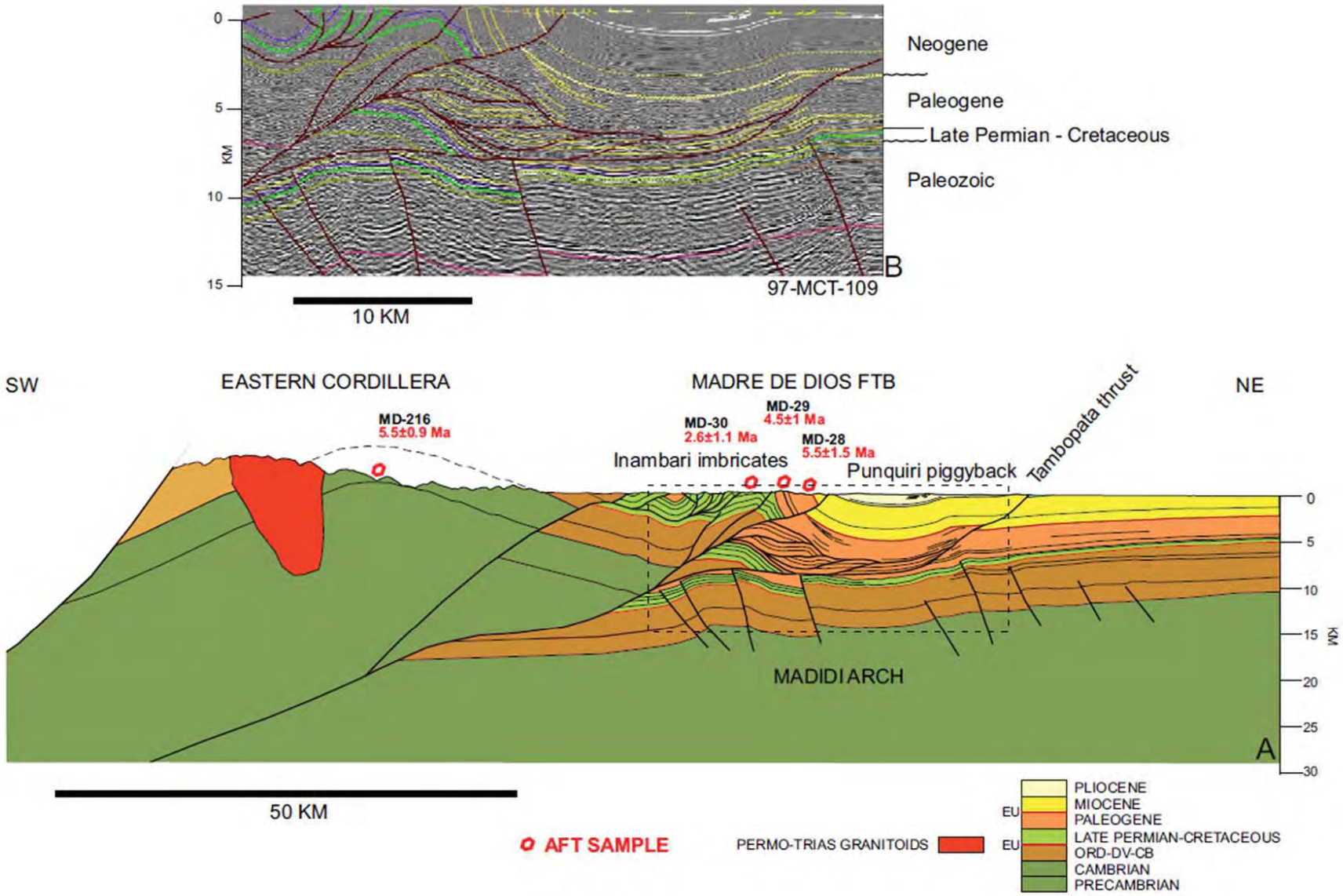
0
5
10
15
KM
Neogene
Paleogene
Late Permian - Cretaceous
Paleozoic
B
97-MCT-109
10 KM
SW
EASTERN CORDILLERA
MADRE DE DIOS FTB
NE
MD-216
5.5±0.9 Ma
MD-30
2.6±1.1 Ma
MD-29
4.5±1 Ma
MD-28
5.5±1.5 Ma
Inambari imbricates
Punquiri piggyback
Tambopata thrust
MADIDI ARCH
A
0
5
10
15
20
25
30
KM
50 KM
AFT SAMPLE
PERMO-TRIAS GRANITOIDS
EU
EU
PLIOCENE
MIOCENE
PALEOGENE
LATE PERMIAN-CRETACEOUS
ORD-DV-CB
CAMBRIAN
PRECAMBRIAN

NE
SO

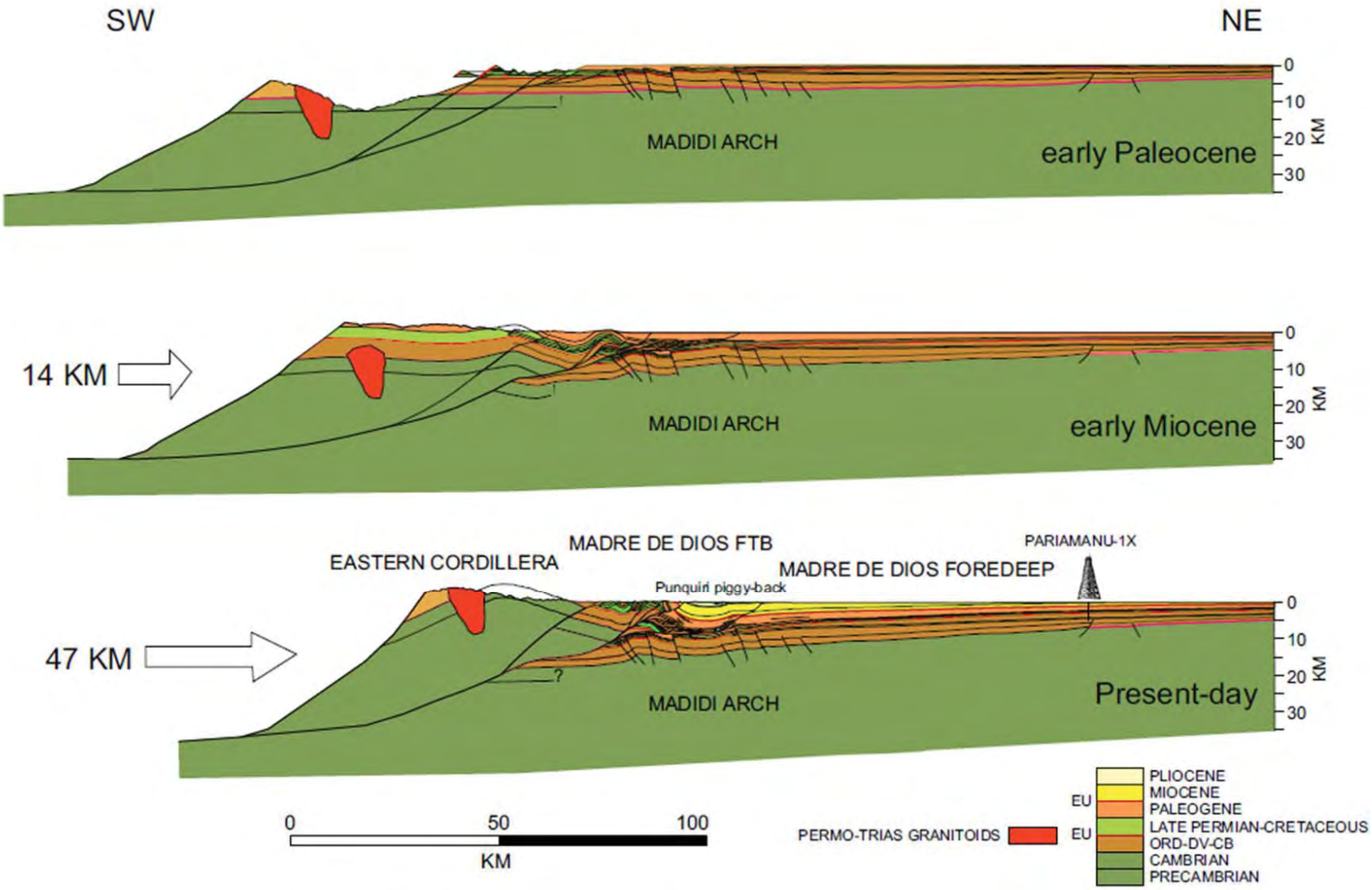
SW
NE
MADIDI ARCH
early Paleocene
0
10
20
30
KM
14 KM
MADIDI ARCH
early Miocene
47 KM
EASTERN CORDILLERA
MADRE DE DIOS FTB
Punquiri piggy-back
MADRE DE DIOS FOREDEEP
PARIAMANU-1X
MADIDI ARCH
Present-day
0
50
100
KM
PERMO-TRIAS GRANITOIDS
EU
PLIOCENE
MIOCENE
PALEOGENE
LATE PERMIAN-CRETACEOUS
ORD-DV-CB
CAMBRIAN
PRECAMBRIAN

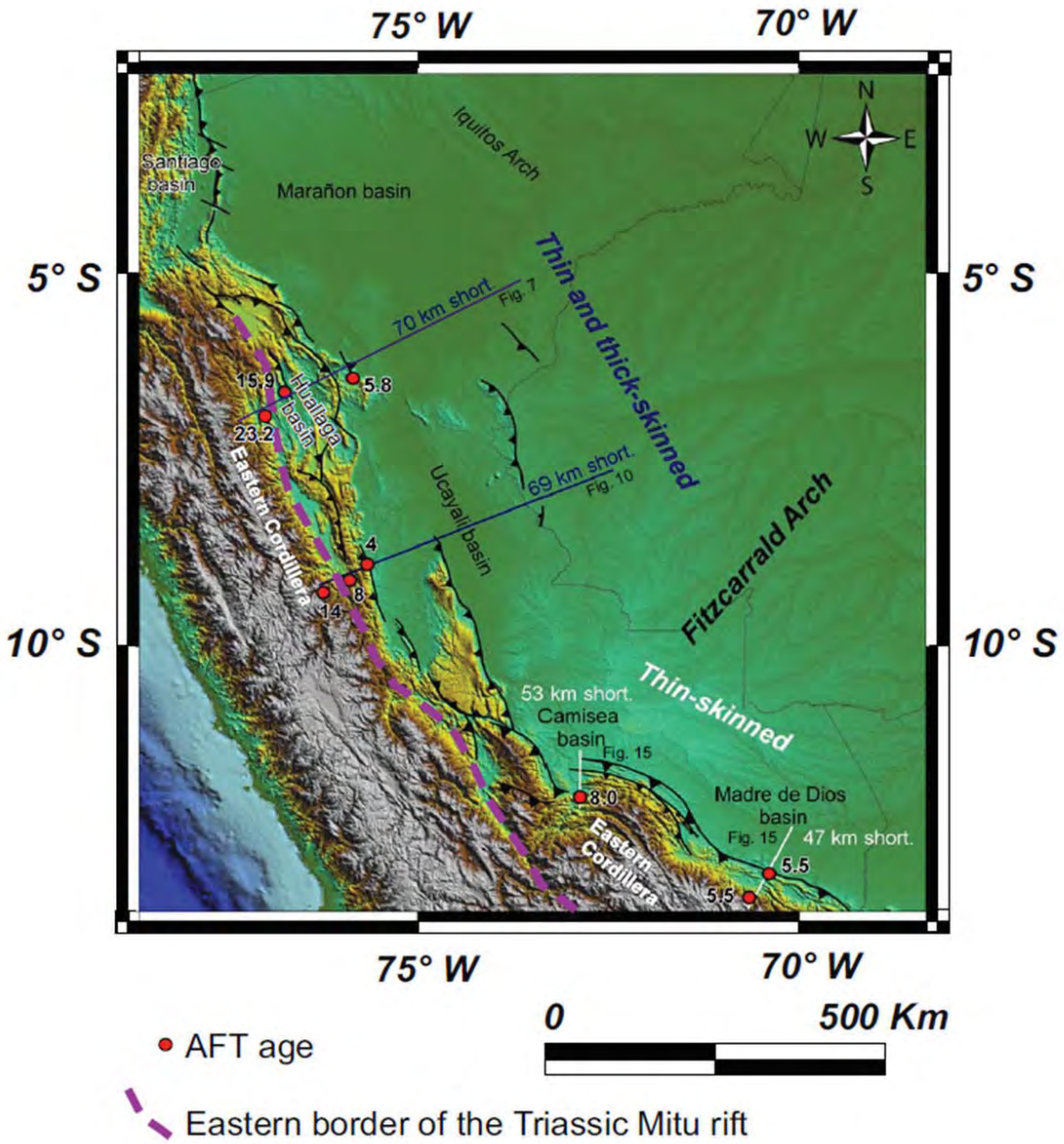
75° W
70° W
5° S
10° S
N
W
E
S
Santiago basin
Marañon basin
Iquitos Arch
Thin and thick-skinned
70 km short.
Fig. 7
15.9
5.8
Huallaga basin
23.2
Eastern Cordillera
Ucayali basin
69 km short.
Fig. 10
4
8
14
Fitzcarrald Arch
Thin-skinned
53 km short.
Camisea basin
Fig. 15
8.0
Madre de Dios basin
Fig. 15
47 km short.
5.5
5.5
Eastern Cordillera
0
500 Km
AFT age
Eastern border of the Triassic Mitu rift

Sample	Stratigraphic age/ Formation	Longiude	Latitude	Elevation (m)	ρs	Ns	ρi	Ni	ρd	Nd	P(X2) (%)	U (ppm)	Cl (wt%)	Central Age (Ma)	Ng	Component ages (Ma)	Cl (± 1б)
BOQ-07	Triassic-Jurassic Lower Nia	-75.67498	-9.065513	431	0.131	49	1.373	515	1.395	2222	<1	11	0.451	25.5 ± 9.7	20	YP: 4.8 OP: 138.4	-1.6 ± 2.3 -26.8 ± 33.1
BOQ-09	Triassic-Jurassic Lower Nia	-75.678211	-9.065779	418	0.079	24	3.686	1118	1.397	2222	<1	30	0.357	13.6 ± 6.6	20	YP: 4.0 OP: 197.7	-0.9 ± 1.2 -43.0 ± 54.7
BOQ-11	Triassic-Jurassic Lower Nia	-75.680089	-9.067837	495	0.033	8	2.317	554	1.399	2222	28	19	0.138	4.0 ± 1.4	20		
BOQ-12	Triassic-Jurassic Lower Nia	-75.680894	-9.070006	480	0.035	11	2.888	907	1.4	2222	43	24	0.229	3.3 ± 1.0	20		
BOQ-15	Triassic-Jurassic Lower Nia	-75.689363	-9.073581	550	0.057	18	4.083	1290	1.402	2222	<1	33	0.219	3.8 ± 0.9	20	YP: 3.5 OP: 75.3	-0.8 ± 1.0 -52.3 ± 169.2
BOQ-20	Triassic-Jurassic Lower Nia	-75.743208	-9.098266	568	0.032	14	1.051	455	1.404	2222	<1	9	0.409	10.7 ± 4.3	20	YP: 4.5 OP: 57.0	-1.6 ± 2.4 -23.2 ± 38.9
BOQ-25	Triassic-Jurassic Lower Nia	-75.781914	-9.142357	1083	0.077	30	1.759	683	1.406	2222	<1	14	0.535	16.4 ± 4.1	20	YP: 8.3 OP: 43.5	-2.7 ± 4.0 -26.8 ± 69.0
TG-03	Triassic Mitu Group	-76.060095	-9.363515	912	0.106	13	1.891	232	1.372	2148	63	16	0.41	14.6 ± 4.2	20		